RADIOMETRIC INVESTIGATION OF SOIL AND BEACH SAND IN ZANZIBAR

GHARIB HAMZA MOHAMED

Thesis presented in fulfilment of the requirements for the degree of Doctor of Philosophiae in the Department of Physics and Astronomy at the University of the Western Cape, South Africa.

Supervisors:

Prof. R. Lindsay,
Department of Physics and Astronomy,
University of the Western Cape.

Dr Peane Maleka,
Department of Subatomic Physics,
NRF/iThemba LABS.

May, 2019

DECLARATION

I, **GHARIB HAMZA MOHAMED**, declare that the work presented in this thesis, **radiometric investigation of soil and beach sand in Zanzibar**, is my original work. It has never been submitted before to any other University for any award and that where other people's works used in this thesis, complete references have been provided.

Gharib Hamza Mohamed **May, 2019**

Student Number: 3417615

Signature: 

RADIOMETRIC INVESTIGATION OF SOIL AND BEACH SAND IN ZANZIBAR

Gharib Hamza Mohamed

KEYWORDS

Absorbed Dose Rate in air

Activity concentration (^{40}K, ^{238}U and ^{232}Th)

Annual Effective Dose Equivalent

Energy Dispersive X-Ray Fluorescence

Gamma ray spectroscopy

Hyper Pure Germanium (HPGe) gamma ray detector

Major elements

MEDUSA gamma ray detector

Multivariate statistics

Trace elements

Radiometric investigation of soil and beach sand in Zanzibar

Gharib Hamza Mohamed

Department of Physics and Astronomy, University of the Western Cape, Private Bag X17, Bellville, South Africa.

ABSTRACT

This study presents the results of radiometric investigation of soil and beach sand in Zanzibar. The activity concentration of natural radionuclides (^{40}K, and ^{232}Th and ^{238}U decay products) in beach sand and soil samples was measured in-situ using the NaI(Tl) and the MEDUSA gamma ray detectors and ex-situ using the low background HPGe detector system.

The activity concentrations of ^{232}Th, ^{238}U and ^{40} K in beach sand are much lower than in soil samples, with one major exception at Kukuu. Two beach sand samples from Kukuu beach were found to have enhanced radioactivity levels due to the presence of heavy minerals.

The spatial distributions maps for ^{40}K, ^{238}U and ^{232}Th show large variation in soil samples for two relatively small islands. These strong variations are unexpected, that could have implications for agriculture, is one of the major outcomes of this study.

The outdoor gamma dose rates obtained in beach sand and soil samples ranged from 3 to 2156 nGy h^{-1} and 50 to 294 nGy h^{-1}, respectively. The highest absorbed dose rates in soil samples and beach sand are respectively 5 and 38 times higher than the average world level of 57 nGyh^{-1} for terrestrial doses (UNSCEAR, 2008). Apart from the Kukuu black sand samples that contain the high ^{238}U and ^{232}Th levels, the beach sands and soil in this study do not pose any radiological threat to the public using beaches for various activities.

Based on elemental concentrations, the beach samples in the study area have been classified into four groups; silicate sand (rich in SiO_2), carbonate sand (dominated with

CaO), mixed sand (with high amount of CaO and SiO_2) and heavy mineral sand (with high contents of Fe_2O_3 and TiO_2.

A strong correlation between SiO_2, Fe_2O_3, TiO_2, Zr, V, Ce, Nb, Hf, Y, La, and Nd show these elements are linked with high activity concentration of ^{232}Th in the studied samples. Moreover, the high concentrations of Y, V, P_2O_5 and Fe_2O_3 in the beach sand samples may relate to high ^{238}U activity concentration.

This study set out to investigate how radiometric studies can quickly and easily provide an idea of the variation of soil type found over a large area as well as provide detailed information on a small scale such as the beach where heavy minerals were found. The in-situ laboratory measurements were supplemented by XRF and ICP-MS measurements of samples to investigate the distribution of heavy mineral sands.

ACKNOWLEDGEMENTS

In the name of Allah, the most Merciful, the most Gracious. All praises and thanks are due to the Allah Almighty; we praise Him, seek His help, the love and ask for His forgiveness. I am thankful to Him, for giving me the blessing, the strength, the chance and endurance to complete this study. Special thanks are to my supervisor Professor Robbie Lindsay, for his guidance, care, encouragement, scientific input and thoughtful remarks he has offered me since the commencement from this study to an end.

I extend my sincere thanks to Dr Peane Maleka, my co-supervisor for his support, expert advices and encouragement during the course of this research. I owe many thanks to Professor Rob De Meijer for his time. I have gained an immense of scientific knowledge, professionalism, skills, and values from him. Many thanks should also go to Dr Joash Ongori for his technical support and fruitful discussions through the entire period of this study.

The financial support of my sponsor, Ministry of Higher Education of the Sultanate of Oman (through the Oman Academic Fellowship, OAF) is highly appreciated. I owe thanks to my employee, the State University of Zanzibar for granting me a study leave in order to achieve this milestone.

The administrative support from the second vice president of Zanzibar's office before and during the field work activities is highly appreciated. To the UWC Physics and Astronomy department, I say thank you for your kind support and offering me a conducive environment for learning. To iThemba LABS, thank you for granting me a permission to travel with MEDUSA detector to Zanzibar for in-situ gamma measurements.

I wish to express my gratitude to Maalim Hamad Juma and Maalim Kassim Hashim of SUZA secondary school as well as locals of Kukuu, Maziwa Ng'ombe, Msuka, Kidoti and Mtende for their support during field work. My special thanks go to Dr Zakaria

Khamis for his input in drawing maps using GIS techniques and to Eldud with his help in statistical analysis. I extend my heartfelt thanks to my colleagues at the UWC Department of Physics and Astronomy especially El Mughera Elhag, Aiman Bashir and Mohammed Bello for their moral support and technical advice.

Ultimate thanks are to my brothers; Mussa, Abdullah, Mohamed, Ahmad, Farid, Fatawi, Abbass and Seif and my sisters; Jokha and Ache for their continuous support during the course of this study. I am pretty sure that when things seems uncertain, your sincere prayers lights my way again.

Furthermore, I would like to acknowledge the role played by my dad; Sheikh Hamza Bin Mohamed bin Ali and my mom Bi Rehema binti Mussa bin Muhammed for quality mentorship and for supporting my education. I am greatly indebted to my inlaws Retired CDR Mwinshamte Mzee Kai and Fatma Omar Kimbau for their support and endless love since I became part of their family.

Last but not least, my special appreciation and thanks go to my caring wife Khadija Shamte Mzee and our lovely children Mohammed and Fatma for your perseverance and patience throughout this tough journey. Thank you for your kind acceptance of the lost evenings and holidays during the course of this study. I pray to Allah Almighty to continue to reinforce our love and bless you all.

CONTENTS

LIST OF FIGURES

LIST OF TABLES

CHAPTER 1

Introduction

1.1 Background

Since time immemorial, human beings have always been exposed to radiation. This radiation originates from cosmic rays and from radioactive nuclides in the earth's crust (Mohanty et al., 2004; UNSCEAR, 2008; Suresh et al., 2011b). Cosmic radiation consists mainly of high-energy particles from the sun and outer space. It interacts with the earth's atmosphere to give rise to a secondary radiation of particles and gamma-rays, which prevail at the earth's surface. Natural radionuclides arising from the earth's crust are not uniformly distributed, their levels and distribution pattern depends upon the local geology of each region of the world, geographical conditions, transport processes as well as sediment formations (Alam et al., 1999a; UNSCEAR, 2008). The most significant natural radionuclides in soils, beach sands and rocks are potassium (^{40}K), thorium (^{232}Th) and uranium (^{238}U) and their decay products (also called terrestrial radionuclides). Since these natural radioactive nuclides have very long half-lives, their presence in soils, beach sands and rocks can simply be considered as permanent (Yasir et al., 2007).

Studies on natural background radiation performed worldwide have resulted in the discovery of areas with high natural background. For instance, in the coastal areas of Guarapari and Rio de Janeiro in Brazil (Carvalho et al., 2007); Kerala and Orissa on the southwest coast of India (Jibiri et al., 2007); and Yangjiang in China (Wei et al., 1990; Tao et al., 2012). In those areas, the high background radiation is due to the presence of monazite sands which are rich in thorium (Jibiri et al., 2007). In some areas in the United States of America such as Denverand Reading Prong, the radiation level is 10 times more than the usual concentration. The soil in these areas were found to be rich in uranium series radionuclides (Saueia and Mazilli, 2006). Additionally, water rich in ^{226}Ra and its decay products from hot springs which flow in Badgastein in Austria (UNESCO, 2003), and Mahallat and Ramsar in Iran (Sohrabi, 1993; L'Annunziata, 2007), have been found to cause elevation of exposure for people working in the spa centres using the hot spring water for therapeutic purposes (Bolca et al., 2007).

As a consequence of being exposed to natural and artificial radiation, mankind receive radiation doses externally due to the gamma ray exposure of the body and irradiation of lung tissue from inhalation of radon and its daughters. Although dose received from natural radiation is small, over exposure may produce damaging biological effects and ingested and inhaled radiation can be a serious health risk (Rowland, 1978). In Kerala, on the west coast of India, residents receive 0.05 – 26 mSv annually, due to the presence of monazite sand (Ramasamy et al., 2013).

Apart from radiation exposures due to living in close proximity to the earth's crust, human beings are also exposed to additional radiation when the earth crust products (oil, gas, coal, coal ash, minerals) are extracted, refined, and used. The NORM (**N**aturally **O**ccurring **R**adioactive **M**aterials) in these products is concentrated into what is called TENORM (**T**echnologically **E**nhanced **N**aturally **O**ccurring **R**adioactive **M**aterials). In general, the hazards of exposure to TENORM during the extraction and processing of earth materials are relatively small compared to the hazards of exposure to other chemicals. The doses received for instance by those intentionally spending time in these environments with high background radiation (e.g., tourists, workers, and miners) are much greater (Eisenbud 1997; UNSCEAR 2008).

Exposure to naturally occurring radiation dose received by the world population accounts for up to 85%, while artificial sources accounts for the remaining 15% as shown in Figure 1.1 (Al Azmi et al., 2013). The inhalation of radon alone contributes about 50% of the total radiation exposure received by the population from natural sources internally, followed by external exposure due to gamma-rays from terrestrial radionuclides and cosmic rays.

The dose from natural radiation varies from one country to another. In general, there is no regulation for limiting the exposure dose received by populations from the natural background radiation because the NORM concentration is generally rather low. Nonetheless, NORM concentrations can be increased above average natural background levels through human activities such as agriculture, use of radioisotopes for medical

purposes, educational activities and electric power generation (Bernard, Z., 1995; Singh et al., 2005). An accidental discharge from these radioisotopes can cause radioactive contamination into the natural environment. Hence, NORM can also be found at elevated levels.

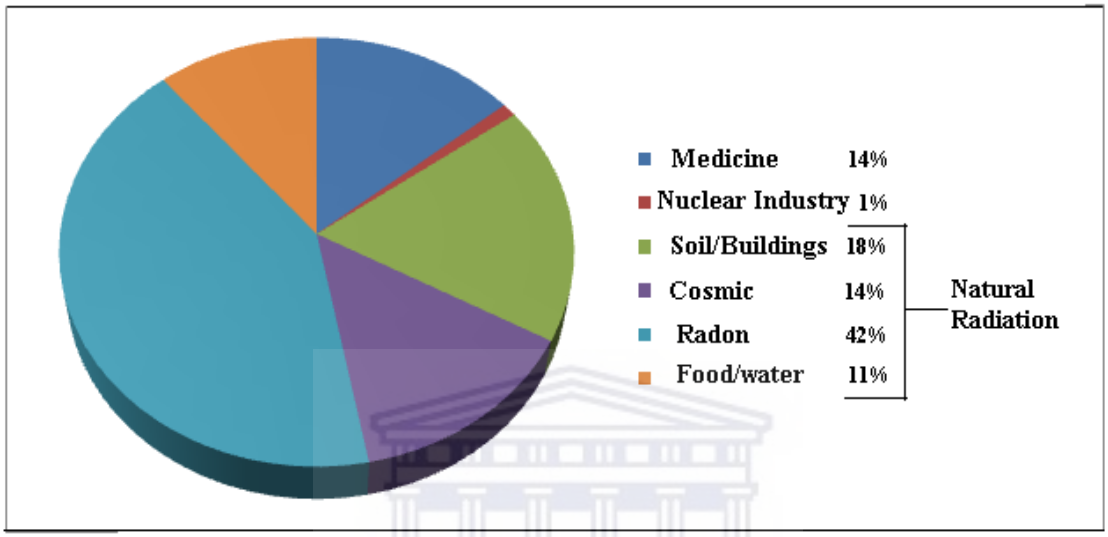

Figure 1.1: Average annual doses to the world population from various sources (Al Azmi et al., 2013)

The IAEA (**I**nternational **A**tomic **E**nergy **A**gency) reports that the exposure from natural radiation to public is of little or no concern in most cases, except those working with mineral ores (Ramli, 1997). However, the WNA (**W**orld **N**uclear **A**ssociation) states that any dose of radiation involves a possible risk to human health (Kannan et al., 2002). The UNSCEAR (**U**nited **N**ations **S**cientific **C**ommittee on the **E**ffects of **A**tomic **R**adiation) established that the world mean dose from natural radiation sources of normal area is estimated to be 2.4 $mSvy^{-1}$ while for all artificial sources including exposure, is about 0.8 $mSvy^{-1}$ (UNSCEAR, 1993).

Studies on the natural radioactivity on beach sands have shown that heavy minerals such as monazite and zircon are among the constituents of minerals available in various beaches around the world. For instance, the studies by the NGD (**N**uclear **G**eophysics **D**ivision) of the University of Groningen to determine whether heavy minerals are found

along the Dutch coast (De Meijer et al., 1990) revealed that in the presence of heavy minerals the exposure rates are higher. The research study included other locations as well e.g. beaches of the island of Texel, Ameland and Baltic coast. In those studies, differences in the radioactivity level were again observed (Greenfield et al., 1989), which showed that the heavy mineral composition of the sands had differences (De Meijer et al., 1990). In all these studies the locations were mapped by collecting samples and measuring them individually on a high purity germanium detector in a laboratory set-up. To map large areas more efficiently the MEDUSA (**M**ulti **E**lement **D**etector system for **U**nderwater **S**ediment **A**ctivity detection) detector was used (De Meijer and Donoghue, 1995).

In various parts of the world where the study of background radiation and NORM were carried out, the results show the variation in the radionuclides distribution as well as the dose received by general public and NORM workers. However, no work has been carried out so far in Zanzibar to investigate the natural radiation background which in turn allows the assessment of the potential hazards associated with natural background radiation. Thus, it is necessary to understand the distributions and levels of radioactive nuclides present in beach and soil since they provide useful information on the monitoring of environmental contamination by radioactive materials in the natural environment. This research study explores the distribution of natural radionuclides by estimating their activity concentrations. Radiological hazards parameters such as the absorbed dose rate, the radium equivalent activity, radiation hazard indices and the annual effective dose of soil and beach sands from the Zanzibar coastline were also investigated. Furthermore, very few geological studies have been carried out in Zanzibar. This study initially measured the radioactivity in the soil and various beaches in-situ. This provided a very useful indication of from which part of the islands samples should to be taken for laboratory analysis.

In this regard, gamma spectrometric techniques which are key analytical tools for the characterization and determination of the isotopic signatures of several environmental samples were utilised together with complimentary chemical analytical tools. The

influence of heavy minerals composition to beach sand natural radioactivity in a selected beach has been carried out in this study.

1.2 Aims of the study

This study aims to examine the distribution of ^{238}U, ^{232}Th and ^{40}K concentration in Zanzibar's coastal and some inland sediments. The exposure associated with natural radioactivity emitted from soil and beach sand will also be investigated. (In this thesis "soil" will usually refer to samples collected inland and "sand" for the samples from the beaches)

The specific objectives of this study are:

- To evaluate the level of natural radionuclides (^{40}K, ^{238}U and ^{232}Th) in soils and beach sands from Zanzibar coastline
- To evaluate the use of the in-situ natural nuclide measurements to guide sampling
- To study spatial distribution of ^{40}K, ^{238}U and ^{232}Th in soils and beaches, thereafter construct radiation maps of the area
- To assess external exposure levels and radiological risks associated with the use of the Zanzibar coasts for various activities for instance tourism and seaweed farming
- To assess the link between major and trace elements composition on level of the natural radiation in beach sand using multivariate data analysis techniques
- To investigate the distribution of heavy mineral sands

1.3 Justification of the study

Various developed countries (e.g Australia, Canada, Switzerland, Slovenia, UK and USA) have performed studies to monitor the distribution of natural radionuclides and have generated their country wide baseline data of natural radioactivity levels on a reasonably small grid size (Darko, 2004). They have also generated radiometric maps of their territories. Some developing countries are also working hard to ensure that the

information regarding natural radioactivity are available. Such projects have been completed through collaborative efforts of research students, scientific institutes and universities. These developments have been possible using gamma (γ) and alpha (α) spectroscopic techniques.

The gamma (γ) radiometry technique is a well developed and consolidated method for radioactive investigation (Chiozzi, 2002; Tyler, 2008). It has a wide range of applications such as mineral exploration (IAEA, 2003), geological mapping (IAEA, 1976a) and study of provenance and transport processes of sediments along the coast (De Meijer, 2001; Anjos et al., 2005, 2011). The method is used to monitor environmental radiation by assessing levels of NORM in soil (Mlwilo, 2010; Santawamaitre et al., 2011; Darko et al., 2015), beach sand (Freitas and Alencar, 2004; Lu, X. and Zhang, X. 2006; Veiga et al., 2006; Malain et al., 2010), building materials (Ahmad et al., 1998; Matiullah et al., 1998) food (Adeniji et al., 2013; Chen et al., 2016) and mine dumps (Lindsay et al., 2004; Ongori et al., 2013).

Despite the interest of the scientific world to study the distribution of natural radiation, its radiological impact on human beings and its application for decades, no published information is available regarding the distribution of natural radiation in Zanzibar. Hence background radiation levels in Zanzibar are not known. This information is required by: (1) the manufacturing and construction industries to determine the radiation they generate, (2) the environmentalists for environmental monitoring and (3) radiation protection experts.

Human activities such as the use of fertilizers, mining, oil and gas explorations may result in changes in the coastal zones as well as the levels of NORM. Recently 2016, the Zanzibar House of Representative has passed a bill to establish ZPUDA (**Z**anzibar **P**etroleum **U**pstream **D**evelopment **A**uthority) which will pave a way for oil and gas exploration in the Zanzibar archipelago. Hence the findings of this study could be used as a baseline in future long term monitoring studies of NORM. The baseline measurement of the activity concentration level in the natural environment will also offer

the opportunity to document present conditions in order to scientifically assess possible future changes due to other external factors.

The coastline of Zanzibar is used for maritime commerce, fishing and seaweed farming. Its beaches are highly popular touristic destinations and are among the famous summer destinations in the Eastern Africa region. The frequently visited beaches include Nungwi (North of Unguja Island), Mchanga Mle, Michamvi and Kizimkazi (South of Unguja Island), Kiwengwa, Matemwe, Pwani Mchangani and Pongwe (East Coast of Unguja Island) and Shangani and Forodhani (in the Stone Town, West of Unguja). In Pemba, Vumawimbi which is situated in the northern part of the island is the only famous tourist site until now. Beach sands are used as building materials in some parts of Zanzibar while soil is used in construction of traditional mud dwellings (Figure 1.2). Hence, it is essential to investigate the potential radiological hazard associated with ionising radiation from the soil and beach sand for people using the Zanzibar coast, its sand and soil for various activities. This will help in creating public awareness on the possible consequences of over exposure to ionising radiation. The information on the radioactive dose received by the people using the Zanzibar coastline will help regulatory bodies in formulation of policies regulating public health and environment. Apart from the above mentioned importance of this project, in case relatively high levels of radiation were found, the possible origin of such an anomaly will be investigated further.

Figure 1.2: Traditional houses built with beach sand (left) and soil (right).

1.4 A review of NORM studies

There is an enormous literature concerning the levels of natural radiation from beach sand, marine environment and soil samples worldwide. However, the number of studies carried out in Tanzania and neghbouring countries (East African region) remains somewhat limited by comparison, and currently no study has been reported on the radioactivity levels of Zanzibar. Most of these studies show that most soils contain nuclides of the ^{238}U and ^{232}Th series and ^{40}K, with a range of concentrations which varies broadly.

1.4.1 Worldwide NORM studies

Chowdhury et al. (1999) conducted a study to determine the activity concentrations of naturally occurring radioactive materials in river sediments and coastal soils in Chittagong, Bangladesh with an aim of evaluating the environmental radioactivity and the radiation hazard. The mean activity of ^{226}Ra, ^{232}Th and ^{40}K observed in Chowdhury's work was approximately 1.6, 3 and 2 times higher than the world average which are 35 $Bq.kg^{-1}$, 30 $Bq.kg^{-1}$ and 400 $Bq.kg^{-1}$ respectively (UNSCEAR, 2000). The previous background radiation survey by the Bangladesh Atomic Energy Commission showed that the external background radiation level of this region is approximately two times higher than the world average value reported by UNSCEAR 1988 Report.

Firyal Bou-Rabee from the University of Kuwait conducted a study in the Arabian Gulf on the levels of activity concentration of ^{238}U, ^{232}Th, ^{40}K, and ^{137}Cs. The soil samples were collected from 83 different locations across Kuwait at a depth of 5 cm to 100 cm. The average activity concentrations were found to be 13 $Bq.kg^{-1}$, 10 $Bq.kg^{-1}$, 370 $Bq.kg^{-1}$, and 3 $Bq.kg^{-1}$ respectively (Bou-Rabee, F., 1997).

In Southern Italy, Bellia et al. (1997) performed gamma ray measurements for ^{238}U, ^{232}Th and ^{40}K on rocks and soils of the island of Ustica. The concentrations obtained ranged

from 15 to 164 $Bq.kg^{-1}$, 16 to 174 $Bq.kg^{-1}$ and 201 to 1350 $Bq.kg^{-1}$, respectively. The gamma activity levels were compared to the mineralogical and chemical data obtained by XRD and XRF analyses. The observed levels of the primordial radionuclides corresponded to the magmatological features of the rocks.

The barren and cultivated soils of Bio-saline Research Station in Pakka Anna, Pakistan were collected by Akhtar et al (2005) for determination of radioactivity levels. In the barren soils radioactivity levels due to ^{238}U, ^{232}Th and ^{40}K were found to be in the range of 26 to 32 $Bq.kg^{-1}$, 51 to 55 $Bq.kg^{-1}$, and 500 to 610 $Bq.kg^{-1}$, respectively. Similar results were found in fertilised soils; 30 to 39 $Bq.kg^{-1}$, 51 to 64 $Bq.kg^{-1}$, and 560 to 636 $Bq.kg^{-1}$, respectively. The results from the two soils segments were found to be within the world median ranges of 17 to 60 $Bq.kg^{-1}$, 11 to 64 $Bq.kg^{-1}$ and 140 to 850 $Bq.kg^{-1}$ respectively (UNSCEAR, 2008).

In 2001, Goddard et al., (2001) measured the levels of activity concentration in soil from 112 locations of the Sultanate of Oman. The soil samples were collected from areas with greater population and geological interest. Goddard found that the capital area, Muscat, had the highest background dose rate and explained that higher levels of dose are due to the presence of shale and quartzite rocks in the geology formation of the area, both of which are rich in ^{226}Ra and ^{232}Th.

Akram et al., (2006) determined the concentration of natural radionuclides in the bottom sediments of Karachi Harbour/Manora channel area. Samples from Layari River were also analyzed to account for background contribution from terrestrial sources. The activity in sea sediment samples from these areas was found to be lower than the world average for ^{226}Ra, ^{232}Th and ^{40}K. The mean values of radium equivalent activity, absorbed dose rate and annual effective dose were 89 $Bq.kg^{-1}$, 44 $nGyh^{-1}$ and 0.06 $mSvy^{-1}$ respectively. The value of effective dose was much less than the level of 1 $mSvy^{-1}$, recommended by ICRP (**I**nternational **C**ommission on **R**adiological **P**rotection).

Veiga et al. (2006) determined the distribution of natural activities produced by ^{40}K, ^{226}Ra and ^{232}Th, for sand samples collected along the coast of four Brazilian States. For some specific beaches, the values of the gamma ray radiation hazard indices exceeded both the mean worldwide exposure (2.4 $mSvy^{-1}$) due to natural sources and the limits proposed by OECD (**O**rganization for **E**conomic **C**ooperation and **D**evelopment for building materials). The mean values of the radium equivalent activities were evaluated and found to be 696 $Bq.kg^{-1}$ in Mambucaba, 1621 $Bq.kg^{-1}$ in Buena, 2289 $Bq.kg^{-1}$ in Anchieta, 10 205 $Bq.kg^{-1}$ in Meaipe, 83 425 $Bq.kg^{-1}$ in Guarapari, 531 $Bq.kg^{-1}$ in Vitória, 2026 $Bq.kg^{-1}$ in Serra, 3240 $Bq.kg^{-1}$ in São Mateus, 3075 $Bq.kg^{-1}$ in Porto Seguro and 1841 $Bq.kg^{-1}$ in Itacaré. These values are above the limit (370 $Bq.kg^{-1}$) recommended for the safe use of building materials for dwelling by OECD.

Radenković et al. (2009) determined the activity concentrations for the radionuclides ^{226}Ra, ^{232}Th, and ^{40}K in the sand samples from Manhattan Beach (USA), Patara Beach (Turkey), Copacabana Beach (Brazil) and Great Beach of Ulcinj (Montenegro). Results of the sand samples randomly taken from both sea and river beach areas of the tourist zone, showed low activity concentration of naturally occurring ^{40}K, as well as natural radioactive series originating from ^{226}Ra and ^{232}Th.

Santawamaitre (2011) investigated the levels of naturally occurring radioactivity in surface soils along the Chao Phraya River, Thailand. Activity concentrations of ^{226}Ra, ^{232}Th, and ^{40}K were found to be 55 to 65 $Bq.kg^{-1}$, 61 to 69 $Bq.kg^{-1}$ and 393 to 478 $Bq.kg^{-1}$, respectively. From the study, Santawamaitre concluded that the radiation hazard from primordial radionuclides in all soil samples from the area studied in his study is not significant.

Ashnani et al. (2010) measured the average activity concentration of ^{226}Ra, ^{40}K and ^{232}Th in water, soil and sediment samples from the Aras River, south west of the Caspian Sea. In water, soil and sediment samples the mean activity concentrations of ^{40}K and ^{226}Ra were 264 $Bq.kg^{-1}$ and 4 $Bq.kg^{-1}$ respectively and in soil and sediment samples the mean concentrations of activity of ^{232}Th was 20 $Bq.kg^{-1}$. From the results obtained, in one third

of the samples, the activity of ^{40}K is very high and other natural activities are in the range of the background radiation.

Ramasamy et al. (2011) studied the contents and mineral characteristics of the natural radionuclides ^{238}U, ^{232}Th and ^{40}K of Ponnaiyar river sediment samples using gamma ray spectroscopy and FTIR (Fourier Transform Infra Red) technique respectively. The findings of their study showed kaolinite is the major mineral to increase the level of radioactivity in the river sediments.

Hamidalddin, (2013) measured the concentrations of $^{238,235}U$, ^{232}Th series, and ^{40}K in the sediments along the Red Sea Coast (South Beach of Jeddah Saudi Arabia) by HPGe gamma spectrometer. They showed that activity concentration values and calculated parameters are within the international limits. They finally concluded that the results can be considered as base values for distribution of natural radionuclides.

Mohery et al., (2014) investigated the natural radiation levels in soil and sediments collected from Jeddah, Saudi Arabia. The activity concentration for ^{238}U, ^{232}Th and ^{40}K were found to be 9 to 17 $Bq.kg^{-1}$, 3 to 8 $Bq.kg^{-1}$and 349 to 486 $Bq.kg^{-1}$, respectively. In all analysed samples, the natural radiation levels are within the acceptable levels.

In some areas around the world, the levels of NORM is very high. Sohrabi (1998), conducted a review study on areas with elevated levels of NORM. This study concluded that elevations of NORM in different regions are attributed to geological structure and geochemical movements of the radioactive materials in the soil. Among the areas mentioned in Sohrabi's work are Morro de Ferro and Meaipe in Brazil (Carvalho et al., 2007), Kerala coast in India (Jibiri et al., 2007) and Yangjiang in China (Tao et al., 2012).

According to Sohrabi, the elevated levels in those areas are due to the presence of monazite sand, phosphate deposits, uniferous granite rocks, alum shale and water rich in ^{226}Ra (Sohrabi, 1997). Other causes of elevated levels of natural radioactivity include use of phosphate fertlizers (Khater and Al-Sewaidan, 2008). Areas such as Joachimstal in

Czech Republic and Schlema, Schneeberg, and Saxony in Germany are well known for higher levels of indoor exposure. The main reason for indoor exposure is due to the use of construction materials rich in ^{226}Ra content such as tailings from uranium mining (Wikimedia Commons, 2009). Kerala and Tamil Nadu in India, Saxony in Germany, Guarapari in in Brazil and Ramsar City in Iran have been classified as areas with very high level of natural radiation with an average dose rate exceeding 10 $mGyy^{-1}$ (UNSCEAR, 1993).

1.4.2 NORM studies in Tanzania and other African countries

In Tanzania, few studies have been conducted to establish baseline data for radiological surveillance. These studies have been conducted in the areas with uranium deposits or in the selected villages in the neighbourhood of the deposit, in phosphate rocks, soil and water samples and staple foods used in Tanzania.

For instance, Lolila (2011) performed dose rate measurement at Mkuju River in Ruvuma, which is close to a proposed uranium mine. An average dose rate in air from external irradiation from Lolila's study was found to be 100 $nGyh^{-1}$ and annual effective dose of about 0.12 mSv at Mkuju River in Ruvuma. The dose rate in air at the proposed Mkuju uranium pit was found to range from 647 - 23360 $nGyh^{-1}$ which corresponds to annual effective dose of 9.6 mSv and 26.4 mSv respectively.

Banzi et al., (2000) measured natural radioactivity at Minjingu phosphate rocks in Tanzania and found that there was high concentrations of ^{226}Ra in phosphate rock, waste rock, wild leaf vegetation and edible leaf vegetation. Banzi et al. (2000) suggested that there is a radiation health risk at Minjingu particularly when the samples are ingested.

The activity concentration of ^{238}U, ^{232}Th and ^{40}K in maize which is one of the staple foods in various regions in Tanzania were determined using HPGe detector (Mlwilo et al., 2007). The mean activity concentrations in maize from five studied regions ranged from 2 to 24 $Bq.kg^{-1}$ for ^{238}U, 2 to 38.9 $Bq.kg^{-1}$ for ^{232}Th and 42 to 435 $Bq.kg^{-1}$ for ^{40}K.

Total annual committed effective dose due to total ^{238}U and ^{232}Th intakes as a result of consumption of maize in five regions were as follows; Manyara (1.46 $mSvy^{-1}$), Mbeya (0.31 $mSvy^{-1}$), Dodoma (0.21 $mSvy^{-1}$), Ruvuma (0.19 $mSvy^{-1}$) and Dar es Salaam (0.08 $mSvy^{-1}$). The dose value from Manyara was almost the same to the annual dose guideline for the general public which is 1 $mSvy^{-1}$, whereas for other regions the doses are low. Mlwilo et al. (2007) concluded that the relatively high mean concentrations of the radionuclides in maize compared to rice may be attributed to the extensive use of phosphate fertilizers in maize production in Tanzania.

Mohamed and Mazunga (2013) determined the radioactivity levels of 30 soil samples and 20 water samples from Likuyu village (South of Tanzania) which is 54 km east of the uranium deposit. The mean radioactivity concentrations of the natural radionuclides ^{238}U, ^{232}Th, and ^{40}K obtained in the soil samples using an HPGe detector were higher than the worldwide mean concentrations value of these radionuclides reported by UNSCEAR (2000). However, the mean activity concentration value of ^{238}U (2.35 Bql^{-1}) and ^{232}Th (1.85 Bql^{-1}) in water samples was similar and comparable to their mean concentrations in the control sample collected from Nduluma River in Arusha.

In Kenya, Kinyua et al. (2011) studied the levels of radionuclides in quarries in the Kisii district and reported a range of 39 to 272 $Bq.kg^{-1}$ for ^{232}Th, 43 to 360 $Bq.kg^{-1}$ for ^{226}Ra, and 245 to 1780 $Bq.kg^{-1}$ for ^{40}K. The average absorbed dose rate 1m above the ground level for the five quarries was found to be 541 $nGyh^{-1}$, while the calculated total absorbed dose rates were found to average 178 $nGyh^{-1}$ below the surface. This is about 4 times higher than the world mean of 43 $nGyh^{-1}$. Assuming a 40% occupancy factor, the corresponding annual effective dose rates due to the radionuclides in the quarries ranged from 0.22 to 0.86 $mSvy^{-1}$, with a mean of 0.44 $mSvy^{-1}$. The internal and external hazard indices were 1.03 and 1.27, respectively, hence slightly exceeding the permissible limits of 1 by ICRP (1990).

Langat et al. (2014) carried out gamma ray spectroscopic analysis of sediment deposits at the shores of Lake Nakuru. The results obtained showed average activity concentrations

of 37, 44 and 708 Bq.kg^{-1} for ^{238}U, ^{232}Th and ^{40}K, respectively. Langat et al. 2014 concluded that the radiation hazard from terrestrial naturally occurring radionuclides in the study area is insignificant. Other studies of natural background radioactivity concentration in the environment and in the building materials in Kenya include those done by Patel el al. (1991), Mustapha et al. (1997), Hashim et al. (2004), Chege (2014) and Kaniu et al. (2018).

Mbatha (2007) carried out radiometric measurements of ^{40}K, ^{238}U and ^{232}Th to study the textural characteristics, heavy mineral composition, provenance, sediment transport and depositional environment of the Melkbosstrand and the Ouskip beach placer deposits, West Coast of South Africa. The measured activity concentrations of ^{232}Th and ^{238}U from Melkbosstrand beach showed higher levels compared to the Ouskip beach. The higher level of ^{40}K concentrations observed in the Ouskip group shows more enrichment of lighter minerals such as potash feldspars and quartz sands. Based on the ^{40}K concentrations in the two beach zones, Mbatha (2007) concluded that the sand particles were derived from the Cape Super group and the Table Mountain Group, occurring in close proximity to the West Coast.

Gamma radiation measurements of sediment samples along the Upper Egypt Nile River region starting from Aswan in the south to the north of El-Minia Governorate were conducted by El-Gamal (2007) using a high resolution HPGe detector. The gamma measurements of the alluvial sediments revealed the presence of the natural long-lived radionuclides ^{238}U, ^{232}Th and ^{40}K with concentrations that varied widely. The ranges of their activity concentrations were 4 to 5 Bq.kg^{-1}, 3 to 30 Bq.kg^{-1} and 112 to 313 Bq.kg^{-1}, respectively. El-Gamal (2007) concluded that the variation is contributed to the pertinent environmental situation such as the presence of dams, barrages and sediments type.

Measurement on the natural radioactivity levels in surface soils of Kitchener in the Nile delta of Egypt was done by Yousef et al. (2007). It was noted that the activity concentration of ^{40}K was in the range of 17 to 99 Bq.kg^{-1} while the concentration of ^{232}Th

series ranged from 1 to 32 Bq.kg^{-1} and for ^{238}U series ranged from 2 to 51 Bq.kg^{-1}. The absorbed dose ranged from 2 to 47 nGyh^{-1}. The variation in concentration of radionuclides was due to the rate of precipitation by currents in the western and eastern parts of the delta and presence of potassium salts.

Agbalagba and Onoja (2011) carried out the analysis of naturally occurring radionuclides in soil samples collected from oil and gas field environment of Delta state, Nigeria. The mean activity concentration of the ^{226}Ra, ^{232}Th and ^{40}K in the samples were 41 Bq.kg^{-1}, 30 Bq.kg^{-1} and 413 Bq.kg^{-1}, respectively. The values obtained are in good agreement with the world range and values reported elsewhere in other countries. The study also examined some radiation hazard indices and was well below the permissible limit.

The activity concentrations of ^{238}U, ^{232}Th and ^{40}K in soil and rock samples collected from Ekiti and Ondo States in the South western Nigeria were performed by using a HPGe detector. The mean activity concentrations of ^{40}K, ^{238}U and ^{232}Th in the soil were 152, 8 and 17 Bq.kg^{-1}, respectively while those of the rock were 554, 26 and 61 Bq.kg^{-1} respectively. Results showed that the activity concentrations of ^{40}K, ^{238}U and ^{232}Th were higher in the rocks than the soils of the areas studied. In the same study, the radiological assessments due to exposure of natural radionuclides on the population in the region were conducted. The mean values obtained for annual effective dose equivalent (AEDE) and annual gonadal equivalent dose (AGED) for the soil were below ICRP recommended limits of 1 mSvy^{-1} and 300 mSvy^{-1}, respectively. AGED for the rocks was higher than the maximum permissible limit (Majolagbe et al., 2014)

Agalga (2013) evaluated the activity concentrations of natural radionuclides ^{238}U, ^{232}Th and ^{40}K in the sediments of the Tono irrigation dam using gamma spectrometry. The study was carried as part of efforts by the Ghana Atomic Energy Commission to acquire data needed to set NORM standards for the country. From the study, the concentrations of natural radionuclides ^{238}U, ^{232}Th and ^{40}K ranged from 5 to 9 Bq.kg^{-1} with a mean of 7 Bq.kg^{-1} for ^{238}U, 6 to 8 Bq.kg^{-1} with a mean of 7 Bq.kg^{-1} for ^{232}Th and 219 to 453 Bq.kg^{-1} with a mean of 380 Bq.kg^{-1} for ^{40}K. The assessment of radiological hazard arising due to the use of dam sediments as a building material for the public was

evaluated. The results were observed to be lower than limits internationally reported and recommended for building materials.

CHAPTER 2

Theory

2.1 Introduction

This chapter presents the background theory of radioactivity. It starts by introducing the origin of natural radioactivity in the environment followed by how a nucleus transform to another nucleus. Special cases of equilibrium associated with radionuclides are introduced in this section together with modes of radioactive decays. The chapter ends by explaining gamma interaction with matter and how gamma rays are detected.

2.2 Origin of Environmental (Natural) Radioactivity

Natural radioactivity originates from both terrestrial and cosmogenic sources within the earth's crust and its surrounding. Natural radionuclides are widespread in all geological formations like soil, sand, rock, air and water (Baeza et al., 1992; UNSCEAR, 2008; Malain et al., 2010; Tzortzis et al., 2004; Ramasamy et al., 2013, Papadopoulos et al., 2015; Kaniu et al., 2018). Apart from natural sources of radioactivity, anthropogenic nuclides have been released in the environment through human activities.

A) Terrestrial (Primordial radionuclides) – these radionuclides have long half-lives comparable to the age of the earth and therefore are only partially decayed to the present day. The principal sources of environmental radioactivity monitored are the ^{238}U, ^{232}Th series and ^{40}K in the earth's crust.

B) Cosmogenic radionuclides – these radionuclides are continuously formed due to the interaction of stable nuclides (mainly oxygen and nitrogen) by cosmic rays in the earth's atmosphere (Eisenbud and Gesell, 1997). Cosmogenic radionuclides include tritium (^{3}H), carbon (^{14}C), and beryllium ($^{7}Be/^{10}Be$). These radionuclides

are pure beta emitters with the exception of ^{7}Be which emits a characteristic gamma-ray of 477.6 keV.

C) Anthropogenic (artificial radionuclides) – these radionuclides are found in the environment due to: (i) nuclear weapons testing (e.g. Alamogordo, New Mexico, 1945); (ii) nuclear power plants (for production of electricity or releases due to nuclear weapon production programs or nuclear fuel reprocessing installations); (iii) nuclear bombing (e.g. Nagasaki and Hiroshima) (iv) commercial fuel reprocessing; (v) nuclear accidents (e.g. Chernobyl accident in 1986, Fukushima Daichi, 2011); (vi) nuclear medicine. Some of the common list of anthropogenic radionuclides include ^{90}Sr, ^{99}Tc, ^{129}I, ^{131}I, ^{137}Cs, ^{237}Np, ^{239}Pu and ^{241}Am.

2.3 Radioactive decay

Radioactive isotopes (also called radionuclides) undergo a process called radioactive decay, a spontaneous transformation of an unstable atomic nucleus (of a parent radionuclide, P) into another nucleus (daughter nuclide, D), accompanied by loss of energy and emission of one or more particles.

In the simple case of radioactive decay, a parent radioisotope (P, unstable) can transform from unstable to stable daughter (D, stable) using alpha (α), beta (β) or gamma (γ) decay modes. In α decay, an α particle (a Helium nucleus, $^{4}_{2}$He) is emitted. In this transformation, the mother nucleus loses two protons and two neutrons. α decay usually occurs in heavy nuclei with Z > 82 (Gilmore, 2008). In β decay, the atomic number (Z) and the neutron number (N) of a nucleus each change by one unit, but the total mass number, A = N+Z, remains constant (Krane, 1988). There are three sub-species of beta decay, and all involve an electron or positron to achieve the conversion. These are β^- decay, β^+ decay and electron capture.

Gamma decay typically occurs after α or β decay in unstable nuclei. For each nuclide, the rate and energy of **γ** emitted during decay is unique, which is the basis for their identification and quantification by means of **γ** spectroscopy. The change of energy level

from an excited to a ground state can proceed via single γ emission or multiple emissions. These emissions are characterized by certain half-life, which is usually very short in comparison to the half-lives of the parent nuclei. An example of γ-ray decay of ^{208}Tl to ^{208}Pb is depicted in Figure 2.1.

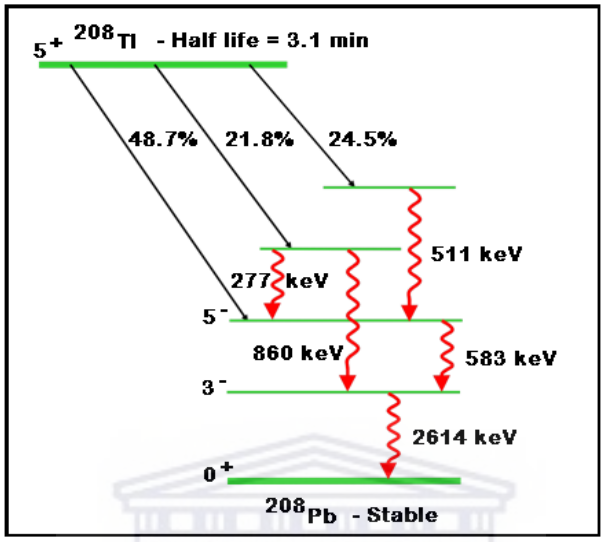

Figure 2.1: Decay scheme of ^{208}Tl to ^{208}Pb, data from: NNDC (2011).

Given a sample of particular radioactive isotope with a decay constant λ, the number of decay events, dN expected to occur in time interval, dt, is proportional to the number of atoms present.

$$\frac{-dN}{dt} = \lambda N \qquad (2.1)$$

Rearranging and integrating with respect to N and t, and with initial conditions that the number of atoms at t = 0 equals N_o, equation 2.1 becomes:

$$N = N_o e^{-\lambda t} \qquad (2.2)$$

Where N is the number of parent atoms remaining at time t and $N_o$is the initial number of atoms at t = 0.

The number of daughters produced, D, is simply: $D = N_o - N$

thus,

$$D = N_o\left(1 - e^{-\lambda t}\right) \qquad (2.3)$$

Equation 2.2 shows that the number of atoms of a given radioactive substance decreases exponentially with time, provided no new atoms are introduced. At the end of certain time interval t, the material will have decayed to half its original value. This can be determined by setting $N = N_o/2$ and $t_{1/2} = t$ in equation 2.2 yielding:

$$t_{1/2} = \frac{\ln 2}{\lambda} \tag{2.4}$$

In practice, it is more useful to consider the activity of a nuclide in a decay chain, rather than the actual number of atoms. The activity, *A*, is the number of atoms of disintegrations per second and is measured in Becquerel (Bq). The historic unit of activity has been the Curie (Ci), 1Ci = 3.7 x 10^{10} Bq, defined as exactly 3.7 x 10^{10} disintegrations/second, which owes its definition as the best available estimate of the activity of 1 gram of pure ^{226}Ra.

$$A(t) = A_o e^{-\lambda t} \tag{2.5}$$

sometimes also expressed as:

$$A(t) = A_o\, 2^{-t/t_{1/2}} \tag{2.6}$$

The use of activities simplifies comparisons between isotopes within the decay chains, as the activities of all the isotopes in a decay chain should all be the same if they are in secular equilibrium (see section 2.6.1). Radioactive decay is the process that enables radioactive dating methods. By determining the decrease of the initial activity, the time elapsed can be derived. The portion of the activity left after n half-lives can be expressed as:

$$A\left(n.t_{1/2}\right) = A_o\,.\,2^{-n} \tag{2.7}$$

Radionuclides decay using one or many of these modes; a) α decay, β - decay and γ-decay. Each mode of decay for every nucleus has a characteristic decay half-life. These half-lives depend on the amount of excess energy, the mode of disintegration and the underlying structure of the nucleus.

2.4 Radioactive decay chains

Nearly all the naturally occurring radioactive elements do not decay directly to a stable state, but rather undergo a sequence of several decays until a stable state is reached. They form radioactive chains (also called radioactive series). These elements have been grouped into three related series: the ^{238}U series, the ^{232}Th series and the ^{235}U series. Each decay series starts with a long-lived isotope, which decays until a stable isotope of lead is achieved.

For instance, the ^{238}U series (Figure 2.2) originates with the uranium isotope with a half life of 4.51 billion years, and goes through a series of transformations that involves the emission of alpha, beta particles and possible emissions of 458 γ-rays before it ends up with ^{206}Pb (De Groot, 2009).

The ^{232}Th series (Figure 2.3) starts with a long-lived isotope of thorium with a half life of 14.1 billion years and goes through a series of alpha and beta-particle decays with 346 possible γ-ray emissions similar in many respects to those of ^{238}U series and terminates with the isotope of ^{208}Pb (De Groot, 2009). Members of the ^{238}U series and the ^{232}Th series are important for assessment of natural radionuclides in both soil and beach sand compartments which are the interest of this study. The details of their distribution in the study area will be discussed in chapter 4.

The ^{235}U series was at one time believed to be an independent series, but its origin has been traced to the rarer isotope of uranium of mass number A = 235. The end product of the ^{235}U series is an odd-numbered isotope ^{207}Pb.

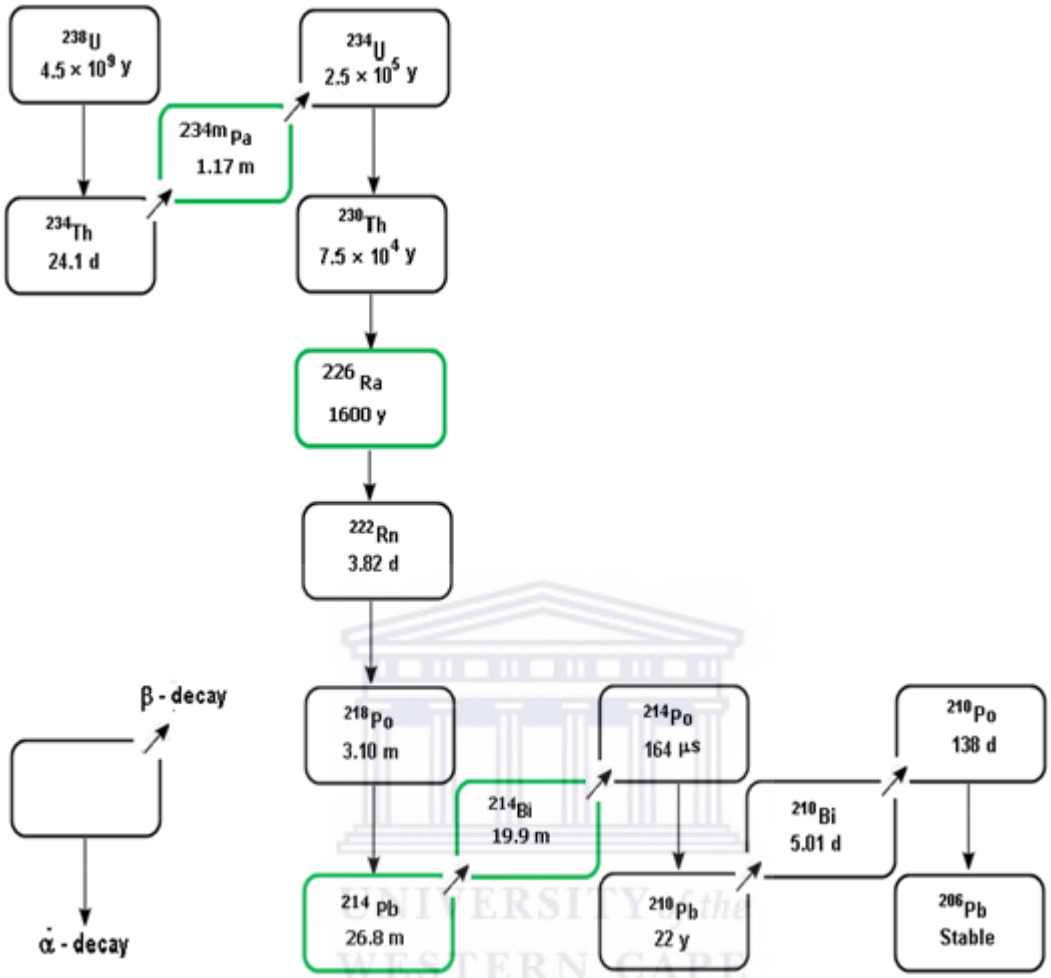

Figure 2.2: A schematic illustration of the ^{238}U decay series. Half-life times are given in years (y), minutes (m), days (d), hours (h) or seconds (s); the most relevant γ-ray emitters are indicated with a green box (data from Browne and Firestone, 1986).

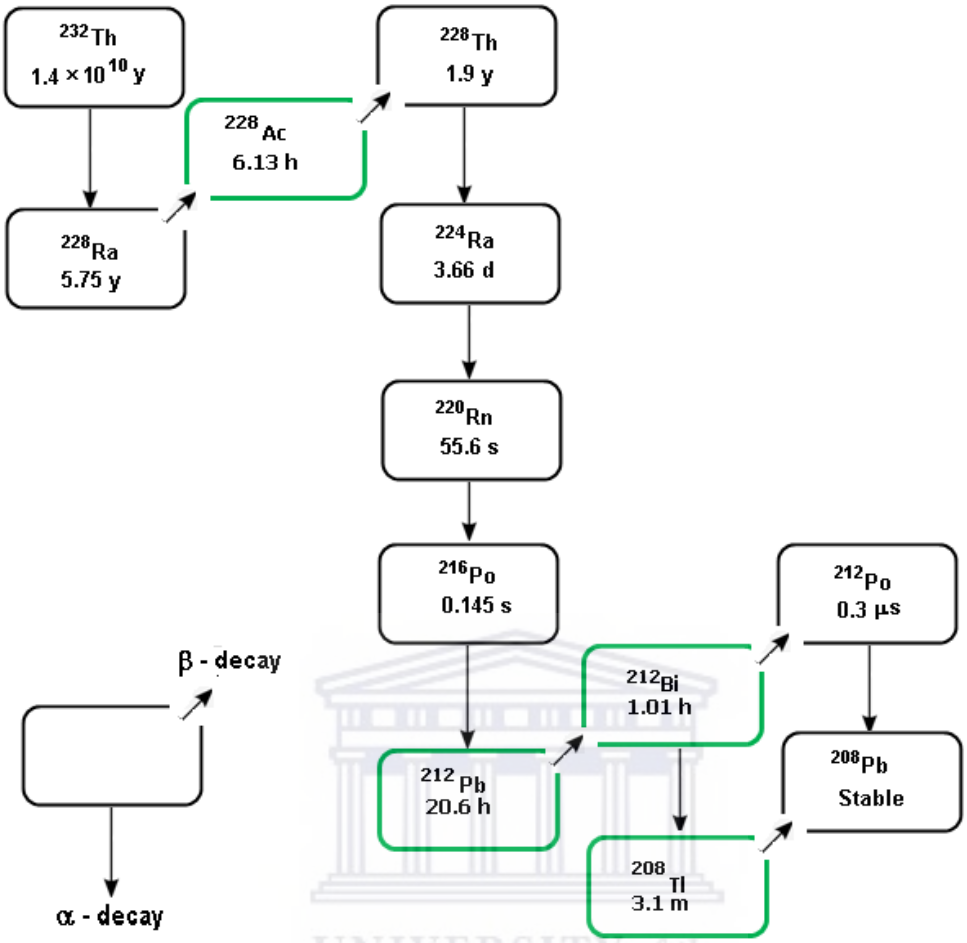

Figure 2.3: A schematic illustration of the ^{232}Th decay series. The half-life of each radionuclide in the series is given in years (y), days, hours (h), minutes (m) or seconds (s); the most relevant γ-ray emitters are indicated with a green box (data from Browne and Firestone, 1986).

In addition to ^{238}U and ^{232}Th series radionuclides, a non-series natural radionuclide ^{40}K, with a half-life of 1.27 x 10^{9} years, is wide spread in all types of rock, healthy animals and human being with varying concentrations. In a human body of 70 kg mass, nearly 4,400 nuclei of ^{40}K decay per second (Knoll, 2010). Out of 24 known isotopes of potassium, three of them occur naturally: ^{39}K (93.3%), ^{40}K (0.0117%) which is the radioactive isotope of terrestrial importance and ^{41}K (6.7%) (Theodorson, 1996).

Although natural potassium contains only 0.0117% ^{40}K in nature, but with an elemental

abundance more than 10^4 times that of uranium and thorium by weight in soil and rock, ^{40}K contributes to the dose received by NORM at a level comparable to that from the ^{238}U and ^{232}Th decay chains.

Naturally occurring ^{40}K decays to stable ^{40}Ca (88.8%) by β^-emission and to stable ^{40}Ar (11.2%) by electron capture (EC) and by positron emission. Following the electron capture decay, a γ-ray at energy of 1.461 MeV is emitted as shown in Figure 2.4.

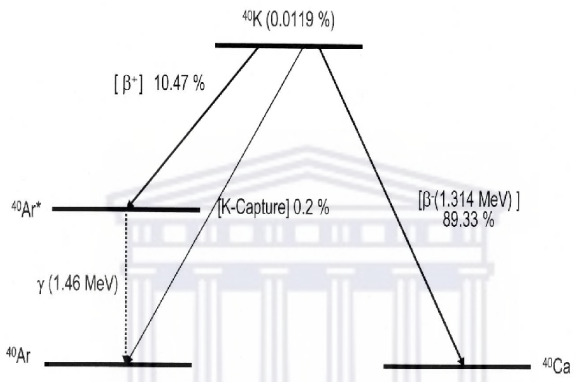

Figure 2.4: The decay scheme of ^{40}K to the excited state of ^{40}Ar by electron capture, releasing its characteristic 1460.8 keV γ-ray (Pradler, et. al., 2013).

The concentrations of ^{238}U, ^{232}Th and ^{40}K in typical rocks, soils and other media varies widely. Table 2.1 shows the ranges of ^{238}U, ^{232}Th and ^{40}K from various countries as reported by NCRP (1987).

Table 2.1: The activity concentrations in Bq.kg^{-1} of ^{238}U, ^{232}Th and ^{40}K in soil samples and coastal sediments from various parts of the world.

Location	^{238}U (or ^{226}Ra)	^{232}Th (or ^{228}Ra)	^{40}K	Medium	Reference
Algeria	5-27	7-27	93-412	Sand	Noureddine et al., 1997
Egypt	3-101	2-117	16-1379	Coastal	El-Reefy et al., 2006
Nigeria	53	26	505	Soil	Ademola et al., 2014
China	18-787	2-225	281-891	Soil	Ziqiang et al., 1988
India	20-62	14-48	61-317	Coastal	Narayana et al., 2001
Syria	1-40	11-25	100-378	Soil	Othman and Yassine,1995
Albania	8-27	13-40	266-675	Coastal	Tsabaris et al., 2007
Spain	10-45	250-600	142-1489	Coastal	Rubio et al., 2003
Greece	7-310	3-190	30-1440	Coastal	Probonas and Kritidis, 1993
Italy	57-71	73-87	580-760	Soil	Bellia et al, 1997
Norway	43	21	283	Coastal	Dowdall et al, 2002
Brazil	10-137	12-191	56-1972	Coastal	Malanca et al, 1996
Ireland	10 - 200	3 - 60	40 - 800	Soil	McAulay and Moran (1998)
Jordan	22-104	21-103	138-601	Soil	Al Jundi et al., 2003
Canada	3-36	2-28	153-817	Sand	VandenBygaart and Protz,1999
Global average	**10-50**	**7-50**	**100-700**	Soil	**UNSCEAR, 2008**

2.5 Radioactive equilibrium

The relationships between two successive radionuclides, parent (P) and daughter (D) with half lives $t_{1/2}$ (P) and $t_{1/2}$ (D), respectively, are described depending on their relative half lives ratio. In the following cases it is always assumed that A (P) = 100% and A (D) = 0 at time t = 0.

2.5.1 Secular equilibrium

There are several successive nuclide pairs in the natural decay chains, where $t_{1/2}$ of the parent nuclide is much longer than the $t_{1/2}$ of its daughter, for example the decay of ^{226}Ra ($t_{1/2}$ = 1600 years) to ^{222}Rn ($t_{1/2}$ = 3.8 days) (see Figure 2.2). If we consider $\lambda_1 \ll \lambda_2$, the relationship between the number of decay events of parent nucleus and its daughter can be expressed as:

$$\frac{N_2}{N_1} = \frac{\lambda_2}{\lambda_1} \qquad \text{or} \qquad N_2\lambda_2 = N_1\lambda_1 \tag{2.8}$$

This is called secular equilibrium, and the activities of both successive nuclides in the chain are the same, i.e A (P) = A (D).

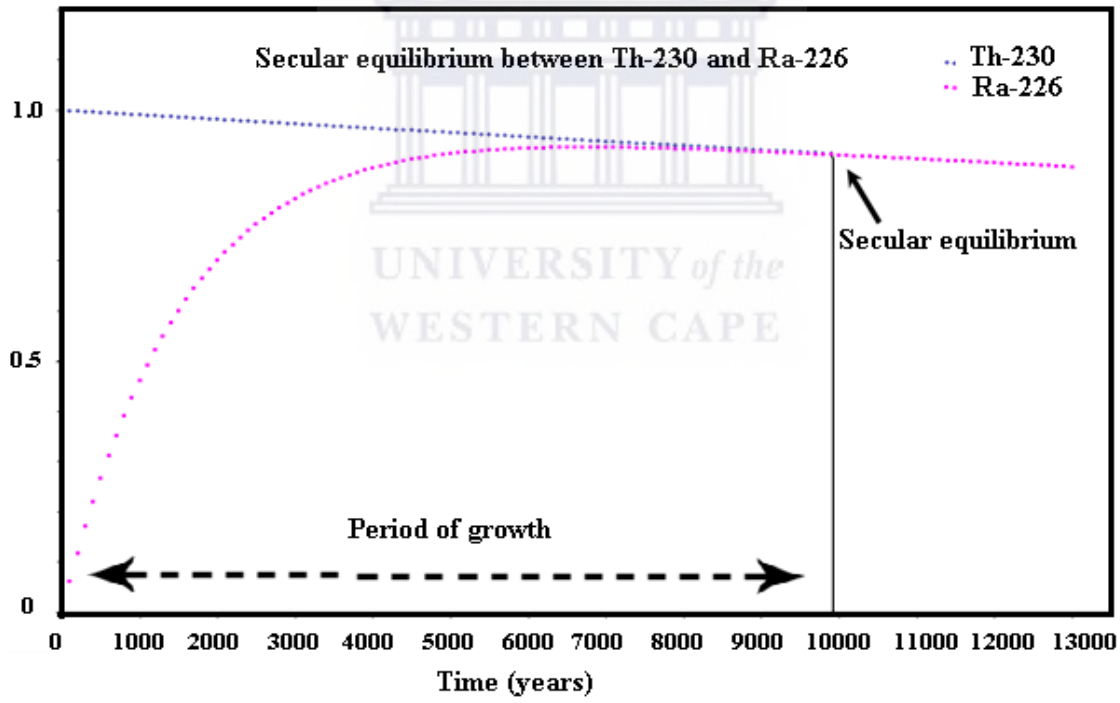

Figure 2.5: An illustration of secular equilibrium (Al Sulaiti, 2011)

Secular equilibrium is a very important phenomenon in the study of environmental radioactivity and this study in particular. Using the assumption that the secular equilibrium is attained between ^{238}U and ^{232}Th decay chains in soil and beach sand used

in this study, the activity concentration of the longer lived isotopes will be determined. This will be possible using the shorter half-lives of their daughters in the decay chains. For instance; after approximately 10000 years, the ^{230}Th/^{226}Ra ratio would be approximately equal to one (see Figure 2.5), which corresponds to approximately 6 times the half-life of the ^{226}Ra. However sometimes, fractionation can occur during geological processes which results in disequilibrium between parent and daughter nuclei.

2.5.2 Transient equilibrium and non-equilibrium

The case when the half-life of the parent is longer ($t_{1/2}$ (P)), but in the same order of magnitude as the daughter nuclide is called transient equilibrium. As an example from ^{238}U natural decay series a nuclide pair ^{238}U - ^{230}Th can be taken, with respective half-lives 2.46 x 10^5 and 7.54 x 10^4 years. After several daughter half-lives the transient equilibrium is established. The activity of the daughter nuclide is then higher than the parent activity due to its shorter $t_{1/2}$. The activity of the daughter isotope in equilibrium state follows the decay of the parent nuclide and can be expressed as:

$$A(D) = A(P)\frac{t_{1/2}(P)}{t_{1/2}(P) - t_{1/2}(D)} \quad (2.9)$$

where A(P) is activity of the parent nuclide, A(P) is activity of daughter nuclide, $t_{1/2}(P)$ is the half life of parent nuclide and $t_{1/2}(D)$ is the half life of daughter nuclide.

When the parent's half-life is shorter than that of its daughter, no equilibrium is established, the parent will decay leaving the orphan daughter behind.

2.6 Gamma interaction mechanisms

Gamma rays (photons) can interact with atomic electrons or the nucleus or the electric field surrounding the nucleus. During interaction a gamma ray's energy can be absorbed or the gamma-ray can be scattered elastically or inelastically. There are three major interaction mechanisms that play an important role in the measurement of photons. These mechanisms are the photoelectric effect, Compton scattering and pair production.

2.6.1 Photoelectric effect

In the photoelectric effect, a γ-ray collides with electrons from an inner shell of the absorber material resulting in the ejection of a bound electron. The ejected electron is subsequently slowed down in the surrounding material and its energy is absorbed. The photon disappears completely, i.e. all its energy is transferred to the electron. If the **γ**-ray energy, E_γ is higher than the binding energy of the electron, E_b, the kinetic energy of the ejected electron can be calculated using:

$$E_e = E_\gamma - E_b \tag{2.10}$$

The ejected electron leaves a hole in the atom; this can be filled by either capturing a free electron or via rearrangement of electrons in other shells, resulting in emission of a characteristic X-ray or Auger electron (see Figure 2.6).

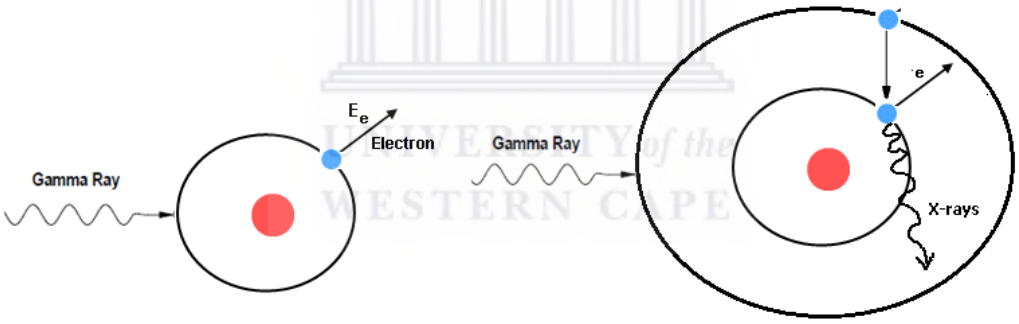

Figure 2.6: An illustration of photoelectric effect (left) followed by emission of characteristic X-rays (right) (Gilmore, 2008).

The cross-section (interaction probability per absorber mass) for photoelectric effect varies with energy in a complicated way and depends on atomic number Z of interacting material. There is also a strong dependence of the photoelectric cross section with photon energy. The probability for the photoelectric effect to take place can be described by the atomic cross section expressed by (Lilley, 2001; Turner, 2007):

$$\tau_a = constant \frac{Z^n}{{E_\gamma}^m} \tag{2.11}$$

where τ_a is the atomic cross section and m and n range from 3 – 5 depending on the gamma energy. The photoelectric effect is the dominant interaction mechanism at low energies (<~100 keV).

2.6.2 Compton Scattering

Compton scattering or Effect is the process whereby an incident photon collides with an electron (usually from an outer shell) and part of its energy is transferred to the ejected electron (Figure 2.7). The γ-ray is scattered from its original direction with the rest energy and a recoil electron is created. A portion of the γ-ray energy is transferred to a recoil electron (Knoll, 2010). The energy of the scattered γ-ray and recoil electron depend upon the angle at which the interaction occurred and is described by the following equations (Debertin, 1998; Gilmore, 2008; Knoll, 2010):

$$\mathrm{E_e} = \mathrm{E_\gamma} - E'_\gamma \qquad (2.12)$$

where $\mathrm{E_\gamma}$ and E'_γ are the incident and scattered γ-ray energies respectively.

If θ is the angle formed by the scattered γ-ray with respect to incident γ-ray, the scattered γ-ray energy can be expressed as:

$$E'_\gamma = \frac{\mathrm{E_\gamma}}{1+\frac{\mathrm{E_\gamma}}{\mathrm{m_o c^2}}(1-\mathrm{Cos}\,\theta)} \qquad (2.13)$$

with $\mathrm{m_o c^2}$ being the electron rest mass of 511 keV and θ is the angle at which the γ-ray is scattered. The dependence of E'_γ and E_e on the scattered angle θ is represented in the Figure 2.7. When θ = 0º, the γ-ray is forward scattered from the interaction point, E_e turns out to be zero and no energy is transferred to the detector. When θ = 180º, the gamma-ray is completely back scattered and for high energy gamma-rays, equation 2.13 reduces to:

$$E'_{\gamma} \cong \frac{mc^2}{2} = 0.256\ MeV \qquad (2.14)$$

In this case, the energy of the electron resulting from the Compton interaction reaches a maximum value which results in a spectral feature called the Compton edge.

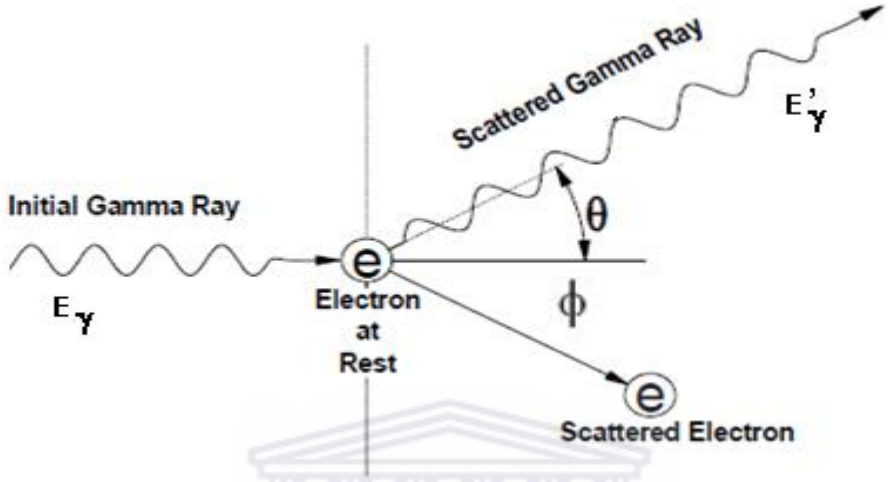

Figure 2.7: Schematic diagram showing Compton Effect: a gamma ray moving to the right collides with an electron at rest and a new gamma ray is scattered at an angle θ and recoil electron at an angle ϕ.

Compton scattering is the dominant interaction process for gamma-ray energies ranging from 0.1 to 10 MeV (Knoll, 2010). The probability of photon Compton Scattering at an angle θ is given by the Klein-Nishina formula:

$$\frac{d\sigma_c}{d\Omega} = r_o^2 \left[\frac{1}{1+\alpha(1-Cos\theta)}\right]\left[\frac{1+Cos\theta}{2}\right]\left[1+\frac{\alpha^2(1-Cos\theta)^2}{(1-Cos^2\theta)[1+\alpha(1-Cos\theta]}\right] \qquad (2.15)$$

where α is the photon energy in units of electron mass energy ($\alpha = \frac{E_\gamma}{mc^2}$), and r_o^2 is the classical electron radius ($r_o = e^2/4\pi\varepsilon_o c^2$ = 2.818 fm).

The strength of each of the three types of gamma ray interactions depends on the initial gamma ray energy and the atomic number, Z, of the material where the interaction takes place. The area where each type is most significant is shown in figure 2.8. For low Z materials and gamma energies less than few hundred keV, the photoelectric effect is the dominant process. Pair production becomes significant at gamma energies above 5 MeV.

This leaves the Compton Effect to be most prominent at mid-range energies around 1 – 2 MeV.

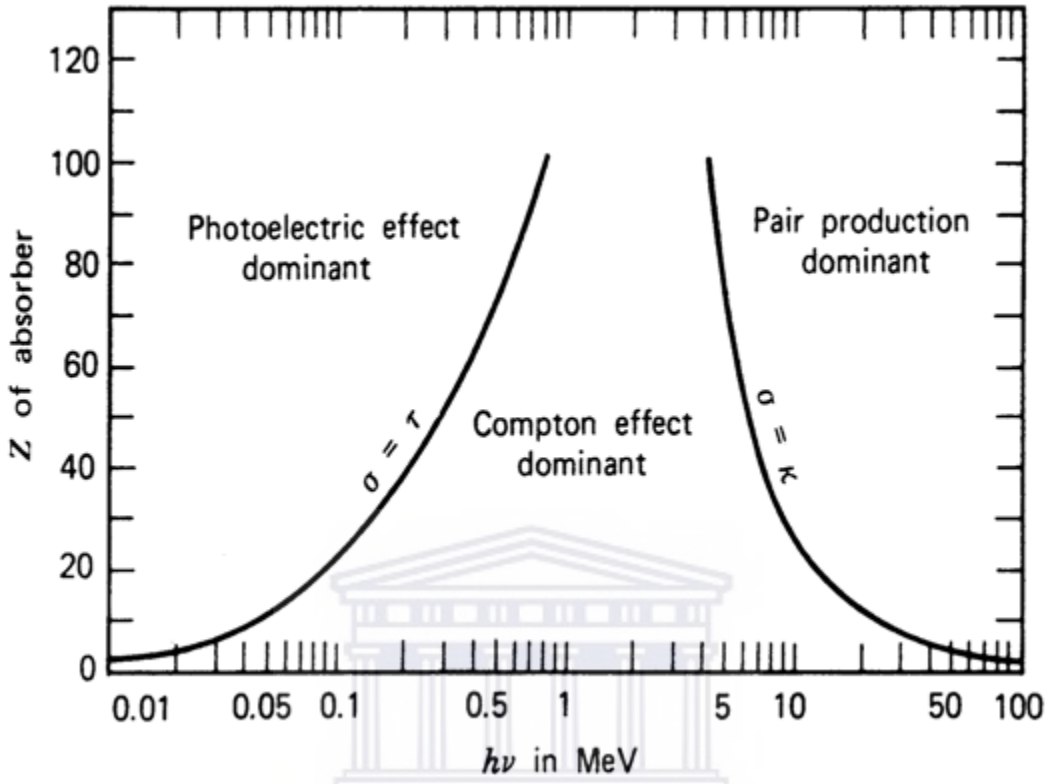

Figure 2.8: The regions of interest where three gamma interaction processes are individually dominant [Knoll, 2010].

2.6.3 Pair Production

This interaction mechanism only takes place within the Coulomb field of a nucleus of an atom. The γ-ray photon is absorbed into the vacuum and is converted into an electron-positron pair (Gilmore, 2008). This is only possible if the incident photon has a minimum energy equivalent to at least the rest mass energy of the pair, that is, $2m_oc^2$ = 1022 keV. After the interaction the electron-positron pair is produced and any excess energy carried by the photon above 1022 keV is converted into kinetic energy and shared equally by the positron and the electron.

After the electron and positron pair is produced, they can go across the medium, losing their kinetic energy by collisions with electrons in the surrounding material through

ionization, excitation and/or *bremsstrahlung*. Once, the positron slows down, it can unite with an atomic electron in the surrounding material and annihilate into two photons of 511 keV each (Gilmore, 2008; Knoll, 2010). These photons are called *annihilation photons*. In order to conserve linear momentum, these two photons must be emitted in opposite directions, *i.e*., back to back. Due to the energy threshold for pair production, this process is dominant at higher energies (E_γ > 5000 keV). The probability of pair production per atom increases with the energy above the threshold energy.

2.7 Gamma (γ)-ray Spectroscopy

For detection of γ radiation and its spectroscopy, two types of detectors are widely used; scintillators and semiconductor detectors. Scintillation detectors generate light in response to an incident charged particle and emit light pulses, the intensity of which is proportional to the incident particle energy. The most common scintillation detectors used for γ spectroscopy are those made of NaI(Tl) crystals. Other scintillation detectors used in gamma radiation measurements include $LaBr_3$ (Ce) and CsI.

The most common semiconductor detector used in γ spectroscopy is high-purity germanium detector (HPGe). Whether scintillators or semiconductor detectors were used in gamma detection, a spectrum representing the gamma rays from a source as a function of gamma ray energy is collected. A typical spectrum collected by the HPGe detector is illustrated in Figure 2.9. In this work three gamma detectors have been used to study the distribution of natural radionuclides in the Zanzibar coastline. Details of these detectors are given in Chapter 3.

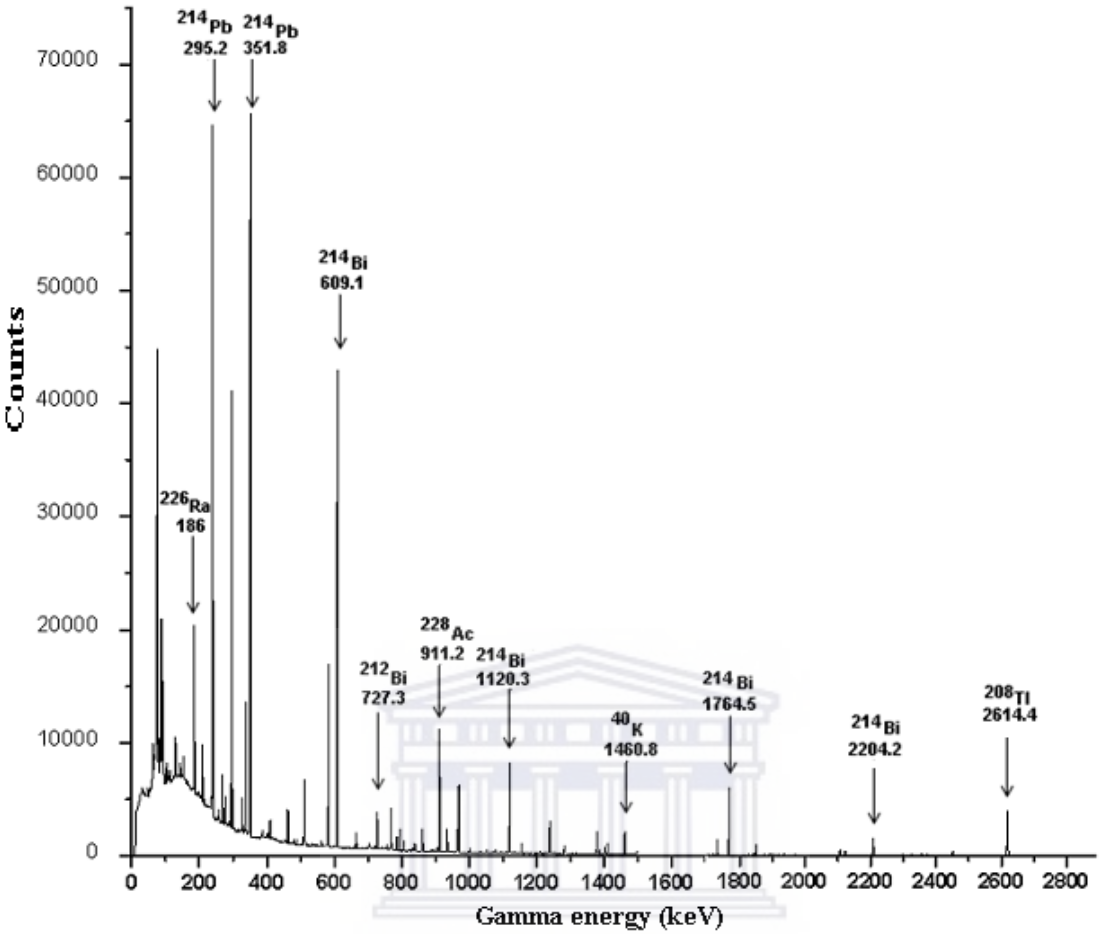

Figure 2.9: An example of a gamma energy spectrum from HPGe detector for sample PBS 9C collected from Kukuu beach.

CHAPTER 3

Study Area, Experimental Setup and Data Analysis Techniques

3.1 Introduction

This chapter presents the measurement methods used in this study. It starts by describing the study area followed by the overview of the three gamma ray detectors used in field (*in-situ*) and laboratory (*ex-situ*) radiometric measurements. The sample collection and preparation as well as data acquisition and analysis methods adopted in this work are also included. Apart from radiometric techniques, a brief description of non-radiometric measurements employed in this study is also given. These include XRF (Energy Dispersive **X-R**ay **F**luorescence) and ICP-MS (**I**nduced **C**oupled **P**lasma **M**ass **S**pectrometry).

3.2 Study area

Zanzibar (Figure 3.1) lies in the Indian Ocean off the coast of mainland Tanzania, between 4° and 6° south of the equator 39° and 40° east. It is a semi-autonomous state within United Republic of Tanzania comprising of Unguja and Pemba Islands and several adjacent islands. Unguja Island (informally called Zanzibar) is 40 km off the Tanzania Mainland and 85 km north-south length and 30 km wide at the widest point. The island is flat and it covers an area of 1658 km^2 (Heguye, 1993; Hassan, 2007). To the north of Unguja, about 50 km is her sister island Pemba, which is approximately 65 km long and 23 km wide. Pemba Island is about 985 km^2 in size. Both islands are covered by mangroves, coral reefs, many long white sandy beaches and the pristine expanse of the sea.

Zanzibar has an estimated population of 1 579 849 (TNBS, 2018) of which 35% reside along the Zanzibar coast. Zanzibar's climate is typically tropical with hot and humid weather most of the year. Zanzibar experiences four main seasons in a year: summer, known locally as Kiangazi (January-March); the heavy rainy season (also called Masika

by locals) from March to May; followed by a relatively cool and dry season, known locally as Kipupwe in Unguja and Mchoo in Pemba (June-August/September), and the short rainy season (also called Vuli by locals) from October to December.

Zanzibar experiences two main windy seasons. These are: 1) the northeast monsoon (locally known as Kaskazi) which blows during December to February towards the coast of both islands and characterised by lower wind speeds and calmer seas and 2) the southeast monsoon which blows away from the shore; this wind pattern is characterised by cooler temperatures, higher winds and rougher seas.

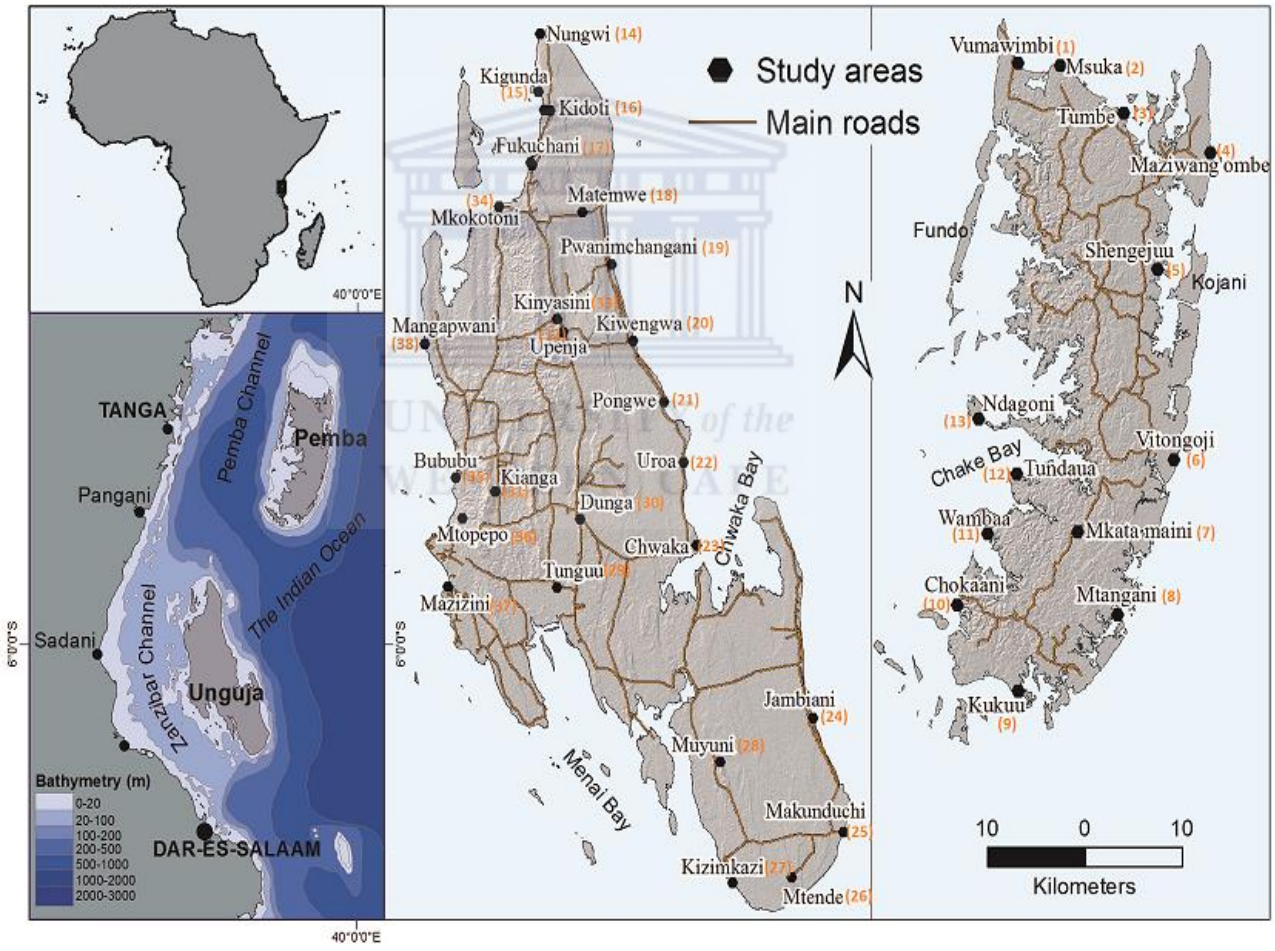

Figure 3.1: Map of Zanzibar showing study areas

In this study, 38 locations have been surveyed as shown in Figure 3.1. Samples were collected in selected locations for laboratory measurements. Each sample was assigned a

code consisting of letters followed with a number (see section 3.4). The number in each code (see Figure 3.1) refers to the area where in-situ measurements were performed or a sample was collected for laboratory measurements.

3.3 In-situ Natural Radioactivity Measurements

In-situ gamma ray spectrometry is a widely used technique for monitoring of natural as well as man-made radionuclides and corresponding gamma fields in the environment. The technique is used in monitoring accidents of nuclear facilities and their surrounding environments, radioactive contamination measurements and mapping, geological prospecting and mapping, and radiation safety studies (De Meijer, 2001; Lindsay et al., 2004; Mlwilo, 2010; Ongori et al., 2015).

Among the most widely used detector for *in-situ* γ-measurements is the sodium iodide thallium activated scintillator, NaI(Tl) (Senthilkumar et al., 2014; Noncolela, 2011; Bezuidenhout, 2012). Other detectors used in γ-in-situ surveys include MEDUSA (De Meijer 1996, Limburg, 2009; Venema and De Meijer, 2001; Speelman, 2004; Modisane, 2005; Hlatshwayo, 2007; Mlwilo, 2010; Ongori, 2013) and HPGe (Al Jundi et al., 2003, 2008; Tzortzis et al., 2004; Kurnaz et al., 2007). In this study, NaI(Tl) and MEDUSA, using a CsI(Na), γ-ray detectors have been used for in-situ measurements with the aim of investigating the levels and distributions of natural radionuclides in the soil surface layer and along the beaches.

3.3.1 NaI(Tl) gamma-ray detector

3.3.1.1 Overview of NaI(Tl) and set up

The 7.62 cm *x* 7.62 cm NaI(Tl) scintillator detector used in this study was manufactured by REXON Components, Inc., Ohio, United States of America. The crystal together with PMT **(P**hoto **M**ultiplier **T**ube) are enclosed by aluminium casing. The detector works through the emission of light due to incident particles making contact with the detector. The emitted light is subsequently collected and amplified in a PMT where the

scintillation is converted into electrical pulses. These pulses are later analysed, each holding important information regarding the interaction of the incident radiation within the scintillator.

The detector is coupled to a scintiSPEC MCA (**M**ulti **C**hannel **A**nalyser) that is produced by FLIR (http://gs.flir.com/). The scintiSPEC MCA uses a USB connection that acts as a power source for operation including the voltage for the PMT and allows data transfer. The system settings and spectrum acquisition was controlled by the winTMCA32 software with 1024 channels, that is also produced by FLIR. The winTMCA32 software was installed in a laptop and was used for both data collection during *in-situ* measurement and analysis. The software is equipped with a hardware set up option to set the gain and high voltage among other settings. The gain was set to 1.5 and high voltage at 1050 V.

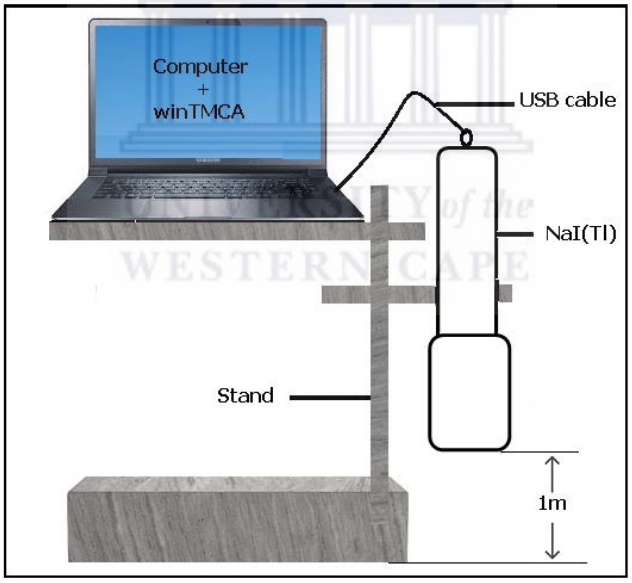

Figure 3.2: An illustration of a NaI(Tl) detector placed 1m above the ground during *in-situ* measurements.

Using the NaI(Tl) detector, stationary field measurements were carried out at 34 different locations. The detector was placed 1 m above the ground as illustrated in Figure 3.2 and subsequently each spectrum was collected for 600 seconds. Before any measurement was carried out, plant residues were removed from each measurement position. The NaI(Tl)

detector was used at these locations to get an idea of the variation in radionuclides present in order to decide where on the islands samples should be collected for laboratory analysis.

3.3.1.2 Calibration of NaI(Tl) detector

Calibration of the detector is an important aspect in radiation detection. The field spectra from various locations were collected, 34 in total. Peaks were identified using the standard spectra; the single peak from ^{40}K and multiple peaks from the ^{232}Th and ^{238}U decay series. The standard spectra were collected from Lanseria Airport calibration pads. The calibration pads were constructed in early 1981 to cater for the needs of airborne spectroscopy. Three calibration pads were constructed; each consists of 8 m diameter by 0.35 m thick concrete structures sunk into the asphalt of a disused runway (Larkin, 2013). The activity concentrations of ^{40}K, ^{232}Th and ^{238}U of the calibration pads are shown in Table 3.1.

Table 3.1: Activity concentration of the three calibration pads (Larkin, 2013).

Pad	**Potassium (%)**	**Thorium** (Bq.kg^{-1})	**Uranium** (Bq.kg^{-1})
1	0.26 ± 0.06	158.0 ± 7.0	4.3 ± 0.3
2	0.24 ± 0.05	7.4 ± 0.1	67.0 ± 4.0
3	6.10 ± 0.20	1.9 ± 0.2	0.9 ± 0.2

When using NaI(Tl) in field measurements, one should expect to observe a shift in the collected spectra (gain shift) as a result of temperature changes, count rate changes and detector electronics (Modisane, 2005). It is therefore important to calibrate the detector before in-situ measurements are performed. For practical reasons, the detector was not routinely calibrated during beach and land mapping but the spectra were re-binned offline. A typical in-situ spectrum after re-binning exercise that was acquired in Kidoti is illustrated in Figure 3.3. Various photopeaks were observed in the spectrum and are associated with ^{238}U, ^{232}Th and ^{40}K radionuclides.

Note that the ^{208}Tl peak (2614 keV) from ^{232}Th is among the peak one should expect to see in Figure 3.3, but this peak is missing since for the used gain the peak is above the highest channel. This is a result of the peak drift during in-situ measurements. To correct

the peak shifts on measured spectra during field measurements and to estimate the ^{232}Th, ^{238}U series and ^{40}K content in the locations surveyed, standard spectra obtained from Lanseria airport were used. The spectral windows were not used to estimate the activity concentration in this work. Instead, full spectrum analysis (see section 3.3.2.3., Hendriks et al., 2001) which utilises the whole spectrum was used.

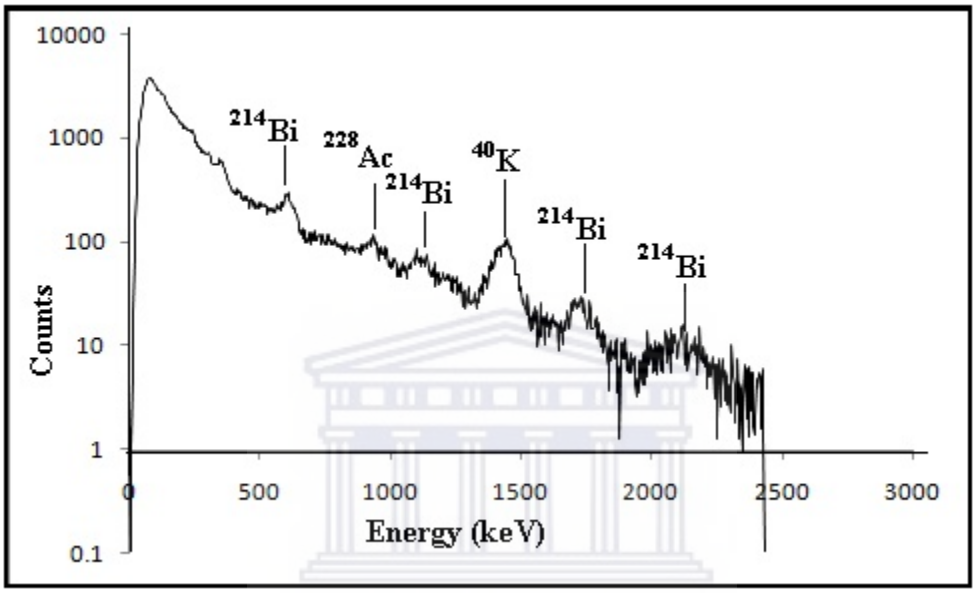

Figure 3.3: The spectrum of the stationary measurement at Kidoti after re-binning.

The field spectra and the standard spectra data were exported to an Excel spreadsheet and a Microsoft Excel VBA program was written to arrange the data to two columns; one for the counts and the other for channels. The spectra were also re-binned such that each channel corresponds to 3 keV. The re-binning was necessary to correct the energy variations between the field spectra and the standard spectra which are usually witnessed because of gain shifts mainly due to temperature variations. The estimated activity concentration obtained during in-situ mapping using NaI(Tl) detector are found in Chapter 4.

3.3.2 MEDUSA γ-ray detector system

3.3.2.1 Overview of MEDUSA and set up

The MEDUSA system available at the ERL (Environmental Radioactivity Laboratory) at iThemba LABS (**L**aboratory for **A**ccelerator **B**ased **S**ciences), was purchased from the NGD **(N**uclear **G**eophysics **D**ivision) of the Nuclear Accelerator Institute (KVI - **K**ernfysisch **V**ersneller **I**nstituut) of the University of Groningen in the Netherlands). The NGD team worked in partnership with the BGS (**B**ritish **G**eological **S**urvey) to develop the MEDUSA system. The detector was initially designed to perform underwater natural gamma ray mapping, but it has been improved to perform the same purpose on land (De Meijer et al., 1997).

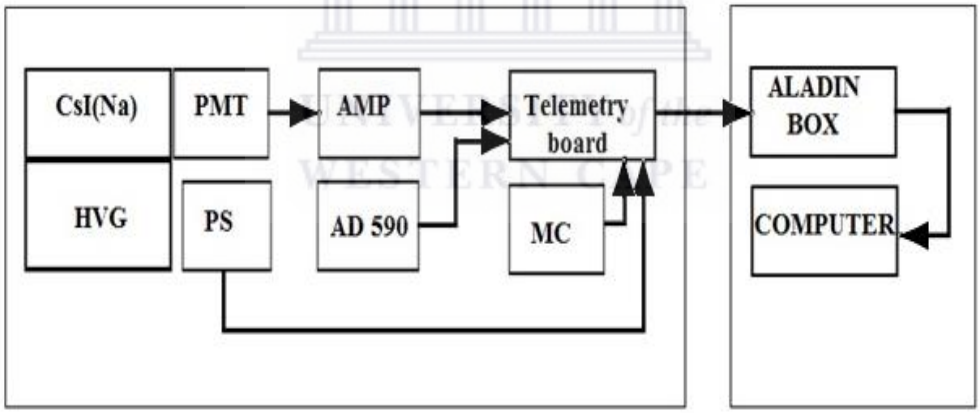

Figure 3.4: Schematic illustration MEDUSA (CsI(Na)) detector crystal and other components.

The MEDUSA system is divided into two main parts. The first part is encased in a stainless steel tube (1.3 m length, 10 cm in diameter) comprising of the CsI(Na) (cesium iodide doped with sodium) γ-ray detector crystal (15 cm long, 7 cm in diameter) and PMT (photomultiplier tube). The first part also include HVG (Cockcroft Walton high-voltage generator), AMP (spectroscopic amplifier), AD 590 (temperature sensor), MC

(microphone), PS (pressure sensor) and a detector telemetry board (data transfer cable). Figure 3.4 shows the schematic diagram of MEDUSA system with the associated electronics connected to it.

The second part of the ERL MEDUSA system consists of a collection of hardware and software apparatus that are used to measure, process and translate into sediment composition the data for natural radioactivity. These include ALADIN (**A**NTARES **L**og **A**cquisition and **D**ata **In**terpretation system) box containing data acquisition system, the laptop computer in which data accumulation, storage and analysis software are installed and the GPS (Global Positioning System) device. The GPS used to log-in the detector position (latitude, longitude and altitude) in this study is a Garmin 76 and was placed above the MEDUSA detector during *in-situ* measurements. The components of the ERL MEDUSA detector system are illustrated in Figure 3.5.

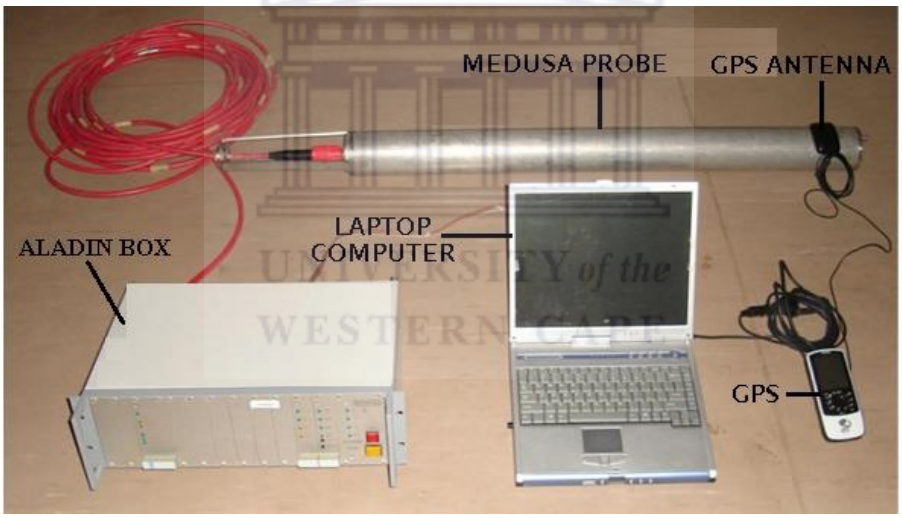

Figure 3.5: Components of the MEDUSA γ-ray detector system.

In this work, the ERL MEDUSA detector is used for both stationary and dynamic measurements. In stationary mode, radioactivity measurements were carried out at discrete points while the detector was placed directly on the ground or was on the vehicle 60 cm above the ground (see Figure 3.6).

Figure 3.6: The ERL MEDUSA γ-ray detector system during *in-situ* gamma-ray mapping, mounted on a 4 x 4 vehicle at Kukuu beach in Pemba (left) and placed on the ground at Msuka (right).

Stationary measurements were performed in the locations that were also observed with high counts during dynamic measurements. To obtain geographical location of the surveyed area, the GPS device was placed directly above the detector and connected to the laptop via a USB port. The laptop and the ALADIN box were placed at the back of the vehicle. The signals of the sensors are digitized and are sent to the laptop for off-line analysis. A 12 V battery was used to supply the required voltage to the ALADIN box via DC/AC inverter.

During dynamic measurements, the detector was mounted on a 4 x 4 vehicle 60 cm off the ground as shown in Figure 3.6. While the detector is mounted on the vehicle, an area was surveyed following a particular pattern depending on the accessibility of the area. The selected areas were traversed while the vehicle was moving at a speed of about 2 ms^{-1}. In this work dynamic measurements were performed at Kukuu, Msuka, Mtende, Kidoti and Tunguu (see Figure 3.1). Where dynamic measurements were not possible, only stationary measurements were made.

3.3.2.2 MEDUSA data processing

In-situ measurements using MEDUSA were conducted in June, 2015. During in-situ measurements, eight different locations were surveyed; five in Unguja and three in Pemba (refer to Figure 3.1). The MEDUSA data are stored in MDL (MEDUSA Data Longer) during acquisition. MDL saves files in the form .nn where nn refers to the number of the file, starting from 01, 02, and 03 and so on.

Apart from MDL, two other programs are used to complete the analysis of acquired data. These are MDS (MEDUSA Data Synchroniser) and Gamman. MDL files acquire various data during surveys. These include gamma ray spectrum data (acquired after every two seconds) and the associated auxillary data (acquired after every one second). Auxillary data include temperature, pressure, sound and total counts. The data collected (spectrum and auxillary) are therefore in unsynchronised format. To establish one to one correspondence between the data, the MDS is used. In order to synchronise the spectrum and auxillary data, the *spectrum data field in action* setting within the MDS software was first changed to synchroniser. Furthermore, the latitude, longitude and altitude was changed to average and all other parameters like temperature and pressure are not changed. The digit tab for latitude, longitude and altitude was changed to 4, 4 and 2 respectively. Table 3.2 shows data field, action changed and acquisition time.

Once the field setting was changed, the synchroniser is pressed to run, and the results were saved in a new file format with an extension (.sdf). The synchronised files are then analysed using a Gamman software package. This software was purchased from Medusa Exploration B.V. in Groningen, the Netherlands. The Gamman accesses data from the MDS to extract activity concentration using the FSA (Full Spectrum Analysis) technique (De Meijer, 1998; Hendriks, 2001). This software is allowed to identify and delete data outliers and to process gamma ray spectra for calculation of individual nuclide concentrations (^{40}K, ^{238}U, ^{232}Th) in Bq.kg^{-1}.

Table 3.2: Data field used for synchronisation.

Data field	Action	Digits	Acquisition time
Spectrum	Synchroniser	-	Every 2 seconds
Total counts	Last known	-	Every 1 second
Time	Last known	-	Every 2 seconds
Latitude	Average	4	Every 2 seconds
Longitude	Average	4	Every 2 seconds
Altitude	Average	2	Every 2 seconds
Temperature	Last known	-	Every 1 second
Pressure	Last known	-	Every 1 second
Cable length	Last known	-	Every 1 second
Cable volts	Last known	-	N/A
Sound	Last known	-	Every 1 second

3.3.2.3 Full Spectrum Analysis (FSA)

FSA is a γ-ray spectrum analysis tool for quantitative determination of radionuclides. Unlike the usual approach which uses spectral windows during analysis, FSA utilises the whole spectrum. In fact, FSA has been found to be a successful spectrum analysis tool for the determination of radionuclides (Hendriks, 2001; Caciolli et al., 2012; Tyler, 2008).

The principle of FSA is based on the assumption that the count rate at each channel, $\boldsymbol{S_i}$, is the sum of the individual radionuclides plus background contribution, ***B(i)***. The event registered in each channel in the measured spectrum ($\boldsymbol{S_i}$) can be expressed as (De Meijer, 2001; Hendriks, 2001; Caciolli, 2012):

$$S_i = \sum_{j=1}^{m} C_j X_j\,(i) + B(i) \qquad (3.1)$$

where,

X_j is the gamma spectrum of radionuclide j for a concentration of 1 Bq.kg^{-1},

i is the channel number and C_j is the activity concentration of the specific radionuclide j. Index j stands for ^{238}U, ^{232}Th and ^{40}K.

With FSA, the spectra acquired in-situ are fitted to the standard spectra of radionuclides of interest which is determined either in the laboratory or via Monte Carlo simulations

(Lindsay et al., 2004). The standard spectra used in analysis of the in-situ MEDUSA data in this work were generated by simulation with the MCNPX (Monte Carlo N-Particle X) code (Hendriks, 2001; Maleka, 2010; Ongori, 2013). The code was used to simulate the flatbed geometry with 30% soil porosity, with 50% water content and 50% air content. The soil was assumed to consist of SiO_2. The simulated standard spectra composed of ^{238}U, ^{232}Th and ^{40}K used in gamma analysis are shown in Figure 3.7.

Since background, mainly cosmic, radiation is an important aspect in gamma ray measurement, the background spectrum was acquired using MEDUSA. The detector was immersed in 15 m deep Theewaterkloof Dam which is located 60 km from iThemba labs (Modisane, 2005; Ongori, 2013).

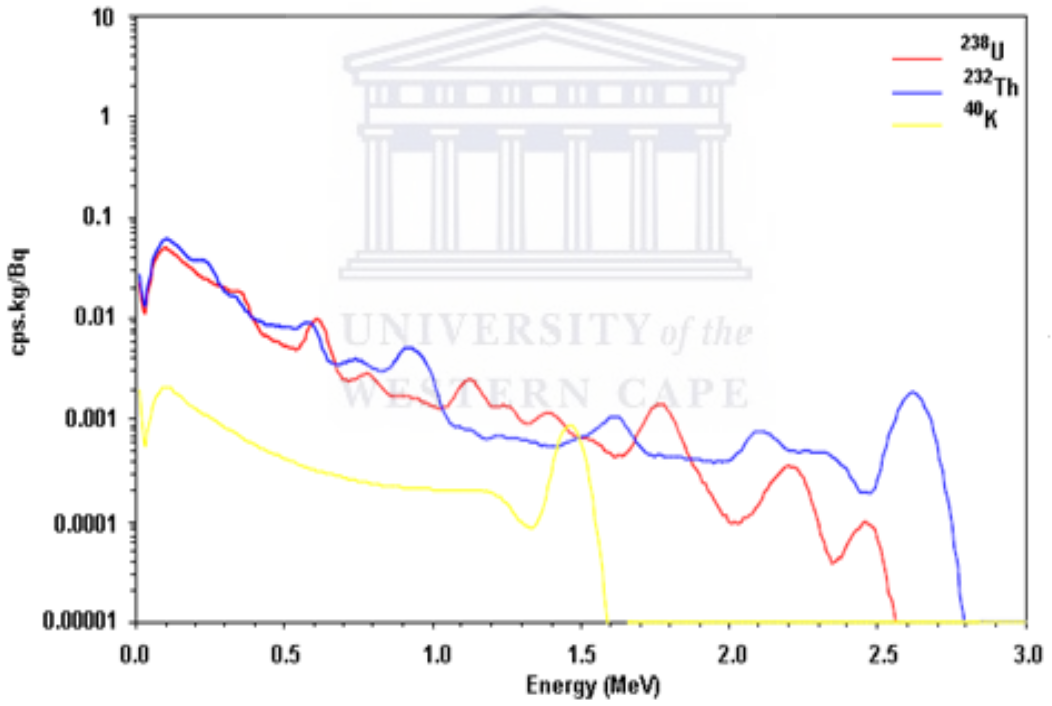

Figure 3.7: A set of simulated standard spectra for ^{238}U, ^{232}Th and ^{40}K [Mlwilo, 2010].

The activity concentration of the radionuclide, j in the measured sample is deduced applying the least square algorithm to rectangular matrix and minimizing the chi-squared as in the following equation:

$$\chi^2 = \frac{1}{n-m}\sum_{i=1}^{n}\frac{1}{\sigma^2(i)}[S(i) - \sum_{j=1}^{m} C_j X_j(i) - B(i)]^2 \qquad (3.2)$$

where, σ^2 is the variance associated with channel ***i*** in the sample spectrum (with counts S(i)), m is the number of standard spectra used (which is 3 in this case) and n is the number of channels used in analysis. The generated FSA are stabilized as discussed in the next section (section 3.3.2.4).

3.3.2.4 Stabilization process

Although the Gamman software package normally stabilizes the imported files automatically, manual stabilization is performed in case the position of the energy spectra of the fit deviate from the standard spectra. For example, the ^{40}K gamma energy peak is supposed to be at 1460 keV and the highest ^{232}Th peak to be at 2614 keV. When this is not the case, manual stabilization is done by adjusting the stabilization value in the stabilization editor in such a way that the peaks fit with the stabilization algorithm (Figure 3.8). There are several factors that may influence the quality of spectra. These include inaccuracy of MCA, crystal, temperature change etc. (Limburg, 2009).

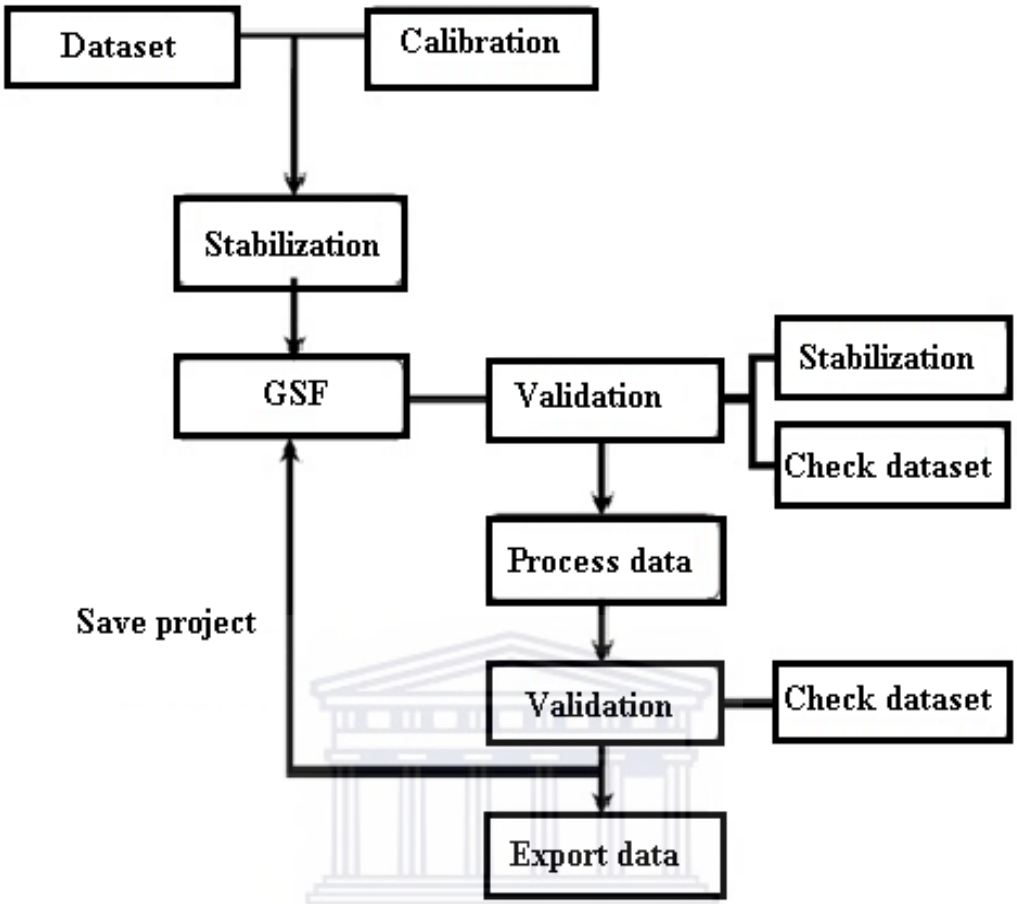

Figure 3.8: A flowchart showing procedure for data analysis of gamma spectra using the MEDUSA and GAMMAN.

The stabilization process is based on a least square method which computes the lowest possible chi-squared. The fitting is considered to be best when the reduced chi-squared is close to one. The best chi-squared achieved in analysis of MEDUSA data in this work is 4.08. Apart from stabilization parameters, the window shows activity concentrations of three principal radionuclides (^{40}K, ^{232}Th and ^{238}U). Figure 3.9 displays an example of a stabilized spectrum from Msuka beach.

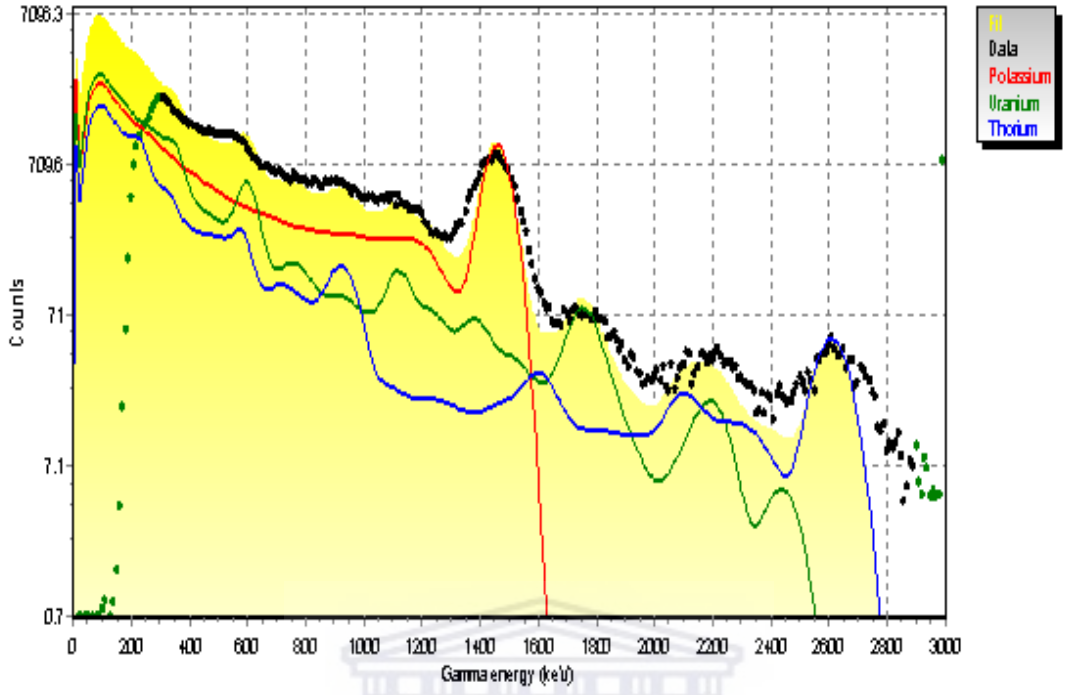

Figure 3.9: FSA fitted spectra acquired with MEDUSA in-situ (black) at Msuka beach with a set of standard spectra for ^{238}U (green), ^{232}Th (blue) and ^{40}K (red).

Once imported files are stabilised, sum and analyse operation is used to extract total counts, activity concentrations of ^{238}U, ^{232}Th and ^{40}K and their uncertainties. Using the extracted data, total counts maps of the surveyed area were plotted (see Figure 3.10 – 3.14) as an example of the results of the MEDUSA system. Activity concentrations maps for ^{238}U, ^{232}Th and ^{40}K were also generated and can be found in Chapter 4 (section 4.3). The processed data are saved with new file extension (.gsf) and exported to Excel spreadsheets. The data were used to generate interpolated maps of ^{40}K, ^{238}U and ^{232}Th using Surfer® 10 Golden software. These interpolated maps are found in Chapter 4 section 4.3.

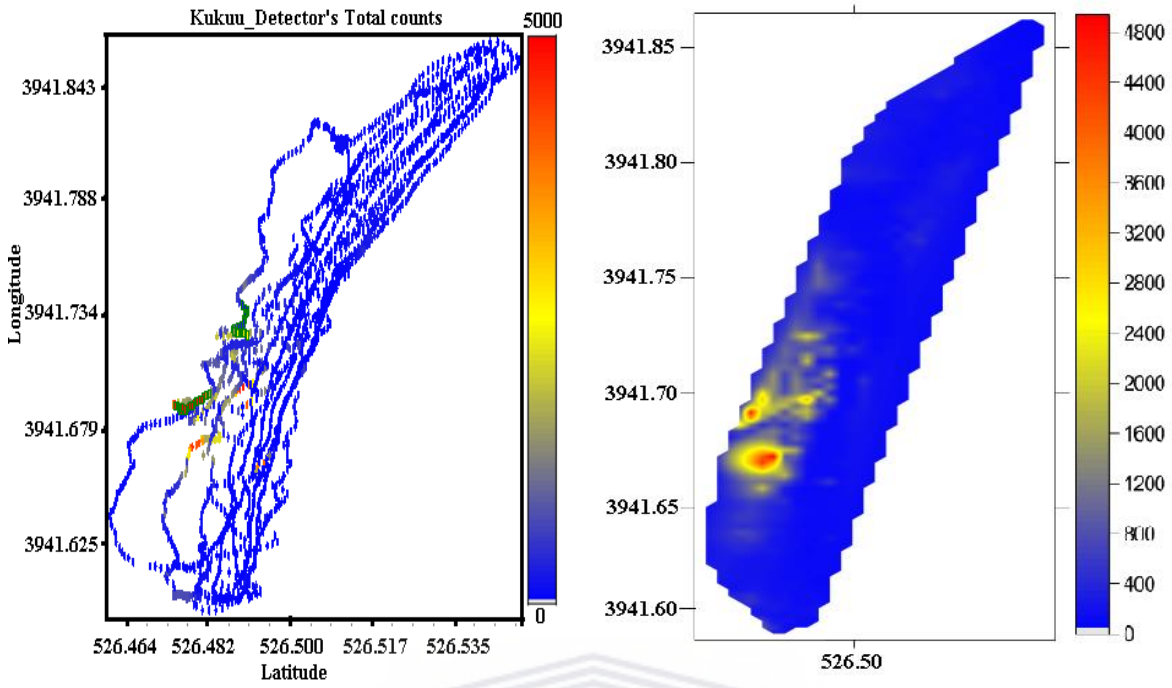

Figure 3.10: A map showing the detector's total counts (left) and an interpolated map (right) of the total counts corresponding to map on the left for Kukuu beach. Red spots indicate high count rate areas. The MEDUSA software algorithm provides the latitude and longitude in the format (m)mnn.nn instead of mmº nn.nn´ where mm and nn.nn match to degrees and minutes, respectively.

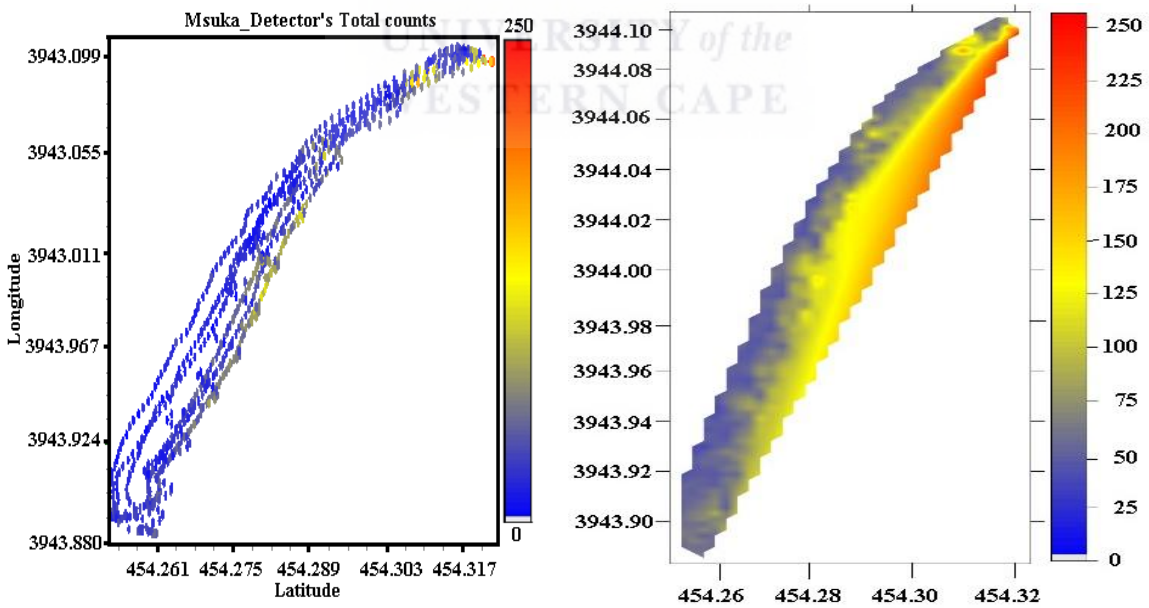

Figure 3.11: A map showing the detector's total counts (left) and an interpolated map (right) of the total counts corresponding to map on the left for Msuka beach.

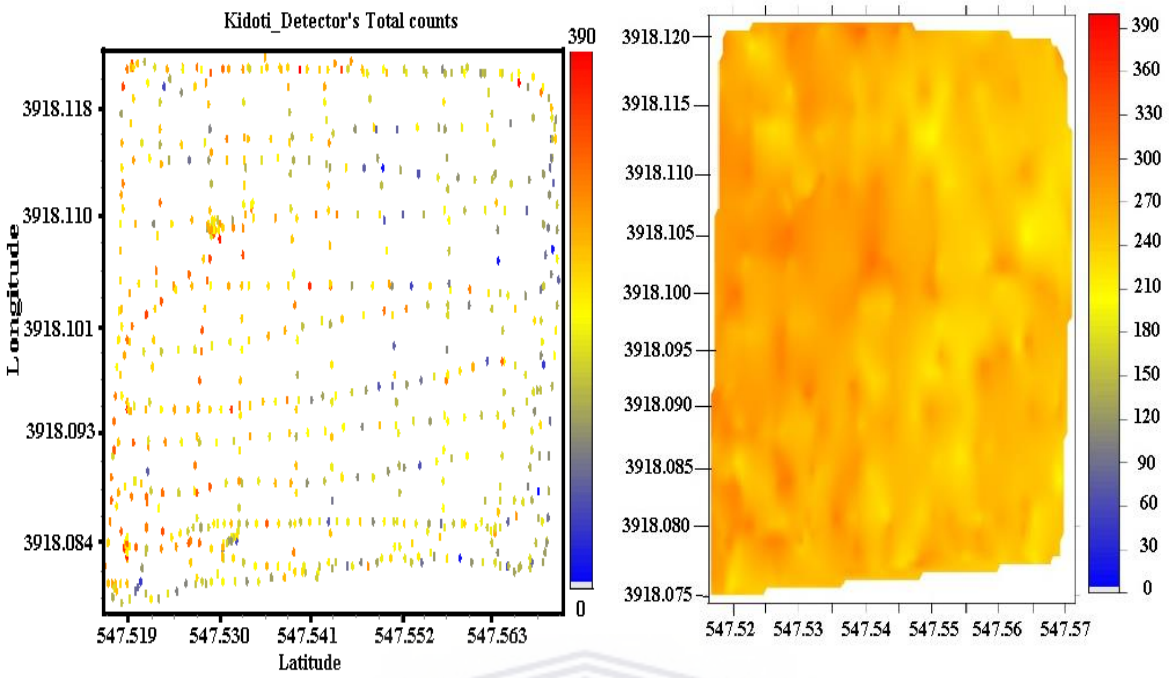

Figure 3.12: A map showing the detector's total counts (left) and an interpolated map (right) of the total counts corresponding to map on the left for Kidoti.

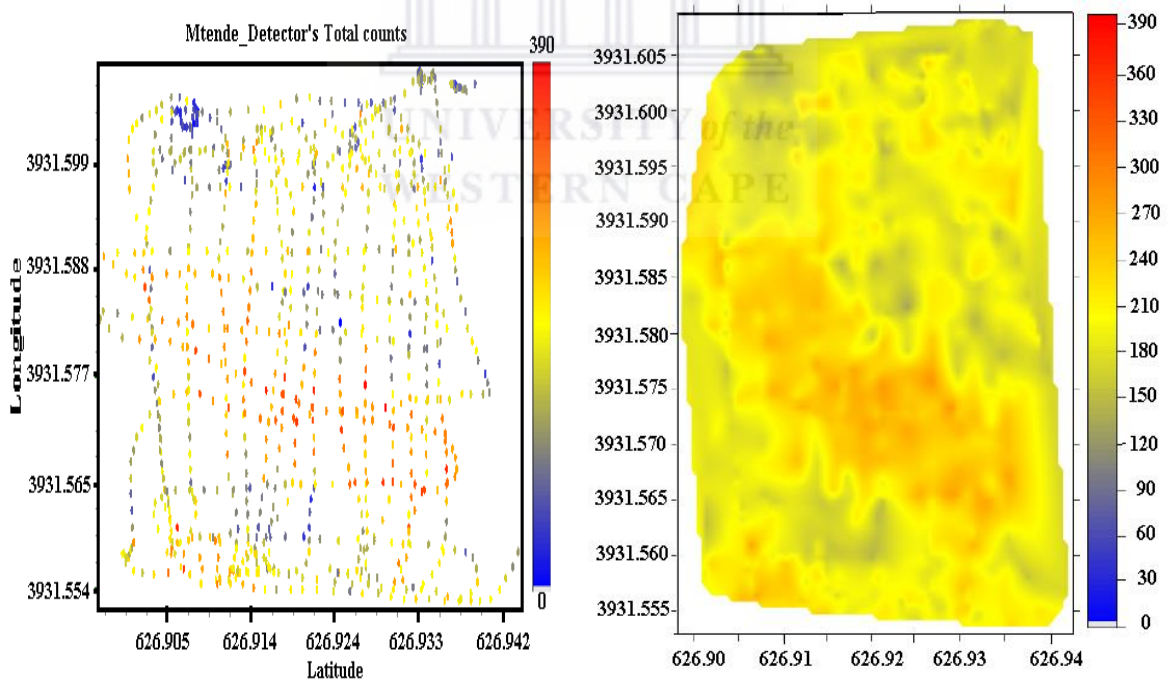

Figure 3.13: A map showing the detector's total counts (left) and an interpolated map (right) of the total counts corresponding to map on the left for Mtende.

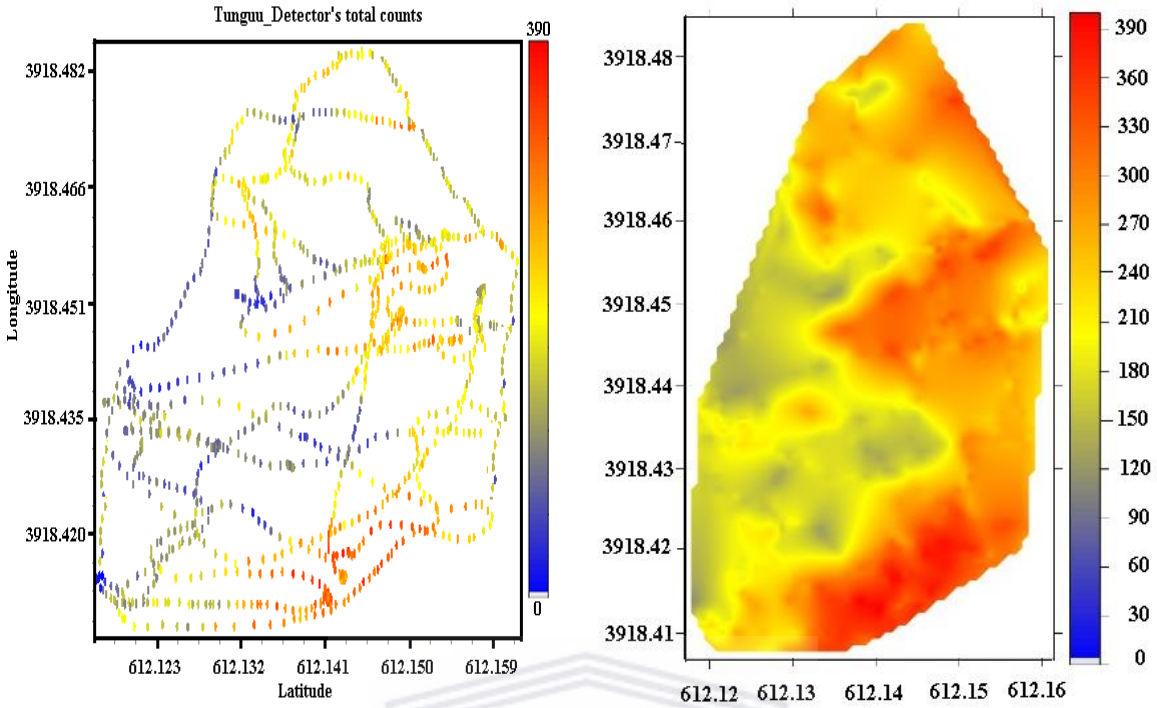

Figure 3.14: A map showing the detector's total counts (left) and an interpolated map (right) of the total counts corresponding to map on the left for Tunguu.

During in-situ measurements, soil samples and beach sands were collected in selected areas for laboratory measurements. The details of the laboratory measurements are discussed in the next section 3.4.

3.4 Ex-situ (laboratory) Natural Radioactivity Measurements

3.4.1 Soil sampling

In-situ measurements usually have fairly large uncertainties and normalisation of the data is problematic. Laboratory measurements can do much better but is only possible for a limited number of samples. Prior to laboratory measurements, the beach sediments and soil samples were collected from several different locations in Zanzibar. Figure 3.15 shows some sampling locations. Beach sands were collected in most popular beaches used by both locals and tourists in Unguja and selected beaches in Pemba.

Figure 3.15: Photographs showing some sampling locations: a) Kiwengwa beach b) Nungwi beach c) Kukuu beach d) Msuka beach.

Altogether 22 samples were collected for laboratory measurements. The samples were obtained at a typical depth of up to 10 cm from the top surface layer of either beach or land. After removing stones and vegetable matter, each soil sample was packed into its own secure water-tight polythene bag to prevent cross contamination. Each sample was assigned a code consisting of three letters followed with a number. The first letter refers to the island where the sample was collected, P for Pemba and U for Unguja while the second and third letters refer to the type of the sample; BS for beach sand and SS for soil sample. The number in each code refers to the area where the sample was collected or surveyed. Where more than one sample was collected in the sample area, the area number was followed by letters A, B, C and so on. The samples were shipped to the University of the Western Cape, South Africa for gamma-ray analysis. The details of the collected samples are presented in Table 3.3.

Table 3.3: The location of the soil and beach sand samples collected by HPGe measurement.

Location	Code	Latitude	Longitude	Density (g.cm^{-3})
Msuka	PBS 2	4.924334	39.763994	1.43
Maziwa Ng'ombe	PBS 4	4.979124	39.874572	1.13
Kukuu	PSS 9	5.441596	39.696035	1.45
Kukuu	PBS 9A	5.441913	39.696070	2.55
Kukuu	PBS 9B	5.441913	39.696070	2.68
Kukuu	PBS 9C	5.442463	39.697159	1.37
Wambaa	PBS 11	5.283715	39.663999	1.43
Kidoti	USS 16	5.798344	39.301315	1.05
Kigunda	USS 15	5.777182	39.293962	0.87
Muyuni	USS 28	6.341888	39.453344	1.09
Dunga	USS 30	6.151539	39.337619	1.10
Tunguu	USS 29	6.195300	29.043100	1.04
Mtende	USS 26	6.469886	39.505475	0.91
Tundaua	PBS 12	5.255771	39.697209	1.51
Nungwi	UBS 14	5.727808	39.291619	1.42
Pwani Mchangani	UBS 19	5.921069	39.357482	1.27
Kiwengwa	UBS 20	5.989350	39.378784	1.22
Uroa	UBS 22	6.094720	39.425662	1.21
Chwaka beach	UBS 23	6.160746	39.438385	1.44
Kizimkazi	UBS 27	6.454623	39.471932	1.28
Bububu	UBS 35	6.108775	39.214257	1.43
Mazizini	UBS 37	6.200971	39.206778	1.48

3.4.2 Sample Preparation

At the nuclear physics laboratory of the University of the Western Cape, samples were air-dried for six days (see Figure 3.16 a). Each sample was then oven dried overnight at a temperature of 110°C until a constant weight was reached (see Figure 3.16 b). The dried soil samples were reweighed to determine the gravimetric moisture content, ground into a fine powder and then homogenised (see Figure 3.16 c).

Figure 3.16: Soil and beach sand sediments preparations: a) Sample drying at room temperature b) Oven drying at 110ºC c) Weighing a dried sample d) A prepared soil sample in the Marinelli beaker.

The dried samples were transferred to the ERL (**E**nvironmental **R**adioactivity **L**aboratory) at iThemba LABS (**L**aboratory for **A**ccelerator **B**ased **S**ciences) for gamma spectroscopic measurements. At the ERL at iThemba LABS, both soil and beach sediment samples were sieved using a standard 2 mm sieve and weighed. The homogenised samples were filled into 1 litre Marinelli beakers, which were then sealed with the aid of glue to prevent the escape of airborne ^{222}Rn (radon) and ^{220}Rn (thoron) from the samples (see Figure 3.16 d).

All samples were weighed and left undisturbed for at least four weeks before measurement. This process provides enough time to establish secular equilibrium between ^{226}Ra (radium 226), ^{222}Rn (radon, with half life 3.83 days) and their decay products in the^{238}U chain. In the case of the ^{232}Th chain, it also guarantees equilibrium between ^{224}Ra (radium 224), ^{220}Rn (thoron, with half life 55. 6 s) and their short-lived daughters (Khater et al., 2001; TRACERCO, 2007). The samples were each counted using a low background HPGe (**H**yper **P**ure **Ge**rmanium) detector for a period ranging from 24 000 to 84 600 seconds.

3.4.3 HPGe detector: Overview and set-up

Laboratory γ-ray spectroscopy measurements of beach sand and soil samples were carried out using a low background HPGe detector system at the ERL iThemba LABS. The detector system consists of a coaxial p-type HPGe detector (Canberra Model GC4520 with a 700µm Aluminium window) and electronics to collect and process the signals produced by the detector. Signals from the detector were fed to the computer with the processing software to generate, display and store the final γ-ray spectrum produced. To minimize the external γ-ray background in the measured spectrum, the HPGe detector capsule was shielded with thick lead castle with a fixed bottom and movable cover. The passive detector shield was made from 10 cm thick lead. When a gamma ray strikes the lead surface, characteristic lead X-rays may escape and hit the detector. For this reason and for structural stability purposes the inner volume of the lead castle is internally lined with a 2 mm copper sheet oxygen free copper housing. The empty space is only devoted to host the sample under investigation. The HPGe crystal has a diameter of 62.5mm and a length of 59.0mm. At 1332.5 keV γ-line of ^{60}Co, it has a relative efficiency of 45% and 2.1 keV FWHM (**F**ull **W**idth at **H**alf **M**aximum) energy resolution.

Figure 3.17: A picture showing components of the HPGe detector system used in this study: a) The lead castle and the liquid nitrogen Dewar, b) the NIM power supply c) the top of the detector

The HPGe detector was coupled to an ATOMKI Palmtop MCA 8k-01 (**M**ulti-**C**hannel **A**nalyzer) from the Institute of Nuclear Research of the Hungarian Academy of Sciences. This includes a successive-approximation type ADC (**A**nalogue to **D**igital **C**onverter), an Ortec Model 572 spectroscopy amplifier, a Silena Model 7716 high voltage supply and a data display terminal. The conversion gain on the ADC was set to display spectra in 8192 channels. The operating bias voltage and pulse shaping time were +3500 V and 6 μs respectively. The gamma ray signals were stored and analysed using the associated MCA software package Palmtop MCA installed on a desktop computer.

The HPGe crystal is cooled with liquid nitrogen to decrease thermal conductivity between the crystal and the surrounding air. The liquid nitrogen dewar of the ERL HPGe has a capacity of 20 litres and is regularly filled with the liquid once a week. The detector is operated at 77 K liquid nitrogen temperature to prevent thermally-induced leakage currents which would result from its small band gap (0.7 eV) [Leo, 1987; Knoll, 2010].

3.4.4 Detector characterisation

Performance of a detector is characterized by its ability to identify various gamma energies and how efficient it is to detect the energy of the incident photon on a detector material. A gamma spectrum is interpreted for identifying and quantifying radionuclides. In order to do that, the HPGe detector was energy and efficiency calibrated prior to sample measurements as discussed next.

3.4.4.1 Energy Calibration

The ability to identify the photo peaks present in a spectrum produced by the detector system is among the important requirements in nuclear spectroscopy measurement (IAEA,1989). This is achieved by carrying out energy calibration of the detection system. In this study, the energy calibration (γ-ray energy as a function of channel number) of the HPGe detector is established by measuring the position of selected full-energy γ-ray peaks with large peak-height to background ratios, and whose energies are known precisely. In order to increase the detection efficiency of the detector an accurate energy calibration of the system and a periodical check is required. The HPGe detector available at the ERL iThemba LABS is energy calibrated every week. The certified standard sources IAEA/RGU-1, IAEA/RGTh-1 and IAEA/RGK-1 for uranium, thorium and potassium respectively are used for energy calibration. These sources emit γ-rays that covers the energy range of interest (100 – 3000 keV). The standard sources are counted for 84600 seconds. This duration was found sufficient to provide counts in the gamma peaks of interest with a precision of less than ± 0.2 keV. The channel number that

corresponds to the centroid of each full energy event on the MCA was recorded and plotted to obtain the fitting function for the energy calibration of the detector. The energy calibration curve is shown in Figure 3.18.

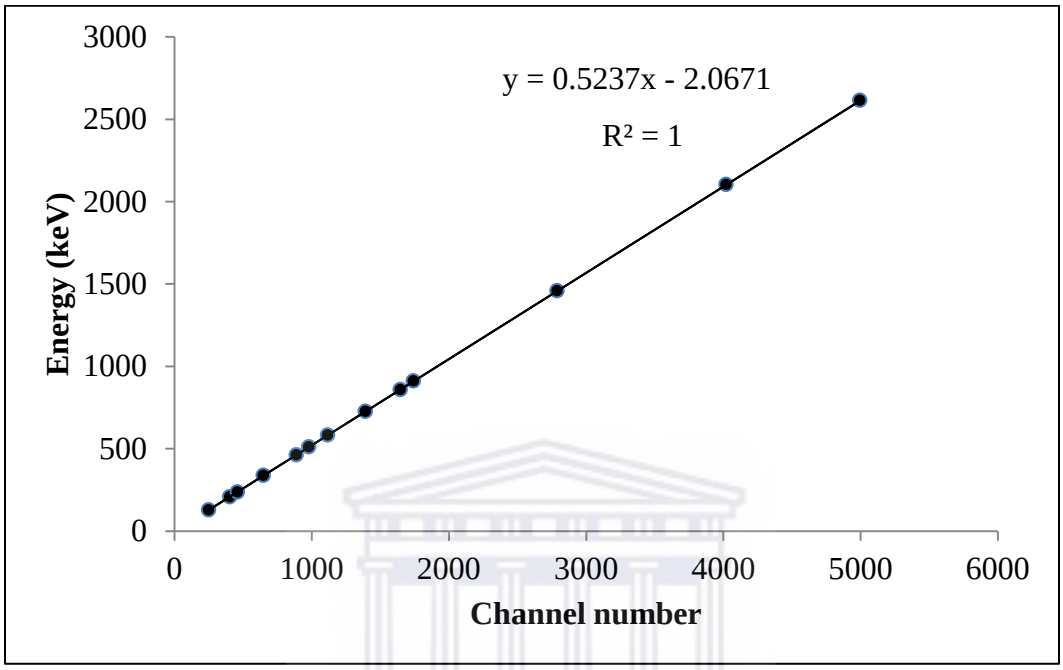

Figure 3.18: Energy calibration curve using IAEA/RTh-1 standard source.

3.4.4.2 Efficiency Calibration

The efficiency of the detector refers to the ratio of the actual events registered by the detector to the total number of events emitted by the source of radiation (Knoll, 2010. An accurate efficiency calibration of the detector is necessary to quantify radionuclides present in the sample. In this work, the photopeak detection efficiency of the HPGe detector was determined using:

A) the IAEA standard reference source approach,

B) relative efficiency approach and

C) Monte Carlo Simulation technique.

Many workers use only one method (usually (A)) but the variation in sample activity and density makes it important to test different methods. Method (B) allows unique efficiency calibrations for each sample as described below.

A) Calibration using IAEA standard reference sources

In the IAEA standard reference source approach, standard sources with known activity are used to determine the efficiency of the detector. Three standard sources IAEA/RGU-1, IAEA/RGTh-1 and KCl (from Merck) of known activity (see Table 3.4) were used in this study.

Table 3.4: The activity concentrations and masses of the IAEA standard sources and KCl powder.

IAEA Standard source	Activity concentration (Bq.kg^{-1})	Mass (kg)
^{238}U	4940	1.14
^{232}Th	3250	1.36
^{40}K	16258	1.29

Since the detection efficiency depends not only on the detection system but also on the sample geometry and matrix, the standard sources were filled in similar Marinelli beakers as samples. The standards were measured for 3600 seconds and net counts in photopeaks of interest were extracted. The efficiencies of the detector at various energies (see Table 3.5) were computed using the relation (Cember and Johnson, 2009):

$$\varepsilon_\gamma = \frac{C_{net}}{AI_\gamma t} \qquad (3.3)$$

where, C_{net} is the net gamma ray counts in the full energy peak, A is the activity of the standard source with its values shown in table 3.4, Iγ is the emission probability and t is the counting time in seconds.

The absolute photopeak efficiency as a function of gamma energy generated using the standard sources is plotted in Figure 3.19.

Table 3.5: γ-ray energies and their associated emission probability per decay [Faires and Boswell, 1981; Wahl, 2007].

	Nuclide	Energy (keV)	Emission Probability
^{238}U Series	^{214}Pb	295.2	0.1842 (4)
	^{214}Pb	351.9	0.3560 (7)
	^{214}Bi	609.3	0.4480 (16)
	^{214}Bi	1120.2	0.1480 (3)
	^{214}Bi	2204.2	0.04924 (18)
^{232}Th Series	^{228}Ac	338.3	0.1127 (19)
	^{208}Tl	583.1	0.3055 (17)
	^{212}Pb	727.3	0.0674 (12)
	^{228}Ac	911.2	0.258 (4)
	^{208}Tl	2614.5	0.3585 (7)
^{40}K	^{40}K	1460.8	0.1066 (13)

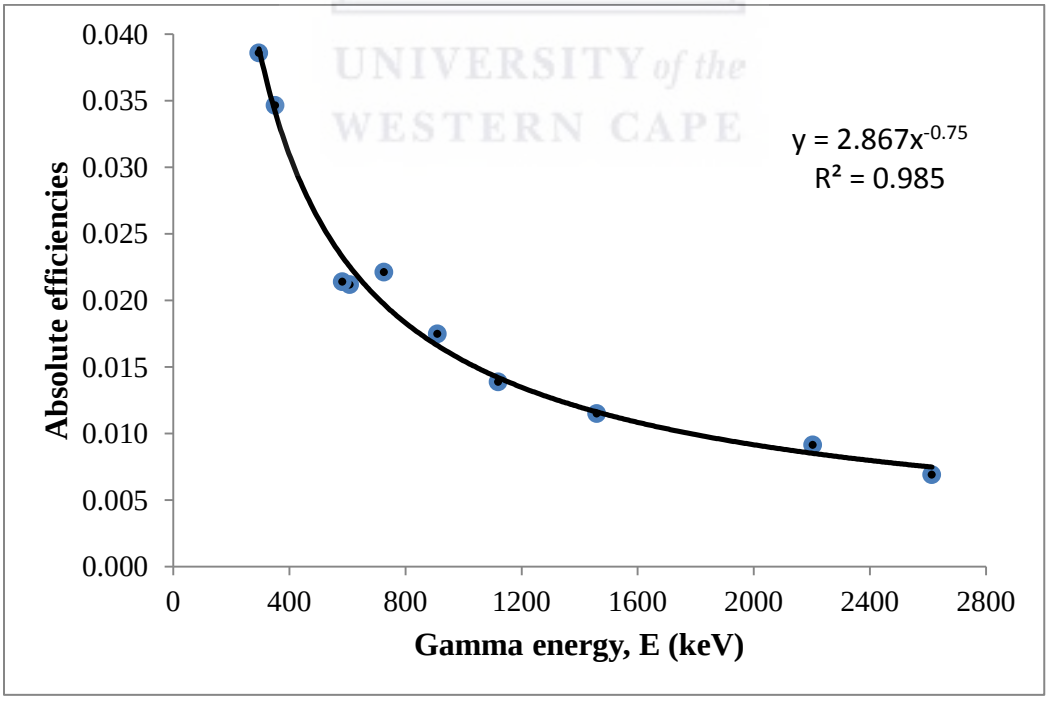

Figure 3.19: The absolute photopeak efficiencies determined using the IAEA standard material sand the KCl powder.

(B) Calibration using relative efficiency approach

Relative efficiency is a simple, inexpensive and effective method for the efficiency calibration of detectors for environmental samples. In this method, the relative efficiency of each sample is determined using gamma lines from the decay series of ^{238}U and ^{232}Th (Croft, 1999). The relative efficiency curves are converted to the measured absolute photopeak efficiency (ε) at 1460 keV obtained by using the KCl (potassium chloride) source which result in the conversion of relative efficiencies to absolute photopeak efficiency (ε) for each soil sample and beach sediment. Using the relative efficiency approach, background spectrum and samples spectra were collected and sample counts were deduced. With the aid of Microsoft Excel the following procedure was followed to generate the efficiency curve:

a) The C_{net} (net counts) from gamma ray lines of interest were obtained by subtracting background counts from each sample counts.
b) Assume that the ^{238}U and ^{232}Th decay series are in secular equilibrium and that the uranium content is determined by the 352 keV line and thorium content by the 338 keV line. The relative efficiency of ^{238}U and ^{232}Th decay chains was determined first by dividing Cnet with I_γ (emission probability) for each gamma line. Then $(Cnet/I_\gamma)_E$ for each gamma line in ^{238}U was divided by $(Cnet/I_\gamma)_{352}$ and for ^{232}Th the ratio of $(Cnet/I_\gamma)_E$ was divided by $(Cnet/I_\gamma)_{338}$.
c) Using equation 3.4, the graph of natural logarithms of ^{238}U relative efficiencies versus energy was plotted.

$$\ln\varepsilon_{\text{relative}} = \ln a + b \ln\left(\frac{E}{E_o}\right) \quad (3.4)$$

The fit parameters (a and b) were obtained from the graph. These fit parameters were used to determine the factor that is needed to normalise the ^{232}Th to the ^{238}U relative efficiencies using the equation:

$$\varepsilon_{\text{relative}} = aE^b \quad (3.5)$$

All the relative efficiency values for thorium were multiplied by this factor. The values obtained in this step represent the normalised thorium relative efficiencies.

d) Again, new fit parameters (a^1 and b^1) were determined based on the new relative efficiency values for uranium and thorium.

e) These relative efficiencies values for uranium and thorium and the 1461 keV gamma line from ^{40}K were used to obtain the final relative efficiencies for all energies.

f) Absolute efficiency calibration – this is found using the KCl sample. First the activity concentration ^{40}K in KCl was determined.

g) To obtain the activity concentration of ^{40}K from the KCl powder (99.5% purity), the KCl powder was counted on the HPGe detector for 3600 seconds. Using the acquired spectrum, net counts in the 1461 keV were extracted and found to be 71 422 counts. The activity of the KCl was then obtained using the equation:

$$A = \lambda N \tag{3.6}$$

where, λ is the decay constant of ^{40}K and N is the number of ^{40}K in KCl powder. But N is calculated as follows,

$$N = N_A . a . n \tag{3.7}$$

where, N_A is Avogadro's number which is equal to 6.02 x 10^{23} atoms/mol (Nir-El Y, 1998), a is the natural abundance of ^{40}K in KCl which is equal to 1.17 x 10^{-4} ± 0.85% (Croft et al., 1999), and n is the number of moles of ^{40}K. The number of moles can be obtained using equation 3.8.

$$n = \frac{m}{M} \tag{3.8}$$

where m is the mass of KCl powder in a Marinelli beaker, 1.291 kg, and M is the molar mass, 74.551 $gmol^{-1}$. Since the half-life ($t_{1/2}$) of ^{40}K is known, that is 4.02 x 10^{16} ± 0.63% seconds (Firestone, 1996), λ can be calculated using:

$$\lambda = \frac{\ln 2}{t_{1/2}} \tag{3.9}$$

The ^{40}K activity concentration in KCl powder was calculated to be 16258 $Bq.kg^{-1}$. By re-arranging equation 3.10, the ^{40}K absolute efficiency is calculated:

$$A = \frac{C_{net}}{\varepsilon_\gamma I_\gamma t_s m} \tag{3.10}$$

h) The ratio of the efficiency of ^{40}K in KCl powder obtained using equation 3.10 above to the relative efficiency of samples calculated using equation 3.7 (step 3) gives a factor (K_f) used to convert all the relative efficiencies to an absolute efficiency curve.

$$K_f = \frac{\varepsilon_{absolute\ 40K}}{\varepsilon_{relative\ 40K}} \quad (3.11)$$

i) The final relative efficiencies are then multiplied by the factor K_f to obtain absolute efficiencies. In fact, thirteen absolute photopeak efficiency curves were generated using the procedure outlined above. An example of the absolute photopeak efficiency curve generated using this procedure outlined above is shown in Figure 3.20. The "a and b" parameters obtained from generated curves are presented in Table 3.6.

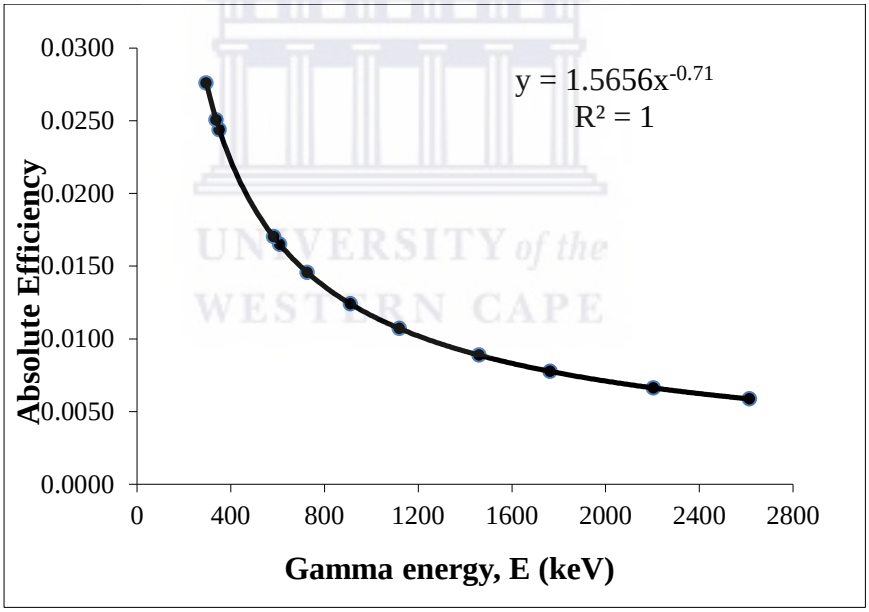

Figure 3.20: The absolute efficiency curve of ^{238}U, ^{232}Th and ^{40}K using KCl.

Table 3.6: The 'a' and 'b' parameters deduced from the efficiency calibration curves using KCl approach.

Location	Code	Parameter a	Parameter b
Msuka	PBS 2	1.455	-0.70
Kukuu soil	PSS 9	0.293	-0.48
Kukuu white	PBS 9C	1.565	-0.71
Wambaa	PBS 11	0.812	-0.62
Tundaua	PBS 12	1.565	-0.71
Nungwi	UBS 14	0.189	-0.42
Pwani Mchangani	UBS 19	0.524	-0.58
Kiwengwa	UBS 20	0.189	-0.42
Uroa	UBS 22	0.564	-0.57
Chwaka	UBS 23	1.473	-0.69
Kizimkazi	UBS 27	0.702	-0.60
Bububu	UBS 35	0.293	-0.48
Mazizini	UBS 37	1.258	-0.68

(C) Calibration using Monte Carlo technique

MCNPX (**M**onte **C**arlo **N**-**P**article e**X**tended) is a general purpose code internationally used for analyzing the transport of gamma rays and neutrons. The code is developed and maintained by Los Alamos National Laboratory [https://mcnp.lanl.gov/]. The technique has been proved to be a useful tool in gamma spectroscopy to correct sample height variations, coincidence summing and self-attenuation (Maurotto et al., 2009). The densities of reference sources used were 1.4 g.cm^{-3}, 1.4 g.cm^{-3} and 1.3 g.cm^{-3} for ^{238}U, ^{232}Th and ^{40}K respectively. On the other hand, the densities of the samples varied from 0.87 g.cm^{-3} to 2.7 g.cm^{-3}. The variations in densities between standard sources used for efficiency calibration and some measured samples may cause variations in detector response due to self-attenuation effects (Croft, 1999; Quindos, 2006; Malain, 2011).

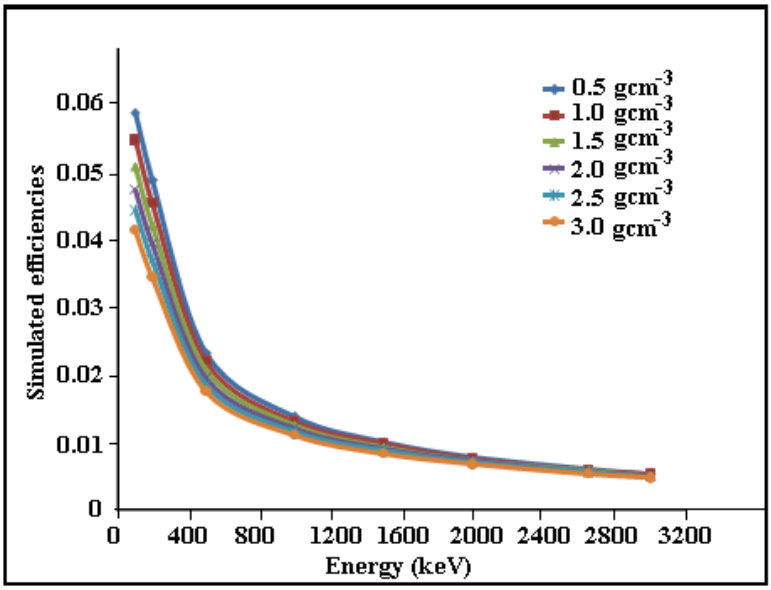

Figure 3.21: MCNPX results for the variation of detector efficiency with energy for different material densities

To address the density variations among the measured samples, the MCNPX code is employed to obtain absolute efficiency values for samples with lower and higher densities than the reference samples. The calculations were performed for this work in collaboration with Dr P. Maleka from NRF/iThemba LABS. The variation of detector efficiency with sample density for different photon energies is presented in Figure 3.21.

It is important to note that the high difference in density and chemical composition of the samples as compared to standard sources may lead to possible error in computed efficiency values. The variation of detector efficiency with energy for different sample densities is depicted in Figure 3.22. The simulated efficiencies obtained from the MCNP simulation were used to calculate the sample activity concentration using equation 3.10.

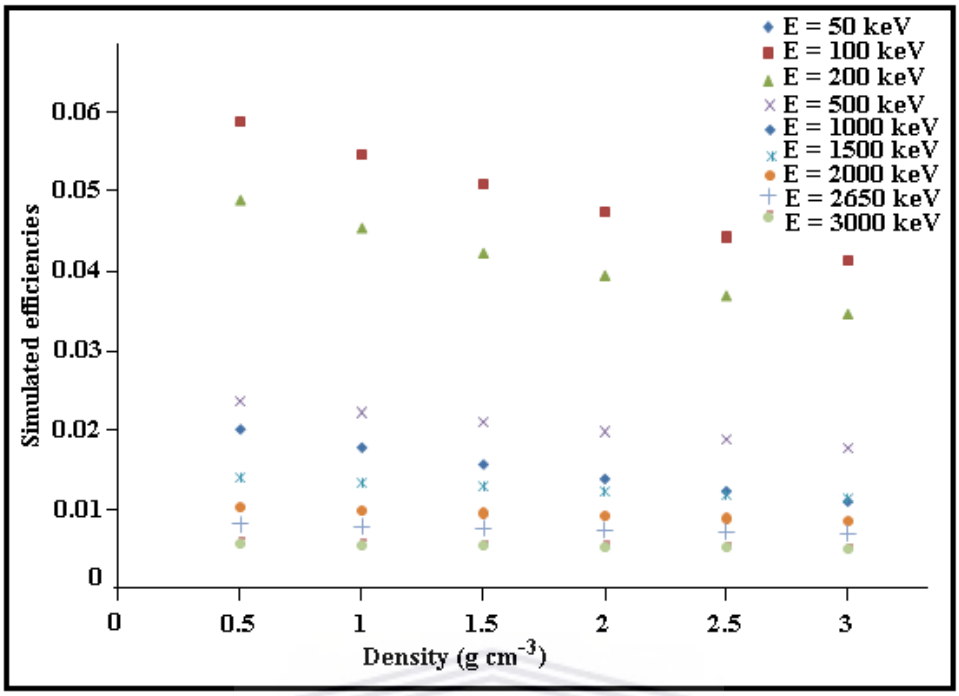

Figure 3.22: MCNPX results of the variation of detector efficiency with sample density for different gamma energies

The simulated efficiencies were used to generate 'a' and 'b' parameters (Table 3.7) for samples with density higher or lower than the standard sources.

Table 3.7: The 'a' and 'b' parameters deduced from the efficiency calibration curves using MNCP approach.

Location	Code	Parameter a	Parameter b
Maziwa Ng'ombe	PBS 4	1.706	-0.71
Kukuu black	PBS 9A, 9B	1.112	-0.66
Tundaua	PBS 12	1.473	-0.69
Kigunda	USS 15	1.706	-0.71
Kidoti	USS 16	1.706	-0.71
Mtende	USS 26	1.706	-0.71
Muyuni	USS 28	1.706	-0.71
Tunguu	USS 29	1.706	-0.71
Dunga	USS 30	1.706	-0.71

3.5 Minimum Detectable Activity

Minimum detectable activity (MDA) is the smallest amount of radioactivity that could be reliably determined for a particular measurement (Gilmore, 1988; Knoll, 2010; Cember and Johnson, 2009). The MDA depends on various factors such as sample composition, the detector efficiency, the energy of the radiation, the source-detector distance, the background radiation level and the measurement time (Debertin, 1988). In this work the background spectrum for gamma measurements was collected using tap water placed in one litre Marinelli beaker counted for 599500 seconds. MDA values were determined according to equation 3.12 (Currie, 1968).

$$\mathrm{MDA} = \frac{2.71 + 4.65\sqrt{N_B}}{I_\gamma \varepsilon_\gamma t} \qquad (3.12)$$

where; N_B is the background count for the region of interest of each radionuclide, t is the background measurement time, I_γ is the gamma emission probability for this line and ε_γ is the photopeak efficiency for the measured γ-ray energy.

The MDA of the HPGe system as used was determined for t = 599500 s from the background measurement using equation 3.12 and ranges from 0.03 Bq for ^{238}U (using 295.2 keV, ^{214}Pb) to a maximum value of 0.47 Bq for ^{40}K. These values show the smallest amount of radioactivity that can be detected and distinguished from the tap water at the respective energies.

3.6 Determination of activity concentrations in samples

Once the detector is energy and efficiency calibrated, the background distribution due to NORM in the environment around the detector was determined. This was achieved by collecting the spectrum using an empty Marinelli beaker for 230317 seconds. The spectra for the samples were collected in the same manner as the background spectrum, with measurement time varying from one sample to another ranging from 24000 to 86400 seconds. A total of 22 samples were measured using the HPGe detector (see Table 3.3). The uncertainty in the determination of the radionuclides, taking into account the

statistical uncertainty and the calibration uncertainty, varied between 5% and l0%, at the 95% confidence level.

The identification of individual radionuclides in the measured spectra was carried out based on their characteristic gamma ray energies. The net counts (Cnet) were extracted which were corrected for the contribution of the background using the relation (Gilmore, 2008):

$$C_{net} = C_s - \frac{t_s}{t_b} C_b \quad (3.13)$$

where C_b is the background counts, C_s is the sample counts, t_b is the time to collect the background spectrum and t_s is the time used to collect the sample spectrum.

The activity concentrations (activity per unit mass of the sample), A, in Bq.kg^{-1} of ^{238}U (^{226}Ra) in soil and beach sands were determined using equation 3.10. The γ-lines of ^{238}U daughters: ^{214}Pb (295 keV, 352 keV) and ^{214}Bi (609 keV) were used. On the other hand the activity concentration of ^{232}Th was determined through gamma emissions of ^{228}Ac (911 keV) and ^{208}T1 (583 keV, 2614 keV). The activity concentration of the singly decaying nucleus, ^{40}K was calculated directly by measurement of its gamma ray transition at 1460.8 keV. The 186 keV peak from ^{226}Ra was not utilised since it will overlap with the 185.7 keV γ-line peak from ^{235}U. The calculated activity concentrations obtained using the HPGe detector from various locations is presented in chapter 4, subsection 4.3.

3.6.1 Estimation of ^{40}K in samples with high ^{232}Th concentration

From the HPGe measurements, it was observed that the sample PBS 9A and PBS 9B are rich in thorium. For this reason, the gamma decay of ^{228}Ac (1459.2 keV) and that of ^{40}K (1460.8 keV) are very close and may interfere (De Meijer et al., 1997b). Subsequently, the contributions to the composite peak at the 1460.8 keV (due to ^{228}Ac) in the gamma ray spectrum may be over estimated and therefore need to be corrected (De Meijer at al., 1997b). Since the decay of ^{228}Ac also emits other gamma rays at several other discrete energies and using peak data from the IAEA/RTh-1 standard source used for energy

calibration, the ratio between the two discrete gamma ray emission lines can be calculated. The ratio of ^{228}Ac from the standard source and from the sample should be the same. The gamma energy yield at 911 keV can be compared with the 1459.5 keV to obtain this ratio. The true counts thus can thus be obtained as follows (Bajoga, 2016):

$$\left[\frac{C_{1459\ keV}}{C_{911\ keV}}\right]^{PBS\ 9A,B} = \left[\frac{C_{1459\ keV}}{C_{911\ keV}}\right]^{IAEA/RTh-1} \quad (3.14)$$

$$[C_{1459\ keV}]^{PBS\ 9A,B} = \left[\frac{C_{1459\ keV}}{C_{911\ keV}}\right]^{IAEA/RTh-1} x\ [C_{911}]^{PBS\ 9A,B} \quad (3.15)$$

where C_{1459} is the net counts in the 1459.5 keV gamma peak of ^{228}Ac obtained from samples PBS 9A, PBS 9B and IAEA/RTh-1.

Using the IAEA/RTh-1standard source spectrum acquired for energy calibration, net counts in the 911 keV and 1459 keV were extracted and found to be 52842 and 1113 counts respectively. On the other hand, the net counts in the 911 keV peak from the PBS 9A sample spectrum was found to be 2081648 counts. The contribution of the 1459 keV gamma-ray to the composite peak was then obtained using the equation 3.15.

Once the contribution of the 1459 keV line in ^{228}Ac is known, equation 3.15 was used to get the true number of counts of the ^{40}K recorded at 1460.1 keV. Tthe ^{40}K net counts was calculated using equation 3.16 and found to be 1793 counts.

$$[C_{1460.1\ keV}]^{PBS\ 9A} = C_{Total} - [C_{1459.5\ keV}]^{PBS\ 9A} \quad (3.16)$$

where C_{Total} is the counts in the composite peak at 1460.1 keV in the γ-ray spectrum.

3.7 Quality control

In this study the HPGe detector used for sample measurements was efficiency calibrated using three different techniques as mentioned in subsection 3.4.4.2. To examine the accuracy of the calculated efficiencies obtained using the KCl and MNCP approaches, a

comparison is made using activity concentration of three samples as shown in Table 3.8. The densities of these samples are comparable to the IAEA standard sources used for efficiency calibration of the detector.

Table 3.8: Comparison of three efficiency calibration techniques

	Activity concentration ($Bq.kg^{-1}$)					
Samples	**^{238}U**			**^{40}K**		
	IAEA	**KCl**	**MNCP**	**IAEA**	**KCl**	**MNCP**
PBS 9C	18 ± 1	18 ± 1	16 ± 0.9	458 ± 23	439 ± 22	403 ± 20
PBS 12	8 ± 0.4	8 ± 0.4	8 ± 0.4	428 ± 21	428 ± 20	428 ± 21
UBS 37	12 ± 0.6	12 ±0.6	11 ± 0.5	359 ± 17	341 ± 16	341 ± 16

From Table 3.8, the activity concentrations of ^{238}U and ^{40}K calculated using absolute efficiencies derived using three efficiency calibration techniques mentioned in section 3.4.4.2 show good agreement between them.

3.8 Estimation of absorbed dose rates and radiation risk factors

External exposure due to irradiation from γ-rays from natural radionuclides emitted by the radioactive decay of ^{40}K, ^{226}Ra, and ^{232}Th from beach sand and soils occurs externally (outdoors) and internally (indoors). The degree of any associated hazard as a result of radiation exposure arising from natural radioactivity is assessed using the absorbed dose rate and the annual effective dose equivalent.

3.8.1 Gamma absorbed rate in air (D)

Gamma absorbed dose rate in the air at 1 m above the ground is one of the parameters with a direct connection between radioactivity concentrations of natural radionuclides and the exposure they cause. Assuming natural radionuclides are uniformly distributed in the environment, the outdoor air absorbed dose rates at 1 m above the ground are determined from the activity concentrations of the relevant radionuclides (i.e ^{226}Ra, ^{232}Th

and ^{40}K). The expression that follows is mostly utilised to calculate dose rate (Tzortzis et al., 2003; UNSCEAR, 2008):

$$D\ (nGyh^{-1}) = CF_K \times A_K + CF_{Ra} \times A_{Ra} + CF_{Th} \times A_{Th} \qquad (3.17)$$

where; A_K, A_{Ra} and A_{Th} and are the activity concentration of ^{40}K, ^{226}Ra and ^{232}Th respectively, and CF_K, CF_{Ra} and CF_{Th} are conversion factors (see Table 3.9) for ^{40}K, ^{226}Ra and ^{232}Th, respectively.

Table 3.9: Conversion factors for various radionuclides as deduced from various studies.

Nuclide	**BECK** (Beck et al., 1968)	**SAITO** (Saito et al., 1995)	**GEANT** (Clouvas et al., 2000)	**MNCP** (Clouvas et al., 2000)	**MC** (Clouvas et al., 2000)
^{238}U series					
^{214}Pb	0.04720	0.05460	0.04342	0.04413	0.04413
^{226}Ra	-	0.00125	0.00100	0.00092	0.00099
^{214}Bi	0.37800	0.40100	0.35554	0.33849	0.38668
Total	**0.43000**	**0.46300**	**0.39996**	**0.38092**	**0.38668**
^{232}Th series					
^{228}Ac	0.27800	0.22100	0.19594	0.18526	0.19120
^{212}Bi	0.02120	0.02720	0.02383	0.02256	0.02305
^{224}Ra	-	0.00214	0.00167	0.00156	0.00167
^{208}Tl	0.32100	0.32600	0.30312	0.28944	0.28871
^{212}Pb	0.02120	0.02770	0.01917	0.01796	0.01926
Total	**0.66600**	**0.60400**	**0.54373**	**0.51678**	**0.52389**
^{40}K	**0.04220**	**0.04170**	**0.03995**	**0.03780**	**0.03808**

In equation 3.17, it can be observed that ^{226}Ra is introduced instead of ^{238}U. This is because about 98.5% of the radiological effects of the ^{238}U series are produced by ^{226}Ra and its decay products. The dose conversion factors reported by various studies (Beck et

al., 1968; Saito et al., 1995; Clouvas et al., 2000) are shown in Table 3.9. In this study, the dose conversion factors derived by Saito et al. (1995) have been used.

3.8.2 Annual Effective Dose Equivalent (AEDE)

The absorbed dose rate in air at 1m above the ground surface discussed in the section 3.8.1, does not directly give the radiological risk to which a human being is exposed (Jibiri et al., 2007). In order to make an estimate for the radiological risk from external gamma radiation due to ^{226}Ra, ^{232}Th and ^{40}K, the absorbed dose rate is converted to the annual effective dose equivalent. The estimation of this radiological parameter is achieved by taking into account two conversion factors, namely the occupancy factor (OF) and the absorbed dose rate in air to effective dose conversion factor (CF). The occupancy factor is the time people spend at a particular location. Since human beings are expected to spend about 20% of their time outdoors, UNSCEAR (2008) has proposed 1752 h y^{-1} (20%) of the time spent outdoors for the outdoor occupancy factor and 7008 h y^{-1} (80%) of the time spent indoor as indoor occupancy factor.

For this study, the default occupancy factors of 20% and 80% for outdoor and indoor, respectively, have been used to calculate ex-situ annual effective dose equivalent for soil samples. On the other hand, various occupancy factors have been utilised to calculate outdoor annual effective dose equivalent in beach sands. The reason for using different occupancy factors in estimating outdoor annual effective absorbed dose equivalent in beach sands is based on the fact that the time spent on the beach by users differ greatly. Hence, three categories of people (locals, tourists and hotel workers) have been considered based on the minimum and maximum time that could be spent by each category on the beach (Table 3.10).

Table 3.10: Occupancy factors for different categories of peoples residing or visiting Zanzibar beaches.

Category of people	Minimum time	Maximum time
Locals	8 hours per day, 1460 hy^{-1}	10 hours per day, 1752 hy^{-1}

Tourists during holidays	42 hy^{-1}	105 hy^{-1}
Hotel workers	208 hy^{-1}	700 hy^{-1}

The annual effective dose equivalent was estimated using the expression (Tzortzis et al., 2004):

$$\text{AEDE } (\mu\text{Svy}^{-1}) = \text{D} \times \text{CF} \times \text{OF} \times 10^{-3} \quad (3.18)$$

where D is the absorbed dose rate in air, CF is the conversion factor from absorbed dose in air to effective dose received by adults which is 0.7 $Sv.Gy^{-1}$ (UNSCEAR, 2008; Ramasamy et al., 2011) and OF is the occupancy factor.

3.9 Energy Dispersive X-Ray Fluorescence (XRF)

Beach sand deposits are composed mainly of feldspar, quartz and other minerals concentrated along the coasts as a result of weathering or erosion processes (Papadopoulos et al., 2015). Heavy minerals found along coasts in various places worldwide include; garnet, ilmenite, monazite, rutile, sillimanite and zircon (Alam et al., 1999; Freitas and Alencar, 2004). These minerals often contain high amounts of Rare Earth Elements (REE) such as U and Th (Alam et al., 1999; Freitas and Alencar, 2004).

In this study beach sand samples that were identified as important based on the radiometry were sent to the CAF (**C**entral **A**nalytical **F**acility) at Stellenbosch University for further analysis by XRF and ICP-MS. The Varian AA 240 FS X-ray diffractometer available at CAF was used for major element analysis of selected samples. The system is coupled with Cu-Kα radiation of 40 kV and a current of 40 mA. The λ for Kα was 0.1541 nm, scanning rate was 1.5º/min, while a step width of 0.05° was used over the 2θ range. It is also equipped with a 400 W Rh window X-ray tube which has a 75 um Be window, and a Si(Li) semiconductor detector with a resolution of less than 150 eV coupled to a sensitive preamplifier (SPECTRO, 2000).

The XRF operation involves the bombarding a sample with X-rays photons. When an X-ray beam hits a sample, an inner shell electron in the sample is excited by an incident

photon in the X-ray region. When a given atom fills the gap of the ejected electron, by the de-excitation from a higher energy level, the energy difference between the two shells appears as an X-ray. The X-ray spectrum acquired during the excitation and de-excitation process reveals a number of characteristic peaks. Since each element generates a unique level in this replacement process, a detector is used to convert produced characteristic X-rays into electric signals. The signals produced are digitised using the spectrometer's electronics and stored in the personal computer for display and analysis. The energy of the peaks leads to the identification of the elements present in the sample (qualitative analysis), while the peak intensity provides the relevant or absolute elemental concentration (semi-quantitative or quantitative analysis).

Loss on ignition (LOI) test was carried out by placing each sample in an oven heated to 1000°C before any measurement was carried out. This allows volatile content in the sample to escape. The LOI is made of contributions from the volatile compounds such as water (H_2O), chlorine (Cl), carbon dioxide (CO_2), fluorine (F) and sulphur (S) as well as organic matters. Potassium (K) and sodium (Na) also escape when a sample is heated for too long. The prepared sample (in powder) on fused glass bead was analysed for major elements. The diffractograms were recorded and the phase identification was done.

Table 3.11: Locations and number of samples analysed for major element analysis.

Location (s)	**Number of samples**	**Location (s)**	**Number of samples**
Vumawimbi	1	Wambaa	1
Tumbe	1	Kiwengwa	1
Maziwa Ng'ombe	1	Uroa	1
Kukuu	7	Jambiani	1
Makunduchi	1	Bububu	1
Msuka	2	Kizimkazi	1
Ndagoni	1	Tundaua	1

The major elements and their corresponding concentrations as found in sample PBS 9A from Kukuu are depicted in Table 3.12 as an example of results obtained. More detailed discussions on these major elements analysis will follow in Chapter 5.

Table 3.12: The major elements found in sample PBS 9A

Elements	Concentration (%)
Al_2O_3	0.69
CaO	0.17
Cr_2O_3	0.14
MgO	0.57
MnO	0.65
P_2O_5	0.01
SiO_2	3.90
TiO_2	41.02
Fe_2O_3	33.50
K_2O	0.02

3.10 Induced Coupled Plasma Mass Spectrometry (ICP-MS)

ICP-MS is among the most successful techniques in many analytical laboratories for the accurate and precise elemental determination for different applications. There are a number of different ICP-MS designs commercially available today. Each design has its own strengths and weaknesses, but they all share many similar components. These include nebulizer, spray chamber, plasma torch, interface and detector, but can differ quite significantly in the design of the mass spectrometer and in particular the mass separation device (Brogioli, 2012; Evans, 2016).

In this study, trace element analyses were carried out on an ICP-MS (ICP-MS-Perkin Elmer SCIEX, Model ELAN R DRCII) at the University of Stellenbosch. Generally, the principle of the ICP-MS technique is based on the assumption that, ions may be generated in a suitable ionising source such as an ICP for all elements in the sediment. Once the sample is introduced for plasma spectroscopy, ions are physically extracted by the plasma into the mass spectrometer and measured using ion detector. Sample introduction for plasma spectrometry is generally accomplished using solution

nebulisation. Sample solutions are aspirated by a nebuliser which shatters the liquid into fine droplets using an Argon stream of approximately 1 litre/minute. These droplets are directed into a spray chamber which removes the unsuitable larger material, and allows only the finest spray to pass into the plasma (Gray, 1983; Brogioli, 2012; Evans, 2016). The ICP-MS offers very low detection levels. The analytical accuracy was checked by analysing international standards (Marine mud / MAG-1). A total of 20 samples (Table 3.11) from various beaches in Zanzibar were analysed.

In an attempt to assess the role of trace and rare earth elements on activity concentration of ^{238}U and ^{232}Th and provenance of beach sand; major and trace elements were analysed. Table 3.13 provides some trace elements found in sample PBS 9A. Among the trace elements found with high concentration in sample PBS 9A is zircon.

Zircon (Zr) is one among the most stable trace element commonly found in rocks; beach and dune sand deposits (Murtty et al., 2007; Laxmi and Rao, 2010). Due to its high melting point, chemical inertness, low thermal conductivity, thermal shock resistance, and low expansion, the use zircon in various mineral industries has been increased over the years. Zircon is used in the ceramic industry, specifically in the manufacture of tiles, sanitary materials, and porcelain products. Owing to high demand of zircon, the attention of engineers, scientists and other users to exploit zircons from different deposits are priority at present. The concentration of zircon along coasts can be attributed to its ability to defy weathering and high specific gravity (Garnar, 1984). Detailed analysis of major and trace elements is presented in Chapter 5, section 5.2.

Table 3.13: The trace elements measured in sample PBS 9A

Element	Concentration (ppm)	Element	Concentration (ppm)
Zr	42250.35	Nb	266.06
V	484.88	Y	147.41
La	602.11	Th	275.43
Nd	463.39	U	42.05
Ce	1132.14	V	262.74

Sr	25.34	Ba	40.13
Rb	0.55		

CHAPTER 4

Results and Discussions on natural radionuclides

4.1 Introduction

Natural radionuclides are present everywhere in the Earth's environment and are widely distributed. The distributions of natural radionuclides are influenced by the local geology and geographical conditions and as such they vary from place to place (Taskin et al., 2009). The natural radioactivity in the environment is usually determined from the ^{238}U, ^{232}Th and ^{40}K contents (OECD, 79). Studies on natural radioactivity have been previously carried out in soil and beach samples in many parts of the world (Patel et al., 1991; Baeza et al., 1992; 1994, Ramli, 1997; Noureddine, 1997; Kannan et al., 2002; Singh et al., 2003, 2005; Veiga et al., 2006; Mehra et al., 2006; Al Sulaiti et al., 2010; Santawamaitre et al., 2011; Arnedo et al., 2013, Kaniu et al., 2018).

This chapter presents the results of in-situ and ex-situ gamma ray measurements of natural radionuclides in beach sands and soils from different locations in Zanzibar. The activity concentration results of ^{238}U, ^{232}Th and ^{40}K and its associated radiological risks are presented and discussed in this Chapter. The results show surprisingly large variations, including the discovery of a deposit of heavy mineral sand on one beach.

4.2 Activity concentrations in beach sand samples

The activities of ^{40}K, and the ^{238}U and ^{232}Th decay series in the beach sand samples collected from different beach locations of the Zanzibar coastal environment are reported in Table 4.1 and shown in Figure 4.1. When the activity of ^{238}U and ^{232}Th is mentioned in this thesis, the value given is under the assumption of secular equilibrium and the activity of the relevant decay series is implied. The lowest (2 $Bq.kg^{-1}$) and highest (1055 $Bq.kg^{-1}$)

^{238}U activity concentration levels were observed in samples PBS 2 and PBS 9A collected from Msuka beach and Kukuu beach respectively. The ^{232}Th activity concentration varies from below detectable limit (BDL) to 2671 Bq.kg^{-1} with a weighted average of 1.0 Bq.kg^{-1}. The lowest activity concentration was measured in sample PBS 4 from Msuka beach and the highest activity concentration was observed from sample PBS 9A from Kukuu beach.

Table 4.1: Activity concentration of ^{40}K, ^{238}U and ^{232}Th in Bq.kg^{-1} of beach sand determined using the HPGe detector.

Sample Code	**Activity concentration (Bq.kg^{-1})**		
	^{40}K	**^{238}U**	**^{232}Th**
PBS 2	381.0 ± 18.9	2.00 ± 0.09	1.0 ± 0.07
PBS 4	BDL	3.0 ± 0.1	BDL
PBS 9A	205.0 ± 10.0	1055.0 ± 48.8	2671.0 ± 101.8
PBS 9B	109.0 ± 5.0	565.0 ± 26.2	803.0 ± 30.9
PBS 9C	439.0 ± 22.0	18.0 ± 0.9	10.0 ± 0.5
PBS 11	471.0 ± 23.4	9.0 ± 0.5	12.0 ± 0.6
PBS 12	428.0 ± 20.4	8.0 ± 0.4	12.0 ± 0.6
UBS 14	3.0 ± 0.1	2.0 ± 0.1	1.0 ± 0.04
UBS 19	9.0 ± 0.5	3.0 ± 0.1	1.0 ± 0.11
UBS 20	7.0 ± 0.4	3.0 ± 0.1	1.0 ± 0.04
UBS 22	14.0 ± 2.0	5.0 ± 0.6	1.0 ± 0.01
UBS 23	351.0 ± 17.7	12.0 ± 0.6	18.0 ± 1.0
UBS 27	11.0 ± 0.5	5.0 ± 0.7	2.0 ± 0.1
UBS 35	409.00 ± 19.0	2.0 ± 0.1	2.0 ± 0.1
UBS 37	341.0 ± 15.8	12.0 ± 0.6	18.0 ± 0.9
Minimum	BDL	2.0 ± 0.1	1.0 ± 0.1
Maximum	471 ± 23	1055 ± 48	2670 ± 100
Weighted Average	**4**	**4**	**1**

BDL stands for below detectable level

In general, the activities of ^{238}U and ^{232}Th in beach sand in the studied area are extremely low with the exception of samples PBS 9A and PBS 9B. In these two samples the ^{238}U and ^{232}Th activity concentrations are much higher (see Table 4.1and Figure 4.2). These

samples are black in colour collected at Kukuu beach, Southern Pemba (see Figure 3.1). The very high ^{238}U and ^{232}Th activity concentrations in samples PBS 9A and PBS 9B can be attributed to the presence of heavy minerals in the sample composition. The presence of heavy minerals such as ilmenite, rutile, monazite, zircon, magnetite and garment in beach sands indicates the presence of significant amount of ^{238}U and ^{232}Th (Kannan et al., 2002; Mohanty et al., 2004; Ramasamy et al., 2014). Other factors that can affect the radioactivity level in any geologic structure include sand type and formation, ambient environment and geochemical properties (El-Arbi, 2005, Papadopoulos et al., 2015). Moreover, transport processes can also be an important factor which can affect the radioactivity levels of sediments (NCRP 1987; Ebaid, 2010).

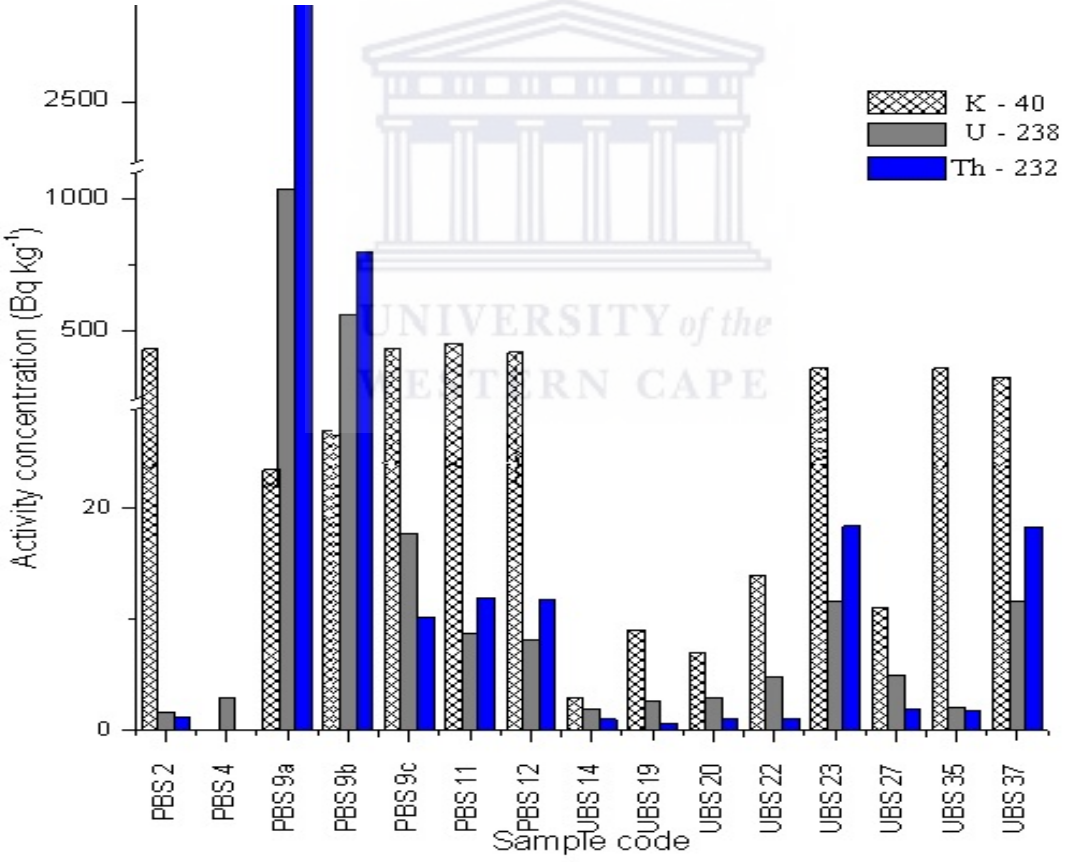

Figure 4.1: Activity concentration of ^{40}K, ^{238}U and ^{232}Th in beach sand

From the Table 4.1, it can be seen that the ^{40}K activity concentration ranges from below detectable limit (BDL) to 471 Bq.kg^{-1} with a weighted average of 3.62 Bq.kg^{-1}. The lowest ^{40}K activity concentration recorded below detectable limit was found in sample PBS 4 collected from Maziwa Ng'ombe beach. The highest ^{40}K activity concentration (471 Bq.kg^{-1}) was recorded in sample PBS 11 from Wambaa beach. In some samples (UBS 14, UBS 19, UBS 20, UBS 22 and UBS 27), the measured ^{40}K activity concentration was less than 20 Bq.kg^{-1}, much below typical world averages. These samples were collected at the northern, southern and eastern coast of Unguja Island. The beaches which yielded low activity concentrations of ^{40}K, ^{238}U and ^{232}Th are among the famous tourist sites in Zanzibar; namely; Kiwengwa, Kizimkazi, Pwani Mchangani and Nungwi.

The very low activity concentration measured in most of the beach samples in this study may be attributed to the presence of shells and carbonates in these samples. The analysis of major elements of these samples shows high calcium carbonate content (see Chapter 5, section 5.2). The findings of this work are consistent with previous findings confirming that sediments rich in carbonates are poor in ^{40}K concentration (UNSCEAR, 2008). On the other hand, some beaches from both Pemba and Unguja Islands (see Table 4.1and Figure 4.1) have intermediate to slightly higher ^{40}K activity concentration values up to 471 Bq.kg^{-1}. These moderate and slightly higher values of ^{40}K activity concentration may be due to the presence of potassium feldspar in the mineral matrix of these samples. The highest value of ^{40}K activity concentration found in this work (471 Bq.kg^{-1}) is slightly higher than the worldwide average value (412 Bq.kg^{-1}) as reported by UNSCEAR, (2008).

The weighted average activity concentrations of ^{40}K, ^{238}U and ^{232}Th in this work are 4, 4 and 1 Bq.kg^{-1} respectively. According to UNSCEAR (2008) the mean activity concentrations of ^{40}K, ^{238}U and ^{232}Th in beach sediments are 30, 35 and 412 Bq.kg^{-1} respectively. This reveals that the average radioactivity concentration levels in beach sediments in Zanzibar are far lower than the corresponding values obtained worldwide, if the very high levels found at Kukuu beach are excluded.

4.3.1 Comparison of activity concentrations of ^{40}K, ^{238}U and ^{232}Th

The activity concentrations of ^{40}K; ^{238}U and ^{232}Th in beach sand in this study have been compared with other countries as shown in Table 4.2. The ^{40}K activity concentration in the Zanzibar beach sand (BDL to 443 $Bq.kg^{-1}$) is higher than the activity concentration from Balochistan coast (7 to 20 $Bq.kg^{-1}$), Rizhao coasts (8 to 35 $Bq.kg^{-1}$) and Adaman coasts (3 to 24 $Bq.kg^{-1}$). In comparison to the literature values, the weighted average activity concentration of ^{40}K (4 $Bq.kg^{-1}$) obtained in this study is lower than the average values reported by other authors for Montenegrin coasts (7 $Bq.kg^{-1}$), Egypt coasts (21 $Bq.kg^{-1}$) and Norway coasts (43 $Bq.kg^{-1}$).

Although the range of ^{40}K activity concentration in Zanzibar beaches is higher than some of the beaches listed in Table 4.2, its values are lower compared to reported values from Kerala coasts (BDL to 23030 $Bq.kg^{-1}$), Rio de Janeiro (7 to 963 $Bq.kg^{-1}$) and Espirito Santo coast (7 to 5553 $Bq.kg^{-1}$). Furthermore, the weighted average activity concentration of ^{40}K in this study is lower than the values reported by other authors (Table 4.2).

Although the range of the activity of ^{238}U and ^{232}Th in this study is higher due to presence of heavy mineral in samples PBS 9A and PBS 9B, the average activity concentration is lower compared to beach sand in other regions of the world (see Table 4.2). The activity of ^{238}U in PBS 9A and PBS 9B (black sand samples) are lower than the black sand from Kerala, Aegean sea and Espiritu Santo coast (see Table 4.2). However, the reported values of ^{238}U activity of black sand from Norway coast, Bangladesh coast and Red sea coast were lower than black sand in this study.

The maximum of the ^{232}Th activity concentration values obtained in this study is higher compared to Kerala beach sand, Rio de Janeiro coast, coasts of Egypt and Espiritu Santo coast as reported by other authors in Table 4.2.

Table 4.2: Activity concentrations of ^{40}K, ^{238}U and ^{232}Th of the Zanzibar coasts and other coastal zones in the world. Number in brackets represents the average value.

Location	**Activity concentrations (Bq.kg^{-1})**			**Reference**
	^{40}K	**^{238}U**	**^{232}Th**	
Zanzibar coasts	3 – 443 (4)	2 – 1067 (4)	1 – 2737 (1)	This study
Kerala beaches, India	BDL – 23030 (2660)	BDL – 15170 (488)	BDL – 713 (362)	Shetty et al. (2010)
Balochistan coast, Pakistan	7 – 20 (14)	16 – 29 (23)	43 – 39 (38)	Akram et al. (2007)
Rizhao beaches, China	8 – 25 (15)	8 – 17 (12)	883 – 1314 (1079)	Lu et al. (2008)
Adaman coasts , Thailand	3 – 35 (19)	3 – 24 (12)	11 – 654 (344)	Malain et al. (2010)
Beaches of Aegean sea, Turkey	97 – 4360 (532)	79 – 1885 (290)	687 – 1421 (1160)	Orgun et al. (2007)
Montenegrin coast (Yugoslavia)	1 – 12 (7)	2 – 16 (8)	16 – 263 (150)	Vukotic et al. (1998)
Rio de Janeiro coast (Brazil)	7 – 963 (95)	5 – 286 (33)	32 – 888 (253)	Veiga et al. (2006)
Red sea, Jordan	9 – 16 (12)	9 – 598 (128)	72 – 755 (477)	Ababneh et al. (2010)
Bangladesh coasts	15 – 94 (37.2)	200 – 772 (438)	28 – 129 (60)	Chowdhury et al. (1999)
Norway coasts	12 – 137 (43)	31 – 564 (283)	4 – 52 (21)	Dowdall et al. (2002)
Coasts of Egypt	10 – 34 (21)	25 – 63 (39)	382 – 419 (402)	Eissa et al. (2010)
Espiritu Santo coast (Brazil)	7 – 5553 (675)	5 – 4043 (637)	27 – 412 (121)	Veiga et al. (2006)

4.4 Activity concentrations of ^{40}K, ^{238}U and ^{232}Th in soil samples

The calculated activity concentrations of ^{40}K, ^{238}U and ^{232}Th in soils measured using the HPGe detector collected from various inland locations in Zanzibar are listed in Table 4.3 and shown in Figure 4.2.

Table 4.3: Activity concentration of ^{40}K, ^{238}U and ^{232}Th of soil samples

Sample Code	**Activity Concentration (Bq.kg^{-1})**		
	^{40}K	**^{238}U**	**^{232}Th**
PSS 9	545.0 ± 25.4	27.0 ± 1.2	24.0 ± 1.1
USS 16	98.0 ± 4.0	225.0 ± 11.3	120.0 ± 5.9
USS 15	84.0 ± 4.0	292.0 ± 12.7	60.0 ± 2.6
USS 28	654.0 ± 28.0	60.0 ± 2.8	49.0 ± 1.9
USS 30	153.0 ± 7.2	158.0 ± 7.7	98.0 ± 4.6
USS 29	30.0 ± 1.0	521.0 ± 23.0	87.0 ± 4.0
USS 26	110.0 ± 5.0	256.0 ± 11.6	130.0 ± 5.6
Minimum	30.0 ± 1.0	27.0 ± 1.2	24.0 ± 1.1
Maximum	654 ± 28	521 ± 24	130 ± 6
Weighted Average	**42.0 ± 0.8**	**41.0 ± 0.9**	**42.0 ± 0.8**
World range	140 – 850	17 – 60	11 – 64
World average	412	35	30

The activity concentrations of ^{40}K ranged from 30 to 654 Bq.kg^{-1} with a weighted average of 42 Bq.kg^{-1}. Two samples (PSS 9 and USS 28) had slightly higher ^{40}K activity concentration than the world average concentration of this radionuclide in the soil, which

is 412 Bq.kg^{-1} (UNSCEAR, 2008). The ^{40}K activity concentrations in the other samples were lower by between 2 to 13 times when compared to the worldwide average.

After determining the ^{238}U activity concentration sample PSS 9 had the lowest activity concentration (27 Bq.kg^{-1}) whereas sample USS 29 had the highest activity concentration (520 Bq.kg^{-1}). These samples were from Kukuu and Tunguu respectively.

The higher ^{238}U activity concentration values were also recorded from samples USS 15 (292 Bq.kg^{-1}) and USS 16 (225 Bq.kg^{-1}) collected from Kigunda and Kidoti respectively. In addition, samples USS 26 (256 Bq.kg^{-1}) collected from Mtende, USS 30 (158 Bq.kg^{-1}) from Muyuni and USS 28 (60 Bq.kg^{-1}) from Dunga were found to have higher ^{238}U activity concentration approximately 1.5 to 7 times higher than the world average concentration of this radionuclide in the soil. All samples which showed higher activity concentration of ^{238}U are reddish in colour with an exception of sample USS 28 which is greyish in colour. The range of ^{238}U activity concentration obtained in the study area varied from 28 to 520 Bq.kg^{-1}. According to UNSCEAR (2008), the range of ^{238}U in soil is 17 to 60 Bq.kg^{-1}. The range found in this study is surprisingly large and the maximum values high. The initial measurements with the NaI(Tl) detector on the islands helped in identifying areas where high values were found, which probably implies a bias to higher values in the samples.

For ^{232}Th, the lowest activity concentration was 24 Bq.kg^{-1} found in sample PSS 9 which was collected from Kukuu (close to but not on the beach), whereas the highest activity concentration was 130 Bq.kg^{-1} found in sample USS 26 which was collected from Mtende. With an exception of sample PSS 9, other soil samples were found to have higher activity concentration of ^{232}Th than the world reported average of 35 Bq.kg^{-1} (UNSCEAR, 2008). The range of ^{232}Th activity concentration in soil samples is also higher compared to world ranges of this radionuclide in the soil. The worldwide range of ^{232}Th in soil is 11 to 64 Bq.kg^{-1} (UNSCEAR, 2008).

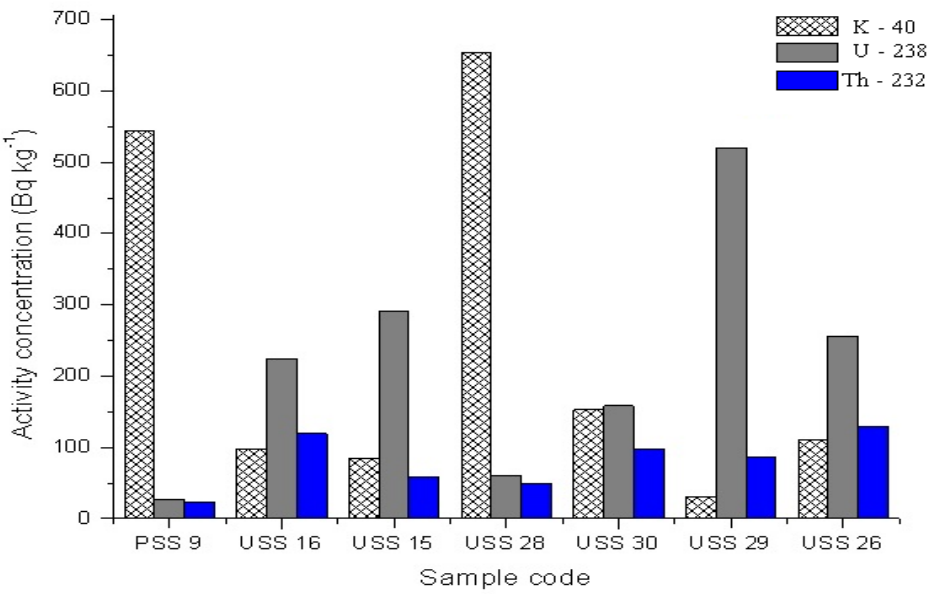

Figure 4.2: Activity concentration of ^{40}K, ^{238}U and ^{232}Th in soil samples

The weighted average activity concentration of ^{238}U and ^{232}Th in measured soil samples are 41 and 42 Bq.kg^{-1} respectively. The world average activity concentrations of ^{238}U and ^{232}Th are 35 and 30 Bq.kg^{-1}, respectively (UNSCEAR, 2008). The average activity concentration values of ^{238}U and ^{232}Th obtained in this study are slightly higher than the world average of these radionuclides in soils.

The higher levels of ^{238}U and ^{232}Th in some soil samples in the studied area could be attributed to their geo-chemical properties as well as geological characteristics of the parent rocks (Myrick et al., 1983; El Taher and Uosif, 2006). The high levels in soils may also be influenced by the use of fertilizers such as phosphate which increase the activity concentration (El Taher and S Makhluf, 2010; Santawamaitre et al., 2011). Based on the findings of this study, it is too early to establish that the higher ^{238}U and ^{232}Th activity concentration is a result of the use of fertilizers or not.

The average ^{40}K activity concentration in the studied soil samples is very low compared to the worldwide average activity concentration of ^{40}K in soils. Only two samples, PSS 9 (545 Bq.kg^{-1}) and USS 28 (654 Bq.kg^{-1}) were found to have higher activity concentration of ^{40}K compared to the world wide reported average. Sample PSS 9 was collected at

Kukuu close to fish landing site while sample USS 28 was collected at the vicinity of Muyuni village. The high activity concentration levels in these samples may be due human activities in these areas (Santawamaitre et al., 2011).

Table 4.4: Activity concentration ($Bq.kg^{-1}$) of ^{40}K, ^{238}U and ^{232}Th in soil samples in various regions in the world. Number in brackets represents the average value.

Location	**Activity concentration ($Bq.kg^{-1}$)**			**Reference**
	^{40}K	**^{238}U**	**^{232}Th**	
Zanzibar soils	**30 – 654 (42)**	**28 – 493 (41)**	**24 – 130 (42)**	**This study**
Greece	12 – 1570 (355)	1 – 238 (25)	1 – 193 (21)	Anagnostakis et al. (1996)
Syria	100 – 378 (247)	1 – 40 (22.2)	11– 25 (18.4)	Othman and Yasmine (1995)
Ireland	8 – 1088 (526)	2.7 – 788 (79)	4 – 479 (104)	O'Dea et al. (1999)
Thailand	178 – 811 (309)	14 – 77 (29)	13 – 143 (30)	Santawamaitre et al. (2014)
Turkey	481 – 807 (667)	19 – 30 (28)	29 – 47 (40)	Taskin et al. (2009)
Spain	617 – 689 (653)	36.2 – 40.5 (38)	38.9 – 43.7 (41)	Baeza et al. (2011)
Malaysia	170 – 430 (310)	49 – 86 (66)	63 – 110 (82)	UNSCEAR (2000)
Portugal	220 – 1230 (840)	26 – 82 (49)	22 – 100 (51)	UNSCEAR (2000)
China	9 – 1800 (440)	2 – 690 (33)	1 – 360 (41)	UNSCEAR (2000)
Pakistan	525 – 602 (562)	25 – 28 (26)	45 – 53 (42)	Akhtar et al. (2004)
Egypt	29 – 650 (320)	6 – 120 (37)	2 – 96 (18)	UNSCEAR (2000)
Japan	15 – 990 (310)	2 – 59 (29)	2 – 88 (28)	UNSCEAR (2000)
United States	100 – 700 (370)	4 – 140 (35)	4 – 130 (35)	UNSCEAR (2000)
World average	**412**	**30**	**35**	**UNSCEAR (2008)**

The observed differences in some results could be attributed to differences in geochemical variations, soil formations and climatic conditions of the study area (Myrick et al., 1983; Kekelidze et al., 2017). Natural radioactivity of soil could also depend on transport processes that were involved since soil formation (Rabesiranana et al., 2008). Gascoyne (1992) pointed out that biochemical and chemical interactions within soil media influence the distribution patterns of ^{238}U, ^{232}Th and their decay products.

In summary, the concentration of radionuclides in beach sands are much lower than in soil samples as expected, with one major exception at Kukuu which will be investigated in Chapter 5. There is surprisingly large variation in soil samples for two relatively small islands.

4.5 Spatial distribution of ^{40}K, ^{238}U and ^{232}Th in the study area

A more detailed study of the distributions of ^{40}K, ^{238}U and ^{232}Th in beach sand and soils has been conducted using the MEDUSA detector (see Chapter 3, section 3.33). Two beaches (Kukuu and Msuka, see Figure 3.1) from Pemba island were mapped. The spatial distribution maps were generated using the MEDUSA γ-ray detector and the Golden Software Surfer® 10 (Surfer®10 Manual, 2011). Data from the MEDUSA γ-ray detector were processed using the Gamman software from MEDUSA Exploration B.V. in Groningen, the Netherlands. The processed data from Gamman were then later transferred to Golden Software Surfer® 10 to generate interpolated maps. Surfer software uses numerous techniques for gridding. These include Inverse Distance to a power, Kriging, Minimum Curvature, Modified Shepard's Method, Natural Neighbour, Nearest Neighbour, Polynomial Regression, Radial Basis Function, Triangulation with Linear interpolation, Moving Average Data Metrics and Local Polynomial (Surfer®10 Manual, 2011; Ongori, 2013). Different gridding techniques provide different interpretations of the data because each method calculates grid node values using a different algorithm.

In this study, the Surfer images were generated using the Natural Neighbour gridding technique to interpolate the spatial distribution maps of ^{238}U, ^{232}Th and ^{40}K in two

beaches (Kukuu and Msuka). The Natural Neighbour gridding technique uses an interpolation algorithm which uses a weighted average of the neighbouring observations, where the weights are proportional to the borrowed area (Surfer®10 Manual, 2011; Ongori, 2013). In addition to the beaches, three places were surveyed on land; namely Kidoti, Tunguu and Mtende. The MEDUSA generated plots and their corresponding interpolated maps using Surfer® 10 software during mobile measurements for ^{40}K, ^{238}U, ^{232}Th and ^{40}K are depicted in Figures 4.4 – 4.18. The colours red, yellow and blue in interpolated maps indicate areas of high, intermediate and low activity concentrations respectively.

4.5.1 Distribution of natural radionuclides on beaches

The ^{238}U activity concentration recorded at Kukuu beach (Figure 4.4) is less than 550 $Bq.kg^{-1}$ on large parts of the beach, while the other part has huge activity concentrations (up to 5500 $Bq.kg^{-1}$). The interpolated map shows zones of the beach with low and very high activity concentrations. This distinct pattern reflects the presence of light and heavy mineral concentrations. The relatively high concentration of ^{238}U as seen in Figure 4.3 was recorded at the section of the beach with the black sand deposits. As mentioned in section 4.2 above, studies on radioactivity on beach sand have shown that black sand are rich in heavy minerals which in turn results in elevated levels of ^{238}U and ^{232}Th (Orgun et al., 2007; Shetty et al., 2010; Ramasamy et al., 2013).

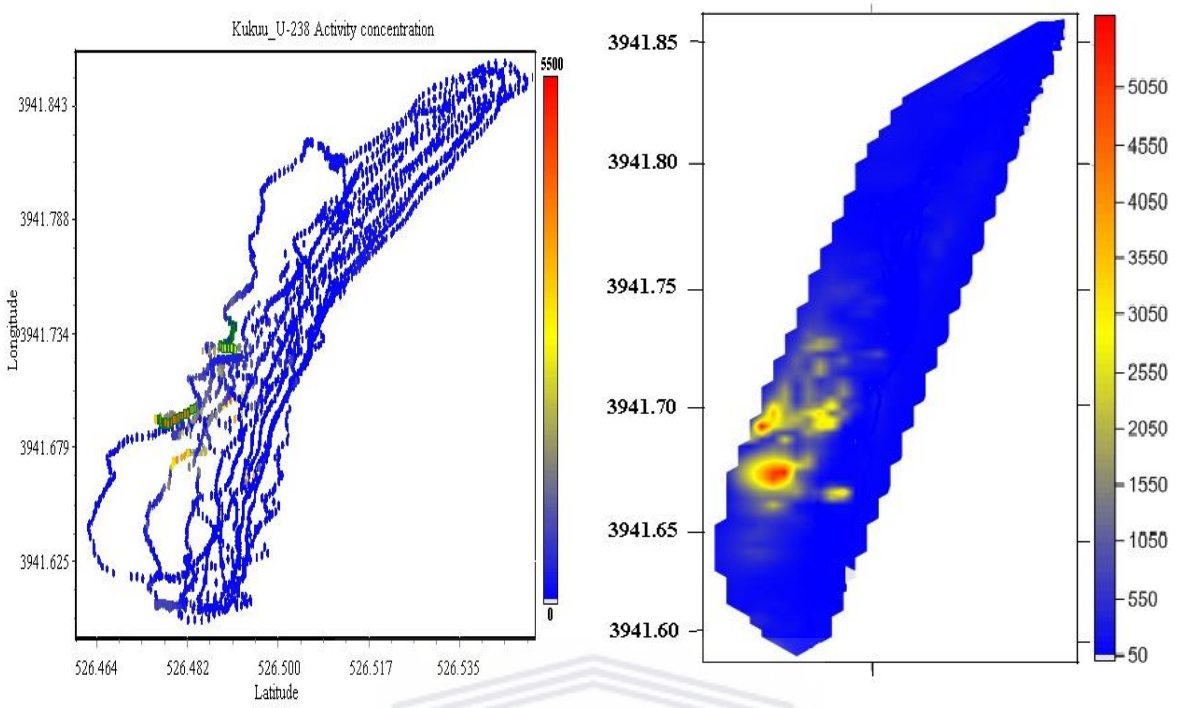

Figure 4.3: A map of Kukuu beach (left) showing ^{238}U activity concentration measured using the MEDUSA γ-ray detector and an interpolated map (right) corresponding to the map on the left. The same notation for latitude and longitude as described in the caption to Figure 3.10 is used in this chapter.

The variation of the activity concentration of ^{232}Th at Kukuu beach was found as illustrated by Figure 4.4. The relatively high ^{232}Th concentration (1050 Bq.kg^{-1}) was measured at the same area of the beach which is localised with black sand deposit. Other sections nearby are also found to have alternating light and dark colour bands depicting different spectroscopic responses during field measurements. This part of the beach appeared to be the one found with black sand during the field visit.

Close inspection of Figure 4.5 shows the concentration of ^{40}K follows a similar pattern as ^{238}U and ^{232}Th. The high concentration of ^{40}K is measured on the section of the beach with black sand and sections close to it. It was also found that high values of activity concentration for ^{40}K were measured close to the land adjacent to the beach. The high levels of ^{40}K close to the land may be caused by soil eroded from land and deposited on the beach.

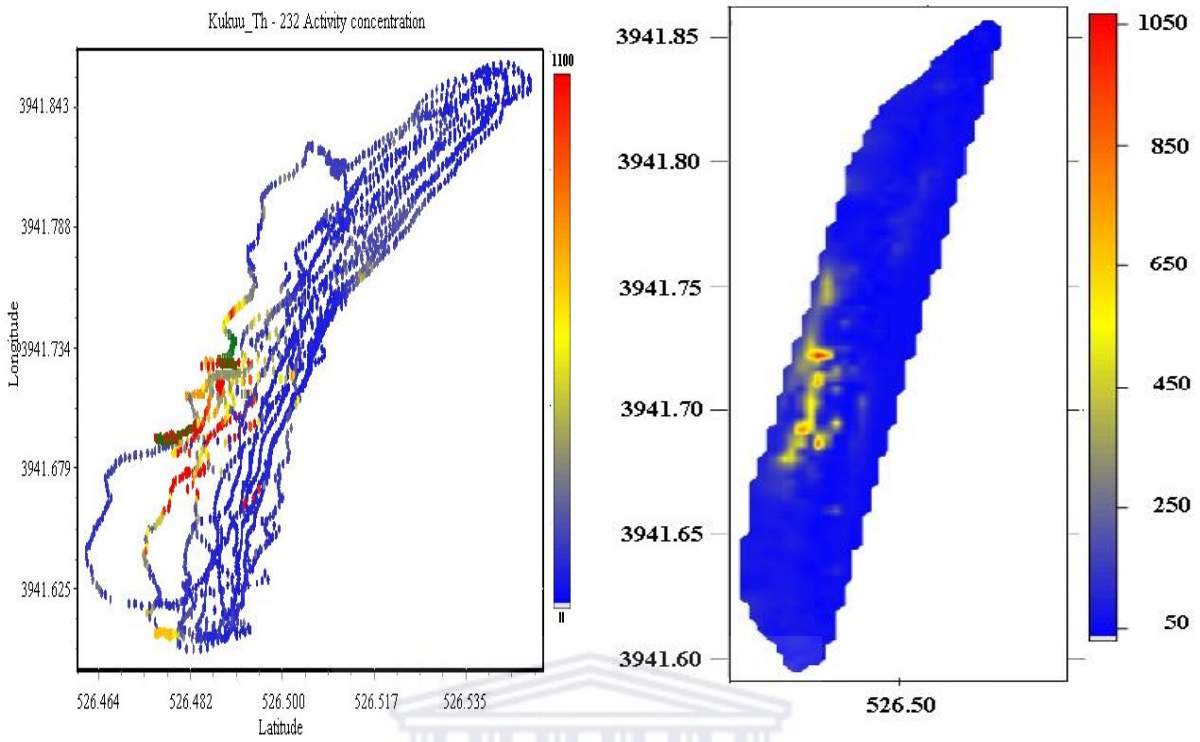

Figure 4.4: A map of Kukuu beach (left) showing ^{232}Th activity concentration measured using the MEDUSA γ-ray detector and an interpolated map (right) corresponding to the map on the left.

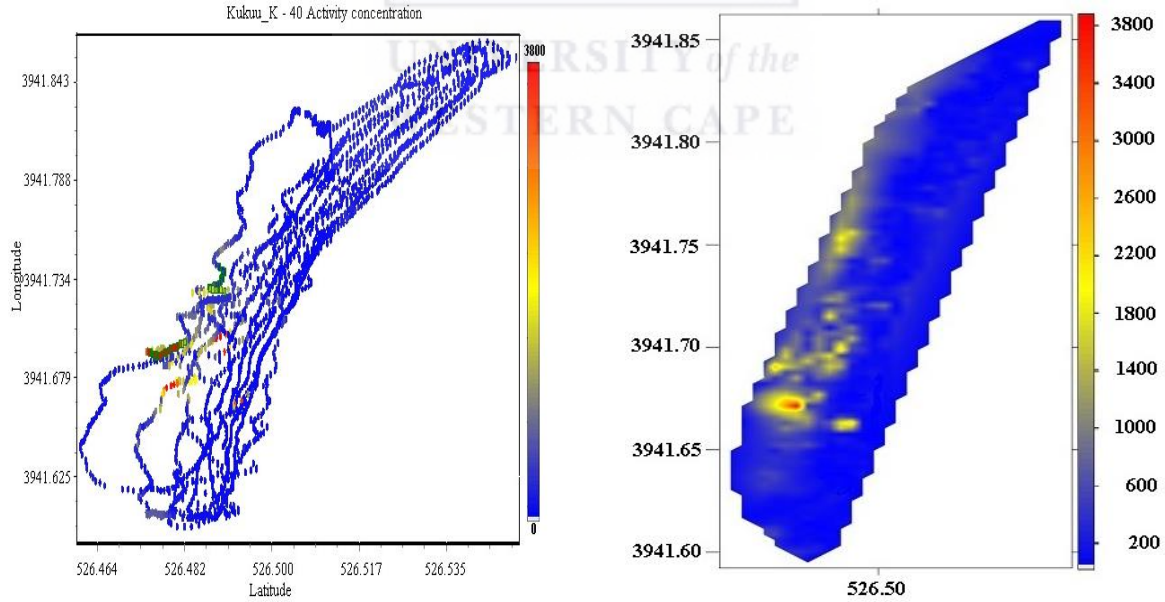

Figure 4.5: A map of Kukuu beach (left) showing ^{40}K activity concentration measured using the MEDUSA γ-ray detector and an interpolated map (right) corresponding to the map on the left.

Apart from Kukuu beach, the spatial distribution measurements of ^{238}U, ^{232}Th and ^{40}K in beaches have been performed at Msuka beach found in northern Pemba and displayed in Figures 4.6 to 4.8.

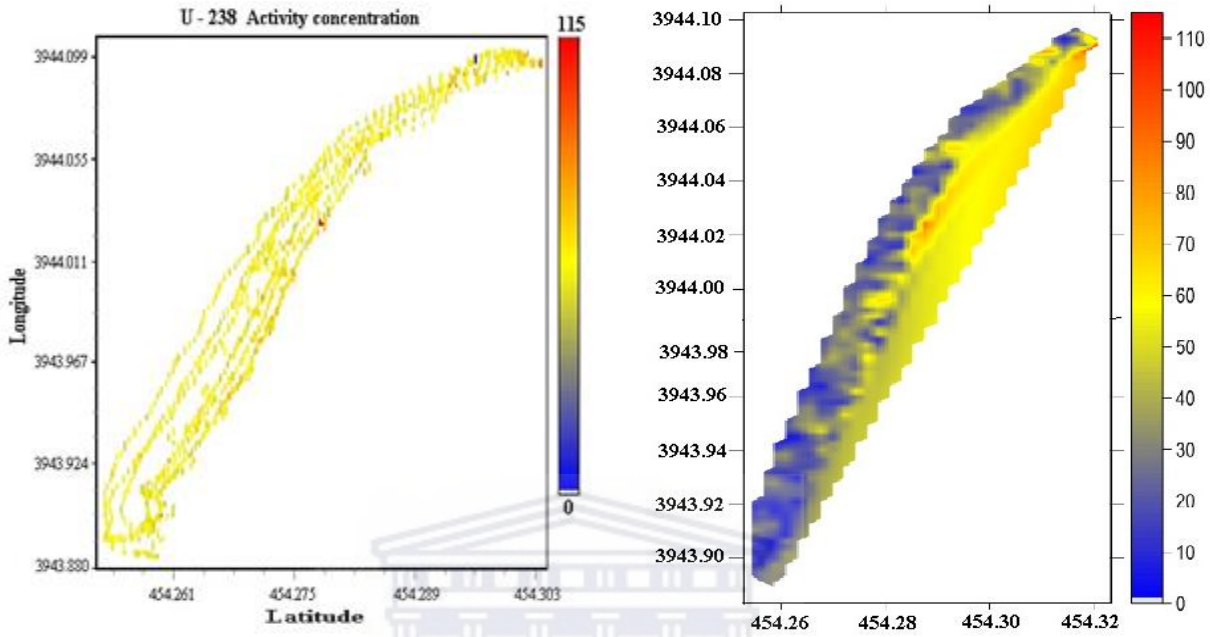

Figure 4.6: A map of Msuka beach (left) showing ^{238}U activity concentration measured using the MEDUSA γ-ray detector and an interpolated map (right) corresponding to the map on the left.

The activity concentrations of ^{238}U and ^{232}Th in Msuka beach are low compared to Kukuu beach. Two distinct regions are clearly observed in the distribution maps, dominated by either yellowish or bluish colours. The differences in colours are an indication of differences in spectroscopic responses during beach mapping. The highest ^{238}U and ^{232}Th activity concentration values recorded at Msuka beach were 115 $Bq.kg^{-1}$ and 210 $Bq.kg^{-1}$ respectively, much lower than at Kukuu but relatively large for beaches in general. The section of the beach which displayed higher values of both ^{238}U and ^{232}Th are the accessible part of the beach which is used by locals for various activities. The maps show that the distribution of radionuclides is not uniform.

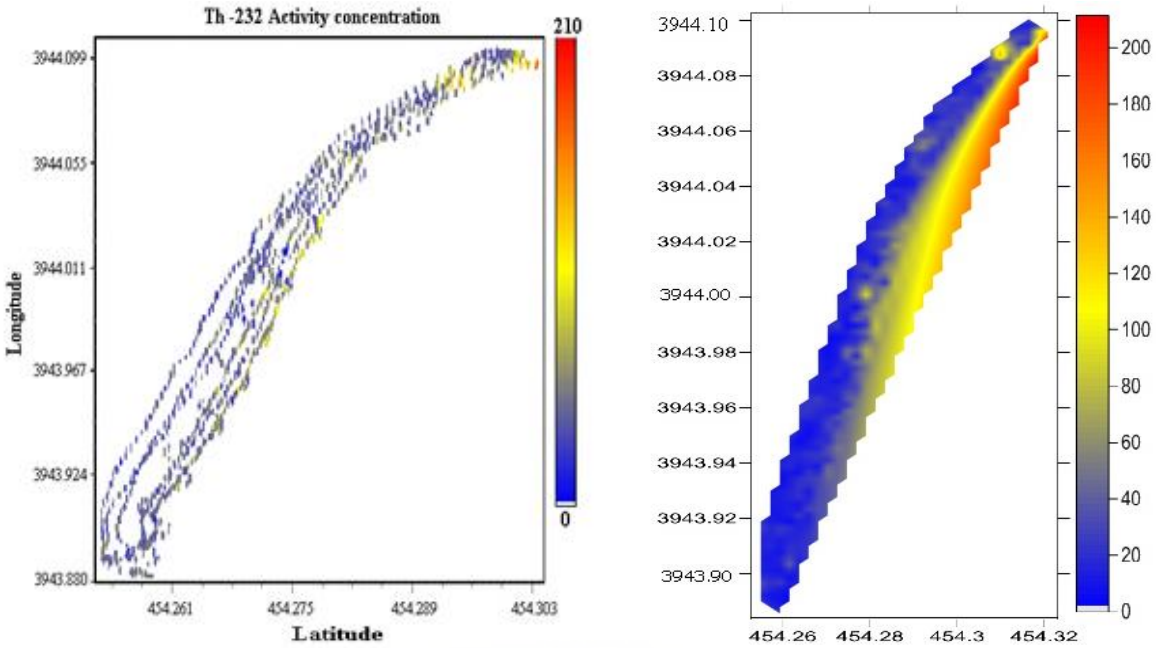

Figure 4.7: A map of Msuka beach (left) showing ^{232}Th activity concentration measured using the MEDUSA γ-ray detector and an interpolated map (right) corresponding to the map on the left.

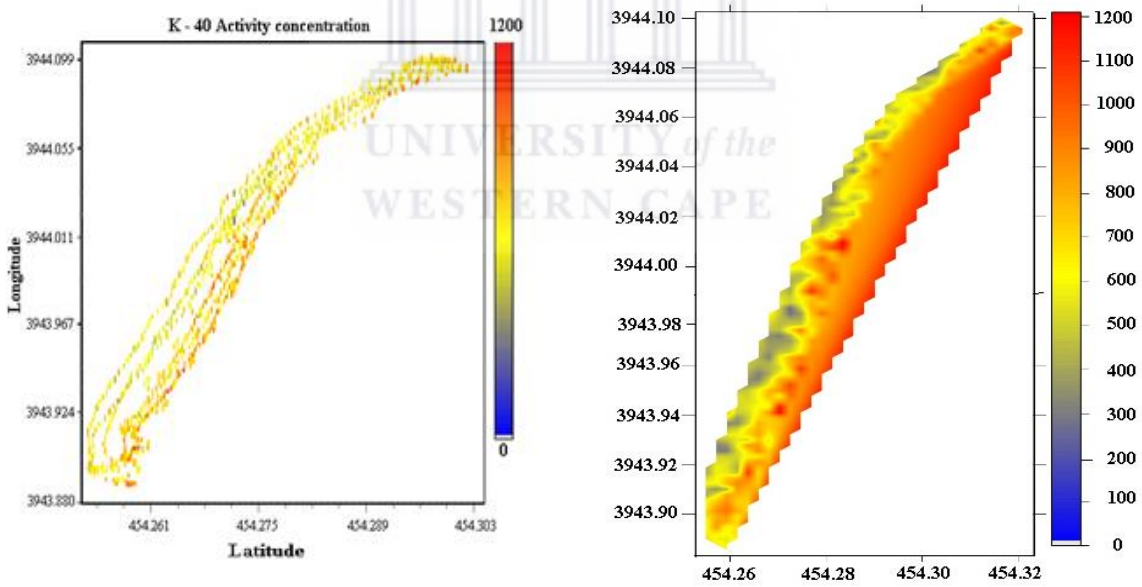

Figure 4.8: A map of Msuka beach (left) showing ^{40}K activity concentration measured using the MEDUSA γ-ray detector and an interpolated map (right) corresponding to the map on the left.

Unlike Kukuu beach, Msuka beach yielded higher concentration of ^{40}K. Clear zones differentiated by yellowish and reddish colours are observed (see Figure 4.8). The highest

values were found when measurements were done close to the land. This section consists of a mixture of beach sand and soil. Also, this part of the beach is characterised by erosion. Therefore, the higher values of ^{40}K may be due to the fact that soil is eroded from land and deposited on the beach.

4.5.2 Spatial distribution of ^{238}U, ^{232}Th and ^{40}K in soils

The spatial distributions of ^{238}U, ^{232}Th and ^{40}K soils measured in three places on land namely Tunguu, Kidoti and Mtende using the MEDUSA detector (see Chapter 3, section 3.33) have been presented in Figure 4.9 – 4.17. While Tunguu village is located at central part of Unguja Island, Kidoti and Mtende are found at the northern and southern part respectively. These areas were identified by the initial NaI(Tl) measurement as areas with relatively high radioactivity.

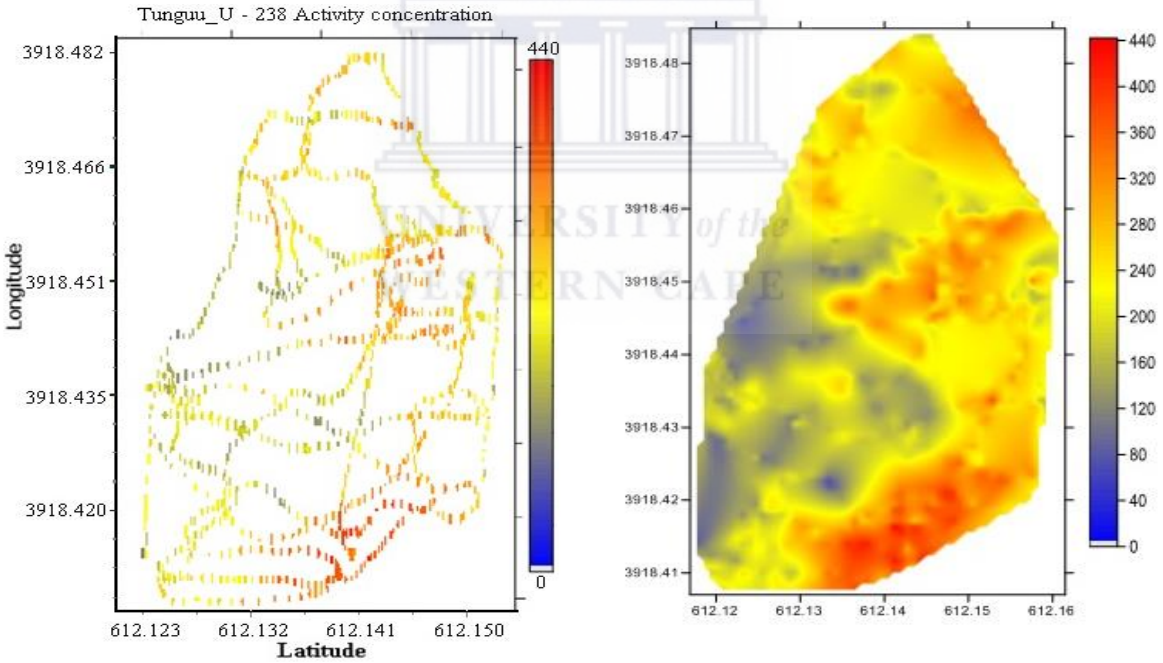

Figure 4.9: A map of Tunguu land (left) showing ^{238}U activity concentration measured using the MEDUSA γ-ray detector and an interpolated map (right) corresponding to the map on the left.

Visual examination of the MEDUSA maps and Surfer maps of ^{238}U, ^{232}Th and ^{40}K measured at Tunguu (Figure 4.7– 4.9) reveal remarkable variations of these radionuclides

on the measured section of the land. The ^{238}U activity concentration distribution (Figure 4.7) varies from 5 – 440 Bq.kg^{-1} with clear distinction of sections of low activity concentration (5 to 120 Bq.kg^{-1}), intermediate activity concentration (120 to 280 Bq.kg^{-1}) and higher activity concentration (280 – 440 Bq.kg^{-1}) levels. The differences in activity concentration of the same radionuclide within a small section of land mapped shows this radionuclide is not uniformly distributed in soils. In the same way, ^{232}Th and ^{40}K maps show similar trends of big radionuclide variations from one section of the land to the other.

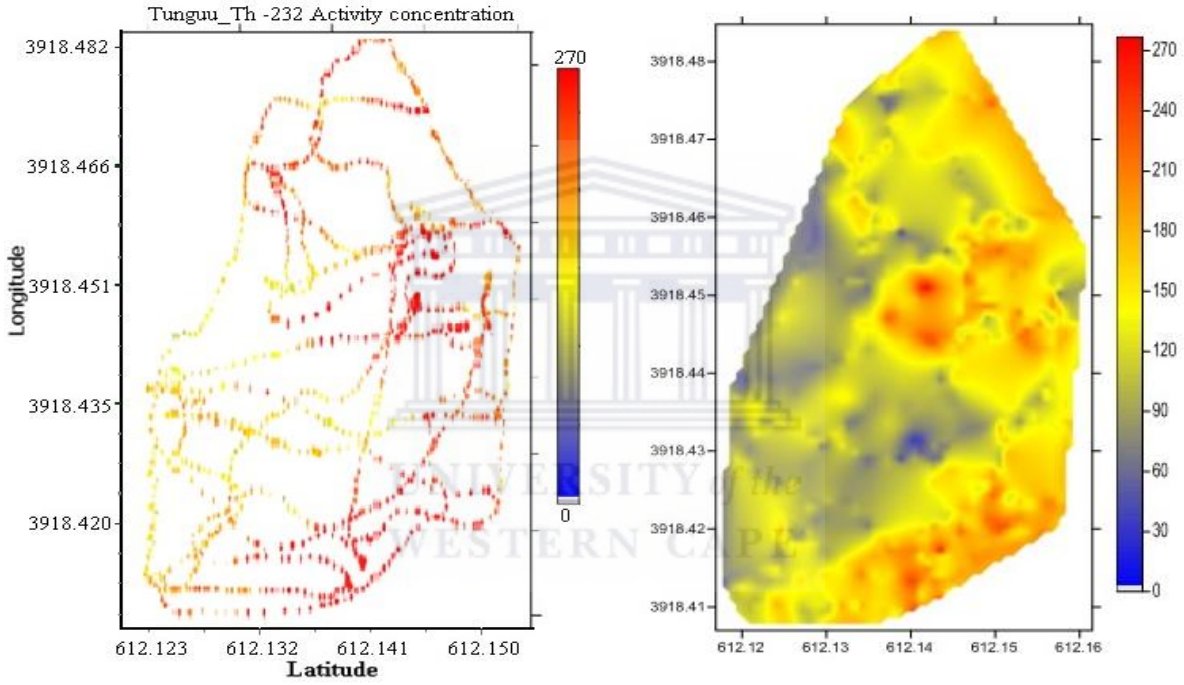

Figure 4.10: A map of Tunguu land (left) showing ^{232}Th activity concentration measured using the MEDUSA γ-ray detector and an interpolated map (right) corresponding to the map on the left.

While ^{232}Th activity concentration ranges from 0 – 270 Bq.kg^{-1} (see Figure 4.10), ^{40}K activity concentration ranges from 0 – 850 Bq.kg^{-1} (see Figure 4.11). Most of the surveyed area of Tunguu has ^{232}Th activity concentration ranging from 60 – 150 Bq.kg^{-1}.

The spatial distribution of ^{238}U, ^{232}Th and ^{40}K of the land mapped at Kidoti is presented in Figure 4.12 to Figure 4.14. The ranges of ^{238}U, ^{232}Th and ^{40}K are 150 – 310 Bq.kg^{-1}, 0 – 100 Bq.kg^{-1} and 0 – 800 Bq.kg^{-1} respectively.

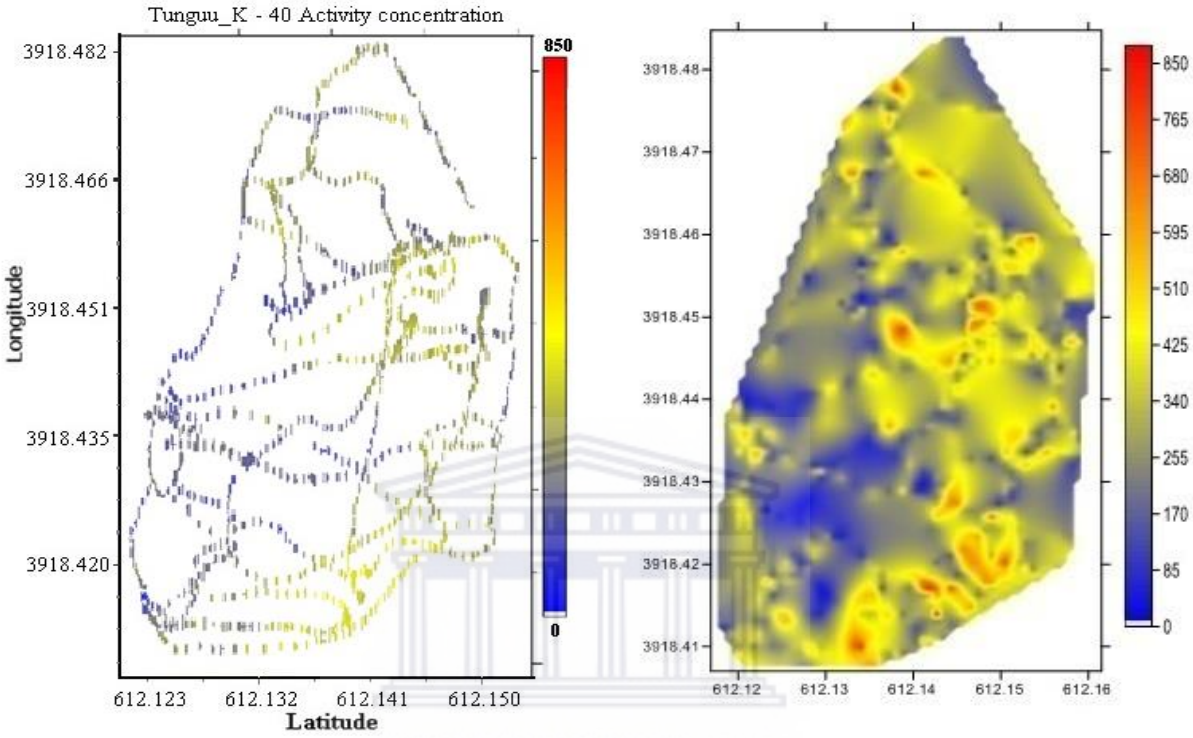

Figure 4.11: A map of Tunguu land (left) showing ^{40}K activity concentration measured using the MEDUSA γ-ray detector and an interpolated map (right) corresponding to the map on the left.

Similar to Tunguu, the most striking feature of ^{238}U, ^{232}Th and ^{40}K distribution maps is the recurring trend of great variation in the activity concentrations in clearly demarked zones. The well-defined boundaries between low, moderate and high activity concentrations reflect an abrupt change in the magnitude of spectroscopic responses during land mapping. The changes in spectroscopic responses imply that there are also mineralogical variations in the surveyed area.

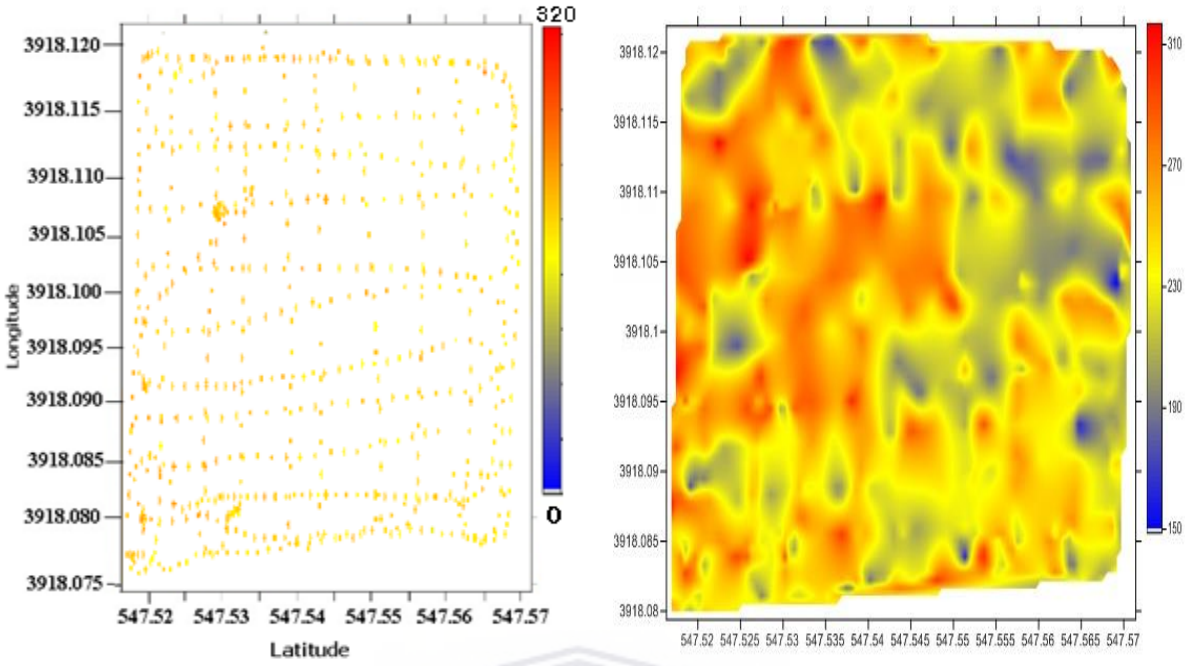

Figure 4.12: A map of Kidoti land (left) showing ^{238}U activity concentration measured using the MEDUSA γ-ray detector and an interpolated map (right) corresponding to the map on the left.

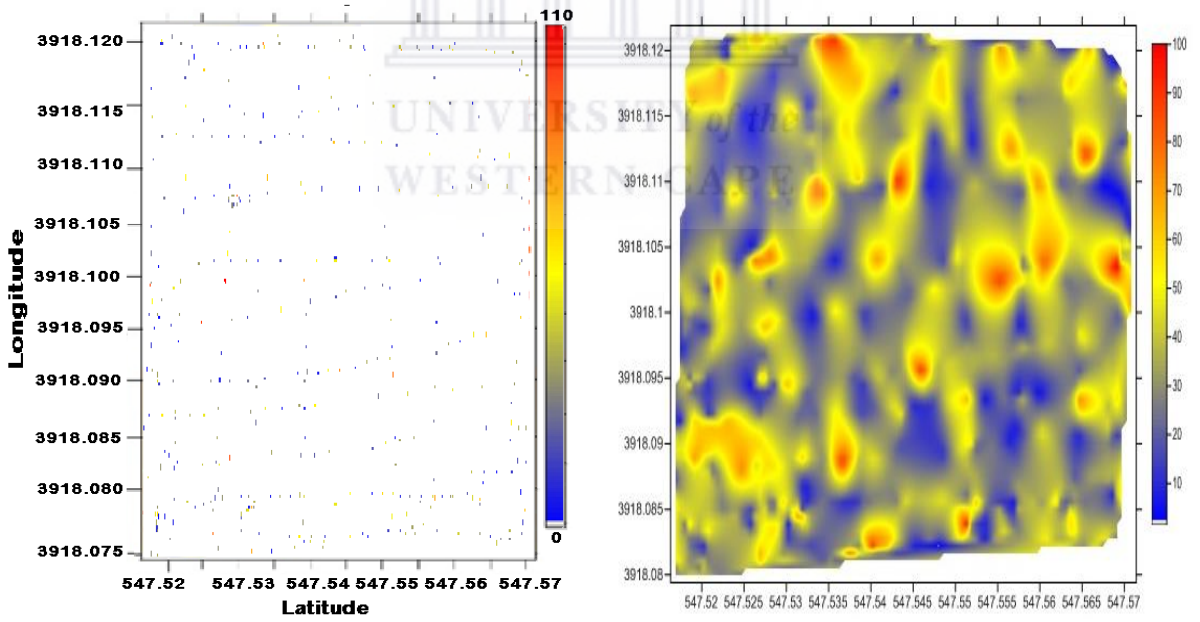

Figure 4.13: A map of Kidoti land (left) showing ^{232}Th activity concentration measured using the MEDUSA γ-ray detector and an interpolated map (right) corresponding to the map on the left.

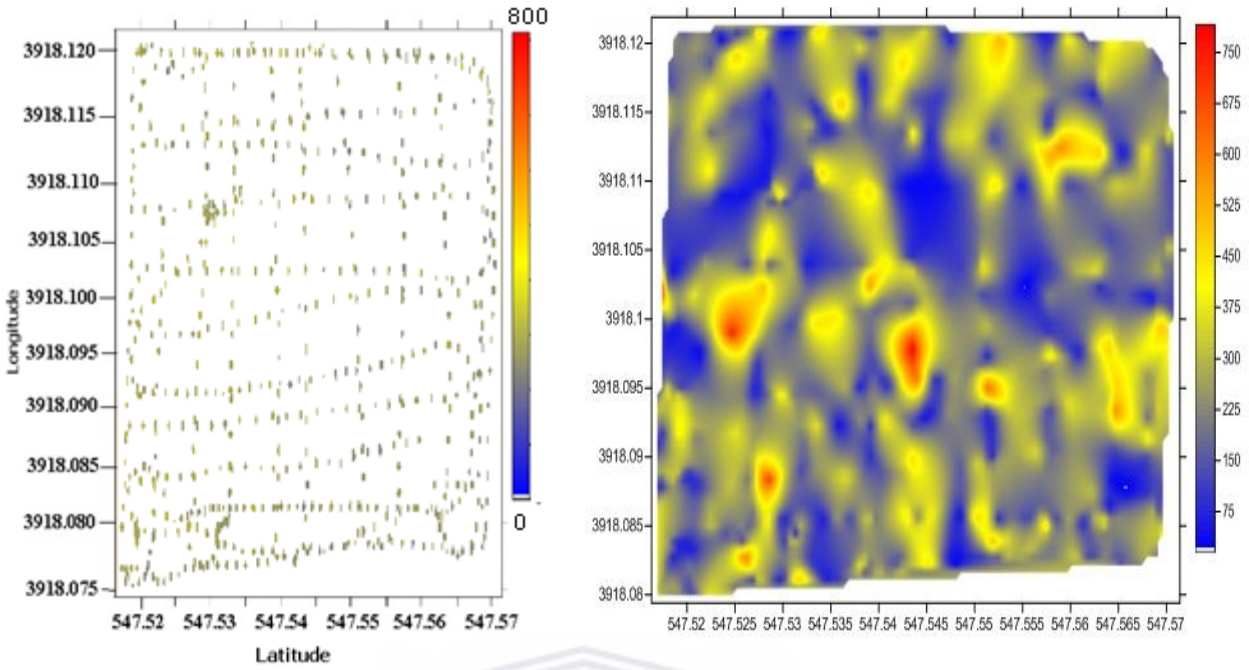

Figure 4.14: A map of Kidoti land (left) showing ^{40}K activity concentration measured using the MEDUSA γ-ray detector and an interpolated map (right) corresponding to the map on the left.

Unlike Kidoti and Tunguu which showed large variations of activity concentrations of ^{238}U, the activity concentration variation at Mtende was small (see Figure 4.15). The slight variations in colours which reflect changes in spectroscopic responses imply minimal variations of ^{238}U in the surveyed area. A large part of the surveyed land shows uniform distribution of ^{238}U with a few spots of low concentration (blue colour).

Figure 4.16, shows the activity concentration variation of ^{232}Th for the land surveyed. The colour variations are due to spectroscopic responses during field measurements which imply the non-uniform distribution of ^{232}Th in the surveyed land.

Close assessment of Figure 4.17 shows the concentration of ^{40}K follows the similar pattern as ^{232}Th. Although the surveyed area is dominated by blue colour implying low concentration of ^{40}K, the high and moderate concentration zones of ^{40}K are observed on the surveyed area by alternating red and yellow.

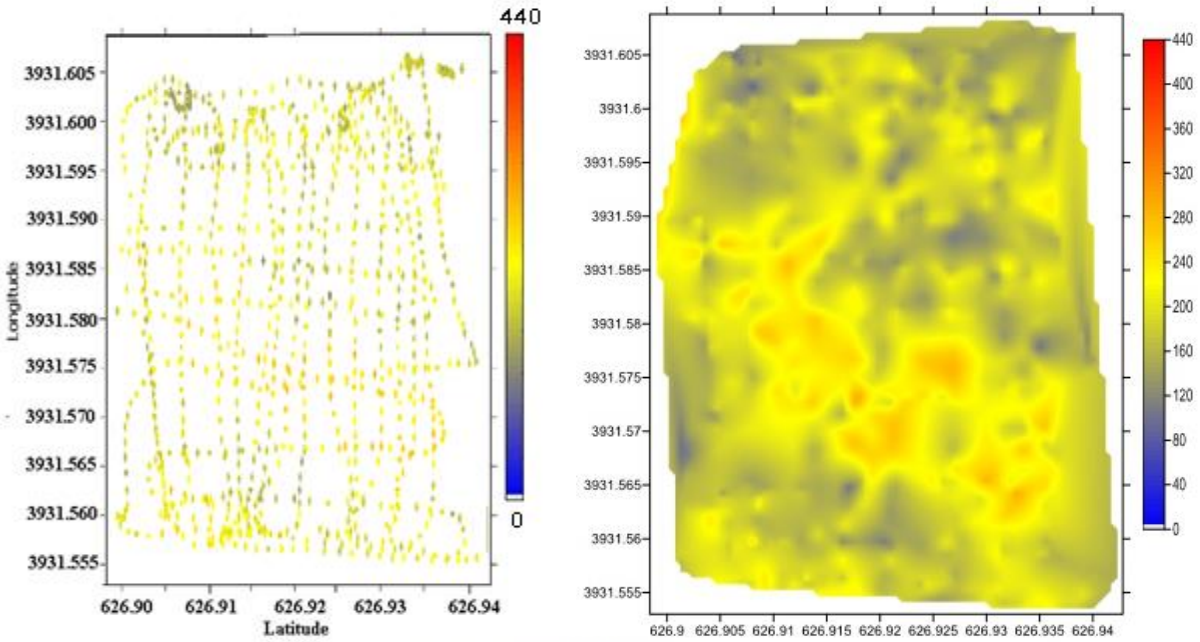

Figure 4.15: A map of Mtende land (left) showing ^{238}U activity concentration measured using the MEDUSA γ-ray detector and an interpolated map (right) corresponding to the map on the left.

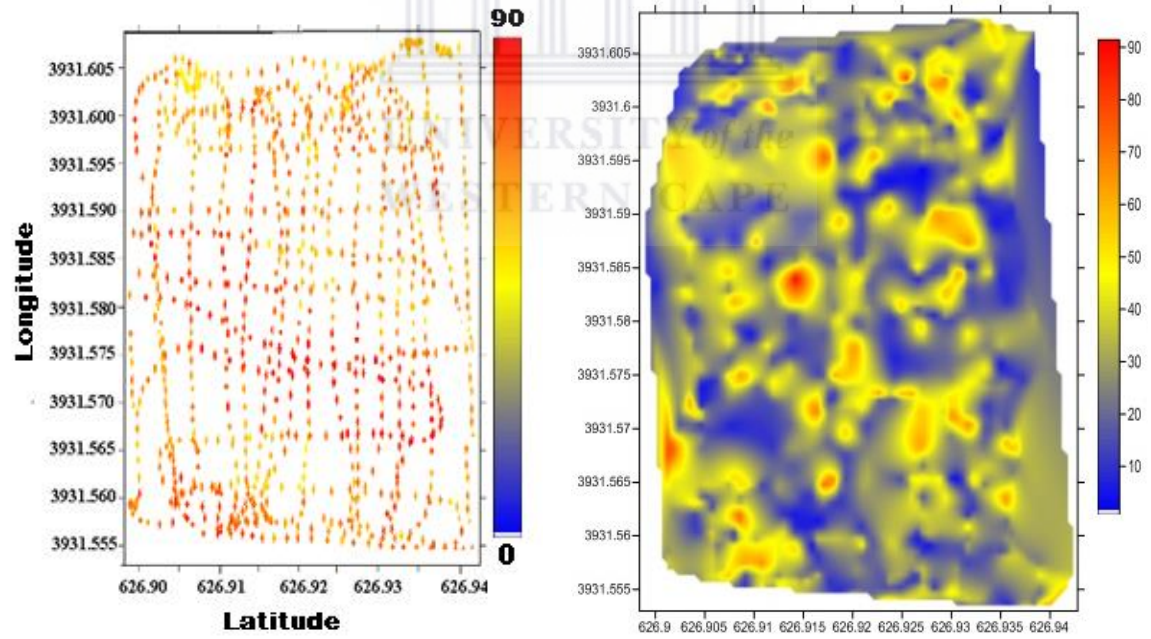

Figure 4.16: A map of Mtende land (left) showing ^{232}Th activity concentration measured using the MEDUSA γ-ray detector and an interpolated map (right) corresponding to the map on the left.

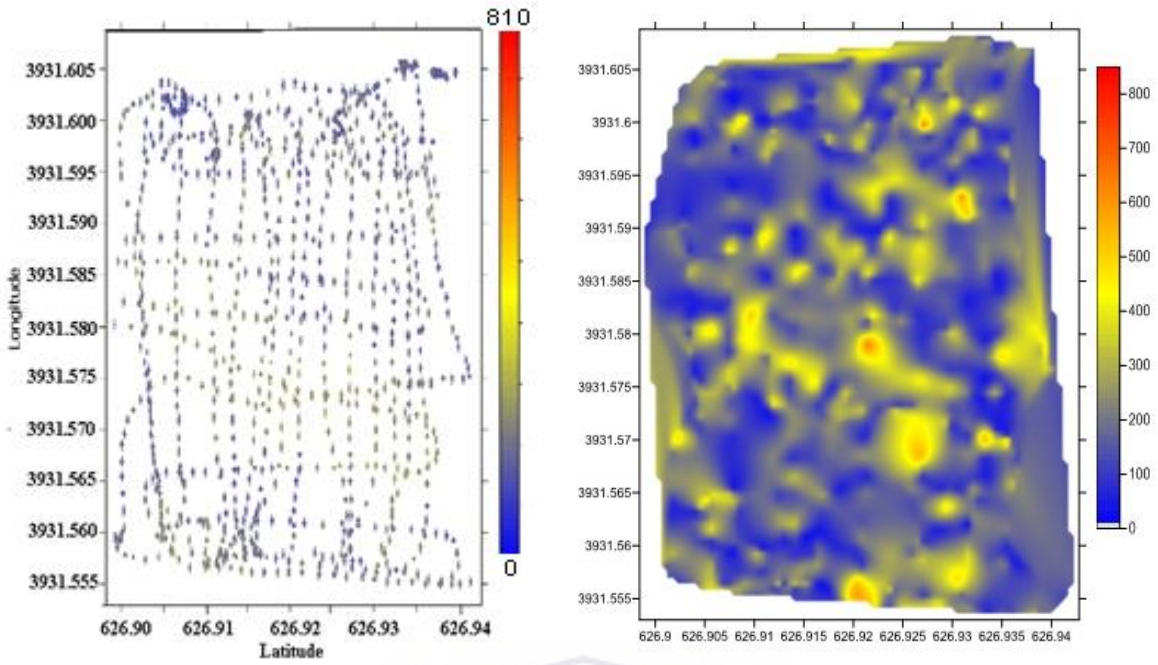

Figure 4.17: A map of Mtende land (left) showing ^{40}K activity concentration measured using the MEDUSA γ-ray detector and an interpolated map (right) corresponding to the map on the left.

4.6 Elemental concentrations of K, Th and U in soil and beach sand

Natural radionuclides in the environment are primarily associated with the geological and geographical conditions and therefore appear at different levels in soils, beaches and rocks across the different regions of the world (Tzortzis and Tsertos, 2004). Concentrations of an element in soil and sand are typically expressed in units of the mass of element (milligrams, mg or micrograms, µg) per mass of soil or sand (kilogram, kg). This is written as mg/kg or µg/kg. Sometimes concentrations in these media are reported as parts per million (ppm) or parts per billion (ppb). For easy comparison, the activity concentration values of ^{40}K, ^{232}Th and ^{238}U in beach sediments and soils obtained in this study (see Table 4.5 and Table 4.6) were converted into % (percentage) for ^{40}K and parts per million (ppm) for ^{238}U and ^{232}Th. Equation 4.1 (Tzortzis and Tsertos, 2004; Malain, 2011) has been used to calculate the elemental concentration in ppm.

$$F_E = \frac{M_E C}{N_A \lambda_E f_{A,E}} A_E. \quad (4.1)$$

where;

F_E is the elemental concentration of radionuclide E in the sample in ppm,

M_E is the atomic mass of radionuclide in kg mol^{-1},

N_A is Avogadro's number,

λ_E is the decay constant (s^{-1}),

$f_{A,E}$ is the atomic abundance of ^{238}U, ^{232}Th and ^{40}K in nature,

A_E is the measured activity concentration (in Bq.kg^{-1}),

C is a conversion factor with a value of 10^2 to convert the potassium concentration to a percentage and 10^6 to convert the uranium and thorium values to ppm.

Alternatively, elemental concentration was calculated using the activity concentration measured. The conversion factors used are given in Appendix A. In these conversion factors, activity concentration containing 1 ppm by weight of ^{232}Th is equivalent to 4.06 Bq.kg^{-1}, 1 ppm by weight of ^{238}U equals 12.35 Bq.kg^{-1} and 1 % of ^{40}K is equivalent to 313 Bq.kg^{-1}. The results obtained for the elemental concentrations using equation 4.1 agree with the results obtained using the expressions in Appendix A. In this study, the elemental concentrations of ^{40}K, ^{238}U and ^{232}Th obtained for beach sand is shown in Table 4.5.

Table 4.5: Elemental concentrations of ^{40}K, ^{238}U and ^{232}Th in beach sand

Samples	Elemental concentrations			$^{232}Th/^{238}U$
	^{40}K (%)	^{238}U (ppm)	^{232}Th (ppm)	
PBS 2	1.22 ± 0.060	0.16 ± 0.01	0.24 ± 0.02	1.50 ± 0.16
PBS 4	0.03 ± 0.002	0.57 ± 0.01	0.49 ± 0.00	0.86 ± 0.02
PBS 9A	0.65 ± 0.030	85.46 ± 3.95	651.52 ± 24.84	2.53 ± 0.15
PBS 9B	0.35 ± 0.020	43.48 ± 2.12	190.00 ± 7.55	4.37 ± 0.27
PBS 9C	1.42 ± 0.070	1.46 ± 0.07	2.44 ± 0.15	1.67 ± 0.13
PBS 11	1.50 ± 0.070	0.81 ± 0.04	0.49 ± 0.14	0.60 ± 0.17
PBS 12	1.37 ± 0.070	1.38 ± 0.03	2.44 ± 0.14	1.77 ± 0.11
UBS 14	0.01 ± 0.001	0.57 ± 0.01	0.24 ± 0.01	0.42 ± 0.02
UBS 19	0.03 ± 0.002	0.49 ± 0.01	0.24 ± 0.01	0.49 ± 0.05
UBS 20	0.03 ± 0.002	0.40 ± 0.01	0.24 ± 0.01	0.60 ± 0.07
UBS 22	0.04 ± 0.010	0.49 ± 0.05	0.24 ± 0.01	0.49 ± 0.05
UBS 23	1.12 ± 0.060	0.97 ± 0.05	4.39 ± 0.25	4.53 ± 0.35
UBS 27	0.03 ± 0.002	0.57 ± 0.06	0.49 ± 0.02	0.86 ± 0.10
UBS 35	1.31 ± 0.060	0.16 ± 0.01	0.49 ± 0.02	3.06 ± 0.23
UBS 37	1.10 ± 0.050	0.97 ± 0.05	4.39 ± 0.21	4.53 ± 0.32
Minimum	**0.03**	**0.16**	**0.24**	**0.42**
Maximum	**1.50**	**85.46**	**651.52**	**4.53**

Weighted Average	**0.38 ± 0.01**	**3.75 ± 0.05**	**1.01 ± 0.00**	1.19 ± 0.15

As seen in Table 4.6, the elemental concentrations for beach sand ranged from 0.03 to 1.50% for ^{40}K, from 0.16 to 85.46 ppm for ^{238}U and from 0.24 to 651.52 ppm for ^{232}Th. Considering the elemental concentrations obtained in beach sand, one can note that the much higher values of ^{238}U and ^{232}Th were obtained from sample PBS 9A and PBS 9B. These two samples are likely composed of heavy minerals which exhibit high ^{238}U and ^{232}Th concentrations. The average elemental concentrations of ^{40}K, ^{238}U and ^{232}Th for beach sediments are 0.71, 6.81 and 6.03 ppm respectively. Excluding sample PBS 9A and PBS 9B, the average elemental concentrations of ^{40}K, ^{238}U and ^{232}Th in beach sand is reduced to 0.71, 0.69 and 1.29 ppm respectively. UNSCEAR (2008) finds that the elemental concentrations in beach sands range typically from 1.88 to 1.99 ppm for ^{40}K, 2.28 to 2.49 ppm for ^{238}U and 9.26 to 10.15 ppm for ^{232}Th.

The results obtained in this study reveal that the average elemental concentrations of ^{40}K, ^{238}U and ^{232}Th in Zanzibar beach sediments are lower by a factor of two to eight times the corresponding values reported worldwide. The elemental concentration for ^{40}K, ^{238}U and ^{232}Th in soils is depicted in Table 4.6. The values obtained varied from 0.09 to 2.09%, 4.45 to 38.30 ppm and 12.68 to 31.71 ppm respectively.

The elemental concentrations in Zanzibar soils range from 0.09 to 2.09% for ^{40}K, from 4.45 to 38.30 ppm for ^{238}U and from 12.68 to 31.71 ppm for ^{232}Th. The average concentrations of these elements are 0.76%, 16.80 ppm and 19.86 ppm. The average elemental concentration of ^{238}U and ^{232}Th in soil obtained in this study are higher than the values given by UNSCEAR (2008). UNSCEAR, 2008 values for ^{238}U, ^{232}Th and ^{40}K are 2.8 ppm, 7.4 ppm and 1.3% respectively.

Elemental ratio analysis of Th/U, K/U and K/Th can also be useful in studying the enrichment/depletion processes due to complex metamorphic history, alteration and weathering processes that affected the rocks under investigation (Chiozzi et al., 2002;

Tzortzis and Tsertos, 2004). The values presented in this thesis can play an important role in further investigations of the geology and historical evolution of the soil on the islands.

Table 4.6: Elemental concentrations of ^{40}K, ^{238}U and ^{232}Th in soil samples

Sample Code	Elemental concentrations			^{232}Th / ^{238}U
	^{40}K (%)	^{238}U (ppm)	^{232}Th (ppm)	
PSS 9	1.74 ± 0.08	2.27 ± 0.10	5.85 ± 0.27	2.58 ± 0.16
USS 15	0.27 ± 0.01	21.94 ± 0.91	14.39 ± 1.43	0.66 ± 0.07
USS 16	0.30 ± 0.01	17.09 ± 1.03	29.27 ± 0.63	1.71 ± 0.11
USS 26	0.33 ± 0.09	20.73 ± 0.23	31.71 ± 0.46	1.53 ± 0.03
USS 28	2.09 ± 0.02	4.45 ± 0.62	12.68 ± 1.12	2.85 ± 0.47
USS 29	0.09 ± 0.01	38.30 ± 1.85	21.22 ± 0.98	0.55 ± 0.04
USS 30	0.49 ± 0.02	12.79 ± 0.94	23.90 ± 1.38	1.87 ± 0.17
Minimum	**0.09 ± 0.01**	**4.45 ± 0.62**	**5.85 ± 0.27**	**0.55 ± 0.04**
Maximum	**2.09 ± 0.02**	**38.30 ± 1.85**	**31.71 ± 0.46**	**2.85 ± 0.47**
Average	**0.38 ± 0.01**	**5.59 ± 0.09**	**14.72 ± 0.21**	**2.63 ± 0.06**

4.6.1 $^{232}Th/^{238}U$ Elemental Ratio

Tables 4.5 and 4.6 provide $^{232}Th/^{238}U$ elemental concentration ratio for beach sand and soil samples respectively, which is important in studying enrichment and depletion of natural radionuclides due to various processes (Tzortzis and Tsertos, 2004; Chiozzi et al., 2002). Adams and Weaver (1958) prove the feasibility of $^{232}Th/^{238}U$ elemental concentration ratio as an indicator of relatively oxidizing conditions or reduction in soil and beach sand samples. ^{238}U has an insoluble tetravalent state which is fixed under reducing conditions, but it turns into a soluble hexavalent state that can be mobilized in the solution. By contrast, ^{232}Th has a single insoluble tetravalent state, one which is geochemically associated with ^{238}U. Therefore, it is a useful standard for comparison purposes (Macfarlane et al., 1989). Adams and Weaver (1958) further suggested that ratios less than 2 were very suggestive of the relative enrichment of ^{238}U and the involvement of the reducing conditions as contrasted with a ratio greater than 7, which refer to the removal of preferential enrichment, perhaps by leaching.

In the present study, the calculated $^{232}Th/^{238}U$ ratio ranges from 0.42 to 4.43 for beach sand and from 0.55 to 2.85 for soil samples. These elemental ratios may provide an indication whether enrichment or relative depletion of radionuclides had occurred. The $^{232}Th/^{238}U$ ratio in most samples is lower than the average continental crust value of approximately 3.8 (Clark et al., 1966; Rogers & Adams, 1969). This suggests that the samples are enriched in ^{238}U. By contrast, $^{232}Th/^{238}U$ ratios of beach sand samples PBS 9B, UBS 23, UBS 27 are 4.37, 4.53 and 4.53 respectively. These values are higher than the average continental crust value, suggesting that these samples are enriched in Th.

From Table 4.7, it can be seen that the concentration of ^{40}K in Zanzibar soil is within the range obtained in Egypt, China, India and Kuwait. On the other hand, the ^{40}K concentration is less than the upper value in Algeria, Italy, Turkey and Pakistan while the ^{40}K concentration is less than the concentration in soils from Jordan, Cyprus and Nigeria.

Table 4.7: The comparison of elemental concentrations of ^{40}K, ^{238}U and ^{232}Th in soil samples and beach sand of the present study with other locations around the world.

Region/Sample type	Elements			References
	^{40}K (%)	**^{238}U (ppm)**	**^{232}Th (ppm)**	
Zanzibar soil	**0.09 – 2.09**	**4.45 – 38.30**	**12.68 – 31.71**	**Present study**
Egypt	0.94 – 2.11	0.40 – 1.94	0.49 – 2.44	Sroor et al. (2001)
Algeria	0.11 – 4.49	0.16 – 10.28	0.49 – 35.12	Baggoura et al. (1998)
Alps-Apennines, Italy	0.14 – 5.14	0.3 – 5.6	0.3 16.7	Chiozzi et al. (2002)
Russaifa, Jordan	0.1 – 1.0	3.9 – 42.4	2.1 – 6.7	Al-Jundi (2002)
Turkey	0.34 – 3.95	0.89 – 15.22	2.44 – 25.61	Kurnaz et al. (2007)
Spain	0.2 – 5.2	1.1 – 13.4	1.7 – 50.3	Baeza et al. (1992)
Bangladesh	1.28 – 2.40	1.05 – 3.48	0.73 – 19.76	Miah et al. (1998)
Cyprus	<1 – 1.9	<1 – 3.2	<1 – 9.8	Tzortzis et al. (2004)
China	1.41 – 2.92	3.24 – 35.79	8.05 – 21.46	Yang et al. (2005)
Jordan	0.32 – 1.21	1.21 – 4.86	0.98 – 7.07	Ahmad et al. (1997)
Pakistan	0.97 – 3.02	1.70 – 3.89	5.37 – 14.39	Tahir et al. (2005)
India	0.06 – 2.73	0.40 – 5.75	3.66 – 18.54	Kannan et al. (2002)
Kuwait	0.24 – 2.23	0.48 - 2.62	0.85 – 6.66	Al Azemi et al. (2015)
Zanzibar beach sand	**0.03 – 1.50**	**0.16 – 85.46**	**0.24 – 651.52**	**Present study**
Melkbosstrand, RSA	0.13 – 0.15	1.60 – 3.94	1.34 – 3.59	Mbatha (2007)
Albania	0.85 – 2.16	0.5 – 2.19	3.17 – 9.76	Tsabaris et al. (2007)
Greece	0.49 – 5.09	2.35 – 8.91	4.63 – 21.46	Florou and Kritis (1992)
French	0.38 – 3.28	0.73 – 5.02	3.90 – 13.41	Lambrechts et al. (1992)
Akkuyu, Turkey	0.43 – 0.92	0.32 – 1.39	3.86 – 9.3	Kurt et al. (2014)
Miami Bay, Malaysia	0.95 – 1.58	1.94 – 213.85	9.02 – 508.78	Shuaibu et al. 2017
Orissa, India	BDL – 4.54	1.21 – 4.53	9.76 - 1400	Rao et al. (2009)
Tamilnadu, India	BDL – 1.82	BDL – 26.48	BDL – 716.66	Punniyakotti and Ponnusamy (2017)
Kocaeli, Turkey	0.04 – 1.64	0.36 – 1.14	0.64 – 4.04	Korkulu and Ozkan

				(2013)
Andaman, Thailand	0.03 – 2.09	0.22 – 1.90	0.73 – 8.44	Malain et al. (2011)
Worldwide range	**0.3 – 4.5**	**0.5 – 4.7**	**1.6 - 20**	**UNSCEAR (2008)**
Worldwide Average	**1.3**	**2.8**	**7.4**	**UNSCEAR (2008)**

The ^{238}U elemental concentration obtained in Zanzibar soil is within the range obtained in China and is less than ^{238}U concentration determined in surface soils from Rusaifa, Jordan. Furthermore, the ^{238}U concentration was found to be higher than the findings from Egypt, Nigeria, Turkey and Spain. Other countries which reported low ^{238}U concentration in soil include Bangladesh, Pakistan, Cyprus, India and Kuwait.

The concentration of potassium in Zanzibar beaches is lower than beaches of Greece, Orisa, Albania and Thailand (see Table 4.7) and greater than Melkbosstrand beach in South Africa and Akkuyu beach in Turkey. The concentration of uranium in beach sediments is higher when compared with other beaches (see Table 4.7) except Miami bay in Malaysia which is 2.5 times higher than Zanzibar. As in the case of ^{238}U, the concentration of ^{232}Th is higher at a majority of the areas except at Orissa, India with ^{232}Th concentration more than two times higher than Zanzibar (see Table 4.7).

4.7 Quality assurance

For the purpose of quality assurance, a reference soil material IAEA-375 was filled up to the 1000 ml mark in the Marinelli beaker and was measured and analysed in the same way as beach sediments and soil samples. The dry mass of the reference sample was found to be 1.254 kg. The IAEA certified sample was treated as an unknown sample. The results obtained from the measurements and the certified values are summarised in Table 4.8.

Table 4.8: Elemental concentrations of reference soil sample IAEA-375 (Ongori, 2013)

Radionuclides	IAEA-375 soil sample certified values	IAEA-375 soil sample measured values
^{40}K (%)	1.33 – 1.38	1.28 – 1.40
^{238}U (ppm)	1.46 – 1.78	1.38 – 1.54

^{232}Th (ppm)	4.90 – 5.20	4.88 – 5.37

One may note the recommended values of ^{40}K, ^{238}U and ^{232}Th are given as activity concentration in Bq.kg^{-1}, which are converted into corresponding elemental concentrations according to equation 4.1. The ERL measured values for ^{40}K, ^{238}U and ^{232}Th were found to deviate from the recommended values by 1%, 10% and 1% respectively. These differences fall within an error margin which demonstrates the good performance of the measurement and the analysis technique used.

4.8 Activity Correlations plots (^{238}U and ^{232}Th; ^{238}U and ^{40}K; ^{232}Th and ^{40}K)

In an attempt to study the relationships that may exist between ^{238}U, ^{232}Th and ^{40}K in beach sediments and soil samples, correlation plots have been plotted. The correlation plots of ^{238}U versus ^{232}Th, ^{238}U versus ^{40}K and ^{232}Th versus ^{40}K in beach sediments and soil samples are presented in Figure 4.18 – 4.20 and Figure 4.21 – 4.23 respectively.

As mentioned in section 4.3, two beach sand samples (PBS 9A and PBS 9B) show very high values of ^{238}U and ^{232}Th concentrations. For this reason, these two samples were treated as outliers; hence they were excluded in correlation plots. The plot for ^{238}U versus ^{232}Th for beach sediments (Figure 4.18) shows a linear relationship between ^{232}Th and ^{238}U with a correlation coefficient of 0.634 between the radionuclides. The positive correlation between ^{238}U and ^{232}Th for beach sediments may indicate similarity in their origin. According to Khater (2001), rocks and/or sand from which the sample originates will have the same chemical behaviour and could be the same for a given pair of nuclei. On the other hand, a weak correlation of 0.405 is observed between the ^{232}Th and ^{40}K (Figure 4.19) and poor correlation between ^{238}U and ^{40}K (Figure 4.20) with coefficient of 0.296. ^{238}U being the most mobile and soluble compared to ^{40}K, the poor correlation between them in beach sediments may be due to relatively high solubility and thus high mobility of ^{238}U compared to ^{40}K (Mamoney and Khater, 2004). Furthermore ^{238}U is associated with organic matter, thus it can leach into sand with high organic content (Valkovic, 2000; Navas et al. 2002).

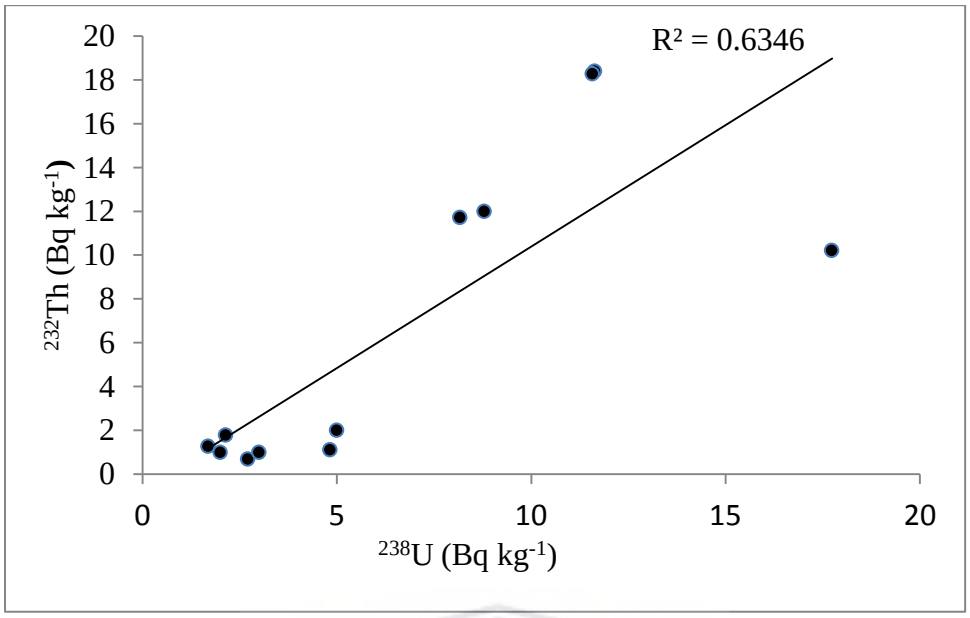

Figure 4.18: Activity correlation plot for ^{232}Th and ^{238}U from measured beach samples

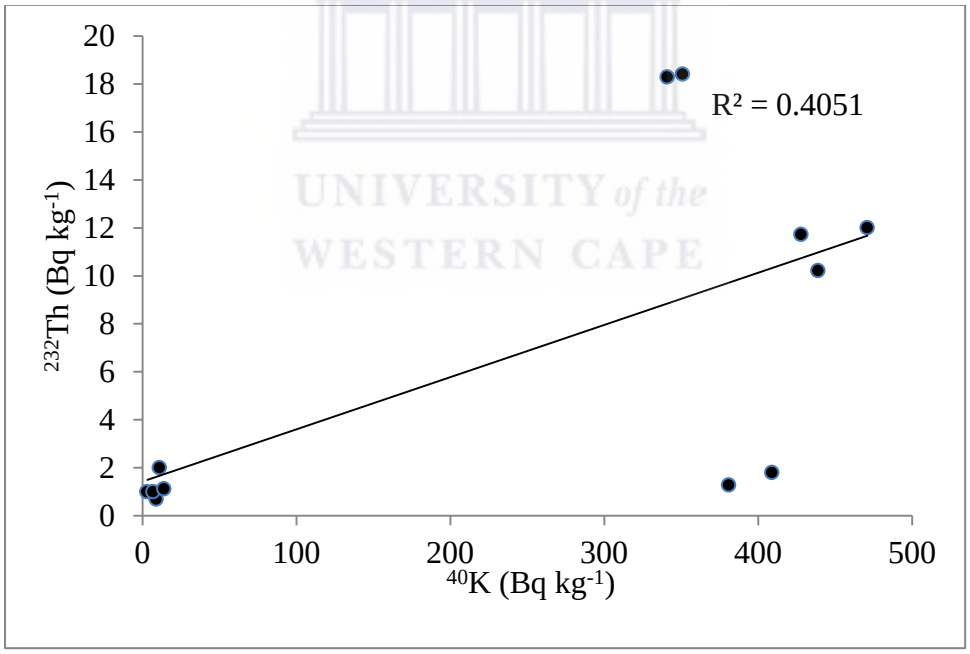

Figure 4.19: Activity correlation plot for ^{232}Th and ^{40}K from measured beach samples

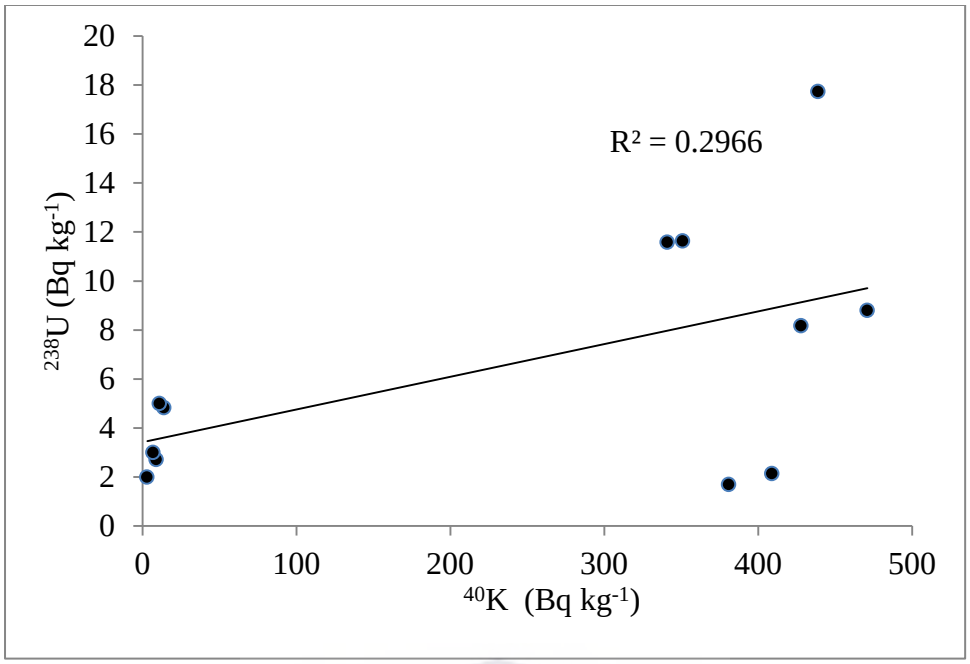

Figure 4.20: Activity correlation plot for ^{238}U and ^{40}K from measured beach samples

The plot for ^{232}Th and ^{238}U (Figure 4.21) in measured soil samples show a weak correlation with a correlation coefficient of 0.205 between the radionuclides. Whereas correlation plots for ^{232}Th and ^{40}K (Figure 4.22) and ^{238}U and ^{40}K (Figure 4.23), show negative correlation coefficients of 0.52 and 0.644 respectively.

The weak positive correlation between ^{238}U and ^{232}Th in soil samples is an indication that environmental processes have affected the distribution of ^{238}U and ^{232}Th in Zanzibar soils (Fujiyoshi and Sawamura, 2004).

Many researchers have attempted to find some correlations between activity concentrations of these radionuclides. Moderate to strong correlation between ^{232}Th and ^{40}K have been reported by many of them (Quindos et al., 1994; Singh et al., 2005; El-Reefy et al., 2006; Mehra et al., 2010; Bajoga et al., 2016; Kardan et al., 2017). The findings of these researchers are in disagreement with the results of this study. Negative correlation between ^{232}Th and ^{40}K as well as ^{238}U and ^{40}K has been found in the inland soil samples. Among the findings which are in good agreement with this work include that of Mehra (2010). The disagreement might be due to a very low number of samples

used in the study of Mehra and this work, or it may indicate that the soil from different parts of the island have different origins or have evolved differently due to environmental conditions such as different weathering and leaching.

Apart from the low number of soil samples in this study, the negative correlation between ^{232}Th and ^{40}K as well as ^{238}U and ^{40}K indicate that the radionuclide concentrations are associated with different chemical and geological properties of the elements. Moreover, the differences in solubility and mobility characteristic of ^{232}Th, ^{238}U and ^{40}K in the environment contribute to negative responses between ^{232}Th and ^{40}K and ^{238}U and ^{40}K. The solubility of ^{238}U changes with reducing and oxidizing environment. On the other hand, ^{232}Th is one of the least soluble elements and it is immobile at low temperatures (Ivanovich and Harmon, 1992; Edsfeldt et al., 2000).

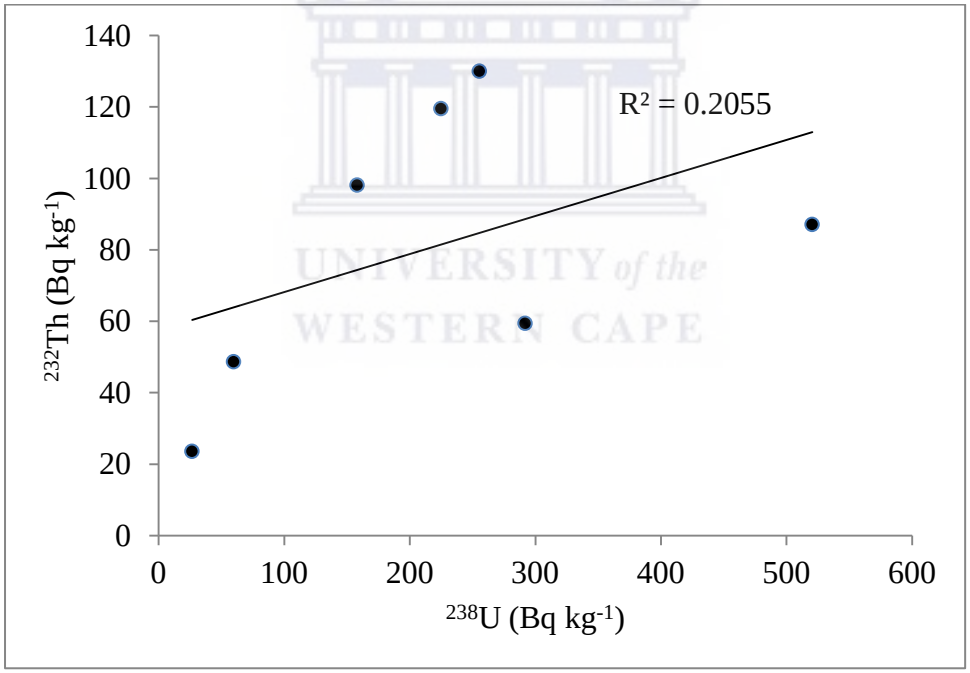

Figure 4.21: Activity correlation plot for ^{232}Th and ^{238}U from measured soil samples

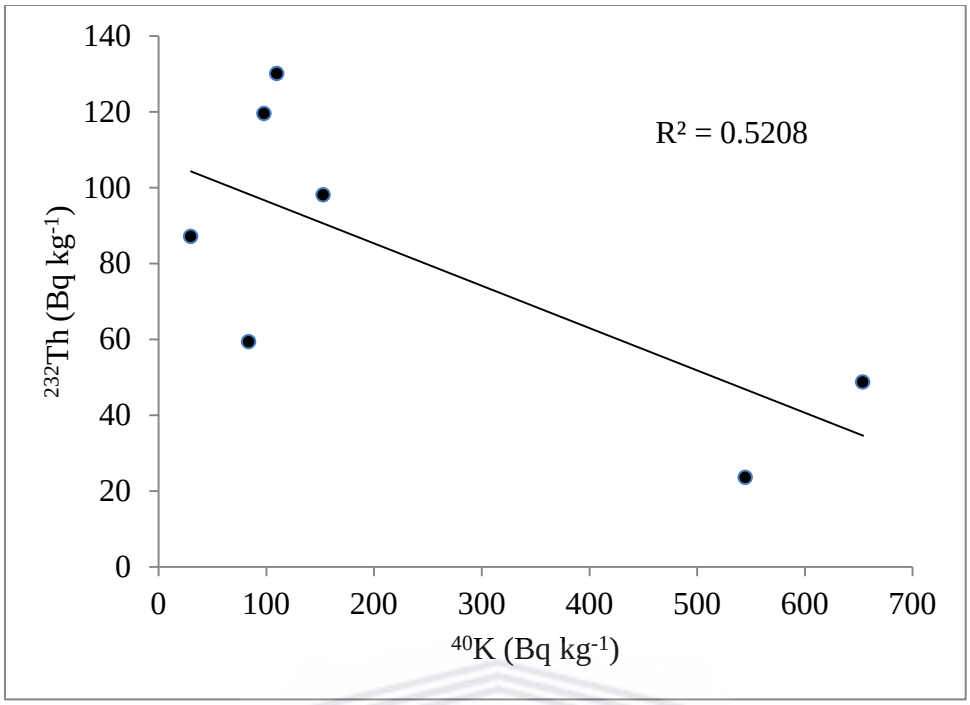

Figure 4.22: Activity correlation plot for ^{232}Th and ^{40}K from measured soil samples

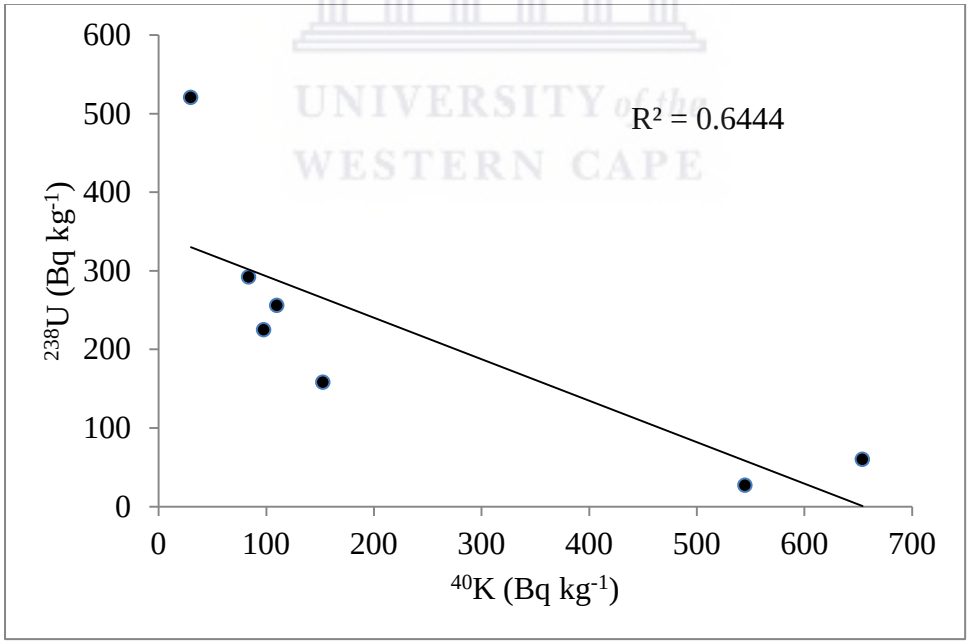

Figure 4.23: Activity correlation plot for ^{238}U and ^{40}K from measured soil samples

4.9 In-situ activity concentration measurements using NaI(Tl) detector

As mentioned in section 3.3.1, a NaI(Tl) detector was used to perform in-situ outdoors terrestrial gamma radiation mapping in 33 locations during initial visit to the islands. The NaI(Tl) detector was placed 1metre above the ground and each spectrum was collected for 600 seconds in each location. Figures 4.24 – 4.26 present maps showing the distribution of the natural radionuclides (^{40}K, ^{232}Th and ^{238}U) from soil and beach in all surveyed areas. The activity concentrations of the ^{40}K, ^{232}Th and ^{238}U were found to vary considerably from one location to another. These measurements were used to select places where samples were taken for the HPGe measurements.

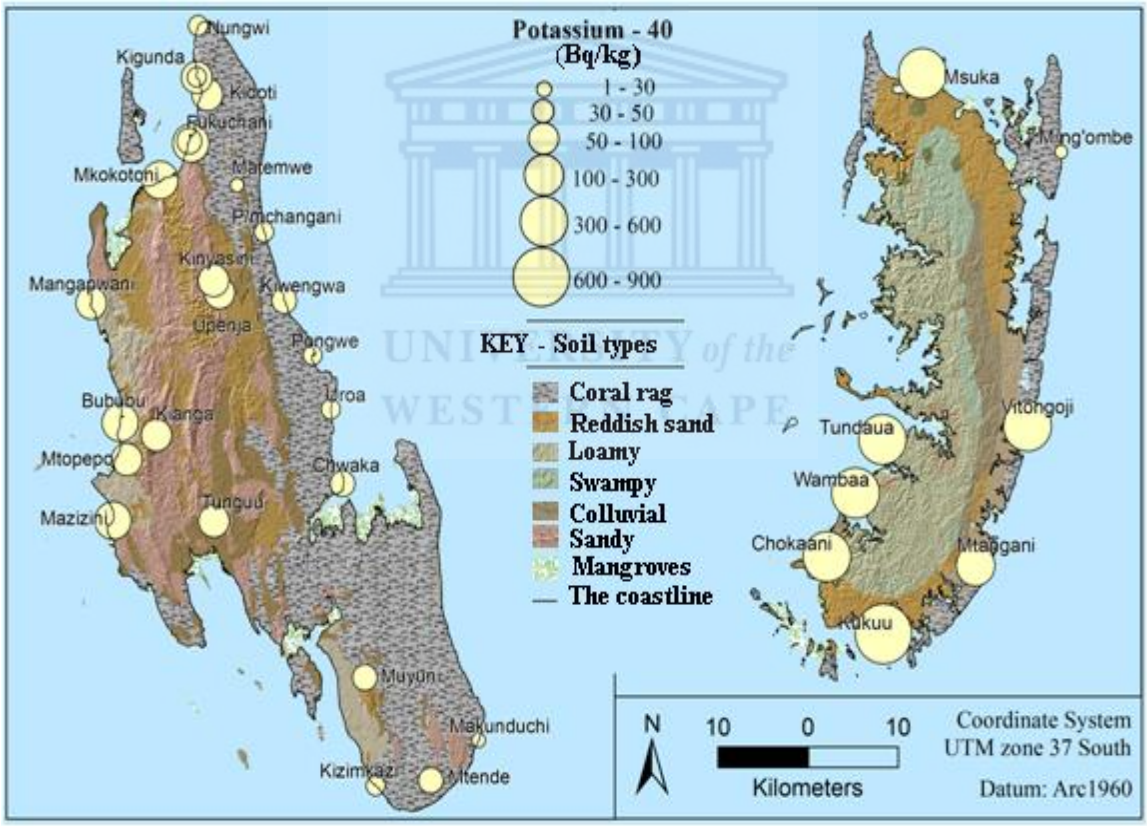

Figure 4.24: The distribution of ^{40}K in Unguja (left) and Pemba (right)

From Figure 4.24, the activity concentration of ^{40}K ranges from a few Bq.kg^{-1} to approximately 900 Bq.kg^{-1} with most of the higher values on Pemba. The low and high

^{40}K activity concentration measured in the surveyed area is related to the underlying geology and type of soil. For instance, the ^{40}K activity concentration of less than 100 Bq.kg^{-1} has been measured along the Zanzibar coastline dominated by corals. The beach sand in these areas was also found to have high percentage of calcium oxide (CaO), suggesting that shells and organic matter are the main constituent of sand in these areas. On the other hand, high ^{40}K activity concentrations of greater than 300 Bq.kg^{-1} were also measured, on beaches that had a pure sandy nature as indicated by a high percentage of silicone dioxide (SiO_2).

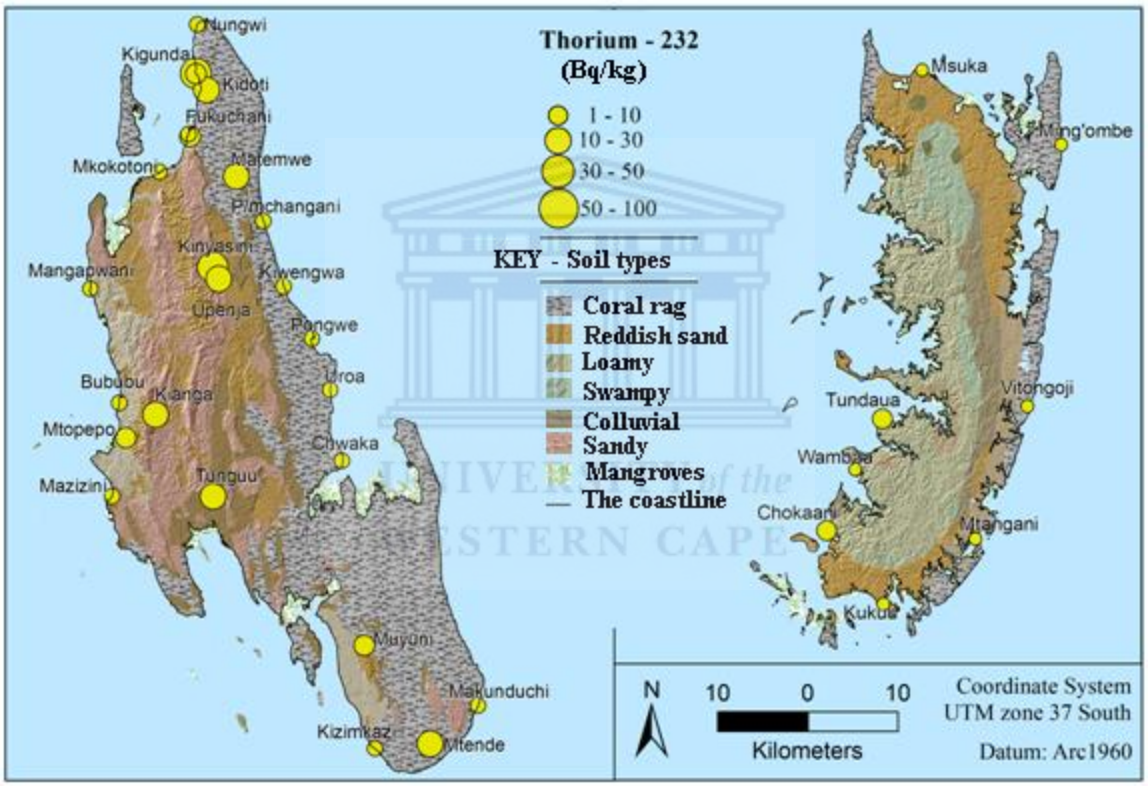

Figure 4.25: The distribution of ^{232}Th in Unguja (left) and Pemba (right)

In the case of ^{232}Th, the activity concentrations of this radionuclide in the surveyed area varied considerably from a few Bq.kg^{-1} up to 100 Bq.kg^{-1}, even among neighbouring regions. This variation is associated with the differences in geological structures of the study area. Rocks and soil always contains some natural radionuclides (uranium and thorium series) at different concentrations. These radionuclides are spread in the area

only after long-lasting geological processes. Low activity concentration values of ^{232}Th were generally observed in the beach sand overlying the carbonaceous rocks in the entire coast of the study area. The highest values of ^{232}Th were recorded in the inland areas as shown in the map.

The distribution of ^{238}U activity concentrations (Figure 4.26) in the surveyed area demonstrates similarity to that of ^{232}Th. The high values of ^{238}U correspond well to the measurements carried out on the land rather than along the coast. The distribution of ^{238}U activity concentration values generally varied from very low (< 10 Bq.kg^{-1}) along the coasts, up to 187 Bq.kg^{-1} reported on land. The high ^{238}U concentration on land is probably associated with the soil type.

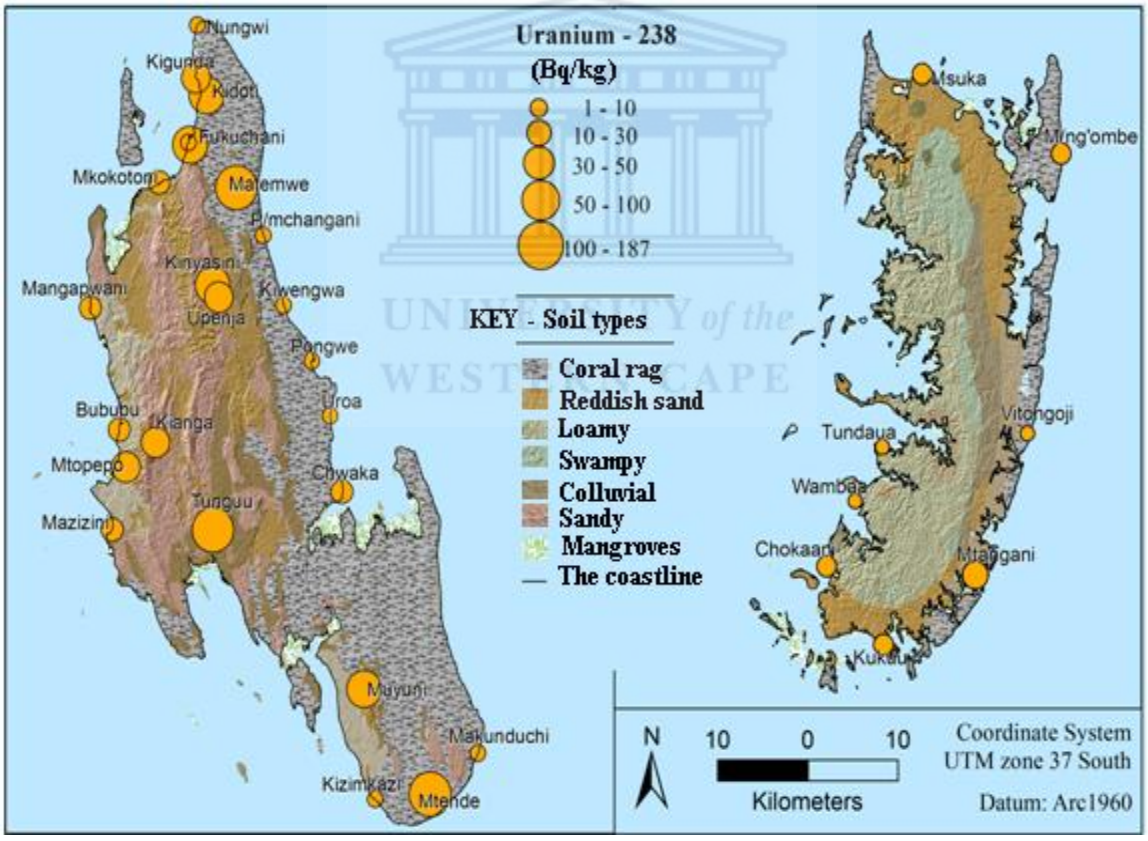

Figure 4.26: The distribution of ^{238}U in Unguja (left) and Pemba (right)

4.9.1 Activity concentrations of ^{40}K, ^{238}U and ^{232}Th measured in-situ and ex-situ

During NaI(Tl) in-situ measurements, soil samples were also collected in selected locations for ex-situ measurements using the HPGe detector (see Chapter 3, section 3.4.3). The summary of in-situ and ex-situ results measurements on the selected locations is presented in Table 4.9.

The variations in activity concentration of ^{40}K, ^{238}U and ^{232}Th obtained using the two detectors (Table 4.9) are as a result of various factors. Most importantly they measure different things. The HPGe measures the activity in the roughly 1.5 kg sample that was collected. The NaI detector measures the concentration from a much larger area from where gamma rays reach the detector. Samples were also not taken from exactly the same spot. The NaI(Tl) detector will obviously have much larger uncertainties associated with the measurements, but has the major advantage that it can be used in-situ to get a good indication if the area has a high or a low activity of the ^{40}K, ^{232}Th and ^{238}U and if it is an interesting area to investigate further by taking a sample. Other reasons for differences include environmental factors, standard gamma energy spectra used for calibration of detectors and data processing techniques (IAEA, 1990). While NaI(Tl) spectra were analysed using standard spectra collected from calibration pads, HPGe detector was calibrated using IAEA certified standard sources for uranium, thorium and potassium.

Table 4.9: Comparison between NaI(Tl) and HPGe measurements

Location		Activity concentration ($Bq.kg^{-1}$)					
		^{40}K		^{238}U		^{232}Th	
		NaI(Tl)	HPGe	NaI(Tl)	HPGe	NaI(Tl)	HPGe
Soils	Kidoti	187 ± 3	95 ± 4	161 ± 5	218 ± 11	97 ± 2	120 ± 6
	Mtende	117 ± 2	110 ± 5	187 ± 6	269 ± 12	47 ± 1	130 ± 6
	Tunguu	103 ± 2	30 ± 1	167 ± 5	520 ± 23	102 ± 2	87 ± 4
	Kigunda	33 ± 1	84 ± 4	53 ± 2	286 ± 12	49 ± 1	59 ± 3
Beach sands	Msuka	494 ± 8	381 ± 19	2 ± 0.1	2 ± 0.09	27 ± 0.6	1 ± 0.07
	Kukuu White	860 ± 14	443 ± 23	12 ± 0.4	18 ± 1	5 ± 0.1	10 ± 1
	Maziwa Ng'ombe	29 ± 0.5	BDL	6 ± 0.2	3 ± 0.1	11 ± 0.2	BDL
	Wambaa	516 ± 9	471 ± 23	2 ± 0.1	10 ± 0.5	8 ± 0.2	2 ± 0.1
	Tundaua	497 ± 8	428 ± 20	9 ± 0.3	8 ± 0.4	19 ± 0.4	12 ± 0.6
	Pwani Mchangani	271 ± 4	9 ± 0.5	28 ± 1	6 ± 0.1	29 ± 0.6	1 ± 0.11
	Chwaka	78 ± 1	351 ± 18	3 ± 0.09	12 ±	18 ± 0.4	18 ± 1

When comparing in-situ and ex-situ measurements, one should expect to see higher concentrations of ^{40}K, ^{238}U and ^{232}Th from in-situ results since the in-situ measurements include other sources of background gamma radiation such as cosmic rays. In this work, high concentration values of ^{40}K were observed in all measured locations except Kigunda soil and Chwaka beach.

The ^{238}U activity concentration values in soils and beaches obtained during in-situ measurements are lower compared to the results obtained by using the HPGe detector except for Pwani Mchangani beach. The estimated ^{232}Th activity concentration in soil follows a similar trend as ^{238}U except for Tunguu soil. The low activity of ^{238}U measured in-situ may be attributed to ^{222}Rn gas escape from the soil or beach since the in-situ measurements are sensitive to gamma emitting nuclei that are dominated by elements below radon in the decay chain. ^{222}Rn gas with a half life of 3.82 days is among the daughters of ^{238}U which escapes easily from drier soils than in moist soils (Ongori et al., 2015). In moist soils, water tends to block soil pores which results in a lower escape rate

of ^{222}Rn in the soil. As a result the build-up of ^{222}Rn in water close to the surface increases the apparent ^{238}U content (Lovborg, 1984; Grasty, 1997). The low activity of ^{238}U in soils measured in-situ could also be caused by vegetation cover (Travassos and Pires, 1994), non-uniform nature of the area (Tesi 2012) and difference in calibration procedure of the detectors (Xhixha, 2012).

The primary objective of using NaI(Tl) in this work was to study the levels and spatial distributions of ^{40}K, ^{238}U and ^{232}Th in the surveyed areas. Despite differences in the results obtained in-situ and ex-situ, NaI(Tl) detector measurements demonstrate that reliable information about the distribution of the radionuclides (^{40}K, ^{238}U and ^{232}Th) can be obtained in a relatively short time and can help to decide where further investigations are needed.

.

4.10 Gamma absorbed rate in air and associated radiological risks

The results of an assessment of the outdoor gamma absorbed dose rates from beach sands and soil samples and its associated radiological dose are presented in the following sections. The in-situ data are presented as maps and ex-situ results are presented in tabular form. These reults are calculated as described in section 3.8.

4.10.1 In-situ mapping of gamma absorbed rate in air from beaches

The in-situ mapping was used to generate spatial distribution patterns of gamma dose rates for the two surveyed beaches as shown in Figure 4.27. The gamma absorbed dose rates ranged from 30 – 210 nGyh^{-1} with an average of 109 nGyh^{-1}. The spatial distribution maps of gamma dose rates are based on the in-situ mobile measurements. Although stationary measurements were performed using the MEDUSA γ-ray detector during in-situ measurements, samples were not collected for ex-situ measurements.

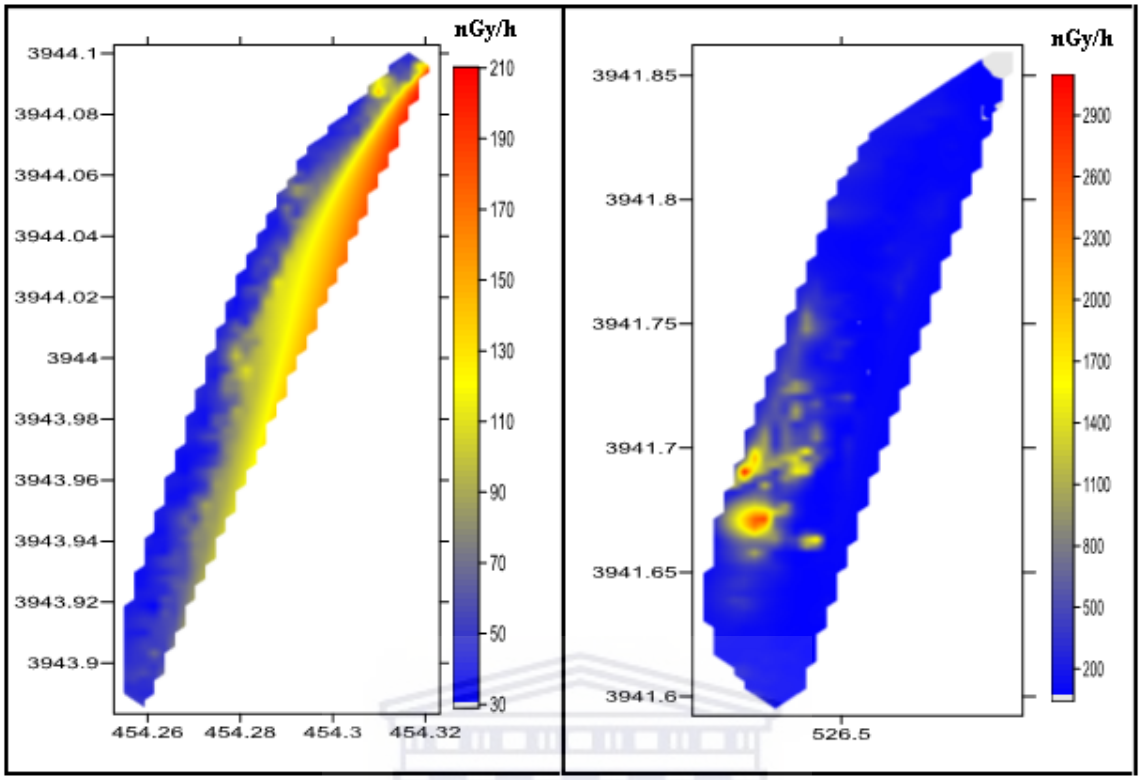

Figure 4.27: Interpolated absorbed dose rate ($nGyh^{-1}$) maps for Msuka beach (left) and Kukuu beach (right).

As seen in Figure 4.27, dose rates measured in a large section of Msuka beach are below the world population weighted average (57 $nGyh^{-1}$). The low gamma dose rates are observed on the sea side of the beach and on the land side part of the beach which is not accessible due to the bushes surrounding the beach. Thus, low gamma dose rates observed can be attributed to presence of light minerals and organic matter which generally contain low level of radioactivity. However, a sharp increase in gamma dose rate was observed on the same beach as shown in Figure 4.27 (left). The section which showed high doses is the accessible part of the beach away from the sea. This section of the beach is used for various human activities such as a landing site where boats offload fish. The high gamma dose rates observed may be attributed to human activities along the beach or the more radioactive soil from the land eroding onto the beach.

The discovery of black sand containing heavy minerals on Kukuu beach obviously needed to be investigated for possible high dose rates. The observed gamma dose rates at

Kukuu beach ranged from 180 – 2200 $nGyh^{-1}$ with an average of 122 $nGyh^{-1}$. As seen in Figure 4.25 (right), the gamma dose rate on nearly the whole of the beach is less than 200 $nGyh^{-1}$. However, an extremely high dose rate (50 times higher) than the world population weighted average was measured at the section of the beach where the black sand is located. The high gamma dose rates observed at Kukuu beach is clearly a result of heavy minerals along the beach.

The spatial variability pattern in measured dose rates (Figure 4.25) was found to correspond to the type of sand present on the surveyed beach as expected. The lower dose is associated with white and grey sand whereas higher dose be associated with black sand which is rich in heavy minerals.

4.10.2 Ex-situ mapping of gamma absorbed rate beach sand samples

During in-situ survey with the NaI(Tl) detector, samples were collected for ex-situ measurements using the HPGe detector. The estimated ex-situ outdoor absorbed gamma dose rate in air due to the presence of ^{226}Ra, ^{232}Th and ^{40}K in the beach sand sediments in the study area and their percentage contributions are given in Table 4.10. Table 4.10 also shows the relative contribution of ^{226}Ra, ^{232}Th and ^{40}K radionuclides to the estimated total dose rates.

It may be noted from Table 4.10 that the ^{226}Ra contributed highest in white beach samples, with an average value of 40% and a maximum of 82%, whereas the average contribution of ^{40}K to the absorbed dose rate is 35%, with a maximum of 91%. ^{232}Th contributed an average of 25% to the absorbed dose rate with a maximum of 77%. However, in samples PBS 9A and PBS 9B, from black sands on Kukuu beach the contribution of ^{232}Th to the total absorbed dose rate is the highest, with an average value of 71%, followed by ^{226}Ra with an average of 28%. ^{40}K contributed the least with an average of less than one percent. This implies that, ^{232}Th contributed significantly to the total dose rate as found in samples PBS 9A and PBS 9B (black sand), whereas ^{226}Ra is the highest contributor to the total dose rate in white beach sand samples. The relative

contributions of ^{40}K, ^{226}Ra and ^{232}Th to the absorbed dose rate are usually about 35%, 25% and 40% respectively (UNSCEAR, 2008). The high thorium value is an indication of the mineral content of the heavy mineral sands.

Table 4.10: Ex-situ gamma absorbed dose rates in air and percentage contribution from ^{226}Ra, ^{232}Th and ^{40}K in beach sand samples

Sample code	**Dose rate ($nGyh^{-1}$)**			**Total dose ($nGyh^{-1}$)**	**Percentage contribution (%)**		
	^{226}Ra	**^{232}Th**	**^{40}K**		**^{226}Ra**	**^{232}Th**	**^{40}K**
PBS 2	0.92	0.60	15.89	**17 ± 2**	5.31	3.47	91.23
PBS 4	2.31	0.60	0.33	**3.2 ± 0.2**	18.14	18.60	10.27
PBS 9A	492.95	1653.15	9.01	**2160 ± 162**	34.31	76.71	0.42
PBS 9B	248.09	470.52	4.55	**720 ± 56**	4.82	65.06	0.63
PBS 9C	8.32	6.04	18.47	**32 ± 3**	71.13	18.40	56.27
PBS 11	4.62	1.21	19.64	**25 ± 8**	23.84	4.74	77.12
PBS 12	7.85	7.25	17.85	**32 ± 3**	73.89	22.00	54.17
UBS 14	3.23	0.60	0.13	**3.9 ± 0.2**	65.99	15.24	3.16
UBS 19	2.77	0.60	0.38	**3.7 ± 0.5**	17.85	16.10	10.00
UBS 20	2.31	0.60	0.33	**3.2 ± 0.2**	25.33	18.60	10.27
UBS 22	2.77	0.60	0.58	**4.0 ± 0.7**	70.00	15.25	14.74
UBS 23	5.54	10.87	14.64	**31 ± 3**	22.87	35.10	47.14
UBS 27	3.23	1.21	0.46	**5.0 ± 0.6**	18.00	24.65	9.36
UBS 35	0.92	1.21	17.06	**19 ± 1.6**	81.60	6.30	88.89
UBS 37	5.54	10.87	14.39	**31 ± 2**	70.00	35.30	46.71
Weighted average				**4.0 ± 0.12**			

The ex-situ outdoor gamma dose rates obtained in beach sand samples ranged from 3 to 2160 $nGyh^{-1}$. The calculated outdoor gamma dose rates obtained from Zanzibar beach samples are extremely low, except for samples PBS 9A and PBS 9B. The low dose rates observed in beach sand sediments may be attributed to the presence of light minerals (Carvalho et al., 2011). The absorbed dose rates obtained in samples PBS 9A and PBS 9B are 38 and 12 times higher than the average level. These two samples were excluded in

calculating the average ex-situ outdoor absorbed gamma dose rate in beach sand samples in the study area.

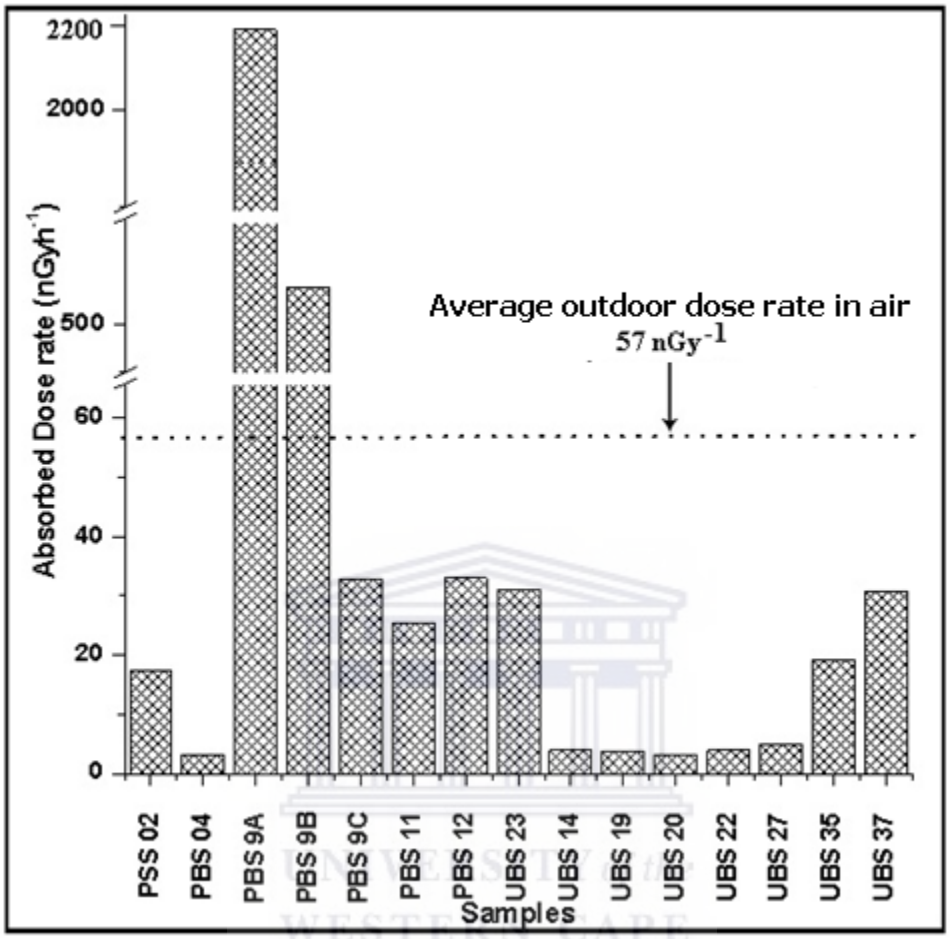

Figure 4.28: Outdoor absorbed dose rates from beach sands.

The obtained average absorbed rate in beach sand sediments is 4.0 ± 0.12 nGy h^{-1}. This value is a factor of sixteen lower than the corresponding population weighted value of 57 $nGyh^{-1}$. The absorbed dose rates obtained in beach sand sediments in the present study is compared with the other studies from other parts of the world as shown in Table 4.11. When compared with other beaches, the absorbed dose rate measured from Zanzibar coastline is lower than the weighted average dose rates measured in other countries (Table 4.11). This shows that the mineral content of Zanzibar beach sand has very low radioactive content.

Table 4.11: Comparison of absorbed dose rates from the Zanzibar beach sand sediments and other studies from other countries.

Location	Dose rate ($nGyh^{-1}$)	Reference
Zanzibar	4 ± 0.12	This study
South coast beaches, Kenya	22 ± 3	Kaniu et al. (2018)
Red sea coast, Egypt	51 ± 2	Harb (2008)
Red sea coast, Sudan	53 ± 19	Sam et al. (1998)
Guarapari, Brazil	985 ± 348	Veiga et al. (2006)
East coast of Orissa, India	1925 ± 718	Sengupta et al. (2005)
Cox's Bazaar, Bangladesh	65 ± 20	Ahmed et al. (2014)
South west coast, Australia	23 ± 19	De Meijer et al. (2001)
Andaman coast, Thailand	31 ± 1	Malain et al. (2010)
Canary island beaches, Spain	44 ± 3	Arnedo et al., (2013)
Tamilnadu, India	59 ± 6	Punniyakotti et al. (2017)

The much higher absorbed dose rate from Kukuu black sand is still lower than the dose rate reported from high background radiation areas such as Orissa, Tamilnadu and Guaraparri. The higher gamma dose rates reported in the other studies has been attributed among other causes, presence of heavy mineral deposits in beach sands and geological setting of the surrounding environments (Mohanty et al., 2004; Ramasamy et al., 2009b).

4.10.3 In-situ outdoor gamma absorbed rate from the soil samples from inland areas

As mentioned in section 3.3.2, the MEDUSA detector was used to map three land sites in Unguja island, namely Kidoti (North), Tunguu (Central) and Mtende (South). The activity concentrations generated by the MEDUSA detector (sections 4.5.1 and 4.5.2) were converted to absorbed dose rate in air using equation 3.2. The dose rates measured in soil in-situ in Tunguu, Mtende and Kidoti ranged from 90 – 320 $nGyh^{-1}$ with an average of 192 $nGyh^{-1}$, 75 – 160 $nGyh^{-1}$ with an average of 109 $nGyh^{-1}$ and 120 – 180 $nGyh^{-1}$ with an average of 143 $nGyh^{-1}$, respectively. The world population outdoor gamma dose rate from soil ranges between 18 – 93 $nGyh^{-1}$ with an average of 57 $nGyh^{-1}$ (UNSCEAR, 2008).

The spatial distribution of outdoor absorbed dose rates (Figure 4.29) in the surveyed land were generated using Golden SURFER software. As seen in Figure 4.29, the dose rate in the surveyed areas is not uniform. While the highest dose rate measured at Tunguu is 310 $nGyh^{-1}$, the highest dose rate measured at Mtende is 155 $nGyh^{-1}$. Although the soil in these surveyed areas looks the same, the Tunguu soil is composed of sandstones. The high dose rate at Tunguu area may also be associated with anthropogenic activities such as land cultivation and human settlement as well as topographical effects such as vegetation and rock outcrops (Santawamaitre el al., 2011).

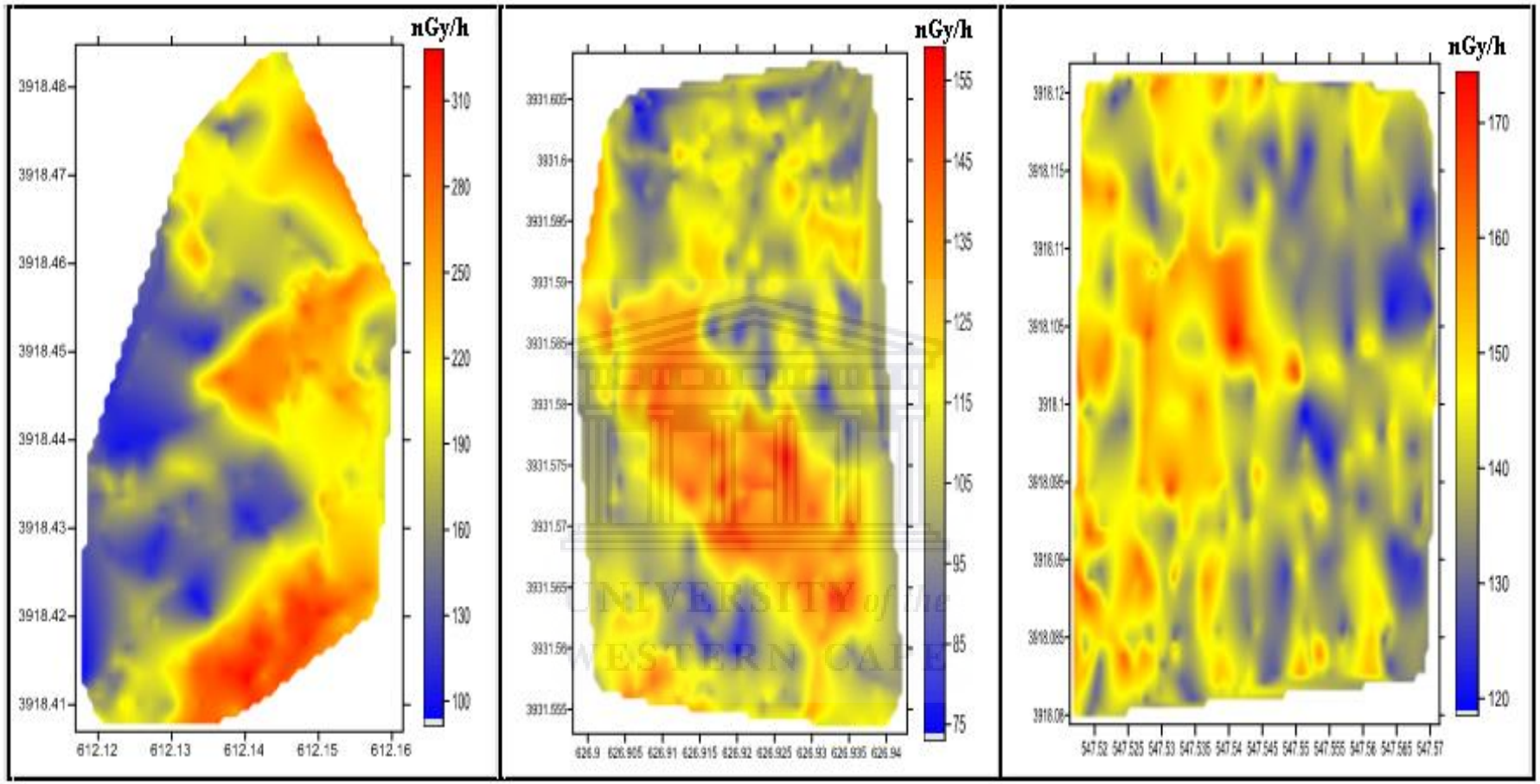

Figure 4.29: Interpolated absorbed dose rate maps for Tunguu (left), Mtende (middle) and Kidoti (right).

4.10.4 Ex-situ outdoor gamma absorbed dose rate in air from soil from inland areas

The relative contribution of ^{226}Ra, ^{232}Th and ^{40}K to the total absorbed dose rate in soil samples collected from various parts of Zanzibar is presented in Table 4.12. As it can be seen, the contribution of ^{226}Ra to the total absorbed dose ranged from 26% to 81% with an average value of 55%, followed by ^{232}Th with an average of 32% ranging from 19% to 43%. The average contribution of ^{40}K is 13% with a maximum of 45%. From Table 4.12, it is clear that the highest contributor to the total absorbed dose in soil samples is ^{226}Ra.

Mishira and Sadasiran (2005) have reported these percentage contributions in the order of 17.7%, 33.6% and 48.7% due to ^{226}Ra, ^{232}Th and ^{40}K for Indian environs. UNSCEAR has reported the worldwide average values for the relative contributions from ^{226}Ra, ^{232}Th and ^{40}K gamma dose rate in air to be 25%, 40% and 35% respectively for normal background areas (UNSCEAR, 2008).

Table 4.12: Ex-situ gamma dose rates in air and percentage contribution from ^{226}Ra, ^{232}Th and ^{40}K in soil samples.

Sample Code	Dose rate (nGyh^{-1})			Total dose (nGyh^{-1})	Percentage contribution (%)		
	^{226}Ra	^{232}Th	^{40}K		^{226}Ra	^{232}Th	^{40}K
USS 9	13	15	23	50 ± 4	26	29	45
USS 15	132	36	4	171 ± 13	77	21	2
USS 16	101	72	4	177 ± 15	57	41	2
USS 26	124	79	5	207 ± 16	60	38	2
USS 28	28	29	27	84 ± 8	33	35	32
USS 29	228	53	1	294 ± 21	81	19	0.4
USS 30	73	59	6	139 ± 11	53	43	5
Average				**86 ± 3**			

The calculated ex-situ outdoor absorbed dose rates for soil samples (Table 4.12) are illustrated in Figure 4.30. The lowest absorbed dose rate (50 nGyh^{-1}) calculated was found in sample PSS 9 from Kukuu village while the highest absorbed dose rate (294

$nGyh^{-1}$) calculated was found at the sample UBS 29 collected from Tunguu. The highest absorbed dose rate calculated and found in sample UBS 29 is approximately five times higher than the average outdoor absorbed dose rate in air from soil. Other soil samples which gave higher calculated dose rates are USS 26, USS 16, USS 15, USS 30 and USS 28. The weighted average dose rate for the soil samples was found to be 86 $nGyh^{-1}$ (see Table 4.12). This is slightly higher than the world average (57 $nGyh^{-1}$) of outdoor dose rate in air (UNSCEAR, 2008), but this may be due to the bias introduced when choosing the sample sites.

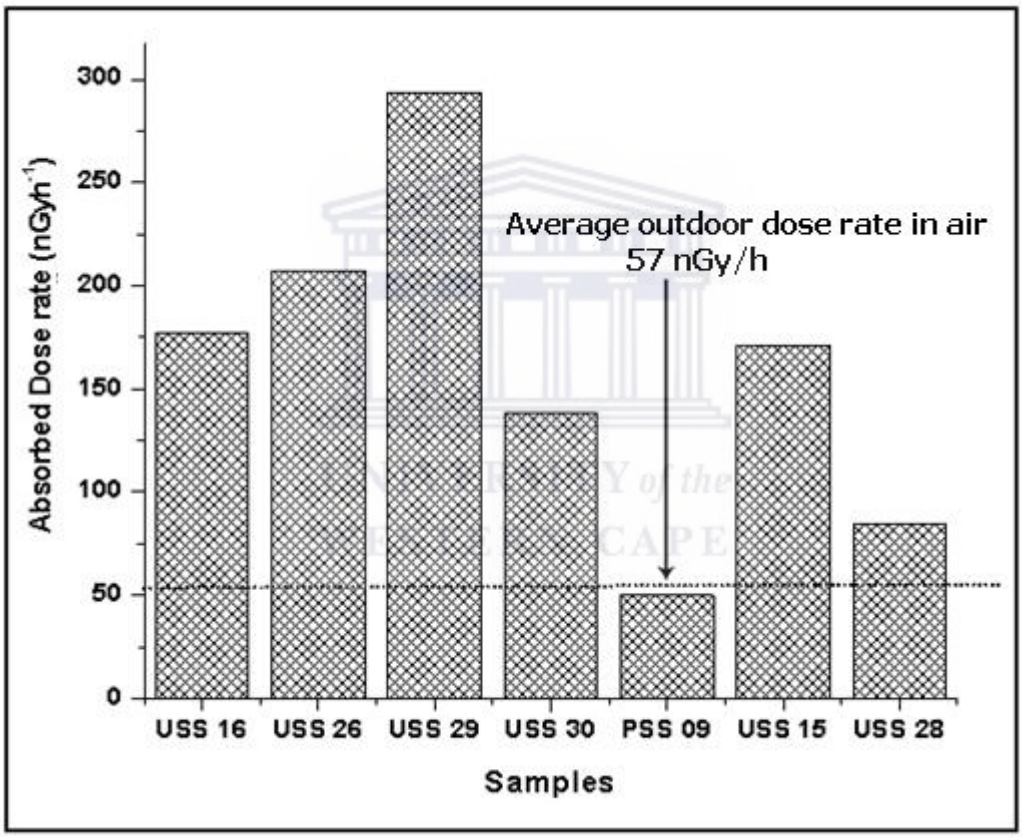

Figure 4.30: Distribution of absorbed dose rate in air in measured soil samples. The solid horizontal line represents the world average (UNSCEAR, 2008).

The absorbed dose rate results obtained from Zanzibar soils were compared with published values from other areas of the world (see Table 4.13). Results from this study are higher than reported values from south western Cameroon, Chao Phraya-Thailand, state of Kuwait, Cyprus, Eastern Canary Islands and Russia. On the other hand, the

calculated absorbed dose rate in soil samples in the present study is comparable with the published data from Izmir-Turkey and Hong Kong. Moreover, the dose rate results obtained in soil samples are lower compared to the published values from Kenya, Malaysia, Namibia and western Ghats-India.

Table 4.13: Comparison of absorbed dose rates from the Zanzibar soils and other studies in the world.

Location	**Dose rate ($nGyh^{-1}$)**	**Reference**
Zanzibar	**86 ± 3**	**This study**
Lambwe east, Kenya	2300 ± 62	Achola et al., (2012)
Mrima Hill, Kenya	967 ± 36	Kaniu et al., (2018)
Izmir, Turkey	86 ± 4	Taskin et al. (2009)
South-Western, Cameroon	29 ± 2	Kardan et al. (2017)
Chao Phraya, Thailand	65 ± 27	Santawamaitre et al. (2011)
State of Kuwait	33 ± 2	Al Azemi et al., (2015)
Cyprus	9 ± 1	Tzortzis et al. (2004)
Melaka state, Malaysia	172 ± 17	Ramli et al. (2005)
Henties Bay, Namibia	126 ± 36	Shimboyo SA & Oyedele J A (2012)
Western Ghats, India	133 ± 18	Manigandan, P.K. & Shekar, B.C. (2014)
Eastern Canary Islands	57 ± 2	Arnedo el al. (2017)
Hong Kong	87 ± 5	Yu et al. (1992)
Perak, Malaysia	222 ± 191	Lee et al. (2009)

4.10.5 Annual Effective Dose Equivalent (AEDE)

The calculated outdoor AEDE values for three categories of people using the Zanzibar beaches are presented in Table 4.14 based on the occupancy values given in Section 3.8.2. The values ranged from 4 to 2644 μSvy^{-1} for locals working on the beaches for their daily living. For hotel workers working on beaches, the outdoor AEDE ranged from 0.47 to 1056 μSvy^{-1} and for tourists using Zanzibar beaches during holidays, the outdoor AEDE ranges from 0.1 to 158 μSvy^{-1}.

Table 4.14: Ex-situ outdoor Annual Effective Dose Equivalent (AEDE) calculated from beach sand samples.

Sample code	AEDE (μSvy^{-1})				
	Locals	Tourists		Hotel workers	
		Minimum	Maximum	Minimum	Maximum
PBS 2	21.36	0.51	1.28	2.54	8.53
PBS 4	3.99	0.10	0.24	0.47	1.59
PBS 9A	2644.33	63.39	158.48	313.94	1056.53
PBS 9B	887.54	21.28	53.19	105.37	354.61
PBS 9C	40.28	0.97	2.41	4.78	16.10
PBS 11	31.25	0.75	1.87	3.71	12.48
PBS 12	40.43	0.97	2.42	4.80	16.15
UBS 14	4.87	0.12	0.29	0.58	1.95
UBS 19	4.61	0.11	0.28	0.55	1.84
UBS 20	3.99	0.10	0.24	0.47	1.59
UBS 22	4.86	0.12	0.29	0.58	1.94
UBS 23	38.10	0.91	2.28	4.52	15.22
UBS 27	6.02	0.14	0.36	0.71	2.40
UBS 35	23.53	0.56	1.41	2.79	9.40
UBS 37	37.79	0.91	2.26	4.49	15.10

The outdoor AEDE corresponding to ordinary white beach sand samples in this study are lower than the average value of 70 μSvy^{-1} (UNSCEAR, 2008). The low outdoor AEDE values in most beach sand samples are due to the presence of low activity concentrations of ^{226}Ra, ^{232}Th and ^{40}K. Highest outdoor AEDE values are observed at sample PBS 9A for locals (2644 μSvy^{-1}) and hotel workers (1056 μSvy^{-1}) which is 38 and 15 times higher than the average level. For tourists using beaches during holidays, the maximum outdoor AEDE value is 158 μSvy^{-1}. The low outdoor AEDE values obtained from white beach sand samples is an indication that the surveyed beaches are safe for use from a radiation safety point of view.

The calculated values of outdoors AEDE for soil samples (Table 4.15) ranges from 61 to 345 μSvy^{-1}. The values obtained for most soil samples are higher than the world average value of 70 μSvy^{-1} for outdoor AEDE in soil samples due to the presence of high activity concentration of ^{238}U and ^{232}Th (UNSCEAR, 2008).

Table 4.15: Annual Effective Dose Equivalent (AEDE) in μSvy^{-1} for soil samples

Sample code	AEDE (μSvy^{-1})
USS 9	61.55
USS 15	202.64
USS 16	217.27
USS 26	253.46
USS 28	104.83
USS 29	345.26
USS 30	173.91

From a radiological point of view, the result from this study indicates that most of the beach sand samples studied are considered to be safe. The radiological hazards to people being exposed to natural radiation emitted from Zanzibar beaches are at the typical level of natural background radiation.

4.11 Summary

The activity concentration of natural radionuclides (^{40}K, ^{232}Th and ^{238}U) in soil and beach sand samples measured in-situ (using the NaI(Tl) and the MEDUSA γ-ray detectors) and ex-situ (using the HPGe detector) and their distributions have been presented and discussed. The MEDUSA detector results were presented as maps showing spatial distributions of natural radionuclides in land surveyed namely, Kidoti, Tunguu and Mtende and beaches surveyed namely, Msuka and Kukuu, whereas HPGe and NaI(Tl) detector results were presented using tables.

The activity concentration of ^{232}Th, ^{238}U and ^{40} K in beach sand ranges from BDL to 2671 $Bq.kg^{-1}$, 2 to 1055 $Bq.kg^{-1}$ and 3 to 471 $Bq.kg^{-1}$, respectively. The obtained weighted average values of ^{232}Th, ^{238}U and ^{40} K in beach sand are 1, 4 and 4 $Bq.kg^{-1}$, respectively. These values are lower than the world average values of 33, 45 and 420 $Bq.kg^{-1}$ (UNSCEAR, 2008). Two black beach sand samples PBS 9A and PBS 9B were found to have greatly enhanced radioactivity levels due to the presence of heavy minerals. Moreover, soil samples were found to have much higher activity concentration of ^{232}Th and ^{238}U compared to white beach sand sediments. ^{40}K activity concentration is lower in

soil samples compared to most beach sand samples. Furthermore, the activity concentration of ^{232}Th, ^{238}U, and ^{40}K radionuclides in this study are lower than the values reported in similar studies conducted elsewhere around the world.

The outdoor gamma dose rates obtained in beach sand samples ranged from 3 to 2156 $nGyh^{-1}$. The highest absorbed dose rate obtained in sample PBS 9A is 38 times higher than the average level of 57 $nGyh^{-1}$ (UNSCEAR, 2008). The calculated ex-situ outdoor absorbed dose rate for soil samples ranged from 50 to 294 $nGyh^{-1}$. The highest dose rate was measured in sample USS 29 which is approximately five times higher than the average outdoor absorbed dose rate in air from soil.

CHAPTER 5

The correlation between major and trace elements and the ^{232}Th, ^{238}U activity concentrations of beach sand

5.1 Introduction

The natural radionuclides of ^{232}Th and ^{238}U are among the constituents of beach sand (Veiga et al., 2006) as also found in this work. The concentration of these radionuclides in beach sand is also associated with the presence of heavy and light minerals**.** Heavy minerals are those minerals with density greater than 2.9 gcm^{-3} whereas light minerals are minerals with density less than 2.9 gcm^{-3} (De Meijer et al., 2001). The contents of heavy and light minerals deposited on coastal areas are also linked to the geochemical (major and trace) composition of beach sand. The variations in major and trace element contents are therefore a tool for interpreting possible origin of heavy minerals in beach sand and for discriminating physico-chemical processes affecting the geology of the area.

This chapter focuses on examining the correlation of major and trace elemental compositions on ^{232}Th and ^{238}U activity concentrations of the beach sand in the study area. The natural radioactivity data provided in Chapter 4 will be complemented with major and trace results to study the influence of the major and trace element variations on or links between the ^{232}Th and^{238}U activity concentrations. Furthermore, major and trace elemental compositions data will be used to trace the origin of heavy minerals along the Kukuu beach.

5.2 Comparison of ^{232}Th and ^{238}U obtained by HPGe gamma ray detector and ICP MS spectroscopy

The elemental concentrations of U and Th in beach sand samples were determined ex-situ using the HPGe γ-ray detector (see Chapter 4, section 4.6). The obtained results are compared with the U and Th elemental concentrations obtained using ICP MS analysis as shown in Figure 5.1.

In general, the ex-situ results obtained using the HPGe detector and ICP MS results for Th and U show a similar pattern (see Figure 5.1). It should be noted that the HPGe results are in general slightly higher compared to ICP MS results. This variation can be attributed to the differences in the two analytical techniques. As discussed earlier in section 3.4.2, with the HPGe detector, samples of approximately 1.5 kg were put in Marinelli beakers whereas analysis by ICP MS was directly made on a split approximately 2.5 g. This can lead to differences since much of the sand is not very uniform.

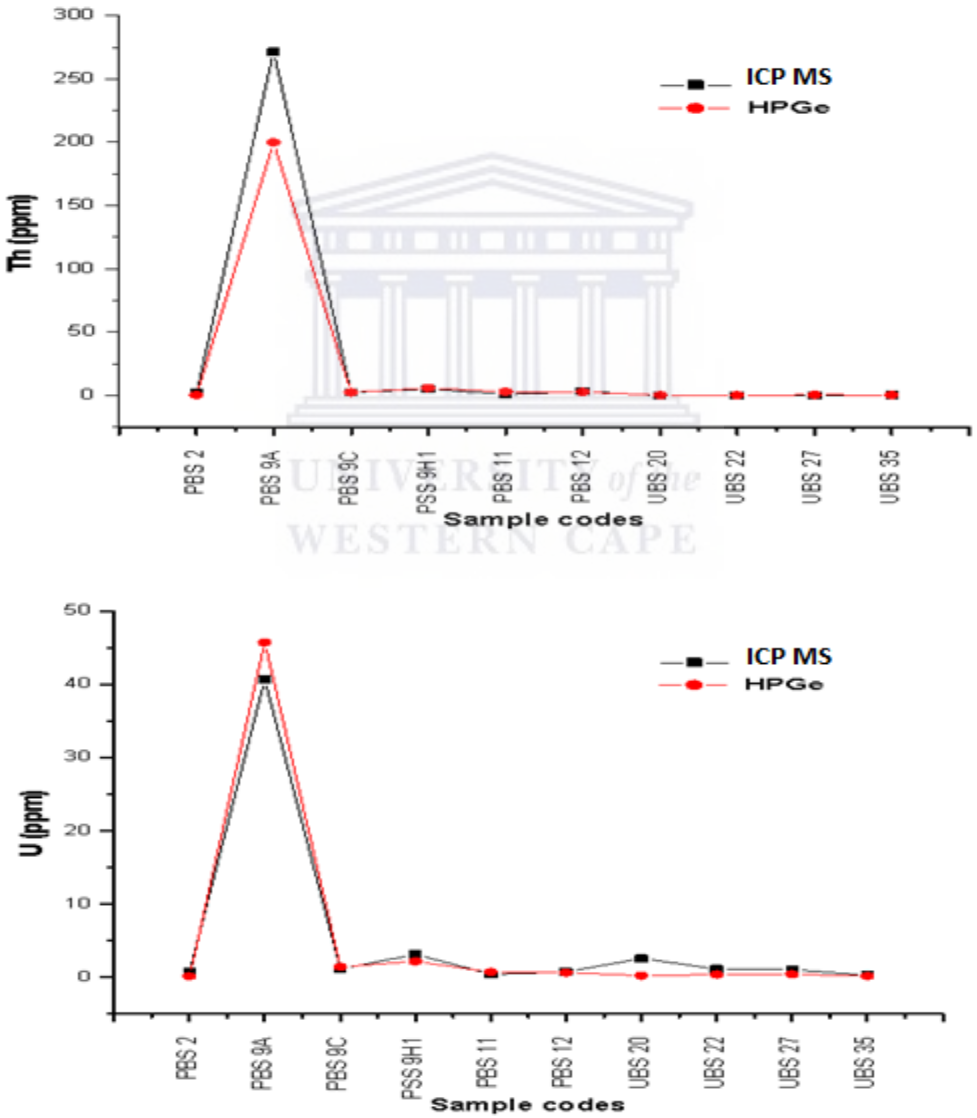

Figure 5.1: Comparison of Th and U concentrations in beach sand measured by HPGe and ICP MS spectroscopic analysis

5.3 Composition of major and trace elements in studied beach sands

The concentrations of major elements (expressed as weight percentage) and trace elements (expressed as ppm) in beach sand representing both low and high levels of natural radioactivity as determined by XRF and ICP MS analyses (see Chapter 3, sections 3.9 and 3.10), respectively, are considered in this section. The results of major elements with corresponding LOI (loss on ignition) values for each sample are presented in Table 5.1, whereas trace elements results of the studied samples are presented in Table 5.2.

5.3.1 Major elements

The concentration of SiO_2 (the most common constituent of sand in inland continental settings) in the studied samples fluctuates between 0.18 and 93.47%, whereas the content of CaO (linked to coral) ranges between 0.11 to 55% and LOI varies from -2 to 45%. The total weight percentage of TiO_2 is between 0.01and 42.02%, Fe_2O_3 contents are in the range of BDL to 33% and Al_2O_3 content ranges from BDL to 16%. K_2O, MgO, MnO, Na_2O and P_2O_5 were found in small amounts in beach sand samples.

Beach sand samples PBS 1, PBS 2, PBS 3, PBS 9C, PBS 11, PBS 12, PBS 13 and UBS 35 were found to have the highest SiO_2 contents among the studied beach sand samples ranging from 69 to 91%. Samples UBS 24, UBS 20, UBS 27, PBS 4, UBS 24 and UBS 22 have surprisingly low SiO_2 contents ranging from BDL to 0.31%. Beach sand samples PBS 9A and PBS 9B (black sand samples) have SiO_2 contents ranging from only 3.9 to 6.81% while samples PBS 9D and PBS 9E from the same beach as black sand samples have SiO_2 contents ranging from 45.19 to 47.68%.

The beach sand samples found with high SiO_2 contents contained low CaO and LOI contents ranging from 0.11 to 7.0% and 0.21 to 6.11% respectively, whereas the high contents of CaO and LOI of 55.92 to 55.34% and 44.08 to 45.13% respectively were

found in samples with low SiO_2 contents. In samples PBS 9A and PBS 9B, the contents of CaO are very low, less than 0.2%.

Table 5.1: Major element concentrations and LOI (Loss on ignition) expressed as weight percentage for the studied samples from the Zanzibar coasts measured by the Central Analytical Facility at Stellenbosch University.

Sample code	SiO_2	CaO	Al_2O_3	K_2O	MgO	MnO	Na_2O	P_2O_5	Fe_2O_3	TiO_2	L.O.I
PBS 1	74.00	7.00	7.83	2.81	0.19	0.01	1.79	0.03	0.28	0.33	5.42
PBS 2	88.10	0.82	4.96	1.73	0.19	0.01	1.26	0.02	0.43	0.41	1.27
PSS 2	85.70	0.60	5.31	1.08	0.15	0.02	0.66	0.05	0.64	0.40	5.09
PBS 3	93.47	0.11	1.37	0.40	0.13	0.02	0.35	0.02	0.84	1.42	0.91
PBS 4	0.31	52.92	0.03	0.02	2.08	BDL	0.87	0.07	0.01	0.04	45.13
PBS 9A	3.90	0.17	0.69	0.02	0.57	0.65	0.14	0.01	33.50	41.02	-2.03
PBS 9B	6.81	0.20	0.95	0.06	0.57	0.66	0.07	0.03	33.19	42.02	-1.99
PBS 9C	87.14	1.76	4.87	1.58	0.19	0.02	1.07	0.02	0.74	0.78	1.49
PSS 9H1	70.22	0.59	15.10	1.86	0.70	0.01	2.28	0.04	2.49	0.74	6.11
PSS 9H2	69.02	0.77	16.83	2.46	0.28	BDL	2.33	0.01	0.67	0.22	6.93
PBS 9D	47.68	25.29	2.73	0.98	0.81	0.02	1.04	0.04	0.19	0.14	22.07
PBS 9E	45.19	27.34	1.57	0.48	0.67	0.01	0.81	0.13	0.51	0.39	23.85
PBS 11	87.34	1.30	6.03	1.69	0.07	0.01	1.52	0.01	0.27	0.33	0.61
PBS 12	91.61	0.42	3.92	1.52	0.06	0.01	0.73	0.01	0.42	0.42	0.21
PBS 13	85.99	0.92	6.13	1.57	0.14	0.03	1.54	0.01	1.12	1.07	0.48
UBS 20	BDL	54.27	0.00	0.02	1.22	0.00	0.60	0.07	0.01	0.02	44.27
UBS 22	0.24	53.35	0.01	0.02	1.74	BDL	0.77	0.08	0.05	0.03	44.94
UBS 24	0.22	55.34	BDL	0.01	0.48	BDL	0.49	0.05	0.02	0.03	44.08
UBS 25	0.18	54.43	BDL	0.03	0.98	BDL	0.84	0.07	0.00	0.03	44.63
UBS 27	BDL	53.85	0.06	0.03	1.44	0.00	0.86	0.08	0.06	0.01	44.39
PBS 35	90.99	2.30	2.66	0.81	0.14	0.00	0.70	0.01	0.09	0.03	1.79

The majority of the studied samples contain low TiO_2 and Fe_2O_3 contents ranging from 0.01 to 1.42% and 0.01 to 2.49% respectively, except for samples PBS 9A and PBS 9B from Kukuu beach. These samples are characterized by much higher TiO_2 (41.02 – 42.02%) and Fe_2O_3 (33.19 – 33.50%) contents. The high TiO_2 and Fe_2O_3 contents in samples PBS 9A and PBS 9B from Kukuu beach is an indication of the presence of heavy minerals deposit along the beach. Heavy minerals such as ilmenite and rutile are rich in TiO_2, hence it is clear that one or both of these minerals are present on Kukuu beach.

Al_2O_3 contents are higher in samples PSS H1 and PSS H2 (soil samples) ranging from 15.10 to 16.83% and low in white beach sand samples ranging from BDL – 7.83%. MnO and P_2O_5 are present in very small amounts in all samples whereas K_2O, MgO and Na_2O are in more noticeable amounts ranging from 0.01 to 2.81%, 0.19 to 2.08% and 0.14 to 2.33% respectively.

5.3.2 Trace elements

Trace element results in the studied samples (Table 5.2) are characterised by higher concentration of zirconium (Zr) in sample PBS 9A. The Zr content measured in this research study ranges from 1.22 – 42250 ppm. The cerium (Ce) and strontium (Sr) content ranges from 0.15 – 1176 ppm and 25.34 – 5446 ppm, respectively. The contents of vanadium (V) and yttrium (Y) ranges from 1.81 – 555 ppm and 0.15 – 147 ppm, respectively. The Nb, Hf, La and Nd contents range between 0.08 – 322 ppm, 0.04 – 922 ppm, 0.09 – 605 and 0.11 – 474 ppm, respectively whereas the content of Ba ranges from 25.34 – 5446 ppm. The U and Th contents vary between 0.29 – 42 ppm and 0.01 – 275 ppm respectively. It is important to note that with the exceptions of Ba and Sr all other trace elements were higher in samples PBS 9A and PBS 9B. The contents of Sr that has similar behaviour as CaO, is high in beach sand samples with high CaO contents.

In summary, although the contents of Fe_2O_3 and TiO_2 and Zr in other samples are low, the high contents of Fe_2O_3, TiO_2 and Zr confirms the presence of heavy minerals in samples PBS 9A and PBS 9B.

Table 5.2: Trace element concentrations (in ppm) for the studied samples from the Zanzibar coast as measured by the Central Analytical Facility at Stellenbosch University.

Sample code	Zr	Y	Nb	Sr	V	Ce	Nd	Hf	Sc	Rb	Ba	Th	U
White sand													
PBS 1	196.60	2.12	5.62	783.00	15.34	6.8	3.09	4.83	5.52	46.3	1138	0.91	0.76
PSS 2	414.79	5.46	4.49	121.59	21.97	17.91	5.38	8.72	5.03	22.92	694	2.62	1.01
PBS 2	366.90	3.61	10.54	186.20	18.36	13.28	7.11	10.01	7.04	28.04	463.15	2.19	0.78
PBS 3	864.10	3.83	18.80	31.50	35.40	23.58	9.02	21.05	7.40	6.56	178.3	5.73	1.22
PBS 4	38.30	0.55	1.27	2310.00	4.01	1.21	0.51	1.26	0.17	0.09	3.07	0.14	0.88
PBS 9C	503.20	4.21	7.97	326.13	25.61	13.17	5.65	12.73	5.42	27.97	689.06	2.55	1.11
PBS 9D	140.46	3.27	1.60	3349.38	11.27	10.02	3.88	3.36	2.69	18.75	385.84	1.34	2.28
PBS 9E	537.63	7.11	4.47	2134.93	18.58	22.78	10.35	12.98	3.58	9.2	197.69	3.55	2.37
PBS 11	157.40	2.02	9.83	271.90	14.80	6.02	2.46	3.89	6.31	27.98	670	0.93	0.40
PBS 12	406.54	2.73	4.45	151.92	16.73	14.76	6.45	9.87	3.28	28.24	605.95	3.20	0.73
PBS 13	822.00	6.28	13.34	220.60	28.80	29.53	11.66	19.44	7.55	23.49	595.6	6.57	1.13
UBS 20	13.87	0.83	0.11	5446.47	5.19	0.83	0.47	0.29	0.43	0.17	8.06	0.11	2.58
UBS 22	3.18	0.45	1.58	2260.00	3.35	0.48	0.34	0.13	0.13	0.07	3.26	0.04	1.14
UBS 24	8.00	0.39	3.45	3300.00	4.09	0.5	0.31	0.68	0.07	0.18	4.1	0.17	1.46
UBS 25	1.22	0.15	0.49	1239.00	1.81	0.15	0.11	0.04	0.07	0.06	1.5	0.01	0.53
UBS 27	1.78	0.6	0.08	2315.97	3.14	0.76	0.52	0.06	0.20	0.17	4.56	0.04	1.05
UBS 35	39.17	0.69	0.29	346.74	7.23	2.26	0.86	1.07	2.79	14.94	324.81	0.35	0.29
Soil													
PSS 9H1	487.28	10.66	8.00	188.46	72.55	30.37	12.32	12.71	12.52	37.06	702.4	5.21	3.13
PSS 9H2	174.30	3.22	3.94	236.80	21.67	13.69	6.25	4.21	6.36	45.2	965	1.93	0.99
Black sand													
PBS 9A	42250.35	147.41	266.06	25.34	484.88	1132	463.39	922.15	38.72	0.55	40.13	275.43	42.05
PBS 9B	36460.00	142.4	322.30	31.96	555.10	1176	474.40	876.20	47.20	1.03	65.1	271.40	40.65

5.4 Classification of beach sand samples

Based on the major element results (Table 5.1) and trace element results (Table 5.2), the studied beach sand samples were classified into their geochemically similar groups using cluster analysis. All the elements listed in Tables 5.1 and 5.2 were used in classifying the samples. Due to variations in elemental compositions in the samples, it is impossible to obtain samples within the same cluster. Instead, more than one cluster is always created. To display the order in which elemental contents with similar properties are shown virtually, dendrograms were generated (see Figures 5.2, 5.3 and 5.4).

The most similar parameters are grouped first. These initial groups are combined according to their similarities. Similarity is a measure of distance between clusters relative to the largest distance between any two individual parameters. In their sample measurements, one hundred percent similarity means the clusters are zero distance apart. Conversely, the similarity of zero percent means the cluster areas are as different as the least similar region. In this research study, hierarchical agglomerative cluster analysis using Ward's method (Ward, 1963) was performed on major and trace elements with Euclidean distances used as a measure of similarity expressed from 0 to 25 (De Meijer et al., 2001; Liu et al., 2003; Sivakumar et al., 2014).

5.4.1 Classification of samples using major elements data

In Figure 5.2, samples are classified into four statistically significant groups based on the similarity of the major elements. Group I consists of PBS 2, UBS 20, UBS 22, UBS 24, UBS 25 and UBS 27 samples. These samples are characterised by low SiO_2 contents and with high percentage of CaO and LOI. The higher values of CaO and LOI in these six samples suggest the presence of significant biogenic $CaCO_3$ component. The high values of CaO and LOI reflect high shell contents in the samples.

The black sand samples (PBS 9A and PBS 9B) are classified in group II. These samples were from Kukuu beach and are characterised by higher TiO_2 and Fe_2O_3 contents. The

high contents of Fe_2O_3 and TiO_2 suggest the presence of heavy mineral such as ilmenite in these samples.

Group III include samples PBS 9C and PBS 9E from Kukuu beach which are characterised by their high percentage of SiO_2, CaO and LOI which reflect the presence of quartz and shells in these samples. These samples can be categorised as mixed sand samples.

Group IV consists of 11 samples; PBS 1, PBS 2, PSS 2, PBS 3, PBS 9C, PSS 9H1, PSS 9H2, PBS 11, PBS 12, PBS 13 and UBS 35. These samples are dominated with high SiO_2 content. The high SiO_2 concentrations reflect the presence of quartz in these samples. Groups III and IV are linked with higher similarity compared to linkage between Groups I and II.

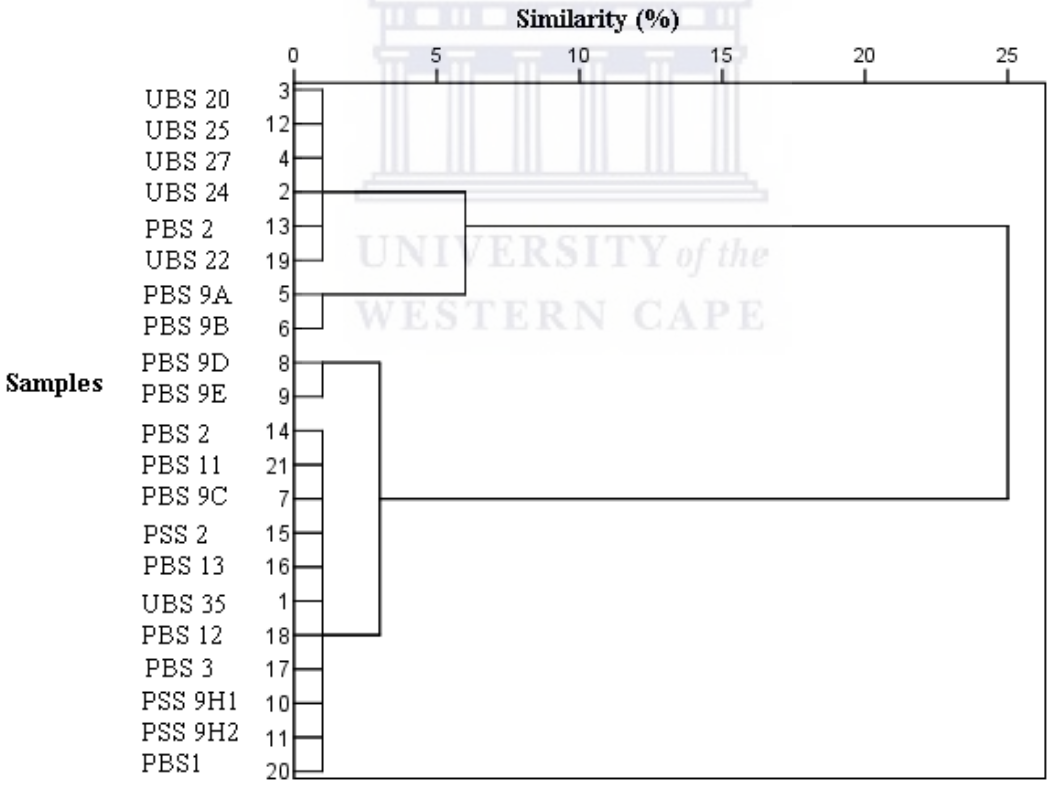

Figure 5.2: Dendrogram using major elements result consisting of 21 samples

One of the interesting findings in Figure 5.2 is that samples from Kukuu beach have been classified into four different groups, namely silicate group (rich in SiO_2), group of mixed sand (with high percent of SiO_2, CaO and LOI), carbonates (rich in CaO) and a heavy mineral sand group (dominated by Fe_2O_3 and TiO_2). The variations in seven Kukuu beach samples into three mineral groups could be attributed to the difference in the origin of these sources (see section 5.6) and a real reflection of the large differences found on the same beach.

5.4.2 Classification of samples using trace elements data

Using trace elements data, a dendrogram comprising of 21 samples was generated as shown in Figure 5.3. In this dendrogram, samples are classified into two clusters. Cluster I consisting of 19 samples characterised by low concentrations of zircon. Cluster II is comprised of two samples with high contents in zircon, samples PBS 9A and PBS 9B.

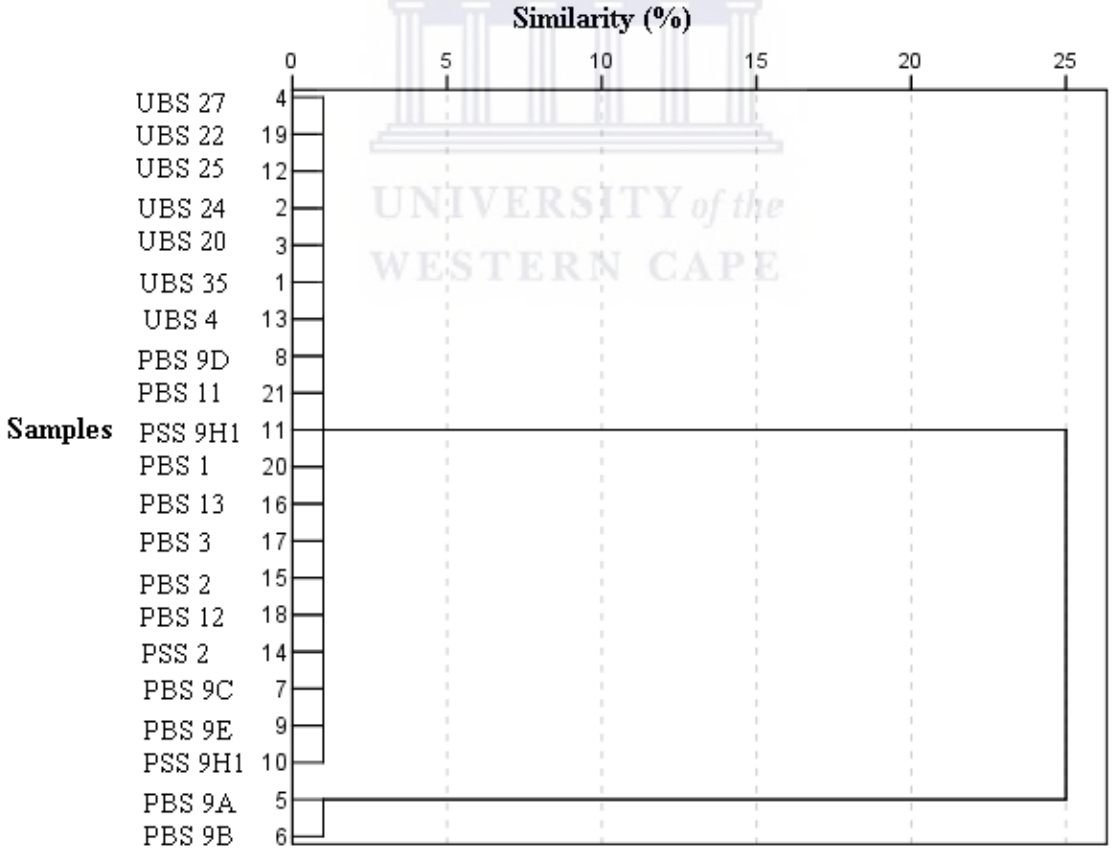

Figure 5.3: Dendrogram using trace elements result consisting of 21 samples.

Due to its high zircon content, these two samples were excluded and a new dendrogram consisting of 19 samples was plotted as shown in Figure 5.4. In this new dendrogram, four groups have been generated.

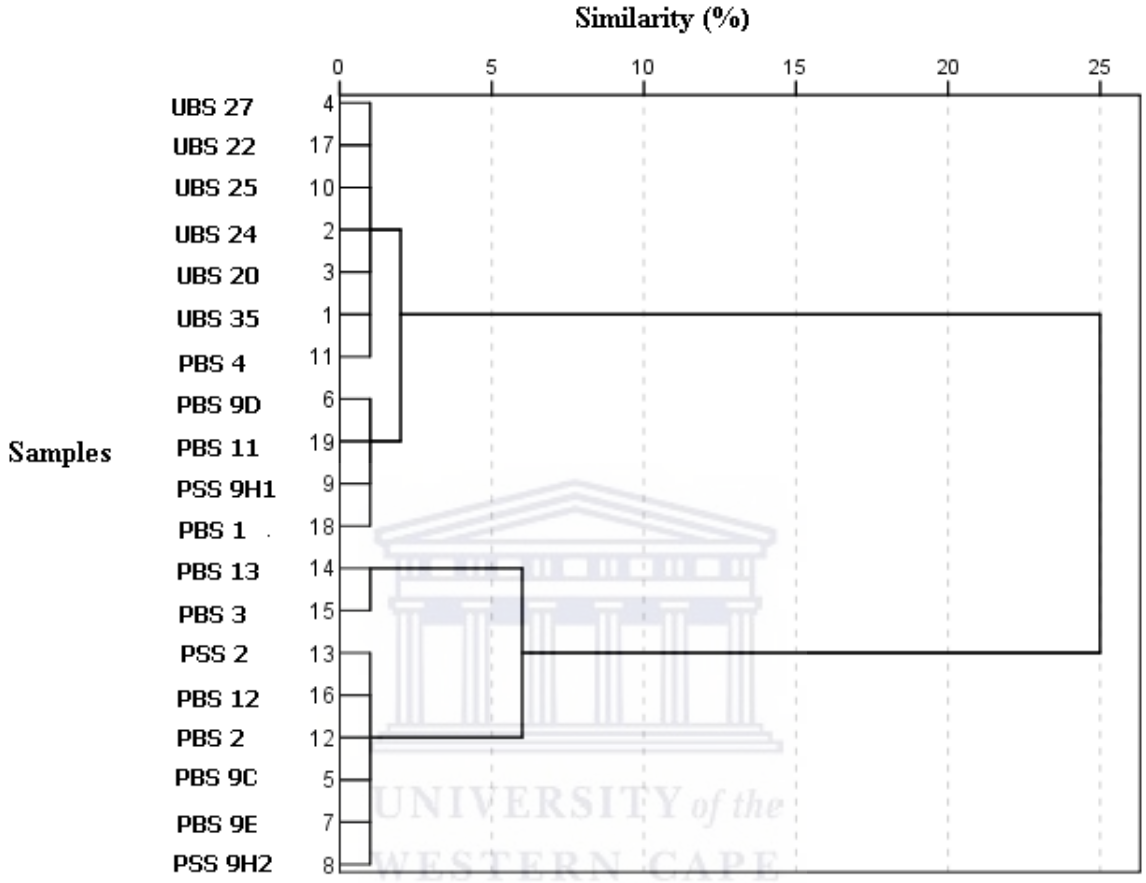

Figure 5.4: Dendrogram using trace elements result consisting of 19 samples

5.5: Correlations between ^{238}U, ^{232}Th concentrations and major and trace element concentrations of beach sand from the Zanzibar coast

In order to examine the possible link between the major and trace elements and the activity concentrations of ^{232}Th and ^{238}U in the beach sand in the study area, Pearson's correlation analysis has been performed. Earlier studies (Macdonald et al., 1997) have shown that the U and Th content that are easily measured by gamma spectroscopy in-situ, can be a valuable indicator of mineral content in soils. The results of the Pearson correlation analysis for both major and trace elements and the activity concentrations of

^{238}U, ^{232}Th are presented as a linear correlation matrix in Table 5.3 and Table 5.4 respectively. The natural radioactivity parameters and major and trace elements (Tables 5.1 and Table 5.2) were used.

Among the major elements, SiO_2, Fe_2O_3 and TiO_2 are significantly correlated with the activity concentration of ^{232}Th at 0.05 significance level. A negative but significant correlation was found between ^{232}Th and CaO and MgO at 0.01 and 0.05 significance levels respectively. The correlations of the remaining major elements namely; Al_2O_3, Na_2O, MgO and P_2O_5 with ^{232}Th activity concentration are insignificant. The strong correlations between SiO_2, Fe_2O_3 and TiO_2 and ^{232}Th suggest a possible connection of these major elements to activity concentration of ^{232}Th in the studied samples.

It can also be noted in Table 5.3 that the ^{238}U activity concentration correlates significantly only with Fe_2O_3 at 0.01 significance level. This suggests that the presence of Fe_2O_3 in beach sand samples is linked to the ^{238}U activity concentration. The correlation between other major elements namely; SiO_2, Al_2O_3, Na_2O, TiO_2, MgO, CaO and P_2O_5 with the ^{238}U activity concentration in the studied samples are insignificant.

A significant positive correlation at 0.05 significance level was found between Zr, V, Ce, Nb, Hf, Y, La, and Nd with the activity concentration of ^{232}Th. This suggests a possible strong link between these trace elements and the ^{232}Th activity concentration in studied beach sand samples. There is also a significant but negative correlation at 0.01 significance level between Sr and ^{232}Th activity concentration. Moreover, correlation between Ba and Rb with ^{232}Th activity concentration is insignificant.

A significant correlation at 0.01 significance level was displayed between Y, V and Sr and the ^{238}U activity concentration. The obtained results also show that the ^{238}U activity concentration correlation with Zr, Ce, Hf, La, Rb, Nb, Ba and Nd is insignificant. This indicates that there is no link between the high ^{238}U activity concentration in studied beach sand samples and a high concentration of minerals such as Zr. Moreover, a significant strong positive correlation is present between Zr and Ce, Nb, Hf, Y, La and

Nd. However, the ^{232}Th activity concentration is only weakly correlated with activity concentration of ^{238}U. These two radionuclides occur together in nature and this weak correlation among them may be attributed to variations in mobility of the two radionuclides (Al-Hamarneh and Awadallah, 2009).

Major and trace element compositions and their linkage to natural radioactivity in this research study have been compared with the findings reported by other researchers. It is important to mention that many researchers reported the relationship that exists between heavy minerals and natural radioactivity but not many have compared the major and trace elements to the natural radioactivity levels. According to Erkul et al. (2016) natural radioactivity levels of some granitoids in Western Turkey have been closely associated with high SiO_2, Na_2O, K_2O, Rb and Ba, whereas no correlation exists between natural radioactivity levels and concentrations of CaO, Sr, Y and Zr.

The ^{238}U and ^{232}Th in plutons of Western Anatolian-Turkey were reported to have no correlation with Zr, SiO_2, Al_2O_3, MgO, CaO, K_2O and TiO_2, whereas significant but weak correlation was found between Hf and ^{238}U and ^{232}Th activity concentration (Papadopoulos et al., 2017).

The contents of organic matter (CaO), clay and magnetic minerals in Kavala beach sand are positively correlated with ^{238}U, ^{232}Th and ^{40}K (Ramasamy et al., 2014). In the present study, CaO neither correlates with ^{238}U nor ^{232}Th.

Table 5.3: Correlation matrix for major elements and ^{232}Th and ^{238}U activity concentrations for selected beach sand samples from the study area. Bold values in the table indicate significant correlation between the variables

	Major elements									Natural radionuclides	
	Al_2O_3	**K_2O**	**MgO**	**Na_2O**	**P_2O_5**	**SiO_2**	**Fe_2O_3**	**TiO_2**	**CaO**	**Th**	**U**
Al_2O_3	1										
K_2O	0.835**	1									
MgO	-0.442	-0.655**	1								
Na_2O	0.903**	0.792**	-0.220	1							
P_2O_5	-0.490*	-0.645**	0.687**	-0.359	1						
SiO_2	0.535*	0.735**	-0.860**	0.324	-0.725**	1					
Fe_2O_3	0.699**	0.470*	-0.319	0.575**	-0.257	0.483*	1				
TiO_2	0.291	0.335	-0.524*	0.143	-0.405	0.651**	0.667**	1			
CaO	-0.659**	-0.800**	0.836**	-0.450	0.725**	-0.988**	-0.569*	-0.644**	1		
Th	0.413	0.365	**-0.494***	0.254	-0.298	**0.627****	**0.791****	**0.911****	**-0.646****	1	
U	0.140	-0.125	0.238	0.121	0.418	-0.225	**0.475***	0.110	0.165	0.287	1

*Correlation is significant at 0.01 significance level
**Correlation is significant at 0.05 significance level

Table 5.4: Correlation matrix for trace elements and ^{232}Th and ^{238}U activity concentration for selected beach sand samples from the study area. Bold values in the table indicatet significant correlation between the variables.

	Trace elements											Natural radionuclides	
	Zr	**Sr**	**V**	**Ce**	**Nb**	**Rb**	**Hf**	**Y**	**La**	**Nd**	**Ba**	**Th**	**U**
Zr	1												
Sr	-.550*	1											
V	0.687**	-0.512*	1										
Ce	0.912**	-0.530*	0.846**	1									
Nb	0.846**	-0.579**	0.601**	0.697**	1								
Rb	0.330	-0.625**	0.541*	0.478*	0.338	1							
Hf	0.999**	-0.553*	0.708**	0.915**	0.847**	0.334	1						
Y	0.739**	-0.415	0.890**	0.928**	0.498*	0.496*	0.751**	1					
La	0.901**	-0.557*	0.822**	0.991**	0.692**	0.532*	0.903**	0.896**	1				
Nd	0.897**	-0.521*	0.835**	0.996**	0.664**	0.494*	0.900**	0.934**	0.991**	1			
Ba	0.345	-0.628**	0.481*	0.444	0.384	0.989**	0.346	0.439	0.500*	0.459*	1		
Th	**0.959****	**-0.530***	**0.795****	**0.967****	**0.787****	0.372	**0.961****	**0.822****	**0.960****	**0.952****	0.357	1	
U	0.167	**0.485***	**0.465***	0.378	-0.043	-0.068	0.182	**0.554***	0.326	0.390	-0.141	0.287	1

*Correlation is significant at 0.01 significance level
**Correlation is significant at 0.05 significance level

5.6 Origin of heavy minerals at Kukuu beach

The major and trace element compositions and their ratios have been regularly used by various researchers to infer the origin of sediments, because they tend to reflect source rock composition (Singh, P., 2009; 2010). In the current research study, samples (PBS 9A and PBS 9B) from Kukuu beach portrayed high contents of TiO_2, Fe_2O_3 and Zr which are associated with heavy minerals. In an attempt to investigate the origin of these heavy mineral samples, three more sand samples (PBS 9C, PBS 9D, and PBS 9E) were collected from various locations of the Kukuu beach. In addition, two soil samples (PSS 9H1 and PSS 9H2) were taken from the cliff adjacent to the beach where black sand was found. In this research study, four trace elements (Ce, La, Nd and Th) and two major elements (TiO_2 and Fi_2O_3) have been considered to trace the origin of heavy mineral sands in the Kukuu black sand.

As can be seen in Figure 5.5, the ratios of the trace elements Th/La, Th/Ce and Th/Nd for three beach sand samples (PBS 9C, PBS 9D and PBS 9E) collected from various parts of the Kukuu beach are comparable, indicating that the samples are from the same origin. On the other hand, the ratios of the similar trace elements for samples PBS 9A and PBS 9B (the black sand) demonstrate no correlation with samples PBS 9C, PBS 9D and PBS 9E. This suggests that samples (PBS 9A and PBS 9B) and (PBS 9C, PBS 9D and PBS 9E) have different origins. In addition, the major elements Fe_2O_3/TiO_2 ratio for the samples PBS 9C, PBS 9D and PBS 9E correlate well, showing these samples have similar origin. Moreover, the Fe_2O_3/TiO_2 ratio for PSS 9H1 and PSS 9H2 (soil samples) neither correlate with the samples PBS 9D and PBS 9E nor with the samples PBS 9A and PBS 9B. The poor correlation between the samples PBS 9A and PBS 9B and the other samples collected in the Kukuu beach is a strong indication that the samples are likely to have different origins. *The black sand is thus likely to be deposited on the beach from elsewhere during storms and spring tides.*

The variations in major and trace element compositions and distribution patterns in beach sand in particular and the coastal environment in general, result from various processes

(Amstrong-Altrin et al. 2014, 2017; Wong et al., 2013). These include wind direction, waves, period of current and river flow acting on the beach. The diverse properties of these elements such as size, shape and specific gravity also play a critical role in the variation of major and trace elemental compositions within a beach deposit (El-Askary and Frihy, 1986). Beach and near shore geomorphology also influences the distribution of these elements (Singh, P. 2010).

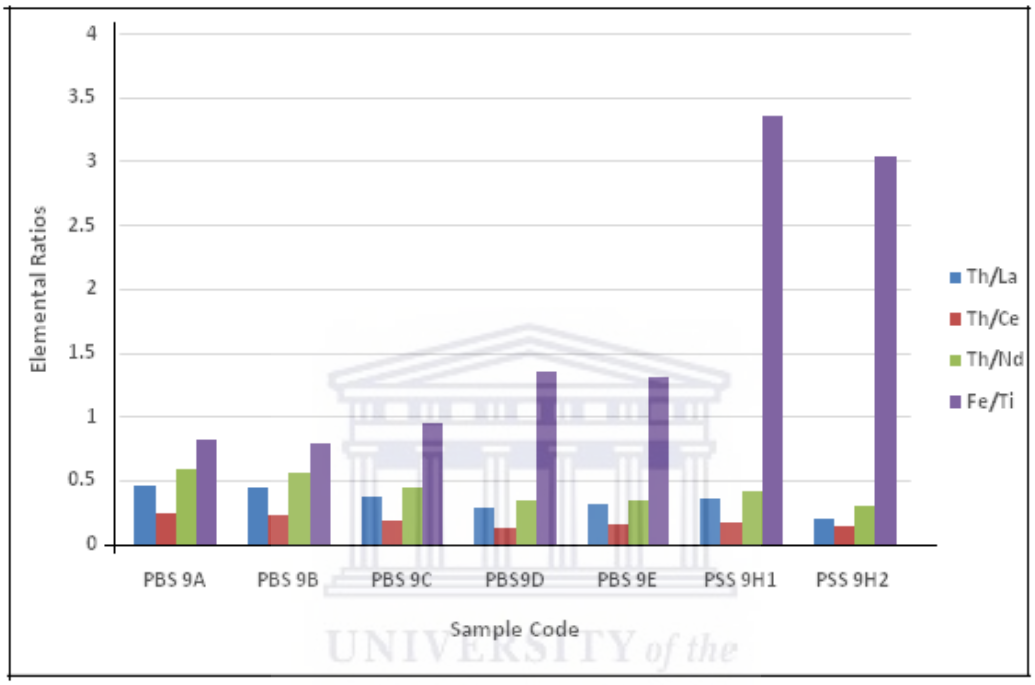

Figure 5.5: Elemental ratios of selected elements from Kukuu beach

Rivers play the main role in transporting sand sediments for most coastal areas (De Meijer at al. 2001). For instance, the main part of the Egyptian black sands originates from the River Nile and its main tributaries (Mowafi and El Tahawy, 2009). In a case where there is no supply of sediments by rivers or water channels, as in the case of Kukuu beach, alternative sources could be either the sediments already available at the beach or the hinterland immediately adjacent to the beach zone. The near shore waves and currents as well as seasonal littoral currents become important. The heavy minerals in the Kavala beach sands in Greece are likely to be derived from granitic rocks of the Kavala pluton through erosion process (Papadopoulos et al., 2015).

The observed variation in degree of darkness in black sand samples from the Kukuu beach that was observed during field visits suggest that weathering conditions influence the elemental compositions of these samples (Papadopoulos et al. 2015). Kukuu beach experiences strong waves during the southwest monsoon, hence the onshore and offshore movements play an important role in sorting the sand and in depositing the heavy minerals along the coast. During harsh currents, light minerals are washed out and heavy minerals remain at the beach shore. The beach is in the shallow channel between the island of Pemba and a smaller island, with normally very calm water that is unlikely to wash away the heavy minerals deposited in the extreme weather conditions.

Since the heavy mineral concentration in the samples collected from Kukuu beach and the surrounding area are not correlated, the heavy minerals found in Kukuu beach samples are likely to be derived from natural erosion process from elsewhere and deposited at Kukuu beach after being washed by the sea waves and re-deposited along the beach.

5.7 Summary

The major and trace element contents in the studied samples vary widely. The samples found with high contents of SiO_2 exhibit low contents of CaO and vice versa. This division is clearly seen between mainly sandy (eroded quartz) samples and samples highly enriched in coral. Only two samples (black sand from Kukuu) were found with high contents of Fe_2O_3 and TiO_2. Major elements like K_2O, MgO, MnO, Na_2O and P_2O_5 were present in small amounts in beach sand samples. Trace element results in all analysed samples were characterised by low concentration of zirconium (Zr) except for samples PBS 9A and PBS 9B. These two samples also contained other trace elements at higher level with the exception of Sr and Ba. The concentrations of Sr and Ba were high in samples with high CaO content.

The studied beach samples have been classified into four groups based on their major element contents namely; silicates (rich in SiO_2), carbonates (dominated by CaO), mixed

sand (with high amounts of CaO, LOI and SiO_2) and heavy mineral sands (with high contents of Fe_2O_3 and TiO_2).

The results obtained from Pearson's correlation analysis suggest that the major elements such as SiO_2, Fe_2O_3 and TiO_2 show strong correlation with ^{232}Th. Moreover, the obtained result indicates that trace elements namely; Zr, V, Ce, Nb, Hf, Y, La, and Nd are associated with high activity concentration of ^{232}Th in the studied samples. In particular, the findings show that the high concentration of Zr, Fe_2O_3 and TiO_2 may coincide with high ^{232}Th activity concentration. On other hand, the high concentrations of Y, V, P_2O_5 and Fe_2O_3 in the beach sand samples may be linked to high ^{238}U activity concentration. Other major and trace elements are insignificantly linked to the level of natural radioactivity.

The investigation of the origin of heavy minerals along the Kukuu beach revealed no connection between black sand samples, white sand samples and soil samples from the cliff adjacent to the beach. The study suggests that the black sands are likely to be derived from the hinterland due to natural erosion process and deposited at Kukuu beach after being transported by the sea waves, probably mainly during the monsoon period when rough seas are present during the southern monsoon.

CHAPTER 6

Summary, Conclusions and Recommendations

6.1 Introduction

This chapter presents a summary of the work done on radiometric investigation of beach sand and selected soil samples in Zanzibar, and provides important findings drawn from the objectives of this study. The chapter also provides recommendations for future work.

6.2 Summary

6.2.1 The activity concentration of natural radionuclides (^{40}K, and ^{232}Th and ^{238}U)

The activity concentration of natural radionuclides (^{40}K, and ^{232}Th and ^{238}U decay products) in beach sand and soil samples from some inland areas was measured in-situ using the NaI(Tl) and the MEDUSA gamma ray detectors and ex-situ using the low background HPGe detector system. The NaI(Tl) measurements were done initially to get an idea of the variation in concentrations on the islands and to identify areas that needed to be further studied with the MEDUSA detector and where the samples needed to be collected for laboratory analysis. The MEDUSA detector was used for both stationary and mobile measurements for detailed study of areas where elevated radioactivity levels had been seen. During stationary measurements, radioactivity measurements were carried out at discrete points while the detector was on the vehicle 60 cm above the ground or was placed directly on the ground. During mobile measurements, the detector was mounted on a 4 x 4 vehicle 60 cm off the ground. While the detector is mounted on the vehicle an area was surveyed depending on the accessibility of the area. The mobile measurements were performed at Kukuu and Msuka beaches, and inland at Mtende, Kidoti and Tunguu. These areas were traversed while the vehicle was moving at a speed of about 2 m.s^{-1}.

The activity concentrations of ^{232}Th, ^{238}U and ^{40} K in beach sand ranges from BDL to 2671 Bq.kg^{-1}, 2 to 1055 Bq.kg^{-1} and 3 to 471 Bq.kg^{-1}, respectively. The obtained values

in this study are lower than the world average values of 33, 45 and 420 $Bq.kg^{-1}$ (UNSCEAR, 2008). The very low activity concentration measured in most of the beach samples in this study may be attributed to the presence of shells and carbonates in these samples.

The activity concentration of ^{232}Th, ^{238}U, and ^{40}K radionuclides in soil samples in this study ranges from 24 to 130 $Bq.kg^{-1}$, 28 to 493 $Bq.kg^{-1}$ and 30 to 654 $Bq.kg^{-1}$, respectively. The average values for ^{232}Th, ^{238}U, and ^{40}K radionuclides in soil samples are 42, 38 and 42 $Bq.kg^{-1}$, respectively. These values are lower than the values reported in similar studies conducted in other places around the world. In this study, two inland soil samples were found to have much higher levels of ^{238}U and ^{232}Th; this could be attributed to geological characteristics of the parent rocks, their geo-chemical properties as well as the use of fertilizers which increase the activity concentration.

The calculated $^{232}Th/^{238}U$ ratio in this study ranges from 0.42 to 4.43 for beach sand and from 0.55 to 2.85 for soil samples. The $^{232}Th/^{238}U$ ratio in most samples is lower than the average continental crust value of approximately 3.8 (Clark, Peterman, & Heier, 1966; Rogers & Adams, 1969). This suggests that these samples are enriched in ^{238}U. The $^{232}Th/^{238}U$ ratios of beach sand samples PBS 9B, UBS 23, UBS 27 are 4.37, 4.53 and 4.53 respectively, which are higher than the average continental crust value, suggesting that these samples are enriched in ^{232}Th.

The comparison between the measurements performed in-situ using the NaI(Tl) detector and ex-situ using the HPGe detector show variations in activity concentration of ^{40}K, ^{238}U and ^{232}Th obtained using these two detectors. The variations may be attributed to various factors. These include the amount of the sample measured, since while the HPGe measures the activity in the approximately 1.5 kg sample that was collected, the NaI(Tl) detector measures the concentration from a much larger area from where gamma rays reach the detector. The measured samples were also not taken from exactly the same spot. Other reasons for differences include environmental factors, standard gamma energy spectra used for calibration of detectors and data processing techniques (IAEA, 1990).

While NaI(Tl) spectra were analysed using standard spectra collected from calibration pads with possibly very different densities to the field soils, the HPGe detector was calibrated using IAEA certified standard sources for uranium, thorium and potassium.

Although the NaI detector will obviously have much larger uncertainties associated with the measurements compared to the HPGe detector, the major advantage of using a NaI(Tl) detector is that it can be used in-situ to get a good indication whether the area has a high or a low activity of the ^{40}K, ^{232}Th and ^{238}U for further investigation.

6.2.2 Spatial distributions maps for ^{40}K, ^{238}U and ^{232}Th

The spatial distributions maps for ^{40}K, ^{238}U and ^{232}Th were generated using the MEDUSA γ-ray detector and the Golden Software Surfer® 10. Colour maps have been used to indicate areas of high, intermediate and low activity concentrations in the interpolated maps. Two beaches (Kukuu and Msuka) from Pemba Island and three inland areas (Kidoti, Tunguu and Mtende) from Unguja Island were mapped. The abrupt changes in activity concentration even among neighbouring regions are associated with strong mineralogical variations and could have implications for agriculture. These strong variations are unexpected and one of the major outcomes of this study.

6.2.3 Radiological assessment

The outdoor gamma dose rates obtained in beach sand samples ranged from 3 to 2156 $nGyh^{-1}$. The highest absorbed dose rates obtained in samples PBS 9A is 38 times higher than the average world level of 57 $nGyh^{-1}$for terrestrial doses (UNSCEAR, 2008). The calculated ex-situ outdoor absorbed dose rate for soil samples ranged from 50 to 294 $nGyh^{-1}$. The highest dose rate was measured in sample UBS 29 which is approximately five times higher than the average outdoor absorbed dose rate in air from soil. Based on the dose rate values obtained from the Kukuu black sand, the sand should not be considered safe for local inhabitants for construction of their dwellings. Apart from the black sands that contain the heavy minerals with high U and Th levels, this study concludes that the beach sand from the Zanzibar coast do not pose any radiological

threat to the locals using beaches for various activities and tourists visiting Zanzibar during holidays.

6.2.4 Major and trace element contents in beach samples

The major and trace element analyses were performed using XRF and ICP-MS respectively. The elemental compositions in the studied samples vary widely. The samples found with high contents of SiO_2 exhibit low contents of CaO and vice versa. The contents of Fe_2O_3 and TiO_2 are small in most samples with the exception of the two samples from Kukuu beach. Major elements such as K_2O, MgO, MnO, Na_2O and P_2O_5 were present in small amounts in beach sand samples. The Zr concentrations in all analysed samples were low except for the black sand samples. Other trace elements with the exception of Ba and Sr were high in the Kukuu black sand. The concentrations of Sr and Ba were high in samples with high CaO content.

The findings of this study show that the major elements such as SiO_2, Fe_2O_3 and TiO_2 have strong correlation with ^{232}Th. Likewise, the trace elements namely; Zr, V, Ce, Nb, Hf, Y, La, and Nd are linked with high activity concentration of ^{232}Th in the studied samples. In particular, the findings of this study show that the high concentration of Zr, Fe_2O_3 and TiO_2 are linked to the ^{232}Th activity concentration. Moreover, the high concentrations of Y, V, P_2O_5 and Fe_2O_3 in the beach sand samples may relate to high ^{238}U activity concentration. Other major and trace elements are not linked to the activity concentration of ^{238}U and ^{232}Th.

6.2.5 Heavy minerals along the Kukuu beach

The investigation of heavy minerals along the Kukuu beach revealed no connection between black sand samples and other beach samples collected on the same beach, and soil samples from the cliff adjacent to the beach. The study suggest that the black sands are likely to be derived from the hinterland due to natural erosion process and deposited at Kukuu beach after being transported by the action of the waves, especially during high tides and storm periods.

6.3 Conclusions

The following are major findings drawn from this study:

- The activity concentration of radionuclides ^{232}Th, ^{238}U and ^{40}K in beach sands are much lower than in soil samples with an exception at Kukuu. Two beach sand samples from Kukuu beach were found to have enhanced radioactivity levels due to the presence of heavy minerals.
- The spatial distribution maps of activity concentrations of ^{40}K, ^{238}U and ^{232}Th in the surveyed area show large variation in soil samples for two relatively small islands. The initial measurements with a portable NaI(Tl) detector showed that this is a powerful method to get an initial idea of variation of activity concentrations and to indicate which areas need to be further investigated.
- The studied beach samples have been classified into four distinct type – normal white beach sand very high in SiO_2, coral sand enriched in CaO, mixed sand with high contents of corals and SiO_2 and black sand high in Fe_2O_3, Zr and $TiO_2$and low in SiO_2.
- The beach sands and soil in the area do not pose any radiological threat to the people living in the area and tourists going to the beaches for recreation in the study area. This is apart from the Kukuu black sand samples that contain the high ^{238}U and ^{232}Th levels.
- A strong correlation between SiO_2, Fe_2O_3, TiO_2, Zr, V, Ce, Nb, Hf, Y, La, and Nd show these elements are linked with high activity concentration of ^{232}Th in the studied samples. Moreover, the high concentrations of Y, V, P_2O_5 and Fe_2O_3 in the beach sand samples may relate to high ^{238}U activity concentration.
- The investigation of the heavy minerals along the Kukuu beach revealed that the heavy minerals are likely to be derived from the hinterland due to natural erosion process.

6.4 Recommendations for future work

- In the current study, in-situ and ex-situ radiometric measurements were performed in selected beaches. It is proposed to extend the analyses of ^{40}K, ^{238}U and ^{232}Th to the entire coast of Zanzibar.
- As only 7 soil samples from inland areas were analysed in this study, it is suggested that a further study is done on the radioactivity concentrations of the Zanzibar topsoil that may lead to useful insights into the geology of the area and possible suggestions for agricultural production.
- A study to establish the radiological map of the activity concentration of the ^{40}K, ^{238}U and ^{232}Th is also suggested. Such a project is likely to discover the origin of the heavy mineral sands assuming that its origin is from Pemba.
- A similar study is proposed to be carried with a view to assess radioactive character of groundwater and food grown in Zanzibar.
- A comprehensive study to investigate the types of the heavy minerals available along the Zanzibar coast is suggested.

References

Ababneh, Z. Q., Al-Omari, H., Rasheed, M., Al-Najjar, T., & Ababneh, A. M. (2010). Assessment of gamma-emitting radionuclides in sediment cores from the Gulf of Aqaba, Red Sea. Radiation Protection Dosimetry, 141, 289–298.

Achola, S.O., Patel, J.P., Mustapha, A.O., Angeyo, H.K. (2012). Natural radioactivity and external dose in the high background radiation area of Lambwe east, South Western Kenya. Radiation Protection Dosimetry, 152 (4): 423-428.

Adams and Weaver (1958). Thorium to uranium ratios as indications of sedimentary processes: Example of concept of geochemical faces American Association of Petroleum Geologists Bulletin 4, pp.387-430.

Ademola et al. (2014). Determination of natural radioactivity and hazard in soil samples in and around gold mining area in Itagunmodi, South-Western Nigeria. Radiation Research and Applies Sciences, 7, 249-255.

Adeniji, A., et al. (2013). Radionuclide concentrations in some fruit juices produced and consumed in Lagos, Nigeria. American Journal of Environmental Protection, 2(2), 7- 41.

Agalga, A. (2013). Preliminary study on the levels of natural radionuclides in sediments of the Tono irrigation dam, Navrongo. International Journal of Science and Technology, Volume 2, No. 11.

Agbalagba, E. O., and Onoja, R. A. (2011). Evaluation of natural radioactivity in soil, sediment and water samples of Niger Delta (Biseni) flood plain lakes, Nigeria. Environmental Radioactivity, 102.7: 667-671.

Ahmad, N., Matiullah, L., Khataibeh, A. (1997). Indoor Radon Levels and Natural Radioactivity in Jordanian Soil. Radiation Protection Dosimetry, 71(3): 231-233.

Ahmad, N., Hussein A. J. A., and Aslam, A. (1998). Radiation doses in Jordanian dwellings due to natural radioactivity in construction materials and soil. Environmental Radioactivity, 41(2): p. 127-136.

Akhtar, Nasim, Tufail M., Ashraf M., and Mohsin Iqbal M. (2005). Measurement of environmental radioactivity for estimation of radiation exposure from saline soil of Lahore, Pakistan. Radiation Measurements, 39(1): pp. 11-14.

Akram, M. et. al. (2007). Determination of Gamma-Emitting Radionuclides in the Inter-Tidal Sediments off Balochistan (Pakistan) Coast, Arabian Sea. Radiation Protection Dosimetry, vol.123, no.2, pp. 268-273.

Akram, M., Qureshi, R. M., Ahmad, N., Solaija, T. J., Mashiatullah, A., Afzal, M., ... & Zeb, L. (2006). Concentration of natural and artificial radionuclides in bottom sediments of Karachi Harbour/Manora Channel, Pakistan Coast (Arabian Sea). *Journal of the Chemical Society of Pakistan*, *28*(3), 306-312.

Alam, M. N. et. al. (1999) The ^{226}Ra, ^{232}Th and ^{40}K Activities in Beach Sand Minerals and Beach Soils of Cox's Bazar, Bangladesh. Environmental Radioactivity, vol. 46, pp. 243-250.

Alam, M. N., et al. (1999). Radiation dose estimation from radioactivity analysis of lime and cement used in Bangladesh. Environmental Radioactivity. Vol. 42.

Alazemi, N. (2015). Determination of Levels of Naturally Occurring Radioactive Materials in Environmental Samples in the State of Kuwait by High-Resolution γ-ray Spectrometry. PhD Thesis, University of Surrey, UK (unpublished).

Al Azmi, D., Karunakara, N. and Mustapha, A. (2013). Teaching about Background Radiation. Physics Education, 48, 506-511.

Al-Hamarneh, Ibrahim F. and Awadallah Mohammad I. (2009). Soil radioactivity levels and radiation hazard assessment in the highlands of northern Jordan. Radiation Measurements, 44(1): p. 102-110.

Al-Jundi, J. (2002). Population doses from terrestrial gamma exposure in areas near to old phosphate mine, Russaifa, Jordan. Radiation Measurements, 35(1), 23-28.

Al Jundi, J. et al. (2003). Natural radioactivity concentrations in soil samples along the Amman Aqaba Highway. Jordan. Radiation Measurements, 36, 555-560

Al-Sulaiti, H., et al., (2010). A preliminary report on the determination of natural radioactivity levels of the State of Qatar using high-resolution gamma-ray spectrometry. Nuclear Instruments and Methods in Physics Research Section A: Accelerators, Spectrometers, Detectors and Associated Equipment, 619 (1-3): p. 427- 431.

Al-Sulaiti, H., (2011). Determination of Natural Radioactivity in the State of Qatar using High Resolution Gamma Spectroscopy. PhD Thesis, University of Surrey (unpublished).

Anagnostakis et al. (1996). Natural radioactivity mapping of Greek surface soils. Environmental International, Volume 22, Supplement 1, pp. 3-8.

Anjos, R. M., et al. (2005). Natural radionuclide distribution in Brazilian commercial granites. Radiation Measurements, 39.3: 245-253.

Anjos et al. (2011). External gamma-ray dose rate and radon concentration in indoor environments covered with Brazilian granites. Environmental Radioactivity, 102: 1055- 1061.

Armstrong-Altrin et al., (2017). Mineralogy and geochemistry of sands along the Monzanillo and El Carrizal beach areas, Southern Mexico: Implications for palaeoweathering, provenance and technonic setting. Geological Journal, 52, 559-582.

Armstrong-Altrin et al., (2018). Provenance discrimination between Atasta and Alvarado beach sands, Western Gulf of Mexico, Mexico: Constrains from detrital zircon chemistry and U-Pb geochemistry. Geological Journal, pp. 1-25.

Arnedo, M. A., et al. (2013). Natural radioactivity measurements of beach sands in Gran Canaria, Canary Islands (Spain). Radiation Protection Dosimetry, 156.1: 75-86.

Arnedo et al. (2017) Mapping natural radioactivity of soils in the eastern Canary Islands. Environmental Radioactivity, 166 (3): pp. 242-258.

Ashnani, M.H.M, Yavari, A.R and Hassani, E. (2010). A survey of pollutions of the Aras river and the south-west of Caspian Sea case study: radioactivity pollutions. World Applied Sciences, 9 (1): 76-80.

Baeza, A. Del Rio, M., Miro, C., Paniagua, J. (1992). Natural radioactivity in soils of the province of Ca´ceres (Spain). Radiation Protection Dosimetry, Vol.45, Issue 1-4, pp. 261-263.

Baeza, A., Del Rio, M., Miro, C., Paniagua, J. (1994). Natural radionuclides distribution in soils of Ca´ceres (Spain) dosimetry implications. Environmental. Radioactivity, 23, 19-37.

Baeza, A., et al. (2011). Analysis of the different source terms of natural radionuclides in a river affected by NORM (Naturally Occurring Radioactive Materials) activities. Chemosphere, 83(7), 933-940.

Baggoura, B., Noureddine A., and Benkrid M. (1998). Level of natural and artificial radioactivity in Algeria. Applied Radiation and Isotopes, 49(7): pp. 867-873.

Bajoga, A. (2016). Evaluation of natural and anthropogenic radioactivity in environmental samples from Kuwait using high resolution gamma-ray spectroscopy. PhD Thesis, University of Surrey (unpublished).

Bajoga, A.D., Alazemi, N., Shams, H., Regan, P.H., Bradley, D.A. (2016). Evaluation of naturally occurring radioactivity across the State of Kuwait using high-resolution gamma ray spectrometry. Radiation Physics and Chemistry.

Banzi, F.P, Kifanga, L.D and Bundala, F.M. (2000). Natural radioactivity and radiation exposure at Minjingu phosphate mine in Tanzania. Radiation Protection, 20: 41-51.

Beck, H.L., De Planque, G. (1968). The radiation, eld in air due to distributed gamma ray sources in ground. New York: US DOE, Environmental Measurements Laboratory, HASL-195.

Bellia, S., Brai, M., Hauser, S., Puccio, P., Rizzo, S. (1997). Natural radioactivity in a volcanic island: Ustica, southern Italy. Appl. Radiat. Isot. 48, 287-293.

Bernard, Z. (1995). Tracers in the Oil Field, Elsevier, ISBN: 044488968X, 978044488968

Bezuidenhout, J. (2012). Mapping of historical human activities in the Saldanha Bay Military Area by using in situ gamma ray measurements. Scientia Militaria, 40/2. 89– 101.

Bolca, M., Sac, M.M., Cokuysal, B., Karali, T. and Ekdal, E. (2007). Radioactivity in Soils and Various Foodstuffs from the Gediz River Basin of Turkey, Radiation Measurements, 42, 263-270.

Bou-Rabee F. (1997). Soil radioactivity atlas of Kuwait. Environment International, 23(1), pp. 5-15.

Brogioli, R. (2012). Electrothermal treatment of laser generated aerosols: online suppression of interferences for laser ablation – Inductively Coupled Plasma Mass Spectrometry. PhD Thesis, University of Zurich (unpublished).

Browne, E. and Firestone, R. B., Shirley, V. S. (Ed.) (1986). Table of Radioactive Isotopes. John Wiley and Sons, Inc. New York.

Caciolli et al. (2012). A new FSA approach for in-situ γ-ray spectroscopy, Science of the Total Environment, 414, 639–645.

Carvalho, F.P., Oliveira, J.M., Lopes, I. and Batista, A. (2007). Radionuclides from Past Uranium Mining in Rivers of Portugal. Environmental Radioactivity, 98, 298-314.

Carvalho, C., Anjos, R M., Veiga, R., Macario, K. (2011). Application of radiometric analysis in the study of provenance and transport processes of Brazilian coastal sediments. Environmental Radioactivity, 102(2), 185-92.

Cember, H. and Johnson, T.E. (2009), Introduction to Health Physics, 4th edition, New York: McGraw-Hill Companies, Inc.

Chege, B.W. (2014). Modelling radon and thoron exhalation and measurement of total natural radiation exposure in Mrima Hill, Kenya. PhD thesis, Kenyatta

University (unpublished).

Chen et al. (2016) A study on the levels of radioactivity in fish samples from the experimental lakes area in Ontario, Canada. Journal of Environmental Radioactivity, 153, 222-230.

Chiozzi, P., Pasquale, V. and Verdoya, M. (2002). Naturally occurring radioactivity at the Alps–Apennines transition. Radiation Measurements, 35(2), pp.147-154.

Chowdhury, M.I., Alam, M.N., Hazari, S.K.S. (1999). Distribution of radionuclides in the river sediments and coastal soils of Chittagong, Bangladesh and evaluation of the radiation hazard. Applied Radiation and Isotopes, 51, 747-755.

Clark, S. P., Peterman, Z. K. and Heier, K. S. (1966). Abundances of uranium, thorium and potassium. In: Handbook of Physical Constants. Clark, S. P., Ed. Geological Society of America Mem. 47, 521–541.

Clouvas, A., Xanthos, S., Antonopoulos-Domis, M. (2000). Monte Carlo calculation of dose rate conversion factors for external exposure to photon emitters in soil. Health Physics, 78 (3), 295–302.

Croft, S. & Hutchinson, I. G. (1999). The measurement of U, Th and K concentrations in building materials. Applied Radiation and Isotopes, 51: 483-492.

Currie, L. A. (1968). Limits for Qualitative Detection and Quantitative Determination. Analytical Chemistry, vol. 40, no. 3, pp. 586-593.

Darko, E. O. (2004). Radiation Risk from NORMS in Mining and Mineral Processing at the Obuasi Goldmines: Modelling, Dose Inter-comparison and Regulatory Control, PhD Thesis, University of Ghana, Ghana (unpublished).

Darko, G., Faanu, A., Akoto, O., Acheampong, A., Goode, E.J., Gyamfi, O. (2015). Distribution of natural and artificial radioactivity in soils, water and tuber crops. Environmental Monitoring and Assessment, 187 (6), 339.

Debertin, K. and Helmer, R. G. (1988). Gamma and X-Ray Spectroscopy with Semiconductor Detectors, Elsevier Science.

De Groot, A. V., van der Graaf, E. R., De Meijer, R. J. & Maucec, M. (2009). Sensitivity of in-situ γ-ray spectra to soil density and water content. Nuclear Instruments and Methods in Physics Research A, 600: 519 – 519.

De Meijer et al, (1990). Estimate of the Heavy Mineral Content in Sand and its Provenance by Radiometric Methods, Nuclear Geophysics, 4(4), 455-460.

De Meijer, R. J. and Donoghue, J. F. (1995). Radiometric fingerprinting of sediments on the Dutch, German and Danish coasts. Quaternary International, 26, 43 - 47.

De Meijer R.J., Tanczos I.C., Stapel C. (1996). Radiometry as a technique for use in coastal research. Geological Society Special Publication, 117, 289.

De Meijer, R.J., Stapel, C., Jones, D.G., Roberts, P.D., Rozendaal, A., Macdonald, W.G. (1997a). Improved and new uses of natural radioactivity in mineral exploration and processing. Explor. Min. Geol. 6, 105.

De Meijer R.J., Stapel C., Rozendaal A., Macdonald W.G., Donoghue J.F. (1997b). New approaches to radiometry in heavy mineral exploration and processing. Heavy Minerals, 187.

De Meijer, R.J., Put L.W., Schuiling R.D., de Reus J.H., Wiersma J. (1998). Provenance of coastal sediments using natural radioactivity of heavy mineral sands. Radiation Protection Dosimetry. 24, 55.

De Meijer, R.J., James, I.R., Jennings, P.J and Koeyers, J.E. (2001). Cluster analysis radionuclide concentrations in beach sand. Applied Radiation and Isotopes, 54, 535- 542.

De Villiers, D. (2011). Characterisation of heavy mineral sands and soils by radiometry and its use in mineral beneficiation and agriculture. PhD Thesis, University of Stellenbosch (unpublished).

Dowdall, M. & O'Dea, J. (2002). $^{226}Ra/^{238}U$ disequilibrium in an upland organic soil exhibiting elevated natural radioactivity. Environmental Radioactivity, 59 (1), 91-104.

Ebaid, Y.Y. (2010). Use of Gamma-Ray Spectrometry for Uranium Isotopic Analysis in Environmental Samples. Romanian Journal of Physics, Vol.55, no.1-2, pp.68-74.

Edsfeldt, C., & Femlund, J. (2000). Differences in radium and uranium distributions in Quaternary deposits.

Eissa, H S., Medhat, M E., Said, S A., Elmaghraby, E K. (2010). Radiation dose estimation of sand samples collected from different Egyptian beaches. Radiation Protection Dosimetry, 147(4), 533-40.

Eisenbud, M. and Gesell, T. (1997). Environmental Radioactivity from Natural, Industrial, and Military Sources, 4th edition, London: Academic Press.

El-Arbi A.M. (2005). Natural Radioactivity in Sand Used in Thermal Therapy at the Red Sea Coast. Environmental Radioactivity, vol.81, pp.11-19.

El Askary, M.A., Frihy, O.E. (1986). Depositional phases of Rosetta and Damietta promontories on the Nile Delta coast. African Earth Sciences, 5 (6), 627-633.

El-Gamal, A., Nasr, S. and El-Taher, A. (2007). Study of the Spatial Distribution of Natural Radioactivity in the Upper Egypt Nile River Sediments. Radiation Measurement, 42, 457-465.

El-Reefy, H., Sharshar, T., Zaghloul, R., Badran, H. (2006). Distribution of gamma-ray emitting radionuclides in the environment of Burullus Lake: Soils and vegetations. Environmental Radioactivity, 87 (2), 148-169.

Erkül et al. (2016). Comparison between natural radioactivity levels and geochemistry of some granitoids in western Turkey. Turkish Journal of Earth Sciences, 25: 242-255

Evans, H.E. (2016). Atomic spectrometry update: review of advances in atomic spectrometry and related techniques. Analytic and Atomic Spectrometry.

Faires, R.A. and Boswell, G.G.J. (1981). Radioisotope Laboratory Techniques (4th edition), London: Butterworth & Co (Publishers) Ltd.

Firestone, R.B. (1996). Table of Isotope, 8th edition, California, John Wiley & Sons Ltd., ISBN: 978-71330561.

FLIR 2015. Available from http://www.flir.com/threatdetection/display/?id=65349. [Accessed 24 October 2015].

Florou, H., & Kritidis, P. (1992). Rate in the coastal areas of a volcanic island, Aegean Sea, Greece. Radiation Protection Dosimetry, 45(1/4), 277–279.

Freitas, A. C., and A. S. Alencar. (2004). Gamma dose rates and distribution of natural radionuclides in sand beaches - Ilha Grande, South-eastern Brazil. Environmental radioactivity, 75.2: 211-223.

Fujiyoshi, R., Sawamura, S. (2004). Mesoscale variability of vertical profiles of environmental radionuclides (^{40}K, ^{226}Ra, ^{210}Pb and ^{137}Cs) in temperate forest soils in Germany. Science of Total Environment. 320, 177-188.

Gascoyne, M. (1992). The geochemistry of the actinides and their daughters. In Uranium Series Disequilibrium: Applications to Environmental Problems, ed. M. Ivanovich and R.S. Harmon, second edition. [Clarendon Press: Oxford], 34-58.

Gilmore, G. (2008). Practical Gamma-ray Spectrometry, 2nd edition., England, John Wiley & Sons Ltd, ISBN: 978-0-470-86196-7.

Goddard, C. C. (2001). Measurements of Outdoor Terrestrial Gamma Radiation in the Sultanate of Oman. Health Physics Society, Oman. pp 874.

Golden Software, Inc. (2012). Surfer 10 User's Guide, Contouring and 3D Surface Mapping for Scientist and Engineers, Colorado, USA.

Grasty, R.L, Shives, R.B.K. (1997). Applications of gamma spectroscopy to mineral exploration and geological mapping. IAEA Technical Report No.174.

Gray, A. L. (1983) Inductively Coupled Plasma Source-Mass Spectrometry Using Continuum Flow Ion Extraction. Analyst, 108, 1033-1050.

Greenfield, M. B., De Meijer, R. J., Put, L.W., Wiersma, J., and Donoghue, J. F. (1989). Monitoring Beach Sand Transport by Use of Radiogenic Heavy Minerals. Nuclear Geophysics, 3 (3), 231-244

Hamidalddin, H.Q.S. (2013), Measurements of the Natural Radioactivity along Red Sea Coast (South Beach of Jeddah Saudi Arabia), 10(1), 121-128

Hassan, I.H. (2007). Reliability of payment for water resources as an environmental service towards the sustainable management of watershed forests in Zanzibar, Tanzania: A case study of Kiwengwa - Pongwe forest reserve. Master's Thesis, Linkopings Universitet, Sweden.

Harb, S. (2008). Natural radioactivity and external gamma radiation exposure at the coastal red sea in Egypt. Radiation Protection Dosimetry, 130, 376-384.

Hashim, N. O., et al. (2004). Natural and artificial radioactivity levels in sediments along the Kenyan coast. Radiation physics and chemistry, 71.3: 805-806.

Heguye, E.S. (1993). Report on findings and recommendations on causes of the problems at the Maziwa Ng'ombe Forest Reserve and surrounding areas. Zanzibar forestry development project phase II, Commission for Natural Resources, Zanzibar. Zanzibar, Tanzania.

Hendriks, P. H. G. M., Limburg, J. & de Meijer, R.J. (2001). Full-spectrum analysis of natural γ-ray spectra. Environmental Radioactivity, 53: 365-380.

Hlatshwayo, I.N. 2007. In-situ Gamma-Ray Mapping of Environmental Radioactivity at iThemba LABS and Associated risk assessment. MSc. Thesis, University of Zululand, South Africa (unpublished).

International Atomic Energy Agency. (2003). Guidelines for radioelement mapping using gamma ray spectrometry data. International Atomic Energy Agency, Vienna, Austria.

ICRP 60 (1990). Recommendations of the International Commission on Radiological Protection, ICRP Publication 60. International Commission on Radiation Protection, Oxford, England.

Ivanovich M, Harmon R.S. (1992). Uranium-series disequilibrium: applications to earth, marine, and environmental sciences. Clarendon Press, Oxford

Jibiri, N.N., Farai, I.P. and Alausa, S.K. (2007). Estimation of Annual Effective Dose due to Natural Radioactive Elements in Ingestion of Foodstuffs in Tin Mining Area of Jos-Plateau, Nigeria. Environmental Radioactivity, 94, 31-40.

Kaniu et al. (2018). Rapid in-situ radiometric assessment of the Mrima-Kiruku high background radiation anomaly complex of Kenya. Environmental Radioactivity, Vol. 188, pp. 47-57.

Kannan,V.et al. (2002). Distribution of Natural and Anthropogenic Radionuclides in Soil and Beach Sand Samples of Kalpakkam (India) using Hyper Pure Germanium (HPGe) Gamma Rays Spectroscopy. Applied Radiation and Isotopes, vol.57, pp. 109-119.

Kardan et al. (2017) A national survey of natural radionuclides in soils and terrestrial radiation exposure. Iran. Journal of Environmental Radioactivity, 178-179, 168 - 176

Kekelidze et al. (2017). Radioactivity of soils in Mtskheta-Mtianeti region (Georgia). Annals of Agrarian Science, 15, 304-311.

Khater, A.E., Higgy, R. H., Pimpl M. (2001). Radiological impacts of natural radioactivity in Abu-Tartor phosphate deposits, Egypt. Journal of Environmental Radioactivity 55, 255–267.

Khater, A. E. M. & Ebaid, Y.Y. (2008). A simplified gamma-ray self-attenuation correction in bulk samples. Applied Radiation and Isotopes, 66: 407-413.

Khater, A. and Al-Sewaidan, H.A. (2008). Radiation Exposure due to Agricultural Uses of Phosphate Fertilzers. Radiation Measurements, 43, 1402-1407.

Kinyua R., Atambo V. O. and Ongeri R. M. (2011). Activity concentrations of ^{40}K, ^{232}Th, ^{226}Ra and radiation exposure levels in the Tabaka soapstone quarries of the Kisii Region, Kenya. African Journal of Environmental Science and Technology, Vol. 5(9), pp. 682-688.

Kluson, J. 2001. Environmental monitoring and in-situ gamma spectrometry. Radiation Physics and Chemistry, 61 (3-6), 209-216

Knoll, G.F. (2010). Radiation Detection and Measurement, 4th edition, New York, John Wiley & Sons Ltd., ISBN: 0-471-07338-5.

Korkulu, Z., and N. Ozkan. (2013) Determination of natural radioactivity levels of beach sand samples in the black sea coast of Kocaeli (Turkey). Radiation Physics and Chemistry, 88: 27- 31.

Krane, K.S. (1988). Introductory Nuclear Physics, 2nd edition, USA, John Wiley & Sons Inc., ISBN:978-0-471-80553-3.

Kurnaz, A. et al. (2007). Determination of Radioactivity levels and Hazards of Soil and Sediment Samples in Firtinia Valley (Rize, Turkey). Applied Radiation and Isotopes, vol.65, 1281-1239.

Kurt, K. & Berker, S. (2014). Measurement of Natural Radioactivity in Beach Sand of Akkuyu Mersin, Turkey. Journal of Natural Sciences Research, Vol.4, No.17.

Lambrechts, A., Foulquier, L., & Garnier-Laplace, J. (1992). Natural radioactivity in the aquatic components of the main French rivers. Radiation Protection Dosimetry, 45(1/4), 253–256.

Langat, W.K., Omar, H.N., Ambuso, W.J. (2014). Gamma ray spectroscopic analysis of sedimental deposits at the shore of Lake Nakuru, Kenya. Natural Sciences Research, Vol.4, No. 21.

Larkin, J.F.S. (2013). Comparative investigation of airborne and ground-based radiometric survey techniques. MSc thesis, University of Witwatersrand

(unpublished).

Laxmi, T. and Bhima Rao, R., 2010, "Bad Land Topography of Coastal Belt Sediment Deposits of India: A Potential Resource for Industrial Minerals." Mines and Minerals Reporter, Vol. 3, No. 7, pp.12-18.

L'Annunziata, M. F. (2007). Radioactivity: Introduction and History, Amsterdam: Elsevier B.V. 173

Lee, S.K. et al. (2009). Radiological monitoring: terrestrial natural radionuclides in Kinta District, Perak, Malaysia. The Journal of Environmental Radioactivity;100:368–374.

Leo, W.R. (1987). Techniques for nuclear and particles physics experiments. Germany: Springer-Verlag Berlin Heidelberg.

Leung, K. C., Lau, S. Y., Poon, C. B. (1990). Gamma radiation dose from radionuclides in Hong Kong soil. Environmental Radioactivity 11, 279-290.

Lilley, J.S. (2001). Nuclear Physics, New York, John Wiley & Sons Ltd., ISBN: 0-471-97936-8.

Limburg, J., Koomans, R. L., Tijs, M. & van der Boor, M. (2009). GAMMAN - a software tool for the analysis of gamma spectra obtained in geophysical research. The Netherlands: Medusa Explorations BV.

Lindsay, R. et al. (2004). Monitoring the radon flux from gold-mine dumps by gamma ray mapping. Nuclear Instruments and Methods in Physics Research B, 213: 775-778.

Liu, WX, Li, XD, Shen, ZG, Wang, DC, Wai, OWH, Li, YS. (2003). Multivariate statistical study of heavy metal enrichment in sediments of the Pearl River Estuary. Environmental Pollution; 121:377-88

Lolila, F. (2011). Establishment of baseline data of external ionizing radiation dose at proposed uranium mining sites and their neighbouring residential areas in Tanzania: The case of Mkuju River, MSc Thesis, University of Dar es Salaam (unpublished).

Løvborg, L. 1984. The calibration of airborne and portable gamma ray spectrometers – theory, problems and facilities: Danish Atomic Energy Commission, RISO report M- 2456.

Lu, X. and Zhang, X. (2006). Measurement of natural radioactivity in sand samples collected from the Baoji Weihe Sands Park, China. Environ. Geol. 50, 977–982.

Lu, X., & Zhang, X. (2008). Measurement of natural radioactivity in beach sands from Rizhao bathing beach, China. Radiation protection dosimetry, 130(3), 385-388.

Lu et al. (2011). Measurement of natural radioactivity and assessment of associated radiation hazards in soil around Baoji second coal-fired thermal power plant, China. Radiation Protection Dosimetry, 1-8.

Macdonald W.G., Rozendaal, A., De Meijer R.J. (1997). Radiometric characteristics of heavy mineral deposits along the west coast of South Africa. Mineralium Deposita, 32, 171.

Macfarlane et al. (1989). The Dakota aquifer program annual report, FY89. Appendix B. Kansas Geological Survey.

Majolagbe, S.B., Faromika O.P. Jeje S.O. (2014). Determination of natural radioactivity in soil samples of some locations in Akure, Ondo State, Nigeria. International Journal of Scientific & Engineering Research, Volume 5, Issue 7. ISSN 2229-5518

Malain, D,. et al. (2010). Measurements of NORM in Beach Sand Samples along the Andaman Coast of Thailand after the 2004 Tsunami. Nuclear Instrument and Methods in Physics Research Section A, vol.619, 441-445.

Malain, D. (2011). Measurements of NORM in beach sand samples along the Andaman coast of Thailand after the 2004 Tsunami. PhD Thesis, University of Surrey (unpublished).

Malanca et al. (1996). Distribution of ^{226}Ra, ^{232}Th, and ^{40}K of Rio Grande do Norte (Brazil). Environmental Radioactivity, 30, 55–67.

Maleka, P.P. (2010). In-situ element analysis from gamma-ray and neutron spectra using a pulsed-neutron source. PhD Thesis, Rijksuniversiteit Groningen.

Mamoney, M. H., and Khater, A.E.M. (2004) Environmental characterization and radio-ecological impacts of non-nuclear industries on the Red Sea coast. Environmental Radioactivity, 73.2, 151-168.

Manigandan, P.K. & Shekar, B.C. (2014). Evaluation of radionuclides in the terrestrial environment of Western Ghats. Radiation Research and Applied Sciences, 7, 310 – 316.

Matiullah, N. Ahmad and Hussein A. J. A. (1998). Natural radioactivity in Jordanian soil and building materials and the associated radiation hazards. Environmental Radioactivity, 39(1): p. 9-22.

Maurotto, A., Rizzo, S., & Tomarchio, E. (2009). MCNP5 modelling of HPGe detectors for efficiency evaluation in γ-ray spectrometry. Radiation Effects and Defects in Solids, 164(5-6), 302-306.

Mbatha, N.B. (2007). Radiometric study of beach sand deposits along the coast of Western Cape Province, South Africa. MSc Thesis, University of the Western Cape (unpublished).

McAulay, I. R. and Moran, D. (1988). Natural radioactivity in soil in the Republic of Ireland. Radiation Protection Dosimetry, 24, 47–49.

Mehra R., Singh S., Singh K. (2006) A study of uranium, radium, radon exhalation rate and indoor radon in the environs of some areas of Malwa region, Punjab. Indoor and
Built Environment, vol.15: 5.

Mehra et al. (2010). Analysis of terrestrial naturally occurring radionuclides in soil samples from some areas of Sirsa district of Haryana, India using gamma ray spectrometry, Environmental Earth Science, 59, pp.1159-1164

Miah, F. K., Roy, S., Touhiduzzaman, M. & Alam, B. (1998). Distribution of Radionuclides in soil samples in and around Dhaka city. Applied Radiation and Isotopes, 49 (1, 2), 133-137.

Mlwilo, N.A., Mohammed, N.K. & Spyrou, N.M. (2007) Radioactivity levels of staple foodstuff and dose estimates for most of Tanzanian population. Radiol. Prot. 27: 271- 480.

Mlwilo, N.A. (2010). Radiometric characterisation of vineyard soils, Western Cape, South Africa, PhD Thesis, University of Western Cape (unpublished).

Modisane T.J.D. (2005). Correlations between natural radionuclide concentrations in soils and vine-growth potential. MSc thesis, University of North-West (unpublished).

Mohammed, N.K. & Mazunga, M.S. (2013). Natural radioactivity in soil and water from Likuyu village in the neighbourhood of Mkuju uranium deposit. International Journal of Analytical Chemistry. ID 501856.

Mohanty, A. K., Sengupta, D., Das, S. K., Vijayan, V., & Saha, S. K. (2004). Natural radioactivity in the newly discovered high background radiation area on the eastern coast of Orissa, India. Radiation Measurements, 38, 153-165.

Mohery et al. (2014). Environmental radiation levels in soil and sediment samples collected from floating water from a land runway resulting from heavy rains in the Jeddah region, KSA. Radiation Physics and Chemistry, 97, 16–24.

Mowafi, W.A., El Tahawy, M.S. (2009). Radiological investigation of the black sand region of the North-East of the Nile Delta. Proceedings of the 7th conference on nuclear and particle physics, 11-15.

Murtty Ch, V.G.K., Upadhyaya and Asokan, S., 2007, "Recovery of Zircon from Sattankulam Deposit in India- Problems and Prospects," The 6th International Heavy Minerals Conference "Back to Basics" The Southern African Institute of Mining and Metallurgy, pp. 69-74.

Mustapha, A.O., Narayana, D.G.S., Patel, J.P., Otwana, D. (1997). Natural radioactivity in some building materials in Kenya and the contributions to the indoor external doses. Radiation Protection Dosimetry, Volume 71, Issue 1, pp. 65-69.

Mustapha, A.O. (1999). Natural radioactivity levels in Kenya. PhD Thesis, University of Nairobi (unpublished).

Myrick et al. (1983). Determination of concentrations of selected radionuclides in surface soil. U.S. Health Physics, Vol. 45, No. 3, 631- 442.

National Council on Radiation Protection and Measurements (NCRP). (1987), Exposure of the Population in the United States and Canada from Natural Background Radiation, NCRP Report no.94, ISBN: 0913392936.

Narayana, et al. (1995), Distribution and Enrichment of Radionuclides in the Newly Discovered High Background Area in Ullal on the Southwest Coast of India, Health Physics 69 (20), 178-186

Navas et al. (2002). Edaphic and physiographic factors affecting the distribution of natural gamma-emitting radionuclides in the soils of the Arna's catchment in the Central Spanish Pyrenees. European Journal of Soil Science, 53, 629-638.

Nir-El, Y. (1998). Application of reference materials in the accurate calibration of the detection efficiency of a low-level gamma-ray spectrometry assembly for environmental samples. Journal of radioanalytical and nuclear chemistry, 227(1-2), 67-74.

Noureddine, I. (1997). Gamma and alpha emitting radionuclides in some Algerian soil samples. Applied Radiation and Isotopes, 48, 1145-1148.

Noncolela, S, P. (2011). Calibration of a NaI(Tl) detector for low level counting of naturally occurring radionuclides in soil. MSc Thesis, University of the Western Cape (unpublished).

NNDC (2011) National Nuclear Data Center http://www.nndc.bnl.gov accessed on 23rd November 2016.

O'Dea, J., Dowdall, M. (1999). Spatial analysis of natural radionuclides in peat overlying a lithological contact in Co. Donegal, Ireland. J. Environmental Radioactivity, 44, 107–117.

Ongori, J.N. (2013). In-situ measurements and calculation of radon gas and exhalation from a tailings mine dump. PhD thesis, University of the Western Cape (unpublished).

Ongori, J.N., Lindsay, R., Newman, R., Maleka, P.P. (2015). Determining the radon exhalation rate from a gold mine tailings dump by measuring the gamma radiation. Environmental Radioactivity, 140, 16-24.

Organisation for Economic Cooperation and Development. (1979), Exposure to Radiation from the Natural Radioactivity in Building Materials, Report by a Group of Experts of OECD Nuclear Energy Agency. Paris, France: OECD.

Örgün, Y., Altınsoy, N., Şahin, S. Y., Güngör, Y., Gültekin, A. H., Karahan, G., & Karacık, Z. (2007). Natural and anthropogenic radionuclides in rocks and beach sands from Ezine region (Canakkale), Western Anatolia, Turkey. Applied Radiation and Isotopes, 65(6), 739-747.

Othman, I. and Yassine T. (1995). Natural radioactivity in the Syrian environment. Science of the Total Environment, 170 (1-2), 119-124.

Pankaj B., Rohit M., Ramola, R.C. (2014). Distribution of natural radioactivity in soil samples and radiological hazards in building material of Una, Himachal Pradesh. Geochemical Exploration 142, 11–15.

Papadopoulos, A., Christofides, G., Koroneos, A., Papadopoulou, L., Papastefanou, C., Stoulos, S. (2013). Natural radioactivity and radiation index of the major granitic plutons in Greece. Environmental. Radioactivity. 124, 227-238.

Papadopoulos, A., Christofides, G., Koroneos, A., Stoulos, S. (2014a), Natural radioactivity distribution and gamma radiation exposure of beach sands from Sithonia Peninsula. Central Eur. J. Geosci. 6 (2), 229-242.

Papadopoulos, A., Christofides, G., Koroneos, A., Stoulos, S., (2014c). Distribution of ^{238}U, ^{232}Th and ^{40}K in plutonic rocks of Greece. Chem. Erde Geochem. 74, 749-764.

Papadopoulos, A., Christofides, G., Koroneos, A., Hauzenberger, C. (2015). U, Th and REE content of heavy minerals from beach sand samples of Sithonia Peninsula (northern Greece). N. Jb. Min. Abh. (J. Min. Geochem.) 192/2, 107-116.

Papadopoulos et al. (2017). Geochemistry of uranium and thorium and natural radioactivity levels of the western Anatolian plutons, Turkey, Miner Petrol, 710-717.

Patel, J.P. et al. (1991). Environmental radiation survey of the area of high natural radioactivity of Mrima Hill of Kenya. Discovery and Innovation, 3 (3): 31-35

Pradler, J. et. al. (2013). On an unverified nuclear decay and its role in the DAMA experiment. Physics Letters B, Volume 720, Issues 4–5, 26, 399–404.

Probonas, M., Kritidis, P. (1993). The exposure of the Greek population to natural gamma radiation of terrestrial origin. Radiation Protection Dosimetry 46, 123-126.

Puniyakotti, J., and Ponnusamy, V., (2017). Radionuclides of 238U, 232Th and 40K in beach sand of Southern Regions in Tamilnadu state, India (Post-Tsunami). Indian Journal of Pure and Applied Physics, 55, pp 218-230.

Quindos, L. S., Fernandez, P.I., Soto, J., Rodeanas, C., Gomez, J. (1994). Natural radioactivity in Spanish soils. Health Physics, 66, 194 – 200.

Quindos, L.S., Sainz, C., Fuente, I., Nicola´s, J., Quindo´s, L., Arteche, J. (2006). Correction by self-attenuation in gamma-ray spectrometry for environmental samples. Radioanal. Nucl. Chem. 270 (2), 339–343.

Rabesiranana et al. (2008). Top soil radioactivity assessment in a high natural radiation background area: the case of Vinaninkarena, Antsirabe-Madagascar. Applied Radiation and Isotopes, vol. 66, 216 – 224.

Radenković et al. (2009). Radioactivity of sand from several renowned public beaches and assessment of the corresponding environmental risks. J. Serb. Chem. Soc. 74 (4), 461–470.

Ramasamy, V., Murugesan, S., Mullainathan S. (2004a). Characterization of minerals and relative distribution of quartz in Cauvery river sediments from Tamilnadu, India- A FTIR study. Bulletin of Pure and Applied Science 23, 1.

Ramasamy, V., Murugesan, S., Mullainathan, S., (2004b). Gamma ray spectrometric analysis of primordial radionuclides in sediments of Cauvery river in Tamilnadu, India. The Ekologia, 2(1-2), 83-88.

Ramasamy, V., Senthil, S., Meenakshisundaram, V. (2009b). Distribution of Natural Radionuclides and Minerals in Beach Sediments from North East Coast of Tamilnadu, India. African Journal of Basic & Applied Sciences, 1 (1-2), pp. 15-20.

Ramasamy, V. et al. (2011). Investigation on natural radiation level and its hazardous nature of river sediments using γ-ray spectroscopy. Radiochemistry, 53 (1), 87-96.

Ramasamy, V., Sundarrajan, M., Paramasivan, K., Meenakashindaran, V., Suresh, G. (2013). Assessment of spatial distribution and radiological hazardous nature of radionuclides in high background radiation area, Kerala, India. Applied Radiation and Isotopes, Volume 73, pp. 21-31.

Ramasamy, V. et al. (2014). Function of minerals in the natural radioactivity level of Vaigai River sediments, Tamilnadu, India - Spectroscopical approach. Spectrochimica Acta Part A Molecular and Biomolecular Spectroscopy, 117, 340-350.

Ramli et al. (2005). Terrestrial gamma radiation dose study to determine the baseline for environmental radiological health practices in Melaka state, Malaysia. Environmental Protection, 25, 435-450.

Ramli, A.T. (1997), Environmental Terrestrial Gamma Radiation Dose and its Relationship with Soil Type and Underlying Geological Formations in Pontian District, Malaysia, Applied Radiation and Isotopes, 48 (3), 407-412.

Rao, N.S., Sengupta, D., Guin, R., Saha, S.K. (2009). Natural radioactivity measurements in beach sand along southern coast of Orissa, eastern India. Environ Earth Sci 59:593– 601.

Rogers, J. J. W., & Adams, J. A. S. (1969). Thorium. Handbook of geochemistry, *2*(4), 90I-90O.

Rowland, R. E., Stehney, A. F. and Lucas, H. F. (1978). Dose Response Relationships for Female Radium Dial Workers. Radiat Res, 76, pp 368-383.

Rubio et al. (2003). Sediment accumulation rate and radiological characterisation of the sediment of Palmones River estuary (southern of Spain). Environmental radioactivity,
65, 67–280.

Saito, K., Jacob, P. (1995). Gamma-ray, elds in the air due to sources in the ground. Radiation Protection Dosimetry. 58, 29–45.

Sam, Adam Khatir, Ahamed Mustafa M. O., Khangi F. A. El, El Nigumi Y. O., et al. (1998). Radioactivity levels in the Red Sea coastal environment of Sudan. Marine Pollution Bulletin, 36 (1), 19-26.

Santawamaitre, T., et al. (2011). Study of natural radioactivity in riverbank soils along the Chao Phraya river basin in Thailand. Nuclear Instruments and Methods in

Physics Research Section A: Accelerators, Spectrometers, Detectors and Associated Equipment 652.1, 920-924.

Santawamaitre, T., Malain, D., Al-Sulaiti, H. A., Bradley, D. A., Matthews, M. C., & Regan, P. H. (2014). Determination of ^{238}U, ^{232}Th and ^{40}K activity concentrations in riverbank soil along the Chao Phraya river basin in Thailand. Journal of environmental radioactivity, 138, 80-86.

Saueia, C.H.R. and Mazzilli, B.P. (2006), Distribution of Natural Radionuclides in the Production and Use of Phosphate Fertilizers in Brazil, Environmental Radioactivity, 89, 229-239.

Sengupta, D., Mohanty, A.K., Das, S.K., Saha, S.K. (2005). Natural radioactivity in the high background radiation area at Erasama beach placer deposit of Orissa, India. International Congress Series, 1276, 210–211.

Senthilkumar et al. (2014). Natural radioactivity measurement and evaluation of radiological hazards in some commercial flooring materials in Thiruvannamalai, Tamilnadu, India. Radiation Research and Applied Sciences, 7, 116 – 122.

Shetty, P.K. and Narayana, Y. (2010). Variation of radiation level and radionuclide enrichment in high background area. Environmental. Radioactivity. 101, 1043–1047.

Shimboyo, S. A., & Oyedele, J. (2015). Determination of natural radioactivity in soils of Henties Bay, Namibia. (http://repository.unam.na/handle/11070/1427)

Shuaibu, H.K., Khandaker, M.U., Al refae, T., Bradley, D.A. (2017). Assessment of natural radioactivity and gamma-ray dose in monazite rich black Sand Beach of Penang Island, Malaysia. Marine Pollution Bulletin 119, 423–428.

Singh et al. (2003). Natural radioactivity measurements in soil samples from Hamirpur district, Himachal Pradesh, India. Radiation Measurements, 36, pp.547-549.

Singh, S, Rani, A. and Mahajan, R.K. (2005). ^{226}Ra, ^{232}Th and ^{40}K analysis in soil samples from some areas of Punjab and Himachal Pradesh, India using gamma ray spectrometry. Radiation Measurements, 39.4, 431- 439.

Singh et al. (2007). Uranium, radium and radon measurements in the environs of Nurpur area, Himachal Himalayas, India. Environmental Monitoring Assessments,128, pp.301- 309.

Singh et al. (2009). Comparative study of natural radioactivity in soil samples from the Upper Siwaliks and Punjab, India using gamma ray spectrometry. Environmental Radioactivity, 100, pp.94-98

Singh et al. (2016). Radionuclide contents and their correlation with radon-thoron exhalation in soil samples from mineralized zone of Himachal Pradesh, India. Radioanalytical Nuclear Chemistry 10.1007/s10967-016-4975-2

Singh, P. (2009). Major, trace and REE geochemistry of the Ganga River sediments: Influence of provenance and sedimentary processes. Chemical Geology, 266, 242-255.

Singh, P. (2010). Geochemistry and Provenance of stream sediments of Ganga River and its major tributaries in the Himalayan region, India. Chemical Geology, 269, pp. 220- 236.

Singh, H.N., Shanker, D., Neelakandan, V.N., Singh, V.P. (2007). Distribution patterns of natural radioactivity and delineation of anomalous radioactive zones using in situ radiation observations in Southern Tamil Nadu, India. Journal of Hazardous Materials, 141, 264–272

Sivakumar et al. (2014). Measurement of natural radioactivity and evaluation of radiation hazards in Coastal sediments of east coast of Tamilnadu using statistical approach. Journal of Taibah University for Science 8, 375–384.

Sohrabi, M. (1993). Recent radiological studies of high-level natural radiation areas of Ramsar. In: Proceedings of the International Conference on High Levels of Natural Radiation Areas, Ramsar, Iran, 1990. IAEA Publication Series, IAEA, Vienna.

Sohrabi, M. (1998). The state-of-the-art on worldwide studies in some environments with elevated naturally occurring radioactive materials (NORM). Applied Radiation and isotopes, 49.3, 169-188.

Spectro (2000). Documentation of SPECTRO X-LAB: Basic Principles of EDXRF. Technical Report, Spectro Analytical Instruments, GmbH.

Speelman, W. J. (2004). Modelling and measurement of radon diffusion through soil for application on mine tailings dams. MSc Thesis. University of the Western Cape, South Africa (unpublished).

Sroor, A., El-Bahi S. M., Ahmed F., and Abdel-Haleem A. S. (2001). Natural radioactivity and radon exhalation rate of soil in southern Egypt. Applied Radiation and Isotopes, 55(6), 873-879.

Suresh G, Ramasamy V, Meenakshisundaram V, Venkatachalapathy R, Ponnusamy V., (2011a). A relationship between the natural radioactivity and mineralogical composition of the Ponnaiyar river sediments, India. Environmental Radioactivity, 102(4), 370-77.

Suresh, G., Ramasamy, V., Meenakshisundaram, V., Venkatachalapathy, R., Ponnusamy, V., (2011b). Influence of mineralogical and heavy metal composition on natural radionuclide concentrations in the river sediments. Applied Radiation Isotopes, 69(10), 1466-74.

Tahir et al. (2005). Measurements of activity concentrations of naturally occurring radionuclides in soil samples from Punjab province of Pakistan and assessment of radiological hazards Radiation Protection Dosimetry 113 421–7

Tanzania National Bureau of Statistics (TNBS), 2018 (available at https:www.nbs.gov.tz accessed on 18th December, 2018).

Tao et al. (2012). Cancer and non-cancer mortality among inhabitants in the high background radiation area of Yangjiang, China (1979-1998). Health Phys., 102:173- 181.

Taskin, H., Karavus, M., Ay, P., Topuzoglu, A., Hindiroglu, S., Karahan, G., (2009). Radionuclide concentrations in soil and lifetime cancer risk due to the gamma radioactivity in Kirklareli, Turkey, Journal of Environmental Radioactivity, 100, 49-53.

Tesi, D. (2012). Indoor and outdoor natural radioactivity in the Vulsini volcanic District (Central Italy): Estimation of doses and radiological risks (unpublished).

Theodorsson, P. (1996). Measurement of Weak Radioactivity, London, World Scientific, ISBN: 978-981-02-2315-1.

TRACERCO (2007). Module 14: Naturally Occurring Radioactive Material in Oil Production, Radiological Safety Course, 1-11.

Travassos, J. M., and Pires, A. C. B. (1994). The screening effect of a tropical forest on airborne gamma- ray spectrometry: Nuclear Geophysics, 8, 461-471.

Tsabaris, C., et al. (2007). Radioactivity levels of recent sediments in the Butrint Lagoon and the adjacent coast of Albania. Applied Radiation and Isotopes, 65, 445–453

Tufail, M. (2006). Measurement of Terrestrial Radiation for Assessment of Gamma Dose from Cultivated and Barren Saline Soils of Faisalabad in Pakistan. Radiation Measurements, vol.41, 443-451.

Turner, J.E. (2007), Atoms, Radiation and Radiation Protection, 3rd edition, Weinheim: Wiley-VCH.

Tyler, A. N. (2008). In situ and airborne gamma-ray spectrometry. Radioactivity in the Environment 11: 407-448.

Tzortzis, M., Tsertos, H., Christofides, S., & Christodoulides, G. (2003). Gamma-ray measurements of naturally occurring radioactive samples from Cyprus characteristic geological rocks. *Radiation Measurements*, *37*(3), 221-229.

Tzortzis, M., Svoukis, E., & Tsertos, H. (2004). A comprehensive study of natural gamma radioactivity levels and associated dose rates from surface soils in Cyprus. Radiation Protection Dosimetry, Volume 109, Issue 3, 1 July 2004, Pages 217–224.

Tzortzis, M. and Tsertos, H. (2004). Determination of Thorium, Uranium and Potassium Elemental Concentrations in Surface Soils in Cyprus, Journal of Environmental Radioactivity 77, 325-338.

United Nations Scientific Committee on the Effects of Atomic Radiation (1993). Sources and effects of ionizing radiation. Report to the General Assembly with scientific annexes. United Nations Scientific Committee on the effects of Atomic Radiation. New York, USA: United Nations.

United Nations Scientific Committee on the Effects of Atomic Radiation (2000). Sources and effects of ionizing radiation. United Nations scientific committee on the effects of atomic radiation. Report to the General Assembly on the Effects of Atomic Radiation. United Nations, New York.

United Nations Scientific Committee on the Effects of Atomic Radiation (2008). Sources and Effects of Ionizing Radiation, Report to the General Assembly, with scientific annexes, United Nations Sales Publication, United Nations, New York.

United Nations Scientific Committee on the Effects of Atomic Radiation (2010). Sources and Effects of Ionizing Radiation, UNSCEAR 2008 Report to the General Assembly, with scientific annexes, United Nations Sales Publication, United Nations, New York.

Uosif, M. A. M. (2007). Gamma-ray spectroscopic analysis of selected samples of Nile river sediments in Upper Egypt. Radiation Protection Dosimetry, 123(2), 215-220.

Valkovic, V. 2000. Radioactive nuclides in nature. Radioactivity in the environment. Amsterdam: Elsevier, 5-31 (Chapter 2).

Vanden Bygaart, A. J., Protz, R., & McCabe, D. C. (1999). Distribution of natural radionuclides and Cs-137 in soils of southwestern Ontario. Canadian Journal of Soil Science, 79, 161–171.

Veiga, R. et al. (2006). Measurement of Natural Radioactivity in Brazilian Beach Sands, Health Physics, vol.41, no.2, 189-196

Venema, L.B. & De Meijer, R.J. (2001). Natural radionuclides as tracers of the

dispersal of dredge spoil dumped at sea. Environmental Radioactivity, 55: 221-239.

Vukotic et al. (1998). Radioactivity on the Montenegrin Coast, Yugoslavia. Radioanal. Nucl. Chem., 235, pp.151-157

Wahl, W. (2007) Radionuclide Handbook for Laboratory Workers in Spectrometry, Radiation Protection, and Medicine, Institute for Spectrometry and Radiation Protection (ISuS), Germany.

Ward Jr, J. H. (1963). Hierarchical grouping to optimize an objective function. Journal of the American statistical association, 58(301), 236-244.

Wei, L., Zha, Y., Tao, Z., He, W., Chen, D. and Yuan, Y. (1990) Epidemiological investigation in high background radiation areas in Yangjiang, China. in In Proceedings of International Conference on High Level Natural Radiation Areas. 1993. Ramsar, Iran, 3-7 November: Publication Series, IAEA, Vienna.

Wong, F.L., Woodrow, D.L., McGann, M. (2013). Heavy mineral analysis for assessing the provenance of sandy sediment in the Fransisco Bay Coastal system. Marine Geology, 345, 170-180.

Xhixha, G. (2012). Advanced gamma-ray spectrometry for environmental radioactivity monitoring. PhD Thesis. University of Ferara (unpublished).

Yang et al. (2005). Radioactivity concentrations in soils of the Xiazhuang granite area, China. Applied Radiation and Isotopes, 63(2): p. 255-259.

Yasir et al. (2007). Study of natural radionuclides and its radiation hazard index in Malaysian building materials. Radioanal. Nucl. Chem.;273:539-41.

Yousef, M. I., Abu El-Ela, A., & Yousef, H. A. (2007). Natural Radioactivity Levels in Surface Soil of Kitchener Drain in the Nile Delta of Egypt. Journal of Nuclear and Radiation Physics, 2(1), 61 - 68.

Yu et al., (1992). The assessment of natural radiation dose committed to the Hong Kong people Environmental Radioactivity, 17, pp.31-48.

Ziqiang, P., Yin, Y. and Minggiang, G. (1988). Natural radioactivity in China. Radiation Protection Dosimetry, 24(1/4), 29-38.

Appendix A

The relationship between the units for the activity concentration, Bq/kg and parts per million (ppm) and percentage (%).

1) Relationship between ppm and Bq/kg

   a) 1 ppm of U_3O_8 corresponds to 1 mg of U_3O_8/kg

      or 1 ppm of U_3O_8 corresponds to 1 g of U_3O_8/kg = $1x10^{-3}$ of U_3O_8/kg

Recall,

Activity, $A = \lambda N$ and $\lambda = \frac{\ln 2}{t_{1/2}}$ where N is number of atoms of ^{238}U per 1 g of uranium

$$N = \frac{m}{M}$$

where m is the mass of ^{238}U (0.9927 g), M is the molar mass of ^{238}U (238.0507828 g) and N_A (6.02×10^{23}) is Avogadro's number

$$N = \frac{0.9927 \times 10^{-3}}{238.0508} \times 6.02 \times 10^{23}$$

$$t_{1/2} \text{ of } ^{238}U = 4.468 \times 10^9 \text{ years}$$

$$= 4.468 \times 10^9 \times 365 \times 24 \times 60 \times 60 \text{ seconds}$$

$$= 1.41 \times 10^{17} seconds$$

Activity of 1 g = ln 2 x 0.9927 x 6.02 x 10^{23} x 10^{-3}/238.0507828 x 1.41 x 10^{17} s

= 12.35 Bq/kg

Therefore, **1 ppm = 12.35 Bq/kg**

   b) 1 ppm of ThO_2 corresponds to 1 mg of ThO_2/kg

      or 1 g of ThO_2/1000kg

let us find N – number of ^{232}Th in 1g of ThO_2

Activity, A = -Dn/dt =- λN

= - ln 2. N/half-life, where N is number of atoms per 1 g of thorium

Half-life of ^{232}Th = 1.405 x 10^{10} yrs = 1.405 x 10^10 x 365 x 24 x 60 x 60 seconds

N = m/M, where m is the mass of thorium, M is the molar mass and N_A is the Avogadro's number.

$A = \ln 2 \times 1x10^{-3} \times 6.02 \times 10^{23} / 232.0381 \times 1.405 \times 10^{10} \times 365 \times 24 \times 60 \times 60$

= 4.06 Bq/kg

For the case of potassium, it is expressed as percentage (%). In nature, potassium exists as K_2O, half-life of $^{40}K = 1.25x10^{9}$ yrs, Abundance of ^{40}K in nature = 0.0117 and molar mass of ^{40}K is 39.9639987